

LITHUANIAN UNIVERSITY OF HEALTH SCIENCES

Justinas Mačiulaitis

**REGENERATIVE POTENTIAL OF
TISSUE ENGINEERED CARTILAGE FOR
THE REPAIR OF OSTEOCHONDRAL
DEFECT IN A PRECLINICAL SPORTS
INJURY MODEL**

Doctoral Dissertation
Medical and Health Sciences,
Medicine (M 001)

Kaunas, 2020

The doctoral dissertation has been prepared at the Clinic of Sport Medicine of the Medical Academy of Lithuanian University of Health Sciences during the period of 2015–2020.

Scientific Supervisor:

Prof. Dr. Rimtautas Gudas (Lithuanian University of Health Sciences, Medical and Health Sciences, Medicine – M 001).

Consultant:

Prof. Dr. Romaldas Mačiulaitis (Lithuanian University of Health Sciences, Medical and Health Sciences, Medicine – M 001).

Dissertation is defended at the Medical Research Council of the Lithuanian University of Health Sciences:

Chairperson:

Prof. Dr. Kęstutis Petrikonis (Lithuanian University of Health Sciences, Medical and Health Sciences, Medicine – M 001).

Members:

Assoc. Prof. Dr. Margarita Pileckytė (Lithuanian University of Health Sciences, Medical and Health Sciences, Medicine – M 001);

Prof. Dr. Liudas Ivanauskas (Lithuanian University of Health Sciences, Medical and Health Sciences, Pharmacy – M 003);

Prof. Dr. Valentinas Uvarovas (Vilnius University, Medical and Health Sciences, Medicine – M 001);

Prof. Dr. Una Riekstina (University of Latvia, Medical and Health Sciences, Pharmacy – M 003).

Dissertation will be defended at the open session of the Medical Research Council of the Lithuanian University of Health Sciences on 28th of August 2020 at 1 p. m. in the Auditorium A-203 of the Center of Advanced Pharmaceutical and Health Technologies of Lithuanian University of Health Sciences.

Address: Sukilėlių 13, LT-50166 Kaunas, Lithuania.

LIETUVOS SVEIKATOS MOKSLŲ UNIVERSITETAS

Justinas Mačiulaitis

**SPORTO TRAUMŲ METU PATIRTŲ
SĄNARIŲ OSTEOCHONDRINIŲ
PAŽEIDIMŲ GYDYMAS, NAUDOJANT
AUDINIŲ INŽINERIJOS PRODUKTUS
IKIKLINIKINIUOSE MODELIUOSE**

Daktaro disertacija
Medicinos ir sveikatos mokslai,
medicina (M 001)

Kaunas, 2020

Disertacija rengta 2015–2020 metais Lietuvos sveikatos mokslų universiteto Medicinos akademijos Sporto medicinos klinikoje.

Mokslinis vadovas:

prof. dr. Rimtautas Gudas (Lietuvos sveikatos mokslų universitetas, medicinos ir sveikatos mokslai, medicina – M 001).

Konsultantas:

prof. dr. Romaldas Mačiulaitis (Lietuvos sveikatos mokslų universitetas, medicinos ir sveikatos mokslai, medicina – M 001).

Disertacija ginama Lietuvos sveikatos mokslų universiteto Medicinos mokslo krypties taryboje:

Pirmininkas:

prof. dr. Kęstutis Petrikonis (Lietuvos sveikatos mokslų universitetas, medicinos ir sveikatos mokslai, medicina – M 001).

Nariai:

doc. dr. Margarita Pileckytė (Lietuvos sveikatos mokslų universitetas, medicinos ir sveikatos mokslai, medicina – M 001);

prof. dr. Liudas Ivanauskas (Lietuvos sveikatos mokslų universitetas, biomedicinos mokslai, farmacija – M 003);

prof. dr. Valentinas Uvarovas (Vilniaus universitetas, medicinos ir sveikatos mokslai, medicina – M 001);

prof. dr. Una Riekstina (Latvijos universitetas, medicinos ir sveikatos mokslai, farmacija – M 003).

Disertacija ginama viešame medicinos mokslo krypties tarybos posėdyje 2020 m. rugpjūčio 28 d. 13 val. Lietuvos sveikatos mokslų universiteto Naujausių farmacijos ir sveikatos technologijų centro A-203 auditorijoje.

Disertacijos gynimo vietos adresas: Sukilėlių pr. 13, LT-50166 Kaunas, Lietuva.

CONTENTS

ABBREVIATIONS	7
INTRODUCTION	8
1. AIM OF THE THESIS.....	11
2. NOVELTY AND PRACTICAL USE OF THESIS	12
3. LITERATURE REVIEW	14
3.1. Pathogenesis of articular cartilage defects	14
3.2. Current treatment techniques	14
3.3. Treatment with three-dimensional scaffolds and cells	16
3.3.1. Characterization of a cellular component	16
3.3.2. Characterization of scaffold component.....	18
3.3.2.1. Scaffold chemical characterization.....	18
3.3.2.2. Scaffold physical characterization.....	19
3.3.2.3. Scaffold mechanical characterization	21
3.3.2.4. Biocompatibility characterization.....	22
3.3.2.5. Clinical application.....	23
4. METHODS AND MATERIALS	24
4.1. Article references.....	24
4.2. Study design.....	24
4.3. Scaffold manufacturing.....	26
4.3.1. Primary study: HOI and collagen scaffold manufacturing	26
4.3.2. Final study: HOI optimization and collagen scaffold manufacturing	27
4.4. Scaffold characterization <i>in vitro</i>	28
4.4.1. Primary study: Morphological analysis of HOI and CS	28
4.4.2. Final study: Morphological and biomechanical analysis of HOI and CS	28
4.5. Cell isolation, culture, and posology <i>in vitro</i>	28
4.5.1. Primary study: Cell isolation, culture, and posology of 3D culture.....	29
4.5.2. Final study: Cell isolation, culture, and posology of 3D culture.....	29
4.6. Cell seeded scaffold biochemical characterization <i>in vitro</i>	29
4.6.1. Primary study: Protein secretion analysis of monolayer and 3D culture	30
4.6.2. Final study: Metabolic activity, cell count, and biochemical analysis of monolayer and 3D culture	30
4.7. HOI scaffold genotypic characterization <i>in vitro</i>	30
4.7.1. Primary study: Gene expression analysis of 3D culture	30
4.7.2. Final study: Gene expression analysis of monolayer and 3D culture	31
4.8. Design of the long-term <i>in vivo</i> study	31
4.8.1. Primary study: 6 months <i>in vivo</i> study design	31
4.8.2. Final study: 3 months <i>in vivo</i> study design.....	32
4.9. Macroscopic evaluation of long-term study.....	32
4.9.1. Primary study: Electromechanical evaluation of cartilage <i>in vivo</i>	32

4.10. Histological evaluation of cartilage <i>in vivo</i>	33
4.11. Statistical evaluation	33
4.11.1. Primary study: Statistical evaluation	33
4.11.2. Final study: Statistical evaluation.....	34
5. RESULTS	35
5.1. Results of the primary study	35
5.1.1. Cell morphology and viability in monolayer	35
5.1.2. Cell Seeding and 3D Growth Analysis	35
5.1.3. Cell Seeded Scaffold Potency Analysis	37
5.1.4. Macroscopic OAS evaluation <i>in vivo</i>	39
5.1.5. Histological O’Driscoll evaluation <i>in vivo</i>	40
5.1.6. Electromechanical evaluation <i>in vivo</i>	41
5.2. Results of the final study	42
5.2.1. Morphological and biomechanical analysis	42
5.2.2. Biocompatibility analysis and pore shape dependence analysis	46
5.2.3. 3D cell redifferentiation and pore shape dependence analysis	49
5.2.4. 3D cell redifferentiation and pore-scale dependence analysis	49
5.2.5. Macroscopic analysis of repair cartilage	52
5.2.6. Histological analysis of repair	54
6. DISCUSSION.....	55
6.1. Biocompatibility of rabbit chondrocytes and microstructured HOI scaffolds <i>in vitro</i>	55
6.2. Safety and efficacy of primary TEC in a long-term rabbit articular cartilage defect model	55
6.3. Biocompatibility of human chondrocytes and optimized HOI scaffold <i>in vitro</i>	57
6.4. Safety and efficacy of final TEC in a long-term rat articular cartilage defect model	61
CONCLUSIONS	63
RECOMMENDATION	64
SANTRAUKA.....	65
REFERENCES LIST.....	99
PUBLICATIONS LIST	107
CONFERENCE PRESENTATIONS	108
COPIES OF SCIENTIFIC ARTICLES	110
ANNEXES	146
Annexe 1	146
Annexe 2	147
CURRICULUM VITAE.....	148
PADĚKA	150

ABBREVIATIONS

AM	–	additive manufacturing
AMIC	–	autologous matrix induced chondrogenesis
CAD	–	computer-aided design
CD	–	cluster of differentiation
COL2A1	–	type II collagen gene
COL10A1	–	type X collagen gene
CS	–	collagen sponge (primary study) or collagen membrane (final study)
DBMP	–	2-benzyl-2-(dimethylamino)-4'-morpholinobutyrophenone
DLW	–	direct laser writing in pre-polymers
DNA	–	deoxyribonucleic acid
ECM	–	extracellular matrix
E _{IT}	–	indentation modulus
ELISA	–	enzyme-linked immunosorbent assay
GAG	–	glycosaminoglycan
GAPDH	–	Glyceraldehyde 3-phosphate dehydrogenase
H&E	–	hematoxylin and eosin dye
H _{IT}	–	indentation hardness
HOI	–	hybrid organic-inorganic
HOI-T	–	tetragonal hybrid organic-inorganic scaffolds
HOI-H	–	hexagonal hybrid organic-inorganic scaffolds
HOI-T1.5	–	HOI-T scaled by a factor of 1.5
HOI-T2	–	HOI-T scaled by a factor of 2
LM	–	light microscope
mRNA	–	messenger ribonucleic acid
OA	–	osteoarthritis
OAT	–	osteocondral graft transplantation
OAS	–	modified Oswestry Arthroscopy Score
RT-qPCR	–	reverse transcription-polymerase chain reaction
TEC	–	tissue engineered cartilage
SEM	–	scanning electron microscopy
SZ2080	–	a two-compound sol-gel composite based on zirconium and silicon
QP	–	quantitative parameter

INTRODUCTION

Articular cartilage defects are some of the most common musculoskeletal problems for a highly active population [1].

Chondral lesions are diagnosed in more than 60% of knee arthroscopic surgeries, therefore present a big challenge to orthopedic surgeons [2].

The innate cartilage capacity to achieve quality tissue regeneration is greatly limited by the avascular origin of the tissue [3, 4]. Despite the self-repair of cartilage after the injury to the osteochondral region, the structural and functional properties of the repair tissue are inferior compared to healthy cartilage [5]. This temporary repair leads to cartilage deterioration and subsequent progression toward osteoarthritis (OA) [6].

Various treatment options to manage an osteochondral injury have been introduced, however complete restoration of hyaline cartilage tissue has not yet been successful [7].

Recently, cell and scaffold-based tissue engineering have progressed rapidly especially in regenerative orthopedics and cartilage repair.

The safety and efficacy quality parameters of the tissue-engineered cartilage (TEC) products are dependent on the interaction between cellular and non-cellular components of TEC and must be established for medicinal products. Successful regenerative products might potentially replace currently used synthetic molecules and implants to treat cartilage diseases.

Regulatory pathways to approve medicinal products of biological origin have been extended to the plethora of new regenerative cell-based therapeutics – advanced therapy medicinal products [8]. European Union guidelines for cell-based medicinal products set forth the requirements and methods to characterize medicinal products [9]. TEC is composed of living cells seeded on scaffolds of different origins, thus characterization requires compliance with quality standards to ensure their safety and efficacy [10].

The cellular component of the TEC is regarded as the active substance for the intended medical use. A correct selection of the type of cells to be used improves the characterization study potential to demonstrate TEC biological activity *in vitro* and their potential and regenerative capacity *in vivo* [11].

The scaffold is regarded as an additional substance and together with cells form an integral part of the final TEC. Biomaterials and fabrication methods used are the initial elements that highly influence active substance proliferation, interaction and deposition of extracellular matrix (ECM) [12]. Highly bioactive properties of natural collagen-based scaffolds are inherent thus this type of scaffold facilitates cell and material interaction, and improves the chondrogenic activity *in vitro* [13, 14]. Similarly, synthetic scaffolds

manufactured by additive techniques such as direct laser writing in pre-polymers (DLW) are currently carefully investigated for cartilage tissue engineering *in vitro*. Custom-tailored physical characteristics of the scaffold, can be reproducibly manufactured, due to DLW three-dimensional structuring capability, high spatial resolution, scaling flexibility and diversity of processable materials [15–18]. Direct laser writing technology for the development of TECs has not yet been studied.

The biocompatibility of TEC is highly dependent on scaffold biomechanical and physical features *in vitro* [19, 20]. Highly predictable and customizable physical characteristics, such as mechanical rigidity, pore size, porosity and pore interconnectivity are enabled by the ability to adjust parameters of synthetic polymeric feed material [21–23]. These structural parameters are critical for TEC and enable a homogenous distribution of cells and nutrient transfer within the scaffold [24, 25]. In addition, the custom design of pore morphology can influence phenotype formation and the superior production of ECM proteins [26]. The surrounding liquid medium can negatively impact soft natural collagen-based scaffolds biomechanics, thus reducing biomechanical properties of the scaffold before implantation. Thus, the favorable biocompatibility of the TEC and the ability to sustain heavy loads *in vivo* is determined by a sufficient physical and biomechanical capacity of the scaffold *in vitro* [13, 27].

The ability of chondrocytes to effectively adhere to the scaffold is highly dependent on cell viability. In addition, viable cell proliferation is indicative of the ability to deposit ECM on the scaffold, thus identification of optimal biomaterial morphological parameters is essential for specific cellular processes [28]. Similarly, TEC potency *in vitro* is established by cartilaginous protein expression and secretion [29]. A lost ability of monolayer cells to express hyaline cartilage genes could be reversed in a 3D culture [30]. Therefore, the upregulation of genes encoding hyaline cartilage-specific type II collagen is indicative of the cell redifferentiation and functionality of TEC *in vitro*. Whether cell proliferation, phenotype, and genotype of chondrocytes will be influenced by innovative three-dimensional scaffolds has not yet been studied.

Safety and efficacy quality parameters are established for TECs and they cover characterization of cellular, non-cellular components and the interaction in between. Despite the regulatory guidelines available for TEC, a lack of detailed guidance from regulatory authorities for adequate characterization remains a challenge for TEC developers [9, 10]. A variety of technologies are available for scaffold fabrication, however clinical adoption of effective TEC is still limited due to inconsistent manufacturing methods, insufficient

characterization and lack of preclinical studies for safety and efficacy evaluation [31].

In this study, we aimed to evaluate the DLW lithography technique to create and characterize custom, hybrid organic-inorganic (HOI) three-dimensional scaffold of optimal morphologies and to evaluate its biocompatibility with animal and human cells *in vitro* and *in vivo* preclinical cartilage repair models.

1. AIM OF THE THESIS

The aim of this study was to evaluate the safety and efficacy of an innovative three-dimensional microstructured TEC in long-term preclinical articular cartilage defect models.

Tasks:

1. To develop primary HOI scaffold and evaluate its *in vitro* biocompatibility with rabbit chondrocytes.
2. To evaluate *in vivo* safety and efficacy of primary TEC in a long-term preclinical rabbit articular cartilage defect model.
3. To optimize HOI scaffold and evaluate its *in vitro* biocompatibility with human chondrocytes.
4. To evaluate *in vivo* safety and efficacy of optimized TEC in a long-term preclinical rat articular cartilage defect model.

2. NOVELTY AND PRACTICAL USE OF THESIS

Articular cartilage is an avascular – aneural tissue and consists of a single cell – chondrocyte – surrounded and embedded by the secreted extracellular matrix (ECM). Lack of tissue vascularity prevents cartilage from self-repair after injury, and lack of innervation leaves patients unacknowledged of the damage, thus further deteriorating the tissue. Despite the relative simplicity of the cartilage tissue, a complete hyaline cartilage regeneration has not been achieved for the last 30 years.

Different cartilage repair techniques have been tested and each with a variable outcome. It has concluded, that some parameters of the regenerative approach have to be met in order to achieve a hyaline, or hyaline-like tissue regeneration. One the most prominent approaches, include the use of scaffolds either with or without seeded cells. Even though many different biomaterials and preparation techniques have been tested to create a safe and efficacious tissue engineered cartilage (TEC) product, the search for a biologically, chemically, and morphologically biocompatible scaffold is still ongoing.

In this work we have tested a new manufacturing approach to create biocompatible scaffolds for articular cartilage regeneration, by employing ultrafast pulse DLW lithography. For the first time femtosecond laser-based technique has been employed for the fabrication of custom three-dimensional HOI scaffolds with micrometers of precision. We have shown that the custom architecture and the resultant biomechanical properties are highly supportive for the ingrowth of new cartilage tissue.

Because the selection of biomaterials and culturing techniques used in manufacturing are key components of fabricating efficacious TEC, a thorough biocompatibility analysis of the morphologically different scaffolds microstructured by the DLW has been carried out in this work. For the first time, the biocompatibility of the organic-inorganic scaffold with the seeded animal and human chondrocytes was tested *in vitro* and *in vivo* and compared to the biocompatibility of seeded collagen scaffolds (CS) in preclinical models. We have shown that HOI and CS materials are biologically compatible and have little to no toxic effect on the seeded chondrocytes in all our studies.

The favorable interaction between chondrocytes and tested HOI scaffolds have yielded new data on the key morphological and culture parameters to be subsequently used in a large animal study.

In addition, collagen-based constructs seeded with chondrocytes demonstrated robust safety and efficacy profile in all of our preclinical studies. Thus, subsequent TEC development according to the monographs of European Pharmacopoeia for eligible use in clinical studies will be pursued.

3. LITERATURE REVIEW

3.1. Pathogenesis of articular cartilage defects

Cartilage is a specialized avascular and aneural connective tissue [3]. It is mainly composed of ECM of collagens and proteoglycans. A relatively sparse population of cells – chondrocytes – form only 1–5% volume of the articular cartilage. Chondrocytes receive their nutrition by diffusion through the matrix. The main function of the chondrocytes is to produce ECM components, such as collagens and proteoglycans and to maintain the integrity of the cartilage [32, 33].

Articular cartilage provides a low-friction gliding surface, it acts as a shock absorber and minimizes biomechanical peak pressures on the subchondral bone. In turn, ECM protects the cells from mechanical damage and acts as storage and transducer of cytokines, growth factors for the cells to maintain a balance of anabolic and catabolic pathways to stabilize cartilage integrity.

A damaged cartilage tissue typically responds with local inflammation, cartilage remodeling and scar tissue formation. The scarce population of chondrocytes distributed throughout the tissue is causing a relatively slow turnover-rate of both chondrocytes and ECM. As a result, a limited intrinsic repair capacity of the cartilage is driven by the avascular nature of the tissue and the low ECM turnover rate by chondrocytes [3, 33]. Insufficient synthesis of new ECM results in incomplete cartilage defect fill and inferior qualitative properties of the cartilage tissue.

Thus, minor lesions of the cartilage if untreated may stay the same or deteriorate and lead to progressive cartilage damage. Isolated osteochondral lesions may significantly impair the quality of life, by causing significant pain and loss of function and potentially leading to disability.

3.2. Current treatment techniques

Ideal articular cartilage repair encompasses restoration of a damaged articular surface with a new cartilage tissue resembling the native cartilage. Neo cartilage tissue is formed during the regeneration process, and the indistinguishable tissue from the surrounding host cartilage is formed [34, 35]. However, current treatment techniques do not fully replicate hyaline cartilage structure and function.

Articular cartilage defects have been previously treated with traditional surgical techniques such as microfracture, autologous matrix-induced chondrogenesis (AMIC), osteochondral graft transplantation (OAT). However, Curl et al., concluded that patients with an active lifestyle have an increased risk for acquiring larger lesions, which often require individualized treatment and have an increased risk of developing early osteoarthritis [2].

The method of treatment is usually based on the patient's clinical condition and the description of the particular lesion [36]. Small and large cartilage defects are often treated differently. It depends on the accepted standards of care, experience and choice of surgeons, and the patient's expectation to return to an active lifestyle.

Microfracture was the first option for patients with less physical activity who were diagnosed with small focal chondral or osteochondral defects ($\leq 2 \text{ cm}^2$) [37, 38].

One of the most commonly used cartilage restoration approaches for small symptomatic lesions is bone marrow stimulation techniques, such as subchondral perforation and microfracture [39]. During the procedure, several holes are made in the subchondral bone to allow the components of the bone marrow to reach the surface of the joint and facilitate repair. The bone marrow contains mesenchymal stem cells that can create new cartilage; however, fibrous cartilage is usually formed instead, which is biomechanically much less resistant to heavy physical loads on the surface of the joint. Although clinical improvement can relieve pain, the reoperation rate of 42% after two years shows the gradual worsening of the repair tissue. Most often this is driven by a partial fibrocartilage, subchondral sclerosis and cyst, intralesional osteophytes and severe bone marrow edema formation [40]. Midterm follow-up studies emphasize the need of accurate patient selection, standardized clinical evaluation, effective rehabilitation protocols and radiological evaluations to improve the operative result of the microfracture procedure [40, 41].

AMIC has been shown to be clinically safe and effective in single, larger ($> 2 \text{ cm}^2$) chondral defects [36, 42, 43]. To maintain the early mechanical stability and cartilage regeneration, the collagen membrane can be applied on top of the a defect after subchondral penetration [44]. Initially, the indicated defect size suitable for AMIC application was 1.5 cm^2 , however, subsequent research demonstrated AMIC to be a viable approach for larger defects [44, 45]. However, approaches to improve the clinical outcome are still being investigated mainly, by selecting patients, careful preparation of cartilage defect, improved scaffolding approaches and improved rehabilitation protocols [46].

OAT has been successfully used in the treatment of small and medium focal chondral and osteochondral defects of the knee [47]. However, the accompanying cartilage damage and the resultant donor site morbidity prevents its application to larger knee defects. The long-term clinical results depend on the age, sex and size of the patient's lesion size [48, 49].

There is currently no "gold standard" for the repair of chondral lesions. All currently employed surgical interventions do not result in the desired cartilage repair, such as little or no fibrous tissue, hyaline cartilage, formation of type II collagen, subchondral and lateral host tissue integration, and subsequent prevention of OA [50]. A population of young and active patients is increasing; thus sports-related injuries are similarly on the rise. A growing unmet need for adequate surgical solutions is needed to delay or halt the widespread cartilage damage and the onset of OA.

3.3. Treatment with three-dimensional scaffolds and cells

3.3.1. Characterization of a cellular component

The researchers have described and characterized the cellular component of cell based medicinal TECs using several analytical methods that are approved by the regulatory bodies. In addition to the general characteristics of TEC, such as cell number and the required dose definition, other less specified categories, such as cell identity and potency, are required for the characterization of TEC. The active substance of the TEC – chondrocyte – is identified by the expression of specific biomarkers on the cell membrane and ECM. Chondrocytes are somatic cells obtained from the cartilage biopsy that lose their phenotype and dedifferentiate after prolonged *in vitro* culture. Culturing conditions influence the innate biochemical activity of the cells, thus changes in the genotypic and phenotypic profile over time are predictive of the biological response *in vitro* and *in vivo*.

Chondrocytes. The secretion of ECM components is mainly driven by chondrocytes which have long been considered the gold standard for cartilage regeneration. These cells were first isolated from human articular cartilage more than 45 years ago [51]. Manning et al. described a promising method for the isolation and growth of chondrocytes *in vitro*. However, the protocols have been optimized properly to better predict the chondrogenic profile.

The identity of the chondrocytes during the monolayer culture is determined by microscopic analysis. The identity of the chondrocytes during the monolayer culture is determined by microscopic analysis. Polygonal morphology, characteristic of healthy chondrocytes, persists in the first passage but is eventually lost changed to the spindle-shaped morphology after

successive passages [52, 53]. Cells are often not sufficiently characterized by their morphological appearance. An objective evaluation is based on the specific expression of the markers. Changes in cell morphology are specific for dedifferentiation and are shown in Fig. 3.3.1.1.

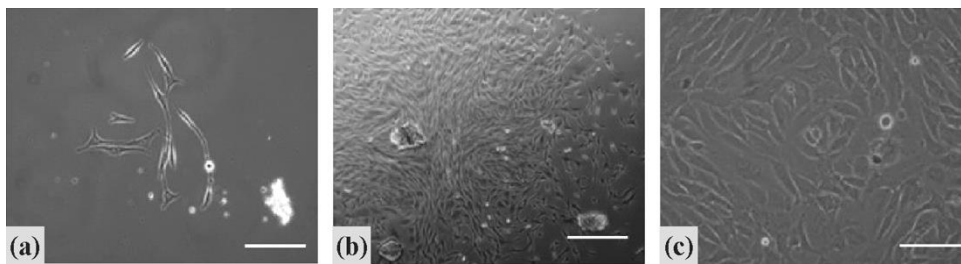


Fig. 3.3.1.1. Light microscopy images of monolayer chondrocytes expanded in the culture at (a) first, (b) second, and (c) third passages

The count of freshly isolated chondrocytes that attached to the surface of the culture flask is scarce. Prolonged chondrocytes cultivation revealed typical chondrocyte morphology at second and third passages in vitro. Scale bars: (a, c) 100 μm , (b) 200 μm .

Data on the direct detection of chondrocyte markers is limited. Grogan et al. described the CD44, CD49 and CD151 markers to be expressed at significantly higher levels by chondrocytes with greater chondrogenic potency [54]. Indirect determination of the biological potency of chondrocytes is performed using ECM mRNA measurements. Reverse transcription-quantitative polymerase chain reaction (RT-qPCR) analysis allows the detection of Aggrecan cartilage-specific protein, type I, type II and X collagen at mRNA levels, thus revealing a strong indicator of dedifferentiation in monolayer cultures [55–57].

Screening of the chondrocyte phenotype profile by expression of type I and type II collagen was performed effectively by incubation with the appropriate antibodies and fluorescence microscopy [56, 57]. In addition to evaluating the morphological changes of chondrocytes, the cytoskeleton synthesized by cells can be similarly evaluated. Although the mRNA profile may represent true protein expression after translation, discrepancies between genotypic and phenotypic chondrocyte characterization have been found in the monolayer culture [57]. Because mRNA expression does not always result in the expression of proteins, genotypic analysis alone is not a sufficient method to provide information on the identity of chondrocytes in monolayer culture [58].

The proliferation of active and proliferative chondrocytes in the monolayer indicates appropriate culture conditions and composition of the growth

medium. The proliferative trait of chondrocytes can be measured directly by counting cells and the synthesis of new DNA, and indirectly by measuring mitochondrial activity [57, 59]. It has been previously shown that modifying the signaling network that regulates the maintenance and growth of the phenotype of chondrocytes can increase cell proliferation [52, 60].

3.3.2. Characterization of scaffold component

3.3.2.1. Scaffold chemical characterization

Scaffolding plays an important role in the engineering of cartilage tissue. The choice of biomaterials and production methods are key elements for the successful production of TEC. The chemical properties of scaffolding are responsible for efficient cell binding and the resultant biological activity. The interactions between scaffolding biomaterials and cells is followed by cell adhesion and the promotion of ECM deposition, so the clarification of the key morphological design parameters determines the success or failure of the biomaterials [12].

Custom-made polymer scaffolds. Recently, additive manufacturing (AM) has received considerable attention in cartilage tissue engineering, which allows the production of customized products using computer-aided design [61]. It is characterized by features such as rapid manufacturing, high precision and ability to adjust the parameters of a synthetic polymer element. Feed materials allow the development of custom-made scaffolds with highly predictable physical properties, such as pore size, porosity and pore interconnectivity [21]. The most common manufacturing techniques applied to modify the physical properties of scaffolds are fusion deposition modeling, liquid frozen deposition, stereolithography, digital light processing, selective laser sintering and electrospinning [61].

A variety of organic-inorganic hybrid polymeric materials can be used for polymeric scaffolding customization. One of the least analyzed materials is a two-compound composite based zirconium and silicon (SZ2080) [62]. It contains inorganic silicon alkoxide and zirconium alkoxide groups that increase the mechanical stability of the materials and the organic part of SZ2080 which contains polymerizable methacrylate moieties.

DLW, using ultrafast pulsed lasers, is a well-established technique for the custom fabrication of three-dimensional scaffolding. The fully three-dimensional structuring capacity, high spatial resolution, scaling flexibility and the variety of materials used in DLW allow the determination of physical parameters such as mechanical strength and wettability [22]. The polymerization reaction is initiated by a strong focus of the laser beam to the volume of the photosensitive polymer, thus converting the liquid or gel material into

solid-state scaffolds during additive manufacturing [63, 64]. Three-dimensional scaffolding manufacturing flow by direct laser writing is shown in Fig. 3.3.2.1.1.

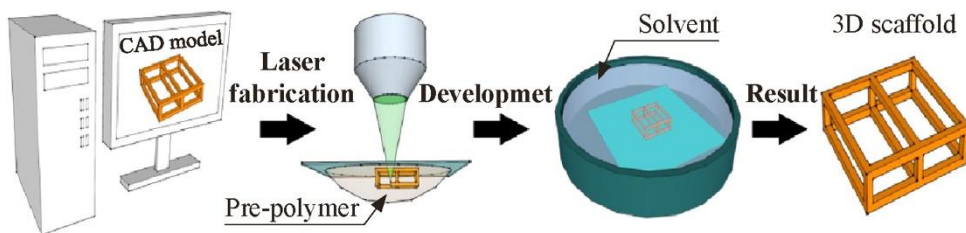


Fig. 3.3.2.1.1. Three-dimensional scaffold custom fabrication steps, employing direct laser writing

A computer-aided design model with custom scaffold physical characteristics is created. After a series of laser fabrication and development steps, the resultant three-dimensional scaffold with desired physical parameters is created.

The ability to apply direct laser writing technology to create scaffolds of the desired morphology for articular cartilage regeneration *in vitro* and *in vivo* is still unknown.

Solid collagen scaffolds. The articular cartilage ECM is formed by a dense network of collagen fibers that support heavy loads in daily activities. To mimic the natural environment of cartilage, solid collagen membrane scaffolds have been widely used in the engineering of cartilage tissues [65]. The macromolecular structure of collagen fibers in membranes that mimic native tissues can have a protein-dependent cellular response. Therefore, choosing a membrane with fibers of a suitable molecular structure can aid in retaining the hyaline cartilage phenotype [66]. The collagen membrane is formed as a mechanically rigid mesh, sponge or nonwoven fabric that provides the necessary support for cell proliferation and facilitates management of TEC during the manufacturing process [67]. The extent of DLW fabricated scaffolds efficacy is still unknown, as there is no comparable articular cartilage regeneration *in vitro* and *in vivo* studies of microstructured and solid collagen scaffolds.

3.3.2.2. Scaffold physical characterization

The three-dimensional physical structure allows sufficient transport of gas, nutrients, and bioactive molecules through the scaffold to allow cells to survive, proliferate and differentiate. The *in vitro* characterization of the speed of scaffold biodegradation helps to determine structural parameters sufficient to maintain the rate of formation of new tissues.

The production of porous cellular scaffolds is an important objective for the production of TEC because these physical properties influence the cellular response *in vitro* [13, 68]. Cell proliferation, metabolic activity and ECM secretion of the active substance depend on pore size, porosity and scaffold connectivity [23, 69]. Regularly interconnected pores improve the chondrocyte phenotype and have been shown to release the abundance of ECM in chitosan and alginate scaffolds [23, 70]. The influence of different pore sizes has also been investigated, which reveals the highest biomechanical and physical properties on the scaffolding with uniform pore sizes, homogeneous environments and high interconnection throughout the scaffold [71]. A uniform porous structure positively influences the uniform cellular distribution and nutrient transport in the scaffold [24, 25]. In addition, a particular pore shape can support a natural cell phenotype with improved functional production of ECM proteins [71]. Uniform pore size, shape and high porosity can be achieved efficiently using the DLW method, with key parameters controlled by precise and flexible microfabrication. Kapyla et al. fabricated scaffolds with the desired pore size, porosity and connectivity were constructed using DLW to provide a novel approach to investigate the effects of scaffolding architecture on cellular behavior *in vitro* [26]. A computer-aided design (CAD) model of hexagonal HOI scaffold and the chondrocytes proliferation is shown in Fig. 3.3.2.2.1.

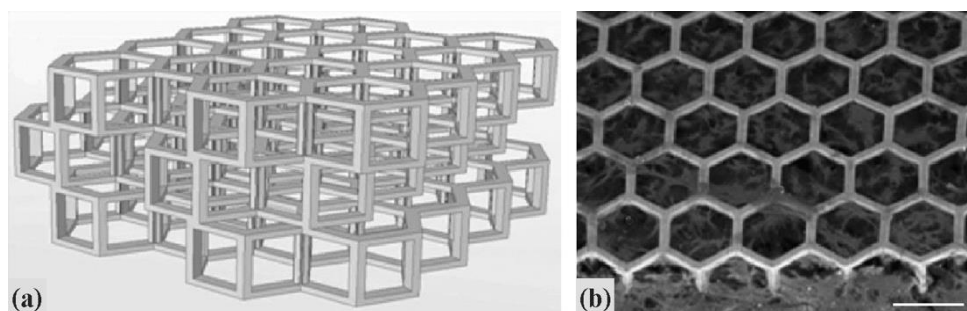


Fig. 3.3.2.2.1. Hexagonal HOI schematics and SEM pictures

(a) CAD model of the three-dimensional scaffold with mathematically precise pore size, shape, uniformity, and high porosity level. (b) SEM image of hybrid organic-inorganic scaffold, fabricated in a layer-by-layer fashion, seeded with viable chondrocytes for subsequent TEC characterization of cellular performance *in vitro*. Scale: 100 μm .

3.3.2.3. Scaffold mechanical characterization

The mechanical properties of articular cartilage and newly fabricated TECs are attributed to its complex structure and ECM composition, which includes the fluid and the solid matrix phases with cells [72]. Understanding the mechanics of a material it is required to know how TEC can resist compression and tensile forces post-implantation. The mechanical properties of TEC depend largely on the source of the scaffold material and the ECM released by the host cells [73, 74]. These properties can be characterized *in vitro* and *in vivo*.

Biomechanical methods. Compression tests or a specific osmotic cartilage loading method can be used to biomechanically characterize the scaffold cartilage engineering [75]. The compression properties of the cartilage can be evaluated using three different measurement configurations: unconfined compression, confined compression and indentation [76]. Destructive tests are irreversible due to increased tension or loads. Correlation between mechanical properties of cartilage and glycosaminoglycan (GAG) content, collagen content, and water content exists. The decrease in cartilage compression stiffness is mostly due to structural alterations rather than changes in the composition of the proteoglycan-collagen matrix [77]. The decrease in cartilage compression stiffness is closely related to the amount of water: the cartilage becomes less rigid and permeable as the amount of water increases [78]. The biomechanical properties of scaffolds microstructured by DLW containing different morphological properties and collagen scaffolds *in vitro* are still unknown.

Electromechanical methods. Electromechanical methods Articular cartilage consists of a protein-rich ECM and GAGs with a negative charge. This specific formulation gives cartilage mechanical rigidity and efficacious load-withstanding properties. The electromechanical properties of the native cartilage tissue have been shown to reflect the composition and structure of the cartilage *in vitro* and *in vivo* [79, 80]. This is an important parameter of a TEC because it can be easily obtained and correlated with histological and biomechanical characteristics [79, 81]. Positively charged mobile ions surrounding the cells in the ECM of TEC are displaced during the compression, relative to the proteoglycan molecules, which are fixed and carry a negative charge. This change creates a streaming potential that can be recorded as an electromechanical quantitative parameter (QP). In the absence of qualitative GAGs, a low streaming potential (high QP) is registered, thus resembling weak electromechanical properties [79]. Changoor et al. found that deterioration of cartilage tissue after prolonged *in vitro* storage can be detected by measuring changes in electromechanical properties [80]. In addition, they

reported that these measurements are even more sensitive to changes than well-established biomechanical properties. Abedian et al. found a significant correlation of QP with multiple histological scores and, therefore, proposed using this parameter as quantitative means to evaluate the cartilage [82]. The electromechanical properties of human tissue cartilage were measured by Sim et. al and a correlation of QP with histological scores and biomechanical properties, as well as GAG and water were documented [79]. They concluded that the acquisition of electromechanical properties allows a more sensitive analysis of the structure and in addition preserves tissue integrity. The electromechanical properties of regenerated cartilage *in vivo* after scaffold implantation are still unknown.

3.3.2.4. Biocompatibility characterization

The expanded chondrocytes are seeded on a three-dimensional scaffold, thus initiating the manufacturing of TEC. Transmembrane cell receptors, integrins, allow cells to bind to ECM components and subsequently form functional support of TEC matrix. This formation process is supported by the appropriate *in vitro* culture conditions which significantly influence key characteristics of TEC.

Viability and proliferation. The ability of chondrocytes to adhere effectively to scaffolding depends largely on cell viability. The detection of living cells that can promote ECM deposition in scaffolding is one of the key aspects in determining the biocompatibility of scaffolding. Cell viability and proliferation in scaffolds have been previously recorded using fluorescent assays to determine the optimal biological parameters of specific cell processes and populations [28, 83]. Therefore, great variability of scaffold-dependent cellular proliferation can be linked to carriers differing in origin, structure and methods of extraction and purification [84]. The ability of chondrocytes to proliferate in innovative DLW microstructured scaffolds of different pore shapes and sizes is still unknown.

Functionality. Being the most abundant cartilage protein, the expression of type II collagen is a hallmark of quality TEC [85]. Biochemical analyses have shown that collagen synthesis is reversed to hyaline cartilage after seeding of dedifferentiated chondrocytes in scaffolds, thus improving the functionality of TEC [55]. The presence of essential collagen molecules is determined by their expression of genes and protein secretion by immunocytochemistry and real-time polymerase chain reaction assays [86]. In addition, the histological staining of Alcian blue and Safranin-O can characterize the distribution of GAGs and chondrocytes in the newly formed ECM [56]. The

ability to form cartilage tissue *in vitro* by different pore shaped and sized DLW scaffolds is still unknown.

3.3.2.5. Clinical application

There has been significant progress in the research and development of TEC in recent years. The basic and clinical research teams made it possible to translate scientifically validated preclinical data into clinical trials using TEC composed of live cells seeded on scaffolds. Despite the clinical success of the first cellular scaffolds for cartilage tissue engineering, custom-made polymeric scaffolds might possess a greater potential for superior clinical outcomes. Laser writing technology allows researchers to produce three-dimensional biocompatible scaffolding of the desired parameters in real-time. If it can take less than twenty-four hours to produce a custom scaffold for medium-sized cartilage defects, the technique can be effectively implemented in standard clinical practice. This enables the production of personalized TECs for cartilage regeneration in patients suffering from highly debilitating chondral defects of the knee, ankle, and shoulder joints.

4. METHODS AND MATERIALS

4.1. Article references

The detailed description of methods used is described in articles:

- (1) Mačiulaitis, Justinas; Miškinienė, Milda; Rekštytė, Sima; Bratchikov, Maksim; Darinskas, Adas; Šimbelytė, Agnė; Daunoras, Gintaras; Laurinavičienė, Aida; Laurinavičius, Arvydas; Gudas, Rimtautas; Malinauskas, Mangirdas; Mačiulaitis, Romaldas. Osteochondral repair and electromechanical evaluation of custom 3D scaffold microstructured by direct laser writing lithography // *Cartilage*. Thousand Oaks: Sage Publications. ISSN 1947-6035. eISSN 1947-6043. 2019, first online, p. 1-11. DOI: 10.1177/1947603519847745
- (2) Mačiulaitis, Justinas; Rekštytė, Sima; Bratchikov, Maksim; Gudas, Rimtautas; Malinauskas, Mangirdas; Počkevičius, Alius; Ūsas, Arvydas; Rimkūnas, Augustinas; Jankauskaitė, Virginija; Grigaliūnas, Valdas; Mačiulaitis, Romaldas. Customization of direct laser lithography-based 3D scaffolds for optimized in vivo outcome // *Applied surface science*. Amsterdam: Elsevier Science. ISSN 0169-4332. eISSN 1873-5584. 2019, vol. 487, p. 692-702. DOI: 10.1016/j.apsusc.2019.05.065
- (3) Mačiulaitis, Justinas; Deveikytė, Milda; Rekštytė, Sima; Bratchikov, Maksim; Darinskas, Adas; Šimbelytė, Agnė; Daunoras, Gintaras; Laurinavičienė, Aida; Laurinavičius, Arvydas; Gudas, Rimtautas; Malinauskas, Mangirdas; Mačiulaitis, Romaldas. Preclinical study of SZ2080 material 3D microstructured scaffolds for cartilage tissue engineering made by femtosecond direct laser writing lithography // *Biofabrication*. Bristol: IOP Pub. ISSN 1758-5082. 2015, vol. 7, no. 1, p. 1-1. DOI: 10.1088/1758-5090/7/1/015015

4.2. Study design

Preclinical proof-of-concept studies have been planned to evaluate a new approach to treat isolated cartilage defects. The primary study was planned to show the preliminary long-term safety and efficacy profile in a homologous rabbit animal model. The final study has been designed to evaluate a clinically relevant xenogeneic cartilage repair model using human cells. The layout for the Primary and Final studies is depicted in Table 4.2.1.

Table 4.2.1. The design of primary and final studies

Study type		Analysis	Attribute	Method
Primary study				
<i>In vitro</i> study (day 4, 8, 12)	SZ material proof-of-concept	Cell culture in 2D	Morphology	LM
			Viability	Trypan blue
		Cell culture in 3D HOI and CS Potency	Morphology and pore coverage	SEM
			Secretion of type II collagen	ELISA
			Expression of type II and X collagens	rt-PCR
<i>In vivo</i> study (6 months)	Safety and efficacy	Macroscopic evaluation	OAS	
		Histological evaluation	O'Driscoll	
		Electromechanical evaluation	QP	
Final study				
<i>In vitro</i> study (day 1, 4, 7)	Pore shape dependence, HOI-H, HOI-T, CS positive comparator	Biocompa- tibility, Cell rediffe- rentiation	Morphology	SEM
			Biomechanical	Indentation
			Morphology	SEM
			Metabolic activity	Presto Blue
			Cell count	Presto Blue
			Secretion of type II collagen	ELISA
	Pore scale dependence, HOI-T1.5, HOI-T2, CS positive comparator	Biocompa- tibility, Cell rediffe- rentiation	Morphology	SEM
			Secretion of type II collagen	ELISA
			Expression of type II collagens	rt-PCR
<i>In vivo</i> study (3 months)	Safety and efficacy	Macroscopic evaluation	OAS	
		Histological evaluation	O'Driscoll	

Note. Primary study analyzed the SZ material ability to form cartilage tissue *in vitro* and *in vivo* using rabbit chondrocytes in autologous articular cartilage defect model. Final study analyzed ability of the human cells to regenerate cartilage in *in vitro* and *in vivo* rat articular cartilage defect model.

4.3. Scaffold manufacturing

A high power and energy femtosecond laser system (Pharos, Light Conversion, Vilnius, Lithuania), with adjustable repetition rate in the 1 to 200 kHz range and generating 1030 nm central wavelength and 300 fs duration pulses was used to fabricate three-dimensional scaffolds of hybrid silicon-zirconium material.

The three-dimensional polymeric scaffolds were microstructured by employing the DLW technique. Computer models were designed using CAD software or specially designed 3D-Poli package (Femtika, Vilnius, Lithuania) and created by focusing a laser beam into the volume of a photosensitive pre-polymer [63, 87, 88].

A hybrid organic-inorganic pre-polymer was photo-sensitized with 1% of photo-initiator (2-benzyl-2-dimethylamino-4-morpholinobu-tyrophenone, Sigma Aldrich, St. Louis, MO, USA) and subsequently used as a structuring material [89]. Pre-polymer was created for DLW applications; therefore it is characterized by its superb three-dimensional micro-/nano-structuring properties.

Collagen scaffolds (CS) were sterile and individually packed; HOI were chemically disinfected in 70% ethanol overnight and heated under UV irradiation for 2 h. The next day, HOI were washed with phosphate buffered saline (Sigma Aldrich) and left for drying and subsequent cell seeding.

The detailed description of the scaffold manufacturing technique is described in articles (1–3).

4.3.1. Primary study: HOI and collagen scaffold manufacturing

HOIs were manufactured as hexagonal structures and consisted of three identical layers formed on top of each other. Each layer had a half-period shift with respect to the lower layer. The overall dimensions of the scaffolds were determined prior to preparation by evaluating the cartilage defect area and thickness of the rabbit joint. The main morphological parameters were determined to be $2.1 \times 2.1 \times 0.21 \text{ mm}^3$, corresponding to the intended cartilage lesion area. Assuming a single cell size of about 20–30 μm , the diameter of one hexagon was set at 100 μm to ensure that the cells would be able to proliferate unobstructed through all layers of the HOI. The height and width of the rod forming the HOI structure were selected to be 15 μm , taking into account previous development work and considering that the cells properly adhered to the rods of this dimension and maintained a spherical rather than a flat morphology. Parameters of upper HOI pores, i.e. the distance between the 2 parallel rods at the same height was determined to be $42 \times 49 \mu\text{m}^2$ width

and length, respectively, and reflected the narrowest transition from the top of the HOI to the bottom for the cells to pass through. The lateral pores were determined according to the upper pore size selection methodology and were $51 \times 54 \mu\text{m}^2$ width and length, respectively. The scanning electron microscopy (SEM) images of manufactured HOI are shown in Fig. 4.3.1 (a, b).

A commercially available CS (Septodont, Maidstone, UK) was used as a direct comparison. CS is composed of native, non-denatured, freeze-dried collagen of bovine origin type I collagen. The CS was cut to the same dimensions to enable comparison with the HOI scaffold. The SEM image of prepared CS is shown in Fig. 4.3.1 (c).

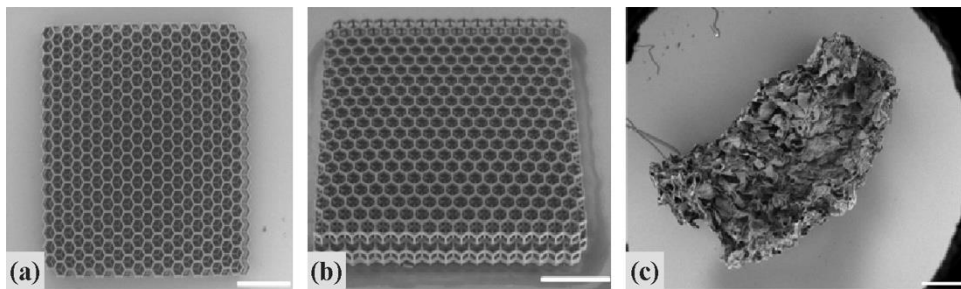


Fig. 4.3.1. SEM images of manufactured HOI top (a), side (b) view, and CS (c)

Three layers consisting of 13 and 14 hexagonal chambers in width and length, respectively, with the single hexagon diameter of $100 \mu\text{m}$ wide. Side pore width and height throughout the scaffold was 51 and $54 \mu\text{m}$, respectively. CS is comprised of native, non-denatured, freeze-dried collagen of bovine origin type I collagen. Scale bar: $500 \mu\text{m}$.

4.3.2. Final study: HOI optimization and collagen scaffold manufacturing

Computer models of four different types of scaffolding were developed and subsequently used in production. In the first phase of the experiment, tetragonal scaffolds (HOI-T) and hexagonal scaffolds (HOI-H) were investigated to determine the influence of pore shape on cell growth.

HOI-T and HOI-H consisted of rectangular and honeycomb-shaped hollow prisms, respectively. They were placed next to each other to form a single layer of scaffolding. Each scaffold had three layers stacked on top of each other. Each layer of the HOI-T had a displacement in both directions to the previous layer, so that four upper square pores formed throughout the scaffold. In contrast, HOI-H had an offset in one direction to the previous layer m, resulting in three upper rhomboid pores throughout the scaffold.

In the second phase of the experiment, to determine the influence of pore size on cell proliferation, the upper and lateral pores of HOI-T were scaled by factors of 1.5 (HOI-T1.5) and 2 (HOI-T2). The scaffold size was as similar as possible ($1.5 \times 1.5 \text{ mm}^2$). The width and height of the rod were constant in all cases: 15 μm .

A commercially available bilayer CS (Chondro-Gide, Geistlich Biomaterials, Wollhusen, Switzerland) was cut to the same dimensions as the HOI and used as a direct comparator. CS is made of highly refined porcine collagen and has been shown to be effective for treating traumatic cartilage defects [90].

4.4. Scaffold characterization *in vitro*

SEM on HOI and CS was performed by Hitachi TM-1000 (Hitachi High-Technologies Co., Tokyo, Japan).

The detailed description of scaffold characterization *in vitro* is described in articles (1–3).

4.4.1. Primary study: Morphological analysis of HOI and CS

Morphological: The cell filling of HOI pores was calculated as the percentage of blank and filled pore areas from SEM photographs on days 4, 8 and 12. CS cell distribution was evaluated at day 12 prior to implantation by histological staining with hematoxylin and eosin dye (H&E).

4.4.2. Final study: Morphological and biomechanical analysis of HOI and CS

Morphological: Manufactured and cell seeded HOI scaffolds were analyzed after 7 days of culture.

Biomechanical: Micro indentation (MCT Micro Combi Tester, Anton Paar, Graz, Austria) of HOI-T, HOI-H and CS was performed according to Oliver and Pharr's method.

4.5. Cell isolation, culture, and posology *in vitro*

All experimental procedures were approved and conducted according to the standard guidelines and protocols by the Animal Health and Welfare Department, State Food and Veterinary Service of the Republic of Lithuania and Kaunas Regional Biomedical Research Ethics Committee.

The detailed description of cell isolation, culture and posology *in vitro* is described in articles (1–3).

4.5.1. Primary study: Cell isolation, culture, and posology of 3D culture

New-Zealand rabbits (male and female; 4–5 months old; 3–4 kg body weight) were housed separately in cages under ordinary conditions ($21\pm 1^{\circ}\text{C}$, 12/12 light/dark and a 45% relative humidity) with free access to food and water.

Allogeneic rabbit articular cartilage biopsy from the non-weight-bearing area was minced, digested, chondrocytes were isolated, plated, cultured, and harvested when 80% confluence was reached. Viability was measured by Trypan blue dye exclusion assay.

Scaffolds were soaked in proliferation medium 1 day before seeding. Third passage cells were seeded in 10 μL doses on sterilized HOI and CS in a dropwise fashion, resulting in 10^5 cells per scaffold.

Scaffolds with cells were harvested after 4, 8, and 12 days of culture and sent for *in vitro* analysis. Also, on day 12 of culturing, scaffolds were prepared for *in vivo* implantation.

4.5.2. Final study: Cell isolation, culture, and posology of 3D culture

Human cartilage tissue was collected during routine knee reconstruction surgery procedures as waste material.

A biopsy was washed extensively, predigested, and digested with enzymes, isolated cells were plated and cultured when reached 80% confluence.

Scaffolds were soaked in proliferation medium one day before seeding. Manufactured HOI and CS scaffold parameters are set at $1,5\times 1,5\text{ mm}^2$ in area, with cell dosage of $4,5\times 10^4$ cells per scaffold used.

Scaffolds with cells were harvested after 1, 4 and 7 days of culture and sent for *in vitro* analysis. Also, on day 7 of culturing, scaffolds were prepared for *in vivo* implantation.

4.6. Cell seeded scaffold biochemical characterization *in vitro*

The detailed description of cell-seeded scaffold biochemical characterization *in vitro* is described in articles (1–3).

4.6.1. Primary study: Protein secretion analysis of monolayer and 3D culture

Type II collagen production was analyzed at 4, 8, and 12 days after seeding using enzyme-linked immunosorbent assay kit (rabbit collagen type II ELISA kit, BioSite, London, UK).

4.6.2. Final study: Metabolic activity, cell count, and biochemical analysis of monolayer and 3D culture

Metabolic activity and cell count: an assay for human chondrocytes growth in HOI-T and HOI-H was performed using Presto Blue Cell Viability Reagent (Invitrogen, Carlsbad, CA, USA) according to the manufacturer's recommendations.

Biochemical analysis: Type II collagen production evaluation was performed on the cells ($n = 4$) used for seeding on the scaffolds and the seeded scaffolds at days 1 ($n = 12$), 4 ($n = 9$) and 7 ($n = 5$) after seeding using enzyme-linked immunosorbent assay kit (human collagen type II ELISA kit, BioSite), according to manufacturer's protocol.

4.7. HOI scaffold genotypic characterization *in vitro*

The total mRNA from the samples was extracted using an Isolate II mRNA Micro Kit (Bioline Reagents Ltd., London, UK) according to the manufacturer's instructions. Elution was performed with 10 μ l RNase-free water included in the kit. SensiFAST Probe No-Rox One-Step Kit (Bioline Reagents Ltd.), primers and hydrolyzation probes (Biolegio B.V., Nijmegen, Netherlands) were used for one-step RT-qPCR.

The detailed description of designed primer pairs, probes, condition of amplification and HOI scaffold genotypic characterization *in vitro* is described in articles (1–3).

4.7.1. Primary study: Gene expression analysis of 3D culture

Scaffolds with cells were harvested after 4, 8, and 12 days of culture and sent for *in vitro* analysis.

For the chondrogenic gene analysis, we examined COL2A1 (coding for type II collagen protein) and COL10A1 (coding for type X collagen protein) genes mRNA expression dynamics of cells before seeding on day 0 and after seeding at day 4, 8, and 12. European rabbit glyceraldehyde 3-phosphate dehydrogenase (GAPDH) gene expression was used for data normalization.

4.7.2. Final study: Gene expression analysis of monolayer and 3D culture

For the chondrogenic gene mRNA analysis, we examined type II collagen (COL2A1) mRNA expression dynamics of cells at day 0 before the seeding on scaffolds and on days 1, 4 and 7 *in vitro*. The primer and probe sequences were designed using Vector NTI Advance program (Thermo Scientific, Waltham, MA, USA) for sequences alignment. The expression of β -actin mRNA was used as an internal standard for normalization of the target mRNA levels between different samples.

4.8. Design of the long-term *in vivo* study

Osteochondral defects were divided into experimental groups based on the randomly received treatment: defects treated using HOI hexagon-pored scaffolds with cultured cells (HOI-cells, n = 4) and without cells (HOI-only, n = 4). Similarly, positive control groups included collagen scaffolds with cultured cells (CS-cells, n = 3) and without cells (CS-only, n = 3). The negative control group comprised defects without scaffolds (scaffold-free, n = 4).

The detailed description of the long-term *in vivo* study design is described in articles (1–3).

4.8.1. Primary study: 6 months *in vivo* study design

Nine rabbits containing 18 bilateral osteochondral defects were used in the study. Surgical procedures were performed aseptically in an operating theatre. Anesthesia was induced intramuscularly and maintained intravenously. Knee joints were approached via the lateral parapatellar approach, followed by medial patellar dislocation. Critical size osteochondral defect (diameter: 3 mm; depth: 2 mm) was created through the articular cartilage and subchondral bone at the weight-bearing area of the medial femoral condyle using an electric drill.

Every defect was extensively washed with saline before implanting a polymerized fibrin clot. Briefly, a mixture of 1 mL of autologous blood plasma, 250 μ L of thrombin, and 250 μ L of CaCl₂ were mixed to prepare the fibrin clot. It was incubated for 5 minutes at room temperature just before adding it to the defect to secure the scaffold or fill the scaffold-free defect.

After intervention, the rabbits were housed under regular conditions and could move freely in individual cages. Rabbits were euthanized after 6 months and samples for subsequent examination were collected.

4.8.2. Final study: 3 months *in vivo* study design

Nine, 10-week-old nude rats (NIHRNU-M, NTac:NIH-Foxn1^{rnu}; Taconic, NY, USA) were used in this study. The animals were anesthetized through an inhalation mask after exposure to 3% isoflurane and O₂ gas. The knee joint was approached by a lateral parapatellar approach, and the trochlear groove was exposed by medial patellar dislocation. Critical size osteochondral defect (diameter: 1.5 mm, depth: 1 mm) was created through the articular cartilage and subchondral bone at the weight-bearing area of the trochlear groove. The defect was extensively washed with saline before scaffold implantation. Fibrin glue (Tisseel, Baxter, Glendale, CA, USA) was added to the defect to secure the scaffold or fill the scaffold-free defect.

After the intervention, rats were housed and allowed to move freely within their cages. Rats were euthanized 3 months after surgery and samples for subsequent examination were collected.

4.9. Macroscopic evaluation of long-term study

Two independent researchers performed macroscopic grading according to a modified Oswestry Arthroscopy Score (OAS) for primary animal and final human cells studies.

Stiffness on probing of the rabbit repair tissue was replaced with a more objective electromechanical parameter. However, it was not applied in the study of the human cells due to insufficient surface area of the rat articular cartilage.

The detailed modified macroscopic OAS and macroscopic evaluation description of the long-term study are described in articles (1–3).

4.9.1. Primary study: Electromechanical evaluation of cartilage *in vivo*

Electromechanical properties of the repair tissue were evaluated with a hand-held arthroscopic Arthro-BST indentator (Biomomentum Inc., Laval, Quebec, Canada, as previously described [91]. Briefly, negatively charged proteoglycan molecules in the collagen network are balanced by mobile positive ions in interstitial fluid. Cartilage compression results in interstitial fluid movement; thus, mobile positive ions are displaced relative to the fixed negative charges. This flow generates streaming potentials that reflect cartilage composition and function [91–93].

A higher electromechanical QP mainly reflects increased extracellular matrix disintegration and inferior load-bearing capacity of the cartilage, while low QP indicates strong electromechanical properties and superior load-bearing capacity.

Measurements of the weight-bearing area on the medial femoral condyle were made before the surgery and at 6 months after implantation. The femoral joint was harvested and QP measurements were recorded 3 times on each control and treated defect to obtain median values.

4.10. Histological evaluation of cartilage *in vivo*

Distal ends of femurs were cut above the condyles, fixed in a 10% neutral buffered formalin solution, and embedded in paraffin blocks for animal and human cell studies. 6 μm thick serial sections were deparaffinized and stained with Toluidine blue (Fisher Scientific, Pittsburgh, PA, USA) and Safranin-O (Fisher Scientific) stains to assess glycosaminoglycans, proteoglycans and collagen production in repaired cartilage [94]. Sections were analyzed using a digital microscope (Olympus BX61, Olympus, Tokyo, Japan) with a camera (Olympus DP72, Olympus) and scored blindly using O'Driscoll histological scoring system [95]. A higher score indicated superior cartilage repair, with 24 representing the maximum score.

The detailed O'Driscoll histological scoring system is described in articles (1–3).

4.11. Statistical evaluation

The quantitative data are expressed as a mean (standard deviation). Statistics were performed using GraphPad Prism 7.04.

4.11.1. Primary study: Statistical evaluation

Statistical results were obtained using Kruskal-Wallis multiple comparison test and presented as the mean and standard deviation (SD). Statistical significance between experimental groups is indicated with (*), which represents a $P < 0.05$ and (**) representing $P < 0.01$.

4.11.2. Final study: Statistical evaluation

Statistical results were obtained using one-way ANOVA with Tukey's post hoc multiple comparison test. Results are presented as the mean and bracketed standard deviation (SD). Statistical significance between the groups is indicated with (*) which represents a $P < 0.05$ and (**) representing $P < 0.01$.

5. RESULTS

5.1. Results of the primary study

5.1.1. Cell morphology and viability in monolayer

During the monolayer culture, chondrocytes showed typical phenotypic changes. The cells progressively lost their natural round shape and became flattened fibroblast-like cells. The viability of chondrocytes prior to seeding on membranes was consistently high and ranged from 98% to 100%.

5.1.2. Cell Seeding and 3D Growth Analysis

Cells seeded on hexagonal-pored HOI exhibited a continuous adherence to the horizontal and vertical rods of the scaffold. The proliferation of cells and ECM production within the scaffold have maintained up to 12 days *in vitro*. The cells could be seen positioned on horizontal and vertical rods, elongated or oval shape. Connections between nearby rods were mainly made by wrapping and bridging the interconnected nearby perpendicular rods. Cell number and interconnecting ECM content have outgrown all the layers of HOI and kept increasing up to day 12, filling the void space and covering most of the pore diameter at day 12. Cell three-dimensional growth in HOI is depicted in Fig. 5.1.2.1.

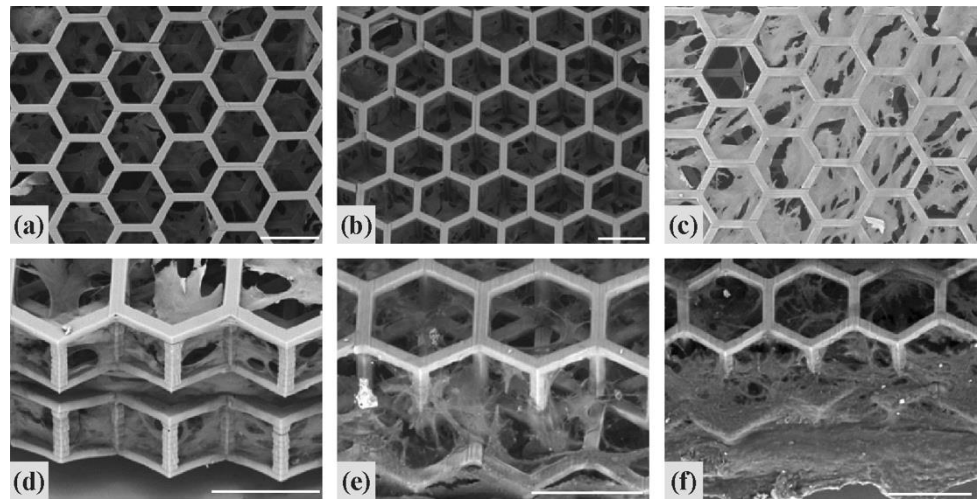


Fig. 5.1.2.1. Cells and interconnecting ECM distribution throughout three-dimensional hexagonal-pored HOI as a percentage of empty and filled pore areas from SEM photographs at days 4 (**a, d**), 8 (**b, e**), and 12 (**c, f**)

Elongated and oval-shape cells continuously adhered to and interconnected horizontal and vertical rods of the scaffold. By wrapping and bridging nearby rods, cells and deposited ECM content incrementally have outgrown all three layers of HOI filling most of the pore volume on day 12. A close-up view from the side is displayed on day 4 (**d**), 8 (**e**), and 12 (**f**). Scale bar: 100 μ m.

Incremental pore coverage was evident throughout the cultures up to day 12 prior to the implantation. It improved significantly at day 12 compared to day 4 ($P = 0.0114$) and covered $71 \pm 6.5\%$ of a single pore. The dynamics of pore coverage is depicted in Fig. 5.1.2.2.

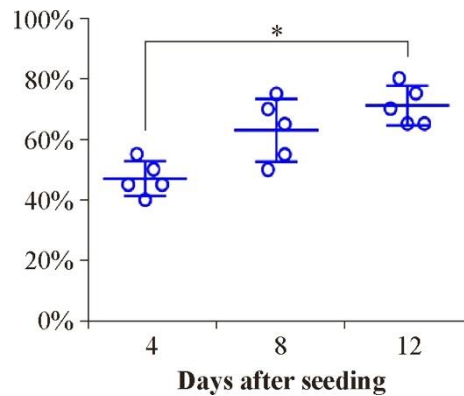


Fig. 5.1.2.2. Dynamics of HOI pore coverage by seeded cells

A percentage of filled pore has increased significantly from day 4 to 12, revealing biocompatible morphological conditions for sustained cell proliferation. $*P < 0.05$.

Positive control of cell-seeded CS revealed random cell distribution from top to bottom and interconnection of nearby collagen folds and creases. Despite all the voids occupied by cells, the bottom layer of CS had fewer cells compared to the top and middle layers. Significantly more iterative pore morphology in HOI allowed superior and more even cell distribution throughout the scaffold compared to CS. Both scaffolds kept physical integrity and did not lose material during *in vitro* culture.

The detailed description of CS scaffold cell distribution is described in articles (1, 3).

5.1.3. Cell Seeded Scaffold Potency Analysis

HOI with cells sustained chondrogenesis under regular culture conditions, by measuring type II collagen secretion to the media when compared to the secretion level of cells that were used for scaffold seeding (monolayer cells). Type II collagen protein secretion is depicted in Fig. 5.1.3.1.

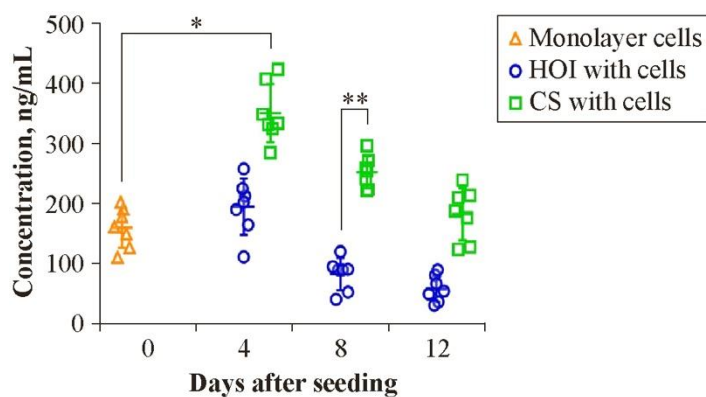


Fig. 5.1.3.1. Type II collagen protein secretion, as measured by ELISA in monolayer, HOI, and CS groups at days 0, 4, 8, and 12

Both groups retained the level of secreted protein from day 4 to 12, with a numerical decrease throughout the period. CS had the superior initial type II collagen secretion capacity at days 4 and 8, when compared to monolayer cells and HOI, respectively. * $P < 0.05$, ** $P < 0.01$.

Protein excretion in the HOI-cells group retained its level up to day 12; however, a slight decrease was evident throughout the period. Protein secretion improved at day 4 ($P = 0.03$) in CS-cells, then retained its previous level up to day 12. Numerical protein secretion decrease was also noted in CS-cells up to day 12. When scaffolds with cells were compared to each other, a greater amount of type II collagen secretion was noted in the CS-cells group at day 8 ($P = 0.0045$), highlighting a superior initial phase of cell-

scaffold biocompatibility in this group. Numerical superiority was noted in CS-cells at day 12 when compared to HOI-cells at the respective endpoint of the study.

Chondrogenic COL2A1 gene expression was upregulated up to day 8 with a numerical decrease at day 12 in both groups. COL2A1 expression is depicted in Fig. 5.1.3.2 (a).

Even though the mean level of COL2A1 expression increased in HOI-cells at days 4 and 8, it was comparable to day 0. CS-cells retained a superior mean level of COL2A1 expression up to day 12 when compared to the gene expression of monolayer cells; however, it improved significantly in the middle of the culture period at day 8 ($p=0.0306$). No significant differences among the 2 scaffolds were observed; however, mean values were lower in the HOI-cells group, compared to CS-cells.

Mean expression of the fibroblastic COL10A1 gene was downregulated in the HOI-cells and CS-cells groups, thus supporting cell redifferentiation on a genotypic level. COL10A1 expression is depicted in Fig. 5.1.3.2 (b).

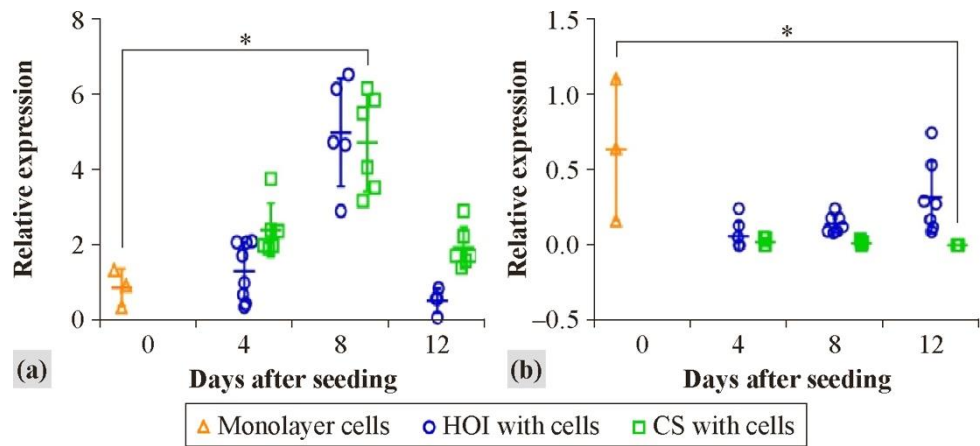


Fig. 5.1.3.2. COL2A1 (a) and COL10A1 (b) genes expression patterns, measured by rt-PCR in monolayer, HOI, and CS groups at days 0, 4, 8, and 12

Chondrogenesis was upregulated in both groups up to day 8. (a) The mean expression level of COL2A1 increased in HOI at days 4 and 8. CS retained superior expression up to day 8, compared to monolayer cells. (b) The mean expression of fibroblastic COL10A1 was downregulated in both scaffold groups up to day 12. CS with cells expressed less COL10A1 at day 12 compared to monolayer cells. COL10A1 expression in CS was lower compared to HOI on day 12. $*P<0.05$.

CS-cells group fibroblastic gene expression level was numerically superior compared to monolayer cells. In addition, it improved significantly, by expressing less COL10A1 at day 12 ($P = 0.0355$).

The detailed description of *in vitro* potency analysis values is described in articles (1, 3).

5.1.4. Macroscopic OAS evaluation *in vivo*

No swelling, signs of inflammatory or immune responses to implanted materials on operated knees were observed at 6 months after implantation. CS-cells group had the highest mean OAS score among all experimental groups. Macroscopic evaluation is depicted in Fig. 5.1.4.1.

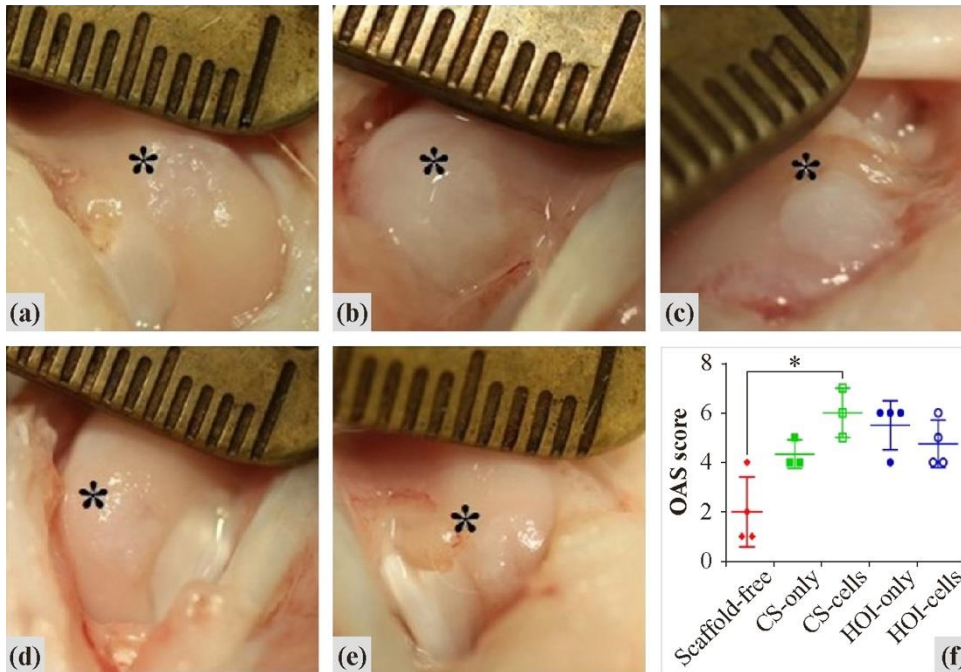


Fig. 5.1.4.1. Macroscopic evaluation of experimental groups at 6 months after intervention in (a) scaffold-free, (b) CS-only, (c) CS-cells, (d) HOI-only, and (e) HOI-cells groups, as expressed by the (f) OAS score

CS-cells had the highest mean OAS amongst all experimental groups. HOI-only and HOI-cells had a tendency for superiority compared to the scaffold-free group. Cartilage repair was evident in all treated groups (Asterix), however fine fronds on the cartilage surface were evident in all HOI-only and HOI-cells defects, whilst smoother cartilage surface was exhibited throughout CS groups. $*P < 0.05$.

CS-cells group OAS evaluation revealed the most hyaline-like cartilage when compared to the scaffold-free group ($P = 0.0347$). Other experimental groups did not differ among each other significantly; however, a tendency for superior outcome in HOI-only ($P = 0.076$) and HOI-cells ($P = 0.69$) compared to scaffold-free group was also noted. A numerically inferior outcome in HOI groups was mainly influenced by more fine fronds on the cartilage surface when compared to a smoother cartilage surface in CS groups.

The detailed description of macroscopic values is described in articles (1, 3).

5.1.5. Histological O'Driscoll evaluation *in vivo*

Mean cartilage repair scores were superior in all treatment groups compared to the scaffold-free group at 6 months; however, a significantly superior histological outcome was scored in CS-cell ($P = 0.035$) group only. A clear numerical advantage of the HOI-cell group over the scaffold-free group was also noted ($P = 0.057$). Other experimental groups were comparable among each other; however, the HOI-only group tended to be superior histological restoration compared to the control group, as well ($P = 0.103$). Restoration of subchondral bone has not been achieved in any of the samples, with slight contour changes throughout experimental groups. HOI structural elements were dispersed in cartilage and subchondral bone layers enfolded in the host tissue. No evidence of infection, donor tissue rejection, or immune response was noted in any histological samples of experimental groups. Histological pictures and evaluation are depicted in Fig. 5.1.5.1.

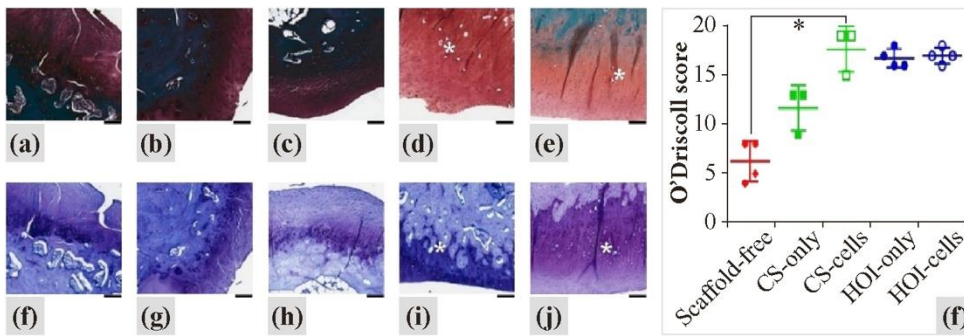


Fig. 5.1.5.1. Histological evaluation of experimental groups at 6 months after intervention in (a, f) scaffold-free, (b, g) CS-only, (c, h) CS-cells, (d, i) HOI-only, and (e, j) HOI-cells groups, as evaluated by (k) a modified O'Driscoll score

The histological score improved in all treatment groups compared to the scaffold-free group as assessed by (a–e) Safranin O and (f–j) Toluidine blue staining. A positive tendency was noted in HOI-cell and HOI-only groups over the scaffold-free group. HOI structural elements (Asterix) were evident in cartilage and subchondral layer. CS-cells group was superior compared to the control group. * $P < 0.05$. Scale bar: 200 μm .

The detailed description of histological values is described in articles (1, 3).

5.1.6. Electromechanical evaluation *in vivo*

Electromechanical parameter measured at the cartilage repair sites treated with HOI-only, HOI-cells, and CS-cells groups were lower than the untreated scaffold-free group, resulting in superior repair for scaffold-based groups, especially cell-seeded scaffolds.

Significantly inferior electromechanical properties were noted in CS-only ($P = 0.002$), HOI-only ($P = 0.022$), and in scaffold-free ($P = 0.0009$) groups compared to healthy cartilage. However, HOI scaffolds with cells ($P = 0.0014$) or without ($P = 0.0059$) exhibited improved values of electromechanical parameter compared to the scaffold-free group. Electromechanical measurement is depicted in Fig. 5.1.6.1.

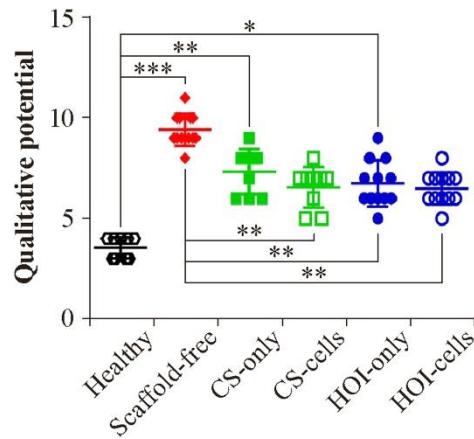


Fig. 5.1.6.1. Electromechanical Arthro-BST measurement of repaired cartilage 6 months after intervention

Electromechanical parameter measured at HOI-only, HOI-cells, and CS-cells was lower than the scaffold-free group, thus resulting in superior repair in these groups. HOI-cells and CS-cells exhibited improved values of the electromechanical parameter and were comparable to healthy cartilage. * $P < 0.05$, ** $P < 0.01$, *** $P < 0.001$.

Despite the non-inferiority between healthy cartilage values compared to CS-cell ($P = 0.069$) and HOI-cell ($P = 0.066$) groups, the best repair potential has been shown for cell-seeded groups, as expressed by improved intrinsic electromechanical properties of cartilage.

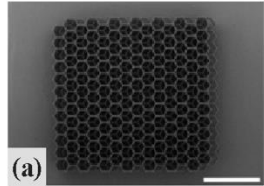
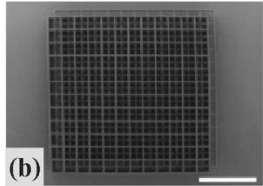
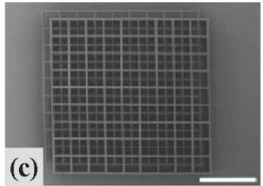
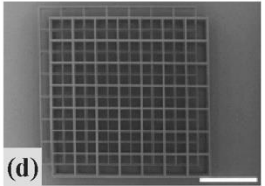
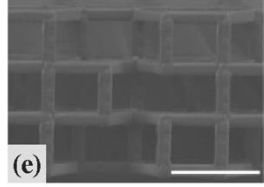
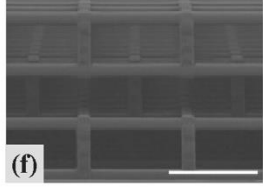
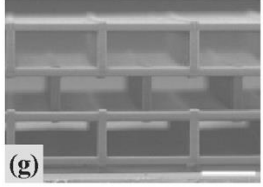
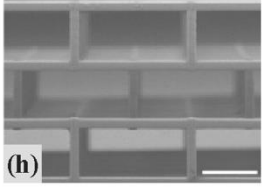
The detailed description of electromechanical values is described in the article (1).

5.2. Results of the final study

5.2.1. Morphological and biomechanical analysis

Morphological characteristics of constructed HOI-H and HOI-T scaffolds were comparable to allow the analysis of pore shape influence on biomechanical properties. Morphological SEM images are depicted in Table 5.2.1.1.

Table 5.2.1.1. Morphological (a–d) top-view and (e–h) side-view SEM images of HOI scaffolds

Scaffold type	HOI-H	HOI-T	HOI-T1.5	HOI-T2
	 (a)	 (b)	 (c)	 (d)
	 (e)	 (f)	 (g)	 (h)
Scaffold size (W×L×H), μm ³	1511×1567×195	1515×1515×195	1582.5×1582.5×262.5	1590×1590×330
Side pore (L×H), μm ²	49×45	105×45	150×67.5	195×90
Top pore (L×H), μm ²	42×49	45×45	67×67	90×90
Porosity, %	87	89	94	96

Note. Pore size effect on cell proliferation was determined in (c, g) HOI-T1.5 and (d, h) HOI-T2 images. Scale bar: (a–d) – 500 μm, (e–h) – 100 μm.

Biomechanical response curves of irregular shape were generated by the indenter tip, as expressed by the obtained crushing force vs. indentation depth. Indentation curves of HOI-H and HOI-T demonstrated that the crushing force increased reaching peaks A, B and C at the depth of three consecutive regions from HOI top to bottom. Force-indentation depth curves are depicted in Fig. 5.2.1.1 (a, b).

Fracture pattern was different amongst HOI scaffolds and was represented by a greater depth required to reach a maximum peak force at II and III layers in HOI-T, compared to HOI-H. Accumulated fractured parts precipitated differently in both scaffolds, thus increasing indentation force in a layer by layer fashion. Indentation force and depth layer-by-layer is depicted in Fig. 5.2.1.1 (c, d).

A clear tendency for superior indentation hardness (H_{IT}) and modulus (E_{IT}) in HOI-H compared to HOI-T was evident. Both HOI scaffolds retained the same H_{IT} and E_{IT} when kept in a wet state (data not shown). On the contrary, a steep and steady incline of crushing force was registered for dry-state CS, while wet-state CS registered a significant force reduction through 140 μm in depth. This simulated a clinical application prior to CS implantation and indicated a reduced resistance for a wet-state CS. In addition, H_{IT} and E_{IT} of CS prepared for implantation was significantly inferior to HOI-T and HOI-H. H_{IT} and E_{IT} average measurements are depicted in Fig. 5.2.1.1 (e).

The detailed description of indentation force and depth values are described in the article (2).

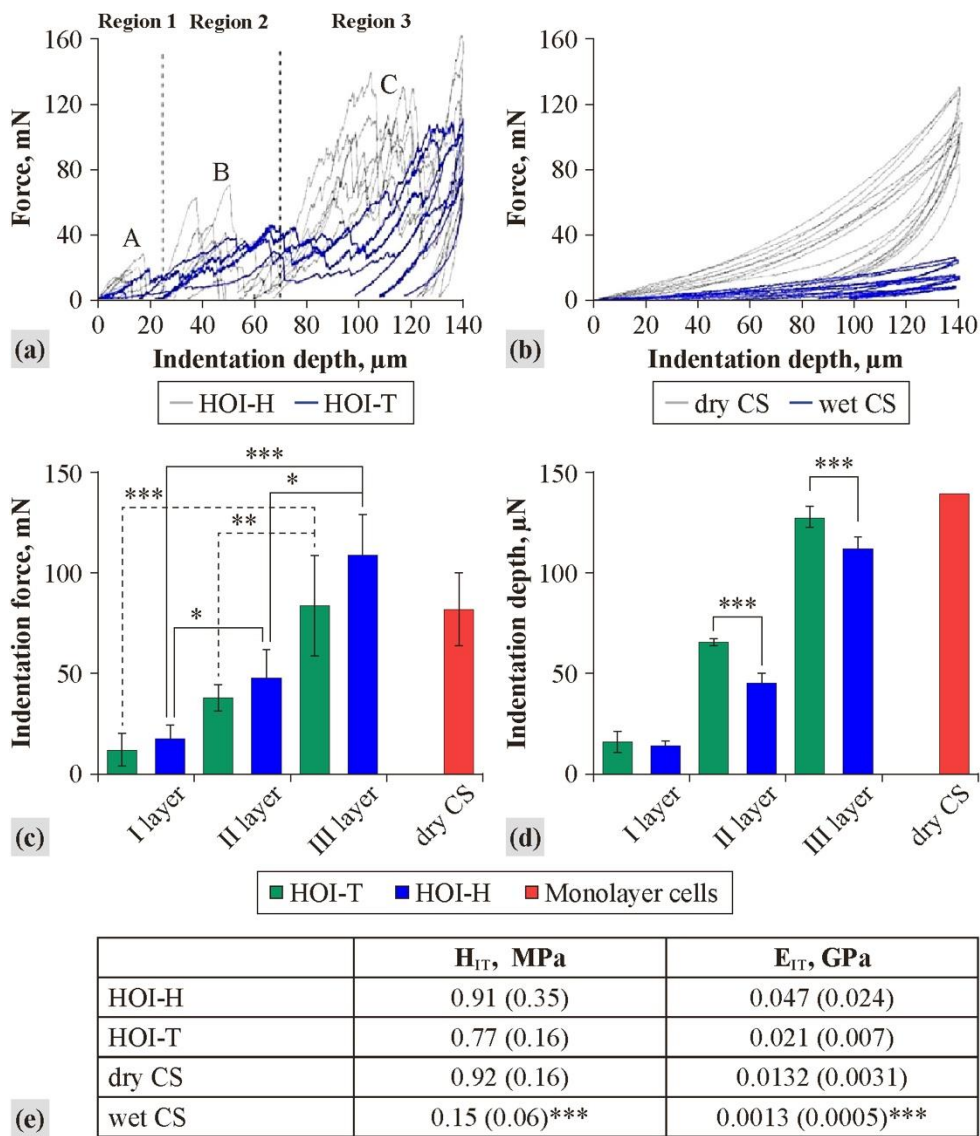


Fig. 5.2.1.1. Force-indentation depth curves obtained during the micro indentation test performed on HOI and CS

(a) Fracture pattern was different amongst HOI-T and HOI-H scaffolds while (b) dry and wet CS deformation patterns indicated reduced resistance for a wet CS. (c, d) The significantly higher force was registered with advancing to deeper layers of HOI scaffolds and was comparable to dry CS. (e) A tendency for superior H_{IT} and E_{IT} in HOI-H compared to HOI-T was noted. H_{IT} and E_{IT} of wet CS was significantly inferior to all scaffolds tested. * $P < 0.05$; ** $P < 0.01$; *** $P < 0.0001$.

5.2.2. Biocompatibility analysis and pore shape dependence analysis

HOI-H cell adherence and increased ECM deposition were maintained up to 7 days *in vitro* by elongated matrix fibers in-between perpendicular rods. SEM images of cell biocompatibility in HOI-H is depicted in Fig. 5.2.2.1 (a, b).

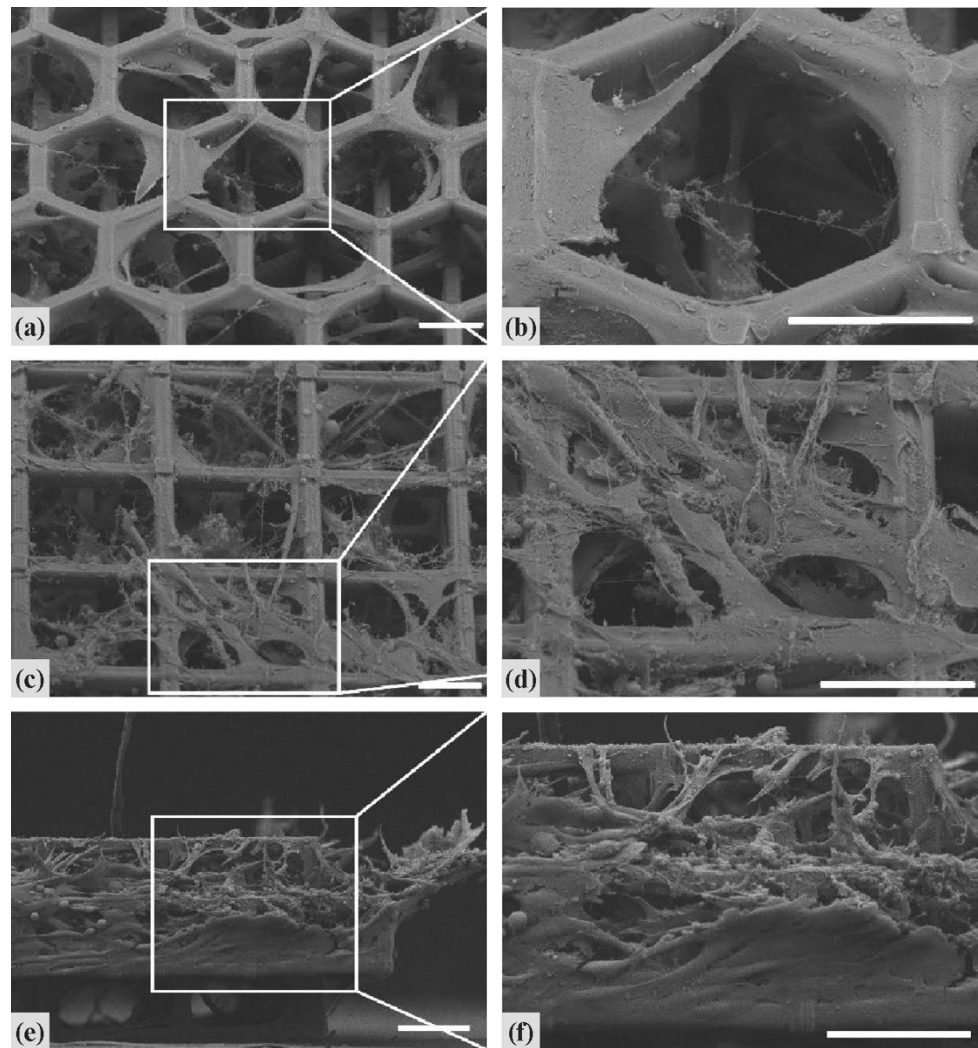


Fig. 5.2.2.1. Distribution of chondrocytes in (a, b) HOI-H scaffold and throughout (c, d) horizontal and (e, f) vertical rods of HOI-T scaffold on day 7 post-seeding

Elongated and oval-shape cells wrapped and bridged horizontal and vertical rods of the HOI-T scaffold and deposited ECM have outgrown all three layers, filling most of the pore volume at day 7. Scale bar: (a–d) 50 μm , (e, f) 100 μm .

Similarly, cells seeded on HOI-T adhered to the horizontal and vertical rods of the scaffold. The proliferation of elongated and spherical shape cells within both scaffolds was sustained up to 7 days *in vitro* and signified cell redifferentiation. Adjacent rods were interconnected by cells and ECM which have outgrown all the layers of HOI and filled the greater part of pore void at day 7, especially in HOI-T. SEM images of cell biocompatibility in HOI-T is depicted in Fig. 5.2.2.1 (c–f).

Cells seeded on HOI-T and HOI-H improved their metabolic activity compared to cells used for seeding (monolayer cells). Even though the metabolic cellular improvement from day 1 to day 7 in both HOI-T and HOI-H groups was significant, it was comparable amongst two groups at all endpoints. Nevertheless, only cells in the HOI-T group improved on day 7, compared to monolayer cells, while HOI-T showed a clear tendency for improvement ($P = 0.057$). Metabolic activity and pore shape dependence are depicted in Fig. 5.2.2.2 (a).

Similarly, cell number increased in HOI-T and HOI-H at day 7, compared to monolayer cells count and was comparable amongst groups in all endpoints. However, a tendency for a higher count of cells was noted in the HOI-T group, compared to HOI-H. Improved metabolic activity is representative to a higher count of cells, thus supporting cellular proliferation on both HOI scaffolds, with a tendency for superiority in the HOI-T group. Count of cells and pore shape dependence is depicted in Fig. 5.2.2.2 (b).

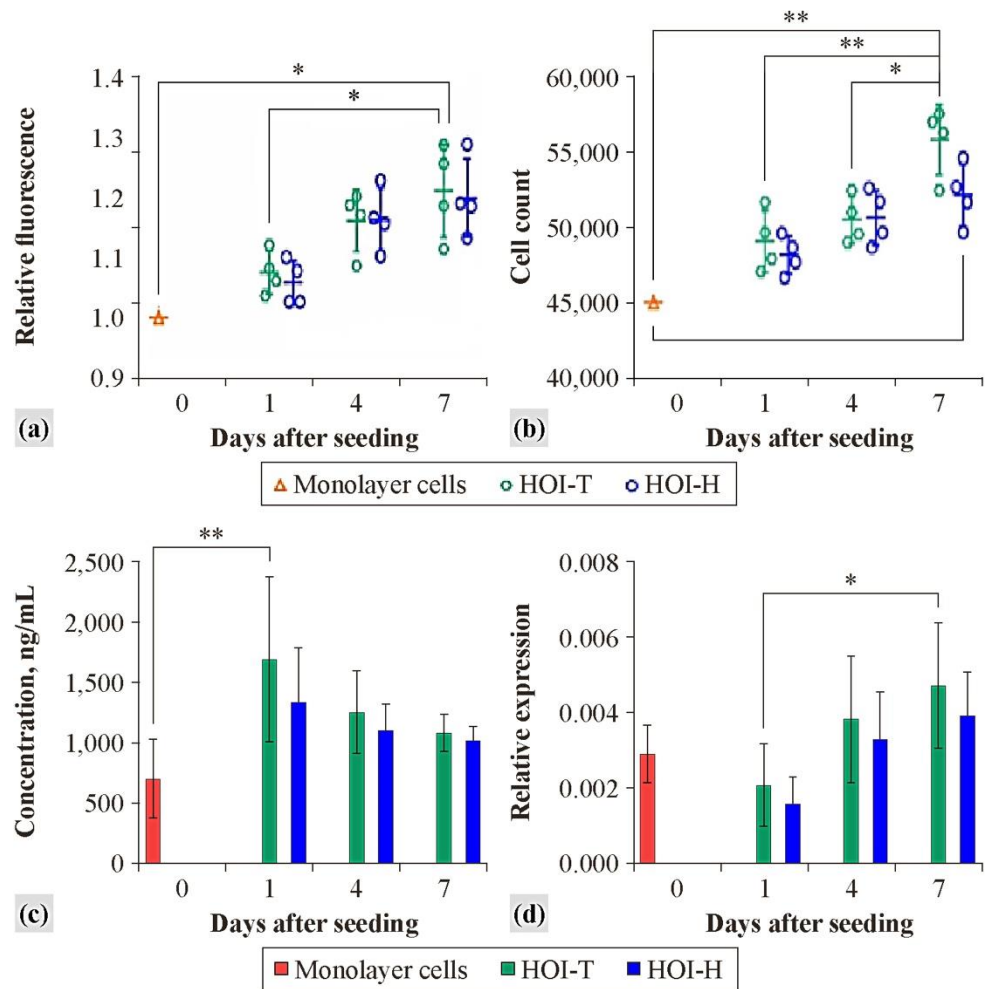


Fig. 5.2.2.2. (a) Metabolic activity, (b) count of cells, (c) type II collagen protein secretion and (d) COL2A1 gene expression of HOI-T and HOI-H seeded with chondrocytes at days 1, 4, and 7

Similar improvement of metabolic activity and cell count to day 7 was seen in both scaffolds, compared to cells used for seeding (cell control). Secretion improved on day 1 in the HOI-T group, compared to cells used for seeding and sustained chondrogenesis up to day 7. Mean protein secretion values were higher in the HOI-T group compared to HOI-H at all endpoints. Relative COL2A1 expression improved only in the HOI-T up to day 7. * $P < 0.05$; ** $P < 0.01$.

5.2.3. 3D cell redifferentiation and pore shape dependence analysis

An improved type II collagen protein secretion at day 1 was noted in the HOI-T group, compared to monolayer cells. Reduced, yet sustained chondrogenesis was evident up to day 7 under regular culture conditions in HOI-T group.

Similarly, protein secretion retained its level up to day 7 in the HOI-H group; however, it was comparable to secretion levels of monolayer cells throughout the period. A decrease in protein secretion was noted in both scaffold groups up to day 7, albeit not significant. Mean protein secretion values were greater in the HOI-T group in all endpoints when scaffolds with cells were compared to each other, albeit not significantly. Therefore, a superior initial phase of HOI-T scaffold and cells biocompatibility indicates at least a numerical superiority of tetragon over hexagon-pored HOI. Type II collagen protein secretion and pore shape dependence are depicted in Fig. 5.2.2.2 (c).

COL2A1 was upregulated up to day 7 in HOI-H and HOI-T groups. Mean values of gene expression were comparable to values of monolayer cells in both groups throughout the culture period. Nevertheless, a significant improvement up to day 7 was noted only in the HOI-T group. COL2A1 gene expression and pore shape dependence are depicted in Fig. 5.2.2.2 (d).

No significant differences amongst two scaffolds were observed, however, mean values of gene expression were higher in the HOI-T group, compared to the HOI-H group, thus supporting a tendency for the superiority of tetragon-pored over hexagon-pored HOI. Type II collagen gene expression is depicted in Fig. 5.2.2.2.

5.2.4. 3D cell redifferentiation and pore-scale dependence analysis

In the second stage of the experiment, top and side pores of HOI-T were scaled by the factors of 1.5 (HOI-T1.5) and 2 (HOI-T2) for the determination of pore size effect on cell proliferation. Morphological SEM images are depicted in Table 5.2.1.1. A comparable proliferation of elongated and oval shape cells within the HOI-T and HOI-T1.5 was sustained up to 7 days *in vitro*. Cells and the secreted ECM were noted on perpendicular and parallel planes of scaffolds, thus supporting the predefined distance between the rods. Cell distribution in HOI-T and HOI-T1.5 is depicted in Fig. 5.2.4.1 (a, b).

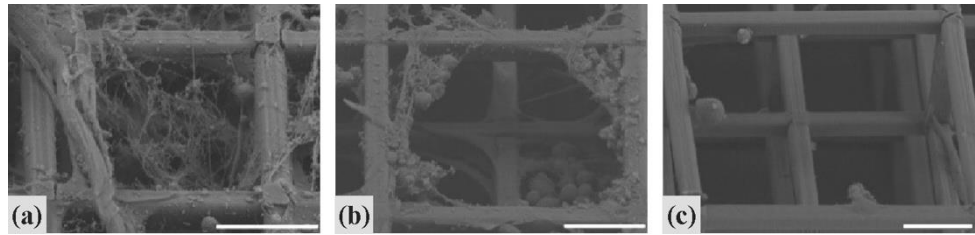


Fig. 5.2.4.1. Cells distribution in a tetragonal pore of **(a)** HOI-T, **(b)** HOI-T1.5, and **(c)** HOI-T2 at day 7 post-seeding

Elongated and oval shape cells and the secreted ECM were noted on perpendicular and parallel planes within the HOI-T and HOI-T1.5 scaffolds. Only sporadic cell adherence was noted on the HOI-T2 rods. Scale bar: 50 μm .

HOI-T2 did not support cell growth and ECM production. Only sporadic cell adherence was noted on the rods, with little ECM production in all HOI-T2 scaffolds tested. Cell distribution in HOI-T2 is depicted in Fig. 5.2.4.1 (c). Cells were randomly distributed in the superficial and middle layers of CS, interconnecting collagen folds and creases. Cell distribution in CS is depicted in Fig. 5.2.4.2 (a, b).

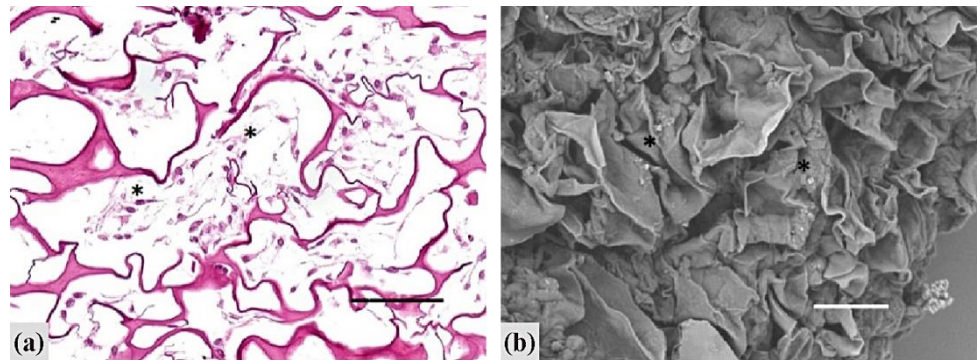


Fig. 5.2.4.2. The distribution of seeded human chondrocytes throughout CS on day 7

A representative **(a)** histological (H&E staining) and close-up **(b)** SEM image reveals chondrocytes (Asterix) distribution in the superficial and middle layers of collagen scaffold interconnecting nearby folds and creases. Scale bar: 50 μm .

Mean values of type-II collagen protein secretion improved at day 1 in HOI-T, HOI-T1.5 and HOI-T2 groups, however only HOI-T had a significant improvement. Protein secretion numerically diminished in all HOI groups up to day 7, indicating decreased, yet sustained release of protein in culture media. HOI-T had significantly superior protein secretion compared to HOI-T1.5 and HOI-T2 after one day in culture. In addition, HOI-T retained its biochemical superiority over HOI-T2 at days 4 and 7. Similarly, mean values of protein secretion numerically diminished in a positive comparator CS group up to day 7, nevertheless it was superior to any other HOI group at all endpoints. Therefore, a biochemical superiority of HOI-T scaffold over HOI-T1.5 and HOI-T2 at least 1 day after the *in vitro* culture is morphological and indicates an advantage of specific pore size in a short-term, yet for clinical implantation acceptable period. Type II collagen secretion is depicted in Fig. 5.2.4.3 (a).

Mean values of COL2A1 expression were upregulated up to day 7 of culture in HOI-T and HOI-T1.5 groups. Mean values of gene expression throughout the culture period were comparable to monolayer cells in all HOI groups. COL2A1 expression improved in the CS group at day 7 compared to day 1, yet it was comparable to all HOI groups at all endpoints. Type II collagen gene expression is depicted in Fig. 5.2.4.3 (b).

HOI scaffolds of scaled pores were comparable amongst each other; however, higher mean values supported a tendency for gene expression superiority of HOI-T scaffolds over HOI-T1.5 and HOI-T2.

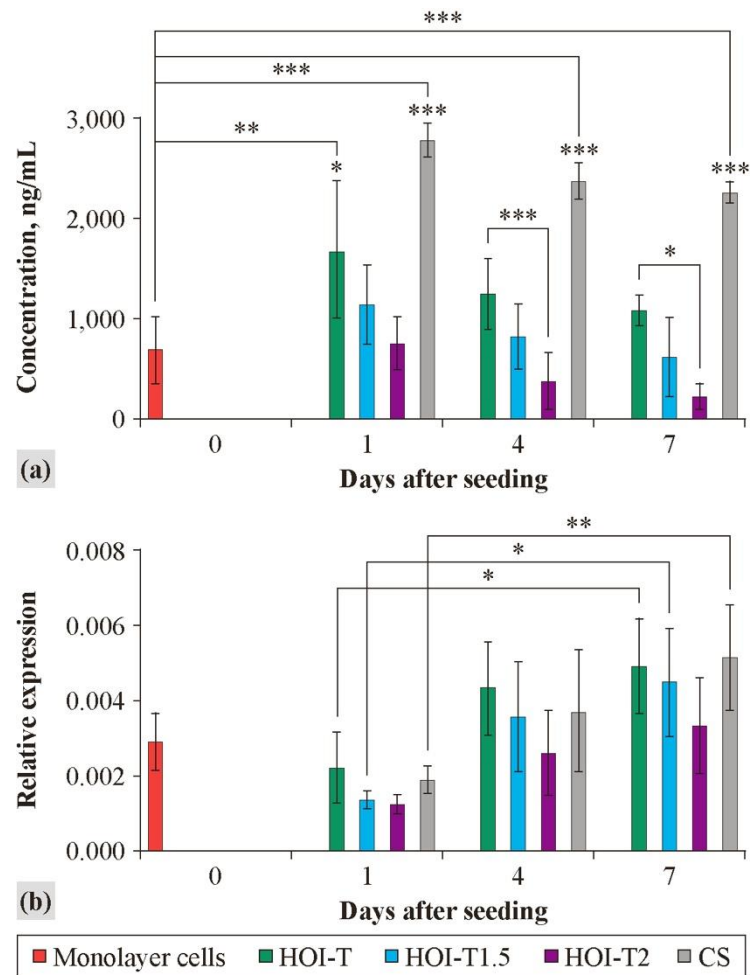


Fig. 5.2.4.3. Pore-scale and biocompatibility dependence

(a) Type-II collagen protein secretion and (b) expression of HOI-T, HOI-T1.5, and HOI-T2 seeded with cells at days 1, 4, and 7. Secretion improved on day 1 in the HOI-T group, compared to cells used for seeding and was superior to HOI-T1.5 and HOI-T2. CS protein secretion was superior to any other HOI group. Mean COL2A1 expression values improved in HOI-T and HOI-1.5T groups and were comparable to CS. * $P < 0.05$, ** $P < 0.01$, *** $P < 0.001$.

5.2.5. Macroscopic analysis of repair cartilage

No swelling, signs of inflammatory or immune responses to implanted materials on operated knees were observed. OAS improved in all groups compared to the scaffold-free group. Interestingly, the addition of cells in the HOI group marginally impaired macroscopic evaluation compared to the HOI-only group. None of the HOI scaffolds restored a smooth cartilage

surface and graft level, integration and coloration resulted in relatively the same. CS-cells group revealed the most hyaline-like cartilage when compared to a scaffold-free group, as evident by the leveled graft with the surrounding cartilage and the smooth appearance of surface throughout all samples. However, CS-only was inferior to the HOI-only group, mainly due to more fine fronds on the cartilage surface when compared to a smoother cartilage surface in both HOI groups. Macroscopic evaluation is depicted in Fig. 5.2.5.1.

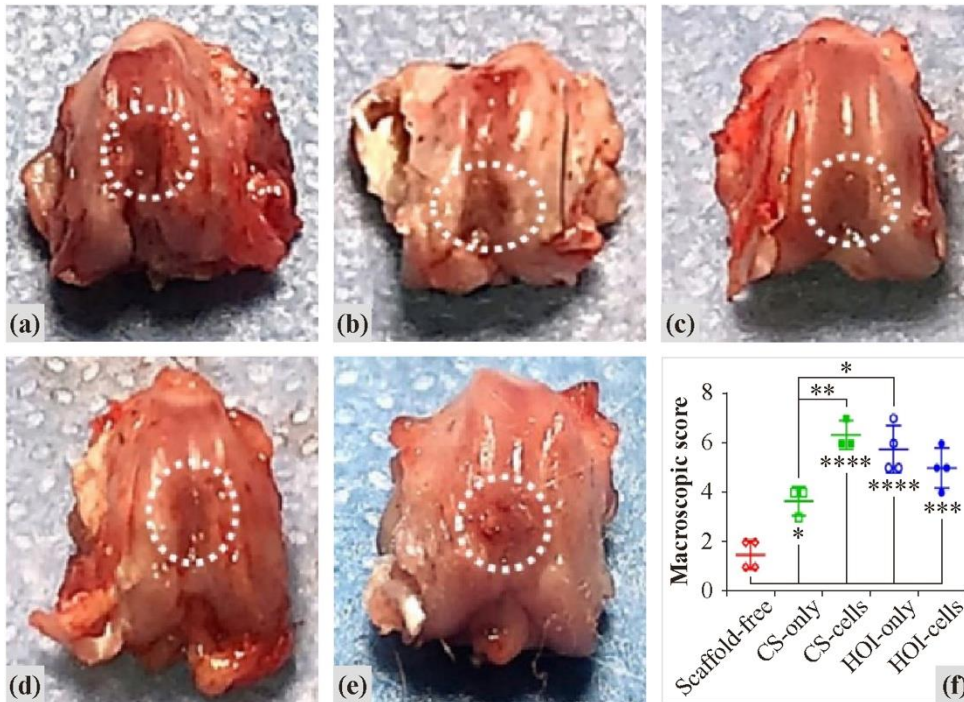


Fig. 5.2.5.1. Macroscopic evaluation of experimental groups at 3 months after treatment in (a) scaffold-free, (b) CS-only, (c) CS-cells, (d) HOI-only and (e) HOI-cells groups

HOI-only and HOI-cells had a clear tendency for superior macroscopic evaluation of repair cartilage (dotted circle) compared to the scaffold-free group. Fine fronds on the cartilage surface were evident in all HOI-only and HOI-cells defects when smoother cartilage surface was exhibited throughout CS groups. CS-cells had the highest mean OAS score amongst all experimental groups, as evident by cartilage defect filling. Statistical significance * $P < 0.05$, ** $P < 0.01$, *** $P < 0.001$, **** $P < 0.0001$.

5.2.6. Histological analysis of repair

O'Driscoll score improved significantly in all treatment groups compared to the scaffold-free group at 3 months. Cell addition in the HOI group did not improve cartilage repair quality. HOI-only group revealed that both sides of repair tissue integrated with host cartilage, compared to HOI-cells group partial integration. Other parameters were comparable amongst the HOI groups. O'Driscoll score in the HOI-only group was superior compared to the CS-only group and was mainly influenced by the smoother cartilage surface in the HOI-only group, whereas isolated pathological fissures on the repair cartilage surface were evident in the CS-only group. CS-cells group revealed the best numerical cartilage regeneration amongst all groups tested, as evident by >75% of repair area filled with cells and both sides of repair tissue integrated with host cartilage in all samples. Complete restoration of subchondral bone was not seen in any of the samples, with slight tidemark contour changes evident throughout experimental groups. Histological evaluation is depicted in Fig. 5.2.6.1.

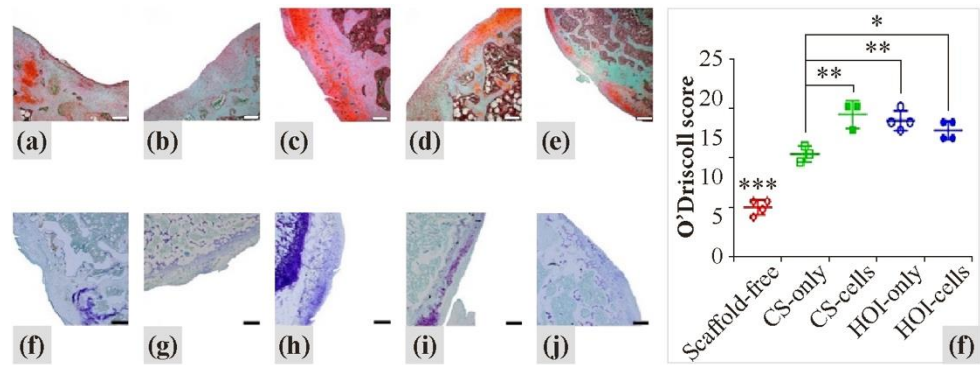


Fig. 5.2.6.1. Histological evaluation of experimental groups at 3 months after treatment in (a, f) scaffold-free, (b, g) CS-only, (c, h) CS-cells, (d, i) HOI-only and (e, j) HOI-cells groups

The histological score improved in all treatment groups compared to the scaffold-free group as assessed by (a–e) Safranin O and (f–j) Toluidine blue staining. Cell addition to the HOI did not further improve cartilage repair, mainly due to more cell clustering in HOI-cell. CS retained numerically superior cartilage repair and was comparable to HOI scaffolds at the follow-up. Scale bar: (a–e) 100 µm; (f–j) 200 µm. Statistical significance * $P < 0.05$, ** $P < 0.01$, *** $P < 0.0001$.

6. DISCUSSION

6.1. Biocompatibility of rabbit chondrocytes and microstructured HOI scaffolds *in vitro*

Because of their genotypic and phenotypic resemblance to the cartilage tissue, chondrocytes have long been the first choice of cells for articular cartilage repair. The morphological, genotypic and phenotypic profiles of chondrocytes have been well established and the efficacy of cellular TECs has been demonstrated in long-term human studies [54, 96, 97].

The physical and chemical properties of TEC influence cell attachment and potency *in vitro* and *in vivo* efficacy. The DLW technique and SZ2080 material allow predefining of parameters such as pore size, shape, and porosity to support cell ingrowth and ECM deposition. The discrepancy described between gene expression and protein secretion led to an *in vitro* RT-qPCR and ELISA analysis [98]. Despite the decrease in protein secretion, HOI maintained the same level of protein translation as the monolayer chondrocytes. The period until 4th day should be analyzed in detail to determine if the increase in gene expression occurred earlier. From the clinical translation perspective, most scaffolds tend to be cultured for a very brief period after seeding, with the focus on accelerated implantation. This enables faster and more qualitative redifferentiation *in vivo*, even when compared to recently introduced bioreactors, which are still ways of solving functional and structural *in vivo* conditions, after a prolonged *in vitro* culture [99].

Ultrafast pulsed lasers became a well-established technique for the creation of custom made free-form 3D micro scaffolds from a variety of materials ranging from proteins to biocompatible glasses. Thus, here we showed for the first time that novel, specially shaped SZ2080 material is a biocompatible material for chondrocytes in a three-dimensional environment and enables them to recover the chondrogenic phenotype, which is otherwise diminished during culturing in a monolayer.

6.2. Safety and efficacy of primary TEC in a long-term rabbit articular cartilage defect model

This study demonstrated a permanent cartilage repair 6 months after implantation of the three-dimensional HOI scaffold. This was confirmed by macroscopic, histological, and electromechanical analysis. To our knowledge, this is the first *in vivo* study to analyze the electromechanical properties of TEC in a long-term preclinical study.

Despite the osteochondral defect used in our study, improvement after 6 months of observation was evident in most experimental groups, especially in HOI and CS scaffold groups with cells. Both HOI groups tended to exhibit a better OAS compared to a scaffold-free group, mainly because of superior tissue integration and smoother regenerated cartilage surface area. Interestingly, the OAS score was slightly lower in the HOI group with cells, when compared to HOI without cells, representing a superior macroscopic result in the HOI without cells group. Seeded cells might have interfered with full scaffold integration by suppressing the ingrowth of the host tissue cells. A recent study showed an increase in fibrosis of cell-based scaffolds compared to non-cell-based scaffolds, indicating that cells might have inhibitory effects on host tissue integration [100]. Future studies should examine the property of cell migration towards scaffolding.

Histologically cell groups tend to be superior over cell-free groups. This is due to the hyaline-like cellular morphology and over 75% of the area filled with chondrocytes, both of which are affected by the addition of cells. The structural elements of the HOI were enfolded in both chondral and subchondral layers without evidence of inflammation. Nevertheless, the subchondral bone was not completely restored, and slight bone plate changes were observed in samples. Biphasic scaffolds with different mechanical and spatial parameters have been proposed to provide superior osteochondral repair [101]. Strategies for selecting the appropriate morphological parameters of scaffolding vary among groups [102–104]. In addition, the subchondral interface between bone marrow and calcified cartilage layer that contains the vessels must be taken into account [105].

A growing number of experimental *in vivo* studies of TECs have led to the need for rapid and reliable evaluation of treatment outcomes, other than invasive diagnostic methods, particularly in long-term preclinical studies. It has been shown that electromechanical properties reflect cartilage quality and correlate with histological and biomechanical parameters, apoptosis and are inversely correlated with the viability of chondrocytes [79–81]. In addition, electromechanical analysis is more sensitive than invasive biomechanical testing [80]. In our study, we have observed a greater electromechanical potential in regenerated cartilage compared to healthy cartilage, revealing incomplete cartilage regeneration. Nevertheless, the score of the scaffold groups with cells was significantly higher compared to the groups without scaffolds, which resulted in better cartilage quality. In addition, the inferiority of both groups with cells compared to healthy cartilage was insignificant and thus revealed satisfactory cartilage regeneration. The results of Arthro-BST were similar to the histological results for the quality of cartilage repair in our study. The inclusion of the QP measurement has already been applied in

explanted human osteochondral cores. Correlation with other cartilage quality parameters has suggested a possible use of this technique to detect underlying and macroscopically not visible cartilage defects [80]. Electro-mechanical measurement can be used as an *in vivo* diagnostic method for cartilage damage and regeneration quantification, by reflecting the key parameters of cartilage quality.

An *ex vivo* histological examination shows that optimization of pore geometry and pre-growing chondrocytes before implantation significantly improves the performance of the created 3D scaffolds. An HOI scaffold with chondrocytes allowed for a better macroscopical and histological evaluation, which was in accordance with PCR results obtained from samples at 3 months after implantation. The HOI scaffold loaded with chondrocytes had the most hyaline-like tissue compared to other groups. The achieved biocompatibility is comparable to the commercially available collagen membrane. A successful outcome of this study supports the idea that hexagonal-pore-shaped HOI microstructured scaffolds in combination with chondrocytes seeding may be successfully implemented for cartilage tissue engineering.

6.3. Biocompatibility of human chondrocytes and optimized HOI scaffold *in vitro*

This study demonstrated the continuous formation of cartilage *in vitro* after an SZ2080 scaffolding was seeded with human chondrocytes. In addition, the shape and size of the pores were investigated to improve cartilage formation outcome. The capacity of HOI cartilage formation was compared with the positive cell-seeded collagen-based scaffold comparator.

The biomechanical properties of scaffolding are important characteristics of a potent TEC and depend on the origin of the material and the morphology design [13, 19]. Moreover, the sufficient biomechanics of TEC *in vitro* allows predicting a sufficient cellular redifferentiation and hyaline cartilage formation to support heavy loads *in vivo* [13, 95]. It is known that the shape of the pores, size, connectivity and other morphological parameters of the scaffold plays a crucial role in the biomechanical properties of the scaffold [27]. In this study, HOI scaffolds were subjected to quasi-static indentation loading from top to bottom, until the failure by cracking of the three horizontal rod layers. Several higher peaks have been observed in regions 2 and 3, or in the middle and lower layers of the scaffold, which may be related to the greater load due to previously fragmented scaffold rods. The increase in the number of fractured rods influenced the number of peaks; therefore, two peaks were generally visible in the second region, while no less than 3 clearly expressed

peaks were registered in the third region. However, compression force peaks were not so expressed in HOI-T compared to HOI-H in the second and third regions which may be due to the higher porosity of HOI-T and a different fracture pattern by the rods. In addition, the influence of pore shape on the fracture pattern significantly increased in the second and third HOI regions HOI. HOI-T revealed less resistance to the cracking under load, compared to HOI-H. Because the force is distributed on the rods, a hexagonal HOI with a higher rod content could withstand a 30–35% higher average force. The different indentation pattern in CS was reflected by irregular shapes and wide variability of response curves. Typically, the force increases to maximum values as the depth of the indentation increases. However, the average force values were highly dependent on the water volume in the sample. The immersion of CS in the proliferation medium shows the real clinical situation prior to implantation, yet the hardness of CS has been already decreased significantly by then. In addition, this reduction is significantly higher compared to both HOI scaffolds, which maintained their H_{IT} and E_{IT} in both conditions tested.

The production and characterization of porous scaffolding have been a key aspect of TEC production, because of the impact the shape, size, porosity and pore interactions have on cellular responses such as cell proliferation, metabolic activity and protein secretion *in vitro* [13, 23, 68, 106]. The shape and size of the pores play a vital role in chondrocyte scaffold penetration because geometry determines the distribution of cells and the resulting pattern of cells embedded in the extracellular matrix. The size of a chondrocyte depends on the cartilage area and generally occupies a volume of 200–2,000 μm^3 , which corresponds to a diameter of 7–15 μm . Being able to easily migrate through larger pores, chondrocyte spanning throughout the scaffold predominantly depends on the cell-scaffold interactions. As the angle between the rods increases, the cell-rod interaction is impeded, and greater cell-to-cell interaction is initiated. This reduces the stability of the structure and spread of the new ECM [107]. Therefore, shorter distances between rods in tetragonal scaffolds and the resulting additional cell binding sites that support cell proliferation can lead to a greater pore coverage by the secreted ECM and cells [108, 109].

It has been shown that the morphological properties of scaffolds, such as high porosity, regularly interconnected pores, improve the chondrocyte phenotype and secrete an abundance of ECM in chitosan and alginate scaffolds [23, 70]. Influence of various pore sizes have also been investigated, revealing superior biomechanical and physical properties in scaffolds with uniform pore sizes, homogenous environment and high interconnectivity throughout the scaffold [71]. In addition, Wang et al. have shown that a particular pore

shape can support normal phenotype by enhancing the functional production of ECM. Di Luca et al. suggested a benefit of different shapes of pores for osteochondral repair [110]. Pore size uniformity, shape and high porosity can be achieved effectively using the DLW method, whose key parameters are controlled by precise and flexible microfabrication. Kapyla et al. fabricated scaffolds with custom pore sizes, porosity and interconnectivity using the DLW technique, providing a novel approach for studying the effect of scaffold architecture on cell behavior *in vitro* [26]. DLW has been known as a promising technology for creating tailored 3D scaffolds with high precision for quite some time now. However, it has been mostly applied for sub-mm size scaffold fabrication and generally limited to *in vitro* cell biology studies [111–114].

In our study, we manufactured a tetragon and a hexagonal HOI to determine the influence of the shape of the pores for the formation of cartilage *in vitro*. HOI-T and HOI-H improved metabolic cell activity and count to day 7. In addition, only cells cultured in tetragon pored HOI improved activity and total cell number compared to monolayer cells. Pore morphology was significantly more iterative in HOI and allowed more uniform distribution of cells throughout the scaffold compared to CS. A superior expression of the COL2A1 gene was similarly upregulated in the tetragon-pored scaffold at least up to day 7. A superior initial culturing phase of HOI-T biocompatibility indicated at least a numerical superiority of tetragon-pored compared to hexagon-pored scaffolds. The previously described discrepancy between gene expression and protein translation *in vitro* prompted a combined RT-qPCR and ELISA analysis *in vitro* and was evident in our study as well [98]. Our study described the inverse correlation between mRNA transcription and protein translation, which has been previously described and is not yet sufficiently defined [115].

Different approaches have been applied to generate three-dimensional microstructures for cartilage regeneration, such as salt leaching, gas foaming, phase separation, and freeze-drying in the past. Conventional manufacturing methods result in pore size and a porosity of 70–860 μm and 30–95%, respectively [116]. However, precise control of scaffold microarchitecture could only be achieved through a customized fabrication, such as DLW [117]. Danilevicius et al. showed an optimal pre-osteoblastic cell ingrowth and proliferation on microstructured DLW scaffolds containing 70 μm squared pores and 86% porosity [118]. Trautmann et al. microstructured stable and reproducible scaffolds with square pore sizes of 10–90 μm . They established a pore size of 90 μm to support the best adhesion and growth of fibroblast cells in the samples [119]. Precisely microstructured pore shapes and sizes require a different design approach compared to conventional methods. The

reduced surface volume for cell binding and the fragile mechanical properties of the DLW scaffold must be compensated by calculated pore morphological and scaffold structural properties and must not interfere with cell growth and proliferation. Therefore, smaller sized pore characteristics combined with the improved structural properties of the scaffold could support a highly customized and sustainable scaffold for cartilage tissue engineering.

Complex cross-link between transcription, translation, post-translational modifications, secretion and extracellular processing of extracellular matrix collagen proteins is essential for efficient protein secretion and stable network formation [120]. Addition of growth medium supplements that catalyze gene splicing, polyadenylation, hydroxylation and other posttranscriptional modifications might enhance the intermolecular connections and type II collagen secretion by the scaffolds. We also speculate that a 7-day timeframe is more useful for determining the shelf-life rather than a clinical surrogacy in the long term.

Despite reduced protein secretion, HOI maintained a superior protein translation compared to monolayer cells used for seeding.

The physical properties of TEC influence cell binding and subsequent potency *in vitro*. After evaluating the influence of pore size, prolonged cell proliferation was observed in HOI-T and HOI-T1.5 scaffolds with pore sizes of $45 \times 45 \mu\text{m}^2$ and $67 \times 67 \mu\text{m}^2$, respectively. Despite the reduced secretion of type II collagen protein up to 7 days *in vitro*, initially, the protein secretion was higher in the HOI-T group compared to other HOI scaffolds. In addition, expression was upregulated in all groups, with a tendency for superiority in HOI-T scaffolds compared to HOI-T1.5 and HOI-T2. Our study supported the findings of Duan et al. who observed 100–200 μm^2 pores in the chondral layer to obtain better results *in vivo* compared to scaffolds of smaller or larger pore sizes [104]. Wang et al. demonstrated a need for sufficient porosity to maintain efficient permeability and cell migration through scaffolding [103]. Pan and the group showed a scaffold with a cartilage layer of 92% porosity that yielded the best *in vivo* efficacy [121]. Despite the 96% porosity in our HOI-T2 scaffold, the void between the rods might have been too large for the number of cells seeded and might suggest the greater number of cells needed to improve binding and pore filling. Therefore, parameters of scaffold pore size, porosity and surface area must be coupled to the cell dosage, as well. In the early stages of preclinical studies, the dosage of inoculated cells should be considered to ensure the efficacy of the treatment [122]. The area of cartilage defect is not two dimensional, but rather organized spatially, therefore manufactured scaffold size area might be better substituted with a size volume and the subsequent cell dosing adjustment. To obtain the most

accurate dose for a successful clinical translation, differences in cartilage thickness between species should be considered.

HOI-T and HOI-H improved metabolic activity of seeded monolayer cells *in vitro*. Tetragon-pored HOI tended to have superior biocompatibility, cartilage-specific protein secretion and gene expression compared to hexagon-pored HOI scaffolds. Tetragonal pore sized $45 \times 45 \mu\text{m}^2$ scaffold was comparable to a $67 \times 67 \mu\text{m}^2$ pore sized scaffold by protein secretion and gene expression for at least up to 7 days *in vitro*.

6.4. Safety and efficacy of final TEC in a long-term rat articular cartilage defect model

This study demonstrated a sustained cartilage repair for 3 months in a xenogeneic model, after the application of the custom three-dimensional silicon-zirconium hybrid organic-inorganic polymer SZ2080 scaffold seeded with human chondrocytes. This was confirmed by macroscopical and histological analysis *in vivo*. This is the first *in vivo* study to analyze a TEC produced by the DLW technique and subsequently seeded with human cells in a long-term preclinical study.

Accelerated implantation of TEC has been demonstrated in other clinical areas and is the main focus of clinical translation for cartilage [123]. Therefore, TECs are generally cultured *in vitro* for a short period, allowing faster transplantation, a more qualitative *in vivo* redifferentiation and preventing overly dense formation *in vitro* that would limit the flow of nutrition and oxygen [99]. In our study, the sustained *in vitro* potency of HOI scaffolds was supported by improved gene expression. Thus, early implantation after cell seeding could support subsequent redifferentiation and cartilage formation *in vivo*.

The initial swelling of the operated knees has later resolved and no signs of immune reaction to implanted materials were observed macroscopically at the late follow-up. Based on the macroscopic and histological evaluation, both HOI-T groups with and without cells improved cartilage repair *in vivo* at a 3-month follow-up compared to a scaffold-free group. This was mainly influenced by the superior tissue integration and a smoother cartilage surface in both HOI groups. Interestingly, the HOI-cells group had numerically inferior results compared to the HOI-only group. This might have been influenced by the seeded cell interference for complete scaffold integration and inhibition of host cell migration to TEC. A recent study showed an increase in fibrosis of cell-based scaffolds, compared to a cell-free scaffold, demonstrating the inhibitory effect of donor cells on tissue integration [100].

CS-cells group revealed the best numerical regeneration of cartilage of all the groups tested; however, the subchondral bone was not completely restored. Cell-based cartilage regeneration has generally been applied for local chondral defects, while subchondral damage requires additional bone replacement [124]. This can be improved by using a biphasic scaffold to completely restore the osteochondral segment [101, 125]. Attention should also be paid to the subchondral interface between bone marrow and calcified cartilage layer containing vessels and innervation [105].

Basic and clinical research teams have enabled the translation of scientifically proven preclinical data to clinical trials utilizing TECs. Despite the clinical success of scaffolds based on natural materials in cartilage tissue engineering, custom synthetic scaffolds have been shown to have a greater advantage for *in vitro* and clinical outcomes. DLW technique allows real-time production of optimal predefined with micron accuracy. The potency and efficacy of customized scaffolds can be constantly improved to achieve optimal osteochondral tissue regeneration in patients suffering from cartilage defects.

All HOI scaffolds improved cartilage repair *in vivo* at a 3-month follow-up. Cell addition to the regular tetragon pored HOI did not further improve cartilage repair *in vivo*. Collagen scaffold retained numerically superior cartilage repair and was comparable to HOI scaffolds at the follow-up. The study supported the hypothesis that pore shape and size influence cell proliferation *in vitro* and gave new insight into cartilage repair with HOI scaffolds seeded with human cells *in vivo*.

CONCLUSIONS

1. Rabbit chondrocytes and microstructured HOI scaffolds are biocompatible for 12 days *in vitro*.
2. Primary TEC is safe and effective in a long-term rabbit articular cartilage defect model.
3. Biocompatibility of human chondrocytes and optimized HOI scaffold is maintained for 7 days *in vitro* and depends on HOI pore shape and size.
4. Final TEC is safe and effective in a long-term rat articular cartilage defect model. Adding chondrocytes to the CS result in improved cartilage regenerative efficacy. However, chondrocytes addition to the HOI-T scaffold does not further improve cartilage repair.

RECOMMENDATION

Collagen scaffold seeded with chondrocytes revealed the greatest *in vitro* and *in vivo* potency thus can be used in clinical practice as a safe and effective tissue-engineered product for cartilage regeneration. Nevertheless, the optimal manufacturing process and quality control should be determined and implemented based on the research carried out in this project and current European Pharmacopeia monographs.

SANTRAUKA

1. ĮVADAS

Sąvarinės kremzlės (SK) pažeidimai yra viena labiausiai paplitusių aktyviai sportuojančių žmonių raumenų ir skeleto sistemos patologijų [1].

SK kremzlinio sluoksnio pažeidimai diagnozuojami daugiau nei 60 proc. kelio sąnario artroskopinių operacijų atveju, todėl ortopedams traumatologams sukelia didelių gydymo iššūkių [2].

Kremzlinis audinys turi ribotas savaiminio gijimo galimybes, nes tai kraujotakos ir inervacijos neturintis audinys [3, 4]. Nepaisant minimalios savaiminės kremzlės regeneracijos po kaulo ir kremzlės (osteocondrinio) pažeidimo, regeneravusios kremzlės struktūrinės ir funkcinės savybės yra prastesnės nei sveikos kremzlės [5]. Ši regeneracija yra trumpalaikė, o kremzlinis audinys vėliau trūkinėja ir progresuoja osteoartrito link [6].

Šiuo metu taikomi osteochondrinų pažeidimų gydymo metodai gali būti efektyvūs, tačiau visiškos hialininės kremzlės audinio regeneracijos dar nepavyko pasiekti [7].

Pastaruosiu metu ląstelių ir karkasų pagrindu paremta audinių inžinerija sparčiai daro pažangą, ypač regeneracinės ortopedijos srityje. Audinių inžinerijos būdu paruoštų sąvarinės kremzlės transplantų (SKT) saugumo ir veiksmingumo kokybės parametrai priklauso nuo ląstelių ir kitų SKT sudedamųjų dalių sąveikos. Siekiant sukurti saugų ir efektyvų vaistinį preparatą klinikiniam taikymui, jis turi būti išsamiai ištirtas ir įvertintas.

Teisiniai biologinės kilmės vaistinių preparatų aspektai buvo pritaikyti ir naujiems regeneracinės medicinos biologiniams vaistams – pažangios terapijos vaistams (PTV) [8]. SKT yra sudarytas iš gyvų ląstelių, pasėtų ant skirtingos kilmės karkasų, todėl jų charakterizavimas turi atitikti kokybės standartus, užtikrinančius jų saugumą ir efektyvumą [10].

Ląstelinis komponentas yra SKT veiklioji medžiaga [11]. Karkasas – papildoma SKT medžiaga, kuri kartu su ląstelėmis suformuoja galutinį audinių inžinerijos prototipą. Tinkamų biomedžiagų ir gamybos metodų parinkimas yra neatsiejami PTV vystymo etapo darbai, kurie turi didelę įtaką ląstelių ir tarpląstelinės medžiagos (TLM) gamybai, vešėjimui šių sudedamųjų dalių sąveikai [12]. Natūralūs kolageniniai karkasai (CS) pasižymi biologiškai aktyviomis savybėmis, todėl jie palengvina sąveiką su ląstelėmis ir pagerina natūralaus kremzlinio audinio formavimąsi *in vitro* [13, 14]. Sintetinės kilmės karkasai gali būti gaminami taikant ir pažangias technologijas – tokias kaip tiesioginio lazerinio rašymo (TLR) litografija ikipolimerinėse medžiagose. Individualios morfologijos karkasai gali būti sukurti dėl TLR litografijos techninių galimybių, tokių kaip trijų dimensijų struktūrizavimo galimybės,

didelė erdvinė skiriamoji geba, mastelio lankstumas ir tinkamų startinių medžiagų įvairovės [15–18]. TLR technologijos galimybės SKT vystymui dar nebuvo tirtos.

SKT biologinis suderinamumas labai priklauso nuo karkasų biomechaninių ir fizinių savybių *in vitro* [19, 20]. Šie struktūriniai ir morfologiniai parametrai yra kritiškai svarbūs SKT biosuderinamumui ir leidžia tolygiai pasiskirstyti pasėtoms somatinėms ląstelėms ir užtikrinti efektyvų mitybinių medžiagų, mikroelementų ir dujų pernašą karkase [24, 25]. Be to, poros morfologija gali būti sukurta, remiantis iš anksto nustatytais parametrais, tai leidžia optimaliai valdyti kremzlinio audinio formavimąsi bei TLM baltymų gamybą sąveiką su ląstelėmis *in vitro* [26]. Taip pat biomechanškai tvirta karkaso struktūra, atsparumas ir pagerėjusios ląstelių prisitvirtinimo charakteristikos *in vitro* sudaro prielaidas tikėtis didesnio SKT biologinio suderinamumo ir didesnių apkrovų po implantacijos palaikymo [13, 27].

Kremzlinio audinio ląstelių – chondrocitų – gebėjimas efektyviai prisitvirtinti prie karkasų labai priklauso nuo šių ląstelių gyvybingumo. Gebėjimas formuoti jungtis su karkaso struktūra turi reikšmingos įtakos ląstelių augimui ir gebėjimui išskirti kremzlinį TLM ant karkasų. Todėl optimalių biomedžiagų morfologinių parametru, tinkamų specifiniams ląstelių procesams, nustatymas yra neatsiejama SKT vystymo dalis [28].

Ikiklinikinis SKT efektyvumas *in vitro* yra nustatomas pagal hialininei sąnarinei kremzlei būdingų baltymų raišką ir išskyrimą [29]. Prarasta vienasluoksnių ląstelių hialininės kremzlės genų raiška gali būti atkurta ląstelių auginimo biologiškai suderinamoje trijų dimensijų karkaso kultūros metu [30]. Todėl genų, koduojančių hialininei kremzlei specifiską II tipo kolageno baltymą, raiškos padidėjimas rodo ląstelių atsikūrimą į pirminį genotipą – rediferenciaciją – ir SKT funkcionalumo – fenotipo – padidėjimą *in vitro*. Ar inovatyvus trijų dimensijų karkasas turės įtakos ląstelių dauginimuisi, genotipui ir fenotipui, dar nebuvo tirta.

SKT apibūdinantys kokybiniai parametrai leidžia vertinti karkaso saugumą ir veiksmingumą, nes išsamiai apibūdina ląstelinę ir papildomasias SKT dalis bei jų tarpusavio sąveiką. Nepaisant žinomų SKT klinikiniam gydymui taikomų teisinių reglamentavimo gairių, tinkamas PTV charakterizavimas yra vis dar didelis iššūkis SKT vystytojams [9, 10]. Taip pat naujausių technologijų, tokių kaip TLR litografijos taikymas karkasų kūrimui, o ypač klinikinis veiksmingų SKT panaudojimas, vis dar yra ribotas dėl nenuoseklių gamybos metodų, nepakankamų charakterizavimo ir ikiklinikinių saugumo ir veiksmingumo tyrimų [31].

Šio darbo metu siekėme įvertinti TLR litografijos metodą, norėdami sukurti ir charakterizuoti optimalių morfologinių parametru, hibridinį organinį ir neorganinį (HOI) trijų dimensijų karkasą ir įvertinti jo biologinį

suderinamumą su gyvūno ir žmogaus ląstelėmis *in vitro* ir *in vivo* ikiklinikiniuose kremzlės regeneracijos modeliuose.

2. Darbo tikslas

Įvertinti pažeistos sąvarinės kremzlės gydymo saugumą ir efektyvumą ikiklinikiniuose modeliuose, naudojant inovatyvų mikrostruktūrizuotą kremzlės audinio inžinerijos produktą.

3. Užduotys

1. Sukurti pirminius HOI karkasus ir įvertinti jų biologinį suderinamumą su triušio chondrocitais *in vitro* studijose.
2. Įvertinti pirminio SKT saugumą ir veiksmingumą ilgalaikiame triušio sąvarinės kremzlės pažeidimo modelyje.
3. Optimizuoti HOI karkasus ir įvertinti jų biologinį suderinamumą su žmogaus chondrocitais *in vitro* studijose.
4. Įvertinti optimizuoto SKT saugumą ir veiksmingumą ilgalaikiame žiurkės sąvarinės kremzlės pažeidimo modelyje.

4. Mokslinis darbo naujumas ir jo praktinis pritaikymas

Sąvarinė kremzlė yra kraujotakos ir inervacijos neturintis audinys, susidedantis iš vieno tipo ląstelių – chondrocitų, – apsuptų ir įterptų į savo pačių išskirtą TLM tinklą. Kraujotakos nebuvimas kremzlės audinyje neleidžia vykti savaiminei kremzlės regeneracijai po pažeidimo, o dėl inervacijos stokos pacientai nejaučia skausmo, esant pažeidimui, todėl gali dar labiau pažeisti sąvarinės kremzlės audinį. Nepaisant santykinai paprasto kremzlės audinio, per pastaruosius 30 metų dar nepavyko pasiekti visiškos hialininės kremzlės audinio regeneracijos.

Šio periodo metu buvo bandomos įvairios kremzlės atkūrimo metodikos, pasižyminčios skirtingais efektyvumo rodikliais. Bandymų metu buvo prieita prie išvados, kad norint pasiekti hialininę ar į hialininę kremzlę panašią audinio regeneraciją reikia įtraukti tam tikrus šios regeneracinės procedūros parametrus. Viena pažangiausių metodikų yra karkasų naudojimas su pasėtomis ląstelėmis arba be jų. Siekiant sukurti saugius ir efektyvius audinių inžinerijos būdu pagamintus SKT, buvo išbandyta daugybė skirtingų biomedžiagų ir jų paruošimo būdų. Nepaisant to, biologiškai, chemiškai ir morfologiškai biologiškai suderinamų karkasų paieška vis dar tęsiama.

Šiame darbe išbandėme naują karkasų gamybos metodą, pasitelkdami greitųjų impulsų TLR litografiją ir sukurdami biologiškai suderinamus karkasus sąvario kremzlės regeneracijai. Pirmą kartą mikrometrų tikslumo femtosekundinio lazerio sistema buvo naudojama, gaminant pasirinktinai

morfologijos trijų dimensijų HOI karkasus. Mes parodėme, kad pasirinktina karkaso morfologija ir jos lemiamos biomechaninės savybės daro didelę įtaką naujos kremzlės susiformavimui.

Kadangi gamyboje naudojamų biomedžiagų parinkimas ir kultivavimo būdai yra pagrindiniai veiksmingo SKT gamybos komponentai, šiame darbe buvo atlikta išsami TLR mikrostruktūrizuotų ir morfologiškai skirtingų karkasų biologinio suderinamumo analizė. Biologinis organinių ir neorganinių karkasų, pasėtų gyvūno bei žmogaus chondrocitais, suderinamumas buvo tirtas *in vitro* ir *in vivo* ikiklinikinėse studijose ir palygintas su ląstelėmis pasėtų kolageno karkasų (CS) biologiniu suderinamumu. Visuose tyrimuose parodėme, kad HOI ir CS medžiagos yra biologiškai suderinamos ir nedaro beveik jokio žeidžiamojo poveikio pasodintiems chondrocitams.

Dėl palankios chondrocitų ir HOI karkasų sąveikos buvo gauta naujų duomenų apie pagrindinius morfologinius ir kultivavimo parametrus, kuriuos vėliau bus galima pritaikyti, atliekant ikiklinikinius tyrimus su dideliais gyvūnais.

Taip pat tyrimai su kolageninių karkasų ir chondrocitų konstruktais parodė gerus saugumo ir veiksmingumo duomenis visuose mūsų atliktuose ikiklinikiniuose tyrimuose. Todėl šie konstruktai bus toliau vystomi, remiantis Europos Farmakopėjos monografijomis bei siekiant šių SKT panaudojimo klinikiniuose tyrimuose.

5. Medžiagos ir metodai

5.1. Karkasų gamyba

Pirminio ir galutinio tyrimų metu trijų dimensijų silicio ir cirkonio karkasams gaminti buvo naudojama didelės galios ir energijos Yb:KGW femtosekundinio lazerio sistema (Pharos, Šviesos konversija, Vilnius, Lietuva), generuojanti 1030 nm centrinio bangos ilgio ir 300 fs trukmės impulsus su reguliuojamu pasikartojimo dažniu 1–200 kHz diapazone. Gamybos metu bangos ilgis buvo padvigubintas iki 515 nm, o pasikartojimo dažnis nustatytas iki 200 kHz. Židinio taško padėtis polimero pirmtako viduje buvo nustatyta, naudojant begalinio matymo lauko režimą ir panaudojant galvanometro skaitytuvą (Scanlab, Miunchenas, Vokietija) ir linijinių padėklų (Aerotech, Pitsburgas, PA, JAV) sinchronizuotą judėjimą.

Trijų dimensijų mikrostruktūrizuoti polimeriniai karkasai buvo pagaminti naudojant TLR litografijos metodą. Skaitmeniniai modeliai buvo sukurti naudojant kompiuterinę dizaino programinę įrangą arba specialiai sukurtą 3DPoli paketą (Femtika, Vilnius, Lietuva), o suformuoti sutelkiant femtosekundinio lazerio spindulį į šviesai jautrų polimero pirmtaką [63, 87, 88].

Hibridinis organinis ir neorganinis polimero pirmtakas, paveiktas 1 proc. 2-benzil-2-dimetilamino-4'-morfolinobutirofenono (DBMP, Sigma Aldrich, Sent Luisas, MO, JAV) šviesos iniciatoriumi, buvo naudojamas kaip pradinė medžiaga [89]. Polimero pirmtakas buvo sukurtas TLR litografijos taikymui, todėl pasižymi puikiomis trijų dimensijų mikro- / nanostruktūrizavimo galimybėmis.

Mėginio paruošimas struktūrizavimui buvo atliktas reikiama dengiamojo stiklo plotą (atsižvelgiant į reikalingų karkasų kiekį) padengiant skystu polimero pirmtaku ir pašildant. Ant iš anksto pašildyto sluoksnio buvo uždėtas dar vienas polimero pirmtako sluoksnis ir vėl pradėtas kaitinimo procesas. Todėl buvo atlikti keli nuoseklūs kaitinimo etapai kaitlentėje, kad polimero pirmtako lašo aukštis viršytų iš anksto nustatytą karkasų aukštį. Vėliau tirpiklis buvo visiškai išgarinamas iš polimero pirmtako, inkubuojant mėginius per naktį 70–75 °C temperatūroje.

Polimerizacijos reakcija buvo pradama sukeldama daugiafotoninę absorbciją, esančią arti židinio. Polimerizacijos metu gelio pavidalo medžiaga yra paverčiama kietos būsenos, pasiekiant nustatytos mikroarchitektūros karkasą.

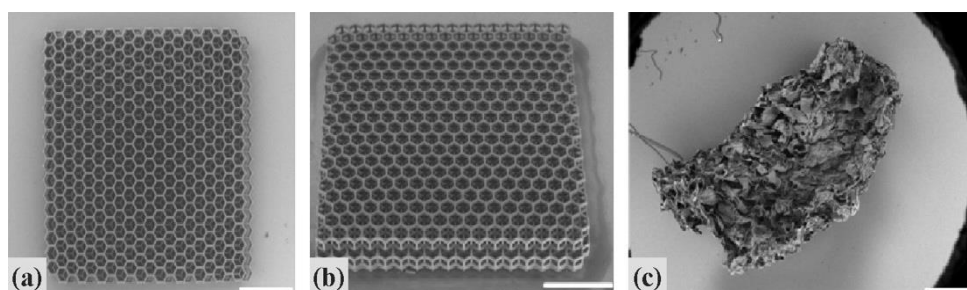
Karkasų gamybai pasirinkta hibridinio organinio ir neorganinio silicio bei cirkonio junginio šviesos polimeras SZ2080 (Forth-Iesl, Heraklionas, Graikija), kuris yra sudarytas iš 20 vienas iš geriausių neorganinių ir 80 proc. organinių dalių [126].

Individualūs CS buvo steriliai supakuoti, o HOI buvo chemiškai dezinfekuojami 70 proc. etanolio tirpale per naktį ir po džiovinimo UV spinduliuote kaitinami 2 val. Kitą dieną HOI buvo plaunami fosfatinu buferiniu druskos tirpalu (Sigma Aldrich) ir paliekami džiuoti bei vėlesniam ląstelių sėjimo procesui.

5.1.1. Pirminė studija: HOI ir CS gamyba

HOI buvo gaminami kaip šešiakampės struktūros, kurias sudarė 3 vieno-di sluoksniai, suformuoti vienas ant kito. Kiekvienas sluoksnis turėjo pusės periodo poslinkį apatinio sluoksnio atžvilgiu. Bendrieji karkasų matmenys buvo nustatyti prieš paruošimą, įvertinant triušio sąnario kremzlės plotą ir storį. Pagrindiniai morfologiniai parametrai buvo nustatyti 2,1×2,1×0,21 mm³, atitinkantys numatytą kremzlės pažeidimo plotą. Įvertinus, jog vienos ląstelės dydis yra apie 20–30 μm, vieno šešiakampio skersmuo buvo nustatytas 100 μm, siekiant užtikrinti, kad ląstelės gebės netrukdomai vežėti per visus HOI struktūros sluoksnius. HOI struktūrą sudarančios sijos aukštis ir plotis parinktas 15 μm, atsižvelgiant į anksčiau atliktus vystymo darbus ir įvertinus, kad ląstelės tinkamai prisitvirtindavo prie tokio išmatavimo karkaso sijos ir

išlaikydavo sferinę, o ne plokščią morfologiją. Viršutinių HOI porų parametrai, t. y. atstumas tarp 2 lygiagrečių viename aukštyje esančių sijų buvo nustatytas atitinkamai 42 ir 49 μm pločio ir ilgio ir atspindėjo siauriausią perėjimą iš HOI viršaus į apačią, siekiant efektyviausio ląstelių gebėjimo pereiti per sluoksnius. Šoninės poros nustatytos remiantis viršutinių porų dydžio parinkimo metodika ir buvo atitinkamai 51 ir 54 μm pločio ir ilgio. CS (Septodont, Maidstone, JK) buvo naudojamas tiesioginei palyginimo kontrolei. CS sudaro natūralus, nedentūruotas, liofilizuotas I tipo galvijų kolagenas. CS buvo supjaustytas tais pačiais matmenimis, kad karkasus būtų galima palyginti tarpusavyje. Pagamintų HOI morfologinės savybės ir skenuojančios elektroninės mikroskopijos (SEM) fotografijos pateiktos 5.1.1.1 pav. (a, b). Paruošto CS SEM fotografija pateikta 5.1.1.1 pav. (c).



5.1.1.1 pav. Pagaminto HOI karkaso SEM vaizdai iš (a) viršaus, (b) šono ir (c) CS

Trys sluoksniai, susidedantys iš atitinkamai 13 ir 14 šešiakampių kamerų, kurių plotis ir ilgis yra 100 μm . Šoninių porų plotis ir aukštis visame karkase buvo atitinkamai 51 ir 54 μm . CS sudaro natūralus, nedentūruotas, liofilizuotas I tipo galvijų kilmės kolagenas. Mastelis: 500 μm .

5.1.2. Galutinė studija: HOI optimizavimas ir kolageno karkasų gamyba

Keturių skirtingų tipų HOI kompiuteriniai modeliai buvo sukurti ir naudoti tolimesnės gamybos ir tyrimų metu. Siekiant nustatyti poros formos įtaką ląstelių augimui, pirmuoju tyrimo etapu buvo tiriami kvadratiniai / tetragoniniai (HOI-T) ir šešiakampiai / heksagoniniai (HOI-H) karkasai. HOI-T ir HOI-H sudarė atitinkamai stačiakampės ir korio formos tuščiavidurės prizmės, kurios buvo sudėtos viena šalia kitos, kad sudarytų vieną karkaso sluoksnį. Kiekviename karkase buvo trys tokie sluoksniai, suformuoti vienas ant kito.

Antruoju tyrimo etapu, norint nustatyti poros dydžio įtaką ląstelių augimui, HOI-T viršutinės ir šoninės poros buvo padidintos 1,5 (HOI-T1,5) ir 2 (HOI-T2) kartus.

Dvisluksniai CS (Chondro-Gide, Geistlich Biomaterials, Wollhusen, Šveicarija) buvo paruošti tokių pačių išorinių matmenų kaip ir HOI ir buvo naudojami tiesioginiam palyginimui. CS yra pagamintas iš labai rafinuoto kiaulės kolageno ir įrodytas, kad jis veiksmingas trauminių kremzlių defektų gydymui [90].

5.2. Karkasų charakterizavimas *in vitro*

Pirminio ir galutinio tyrimo metu morfologijos analizei atliktas SEM tyrimas, skalaujant karkasus su šiltu fosfatiniu buferiniu tirpalu ir fiksuojant 2,5 proc. vandeniniu glutaraldehido tirpalu 30 minučių. Karkasai buvo skalaujami ir dehidratuojami didėjančios etanolio koncentracijos tirpalais – 25 proc., 50 proc., 75 proc., 90 proc. ir 96 proc. Mėginiai buvo džiovinami kritinio taško džiovintuve (K850, Quorum Technologies, Lewes, JK), padengiami 20 nm storio aukso sluoksniu, naudojant rotorinį dengiklį (Q150R, Quorum Technologies) ir tiriami.

5.2.1. Pirminė studija: HOI morfologinė analizė

Morfologija: HOI konstrukto porų užpildymas ląstelėmis buvo apskaičiuotas, vertinant SEM tyrimo duomenis 4-ą, 8-ą ir 12-ą kultivavimo dienomis. Vertinant SEM fotografijas buvo apskaičiuota tuščių ir užpildytų porų procentinė išraiška.

5.2.2. Galutinė studija: HOI ir CS morfologinė ir biomechaninė analizė

Morfologija: Pagaminti ir ląstelėmis sodinti HOI konstruktai buvo vertinami po 7 dienų trijų dimensijų *in vitro* auginimo.

Biomechaninis: Tyrimams naudota modulinė matavimo sistema (OPX-MCT, Anton Paar, Gracas, Austrija) su neporingu pusiau sferinės formos 200 μm spindulio deimantiniu antgaliu, o išspaudimo vaizdas buvo stebimas optiniu mikroskopu. Karkasas buvo tiriamas, naudojant ciklinį apkrovimo ir nukrovimo režimą. Pirmiausia bandinys 300 mN/min. greičiu buvo apkraunamas pradine 8–10 mN jėga, kuri per 30–90 apkrovos ciklų buvo didinama iki maksimalios 150–350 mN vertės. Kai kuriais atvejais buvo naudota 120 apkrovos ciklų, o maksimali apkrova buvo didinama iki 900 mN. Kiekvieno apkrovimo ciklo atveju pasiekus maksimalią vertę, ciklo apkrova buvo laikoma 10 s, po kurių karkasas buvo nukraunamas 20–60 mN/min. greičiu. Trukmė tarp apkrovimo ir nukrovimo ciklų buvo 10 s. Karkaso

apkrovimas ir nukrovimas įspaudėju buvo atliekamas pagal trapezoidinę funkciją. Vidutinė HOI gniuždymo jėga buvo nustatyta pagal apkrovos ir įdubimo gylio kreives. Įdubimo kreivės buvo padalytos į 1-ą, 2-ą ir 3-ą sritis arba atitinkamai į viršutinį, vidurinį ir apatinį karkaso sluoksnius. Kiekviename HOI sluoksnyje gautas didžiausias jėgas žymi atitinkamos A, B ir C smailės. HOI ir CS biomechanines savybes atspindi viena smailė maksimaliame įdubimo gylyje, esant sausai ir šlapiai būsenai. Ciklinio proceso metu buvo užrašoma kiekvieno ciklo apkrova ir poslinkis (įspaudimo gylis), gaudant apkrovos – poslinkio kreivę. Naudojantis nanoįspaudimo bandymo metu gautomis apkrovos ir poslinkio kreivėmis, Oliverio–Faro metodu, poslinkio kitimo duomenimis ir jų tarpusavio santykiais, buvo nustatyti tirtųjų biomechaninių kietumas H_{IT} ir redukuotas modulis E_{IT} (antgalio ir bandinio kombinuotas modulis).

5.3. Ląstelių išskyrimas, kultivavimas ir pozologija *in vitro*

Pirminio ir galutinio tyrimų metu visos eksperimentinės procedūros buvo patvirtintos ir atliktos vadovaujantis Gyvūnų sveikatos ir gerovės departamento, Lietuvos Respublikos valstybinės maisto ir veterinarijos tarnybos bei Kauno regiono biomedicininų tyrimų etikos komiteto standartinėmis gairėmis ir protokolais.

5.3.1. Pirminis tyrimas: Ląstelių išskyrimas, kultivavimas ir trijų dimensijų kultūros pozologija

Naujosios Zelandijos triušiai (patinai ir patelės; 4–5 mėn. amžiaus; 3–4 kg kūno svorio) buvo laikomi įprastomis sąlygomis (21 ± 1 °C temperatūros, 12/12 šviesos / tamsos ir 45 proc. santykinės drėgmės režimai), atskirai narvuose su laisva prieiga prie maisto ir vandens.

Alogeninė triušio sąnario kremzlės biopsija iš krūvio negaunančios srities buvo sumalta ir skaidyta 2,5 proc. tripsino (Invitrogen, Carlsbad, CA, JAV) ir kolagenazės XI (Sigma Aldrich) tirpalais. Išskirtos ląstelės buvo išsėtos, kultivuojamos ir surinktos, kai buvo pasiekta 80 proc. flakono dugno padengimas. Ląstelės buvo auginamos mitybinėje terpėje (DMEM/F12, Sigma Aldrich) papildytoje 10 proc. veršelio serumo (Lonza, Bazelis, Šveicarija), 100 VV/ml penicilino ir 100 µg/ml streptomicino (Sigma Aldrich). Flakonų inkubacija buvo atliekama CO₂ inkubatoriuje (37 °C temperatūra, 90 proc. drėgmės atmosfera su 5 proc. CO₂ dujų).

Karkasai 1 dieną prieš sėjimą buvo laikomi dauginimo terpėje. Karkaso sėjimui reikalingas ląstelių kiekis buvo apskaičiuotas įvertinus kremzlės defekto dydį ir turimą karkaso morfologiją. Po tripsinizacijos su 0,25 proc. tripsinu trečiojo persėjimo ląstelės buvo suskaičiuotos ir suspenduotos

10^7 ląstelių / 1 ml koncentracijos tirpale. Ląstelės buvo sėjamos 10 μ l dozėmis ant sterilių HOI ir CS. Pasėti konstruktai 2 valandoms buvo dedami į CO₂ inkubatorių, siekiant ląstelių prisitvirtinimo, o vėliau papildomi mitybinės terpės.

Terpė buvo keičiama kas 3–5 dienas, o pasėti konstruktai kultivuojami iki 12-os dienos. Konstruktai su ląstelėmis buvo surinkti po 4-į, 8-į ir 12-os dienų auginimo ir išsiųsti *in vitro* tyrimams. Taip pat 12-os auginimo dienos karkasai buvo paruošti implantavimui *in vivo*.

5.3.2. Galutinis tyrimas: Ląstelių išskyrimas, kultivavimas ir trijų dimensijų kultūros pozologija

Žmogaus sąnarinės kremzlės audinys buvo imamas kelio kryžminio raiščio rekonstrukcijos metu.

Biopsija buvo plaunama fosfatiniu buferiu, dvi valandas skaidoma proteazės (Sigma Aldrich) ir per naktį – kolagenazės A (Worthington, Lakewood, NJ, JAV) fermentais. Išskirtos ląstelės buvo pasodintos ir kultivuojamos mitybinėje terpėje (DMEM, Thermo Fisher, Logan, UT, JAV), papildytoje 10–20 proc. galvijo serumo (Sigma Aldrich), 100 VV/ml penicilino ir 100 μ g/ml streptomocinas (Sigma Aldrich) 37 °C temperatūroje, drėgnoje atmosferoje su 5 proc. CO₂ dujų. Ląstelės buvo surinktos, kai flakono padengimas siekė 80–90 proc.

Karkasai vieną dieną prieš sėjimą buvo mirkomi dauginimo terpėje. Ląstelių dozavimas buvo susietas su poreikiu 1×10^6 ląstelių padengti 1 cm² karkaso plotui. Pagaminti HOI ir CS parametrai buvo $1,5 \times 1,5$ mm² dydžio, todėl apskaičiuota $4,5 \times 10^4$ ląstelių dozė atitinka numatytąjį gydymui skirtą ląstelių kiekio poreikį.

Po tripsinizacijos su 0,25 proc. tripsino (Invitrogen), trečiosios persėjimo ląstelės buvo suskaičiuotos ir vėl suspenduotos. Ląstelės buvo sėjamos 40 μ l dozėmis ant sterilių HOI ir CS. Pasėti karkasai dviem valandoms buvo dedami į CO₂ dujų inkubatorių.

Terpė buvo keičiama kas 2–3 dienas, o pasėti konstruktai buvo kultivuojami iki 7-os dienos. Konstruktai su ląstelėmis buvo surinkti po 1-os, 4-į ir 7-į dienų auginimo ir siunčiami *in vitro* tyrimams. Taip pat 7-tą kultivavimo dieną karkasai buvo paruošti implantavimui *in vivo*.

5.4. Pasėtų karkasų biocheminis charakterizavimas *in vitro*

Pirminio ir galutinio tyrimų metu II tipo kolageno baltymo išskyrimui nustatyti buvo taikytas imunofermentinis ELISA tyrimo metodas, remiantis gamintojo protokolu. 200 μ l mėginio buvo įpilta į 96 šulinėlių plokštelę ir

optinio tankio sugertis buvo nuskaityta mikroplokštelių skaitytuvu (Multiskan GO, Thermo Scientific), naudojant 450 nm ilgio apšvietą. Standartinė kreivė buvo išreikšta kaip santykinis kiekvieno standartinio tirpalo optinis tankis su atitinkama standartinio tirpalo koncentracija. II tipo kolageno baltymo koncentracija mėginiuose buvo vertinama pagal standartinę kreivę.

5.4.1. Pirminis tyrimas: Monosluoksnio ir trijų dimensijų kultūros baltymų išskyrimo vertinimas

II tipo kolageno baltymo išskyrimo vertinimas buvo atliktas, tiriant ant karkasų sėjamas vienasluoksnes ląsteles, taip pat HOI ir CS konstruktus, sodintus ląstelėmis 4-ą, 8-ą ir 12-ą dienomis po sėjimo. Tyrimui naudotas triušio II tipo kolageno baltymo ELISA rinkinys (Biosite, Londonas, JK), o tyrimas atliktas pagal gamintojo protokolą.

5.4.2. Galutinis tyrimas: Monosluoksnio ir trijų dimensijų kultūros metabolinio aktyvumo, ląstelių skaičiaus ir biocheminis vertinimas

Ląstelių metabolinis aktyvumas HOI-T ir HOI-H konstruktuose buvo atliktas, naudojant gyvybingumo reagento (Presto Blue, Invitrogen) tirpalą pagal gamintojo rekomendacijas. Gyvybingumo reagentas yra citotoksiškas, resazurinu pagrįstas metabolinis tyrimas ir yra skirtas ląstelių gyvybingumui nustatyti. Jis matuoja mitochondrijų ląstelių gebėjimą versti nefluorescencinį mėlyną resazurinę į rožinį rezorufino, tokiu būdu įvertinant ląstelių ir karkasų biologinį suderinamumą. Tyrimas buvo atliktas 1-ą, 4-ą ir 7-ą dienomis po sėjimo ant karkasų. Kiekvienas karkasas buvo panardinamas 10 proc. gyvybingumo reagento tirpale ir inkubuojamas 30 minučių 37 °C temperatūroje CO₂ dujų inkubatoriuje. Mėginiai buvo surinkti, o spalvos sugertis įvertinta plokštelių skaitytuvu (Multiskan GO, Thermo Scientific), naudojant 570 nm apšvietą. Po tyrimo buvo nubrėžta konstrukto ir vienasluoksnių ląstelių spalvos sugerties ir metabolinio aktyvumo santykio standartinė kreivė. Ląstelių skaičiui konstruktuose įvertinti buvo naudojama standartinė spalvos sugerties ir ląstelių tankio monosluoksnyje kreivė.

II tipo kolageno baltymo išskyrimo vertinimas atliktas matuojant vienasluoksnes ląsteles, naudojamas sėjimui ant karkasų, taip pat HOI ir CS sodintų ląstelėmis 1-ą, 4-ą ir 7-ą dienomis po sėjimo. Tyrimui naudotas žmogaus II tipo kolageno baltymo ELISA rinkinys (Biosite, Londonas, JK), o tyrimas atliktas pagal gamintojo protokolą.

5.5. HOI konstrukto genotipinis charakterizavimas *in vitro*

Pirminio ir galutinio tyrimų metu informacinė ribonukleininė rūgštis (iRNR) iš mėginių buvo išskirta, naudojant išskyrimo rinkinį (Isolate II RNA, Bioline Reagents Ltd, Londonas, JK) pagal gamintojo instrukcijas. Eliucija buvo atliekama naudojant 10 µl vandens be RNazės. Atvirkštinės transkriptazės kiekybinės polimerazės grandinės reakcijai (RT-kPGR) atlikti buvo naudojami pradmenys (SensiFAST Probe No-ROX One-Step Kit, Bioline Reagents Ltd) ir hidrolizės zondai (Biolegio B. V., Nijmegen, Olandija). Visos vienos pakopos reakcijos buvo atliktos iš viso 15 µl tūrio, naudojant 6,75 µl išskirto iRNR mėginio ir pradmenis, kurių kiekvieno koncentracija buvo 200 nM, ir zondus, kurių kiekvieno koncentracija buvo 100 nM. Vieno žingsnio RT-kPGR tyrimai buvo atlikti naudojant realaus laiko termociklerį (Rotor-Gene-Q-5-plex, Qiagen GmbH, Hildenas, Vokietija) šiomis sąlygomis: pirmosios grandinės kopijinė DNR (kDNR) buvo susintetinta 45 °C temperatūroje 20 min. (1 ciklas), tada denatūruota 95 °C temperatūroje 2 min. (1 ciklas); po to 50 denatūravimo ciklų 10 s 95 °C temperatūroje ir 1 min. atkaitinimas / pailginimas 60 °C temperatūroje. $2^{-\Delta\Delta CT}$ algoritmas buvo naudojamas apskaičiuojant amplifikacijos produkto santykinius kiekius, atspindinčius tikslinės iRNR santykinius lygius [127].

5.5.1. Pirminis tyrimas: trijų dimensijų kultūros genų raiškos vertinimas

Konstruktai su ląstelėmis buvo surinkti po 4-ių, 8-ių ir 12-os dienų augimo ir išsiųsti genų raiškos tyrimams.

Kremzlinių genų iRNR analizei buvo ištirtos COL2A1 geno, koduojančio II tipo kolageną, ir COL10A1 geno, koduojančio X tipo kolageną, iRNR raiškos dinamikos ląstelėse prieš sėjimą ant karkasų bei 4-ą, 8-ą ir 12-ą dienomis po sėjimo. Duomenų normalizavimui buvo naudojama Europos triušio GAPDH geno raiška.

5.5.2. Galutinis tyrimas: vienasluoksnės ir trijų dimensijų kultūros genų raiškos vertinimas

Kremzlinio geno iRNR vertinimui buvo ištirta COL2A1 geno, koduojančio II tipo kolageną, iRNR raiškos dinamika ląstelėse prieš sėjimą ant karkasų bei 1-ą, 4-ą ir 7-ą dienomis po sėjimo. Pradmenų ir zondo sekos buvo sukurtos naudojant kompiuterinę programą (Vector NTI Advance, Thermo Scientific). β-aktino iRNR raiška buvo naudojama kaip vidinis standartas, normalizuojant tikslinės iRNR raiškos lygį skirtinguose mėginiuose.

5.6. Ilgalaikio *in vivo* tyrimo dizainas

Pirminio ir galutinio tyrimų metu osteochondriniai defektai buvo suskirstyti į tiriamąsias grupes, kurioms atsitiktiniu būdu buvo paskirtas gydymas: pažeidimai, gydyti HOI šešiakampi konstruktu su ląstelėmis (HOI ląstelės, n = 4) ir be ląstelių (tik HOI, n = 4). Į teigiamos kontrolės grupes buvo įtraukti CS konstruktai su ląstelėmis (CS ląstelės, n = 3) ir be ląstelių (tik CS, n = 3). Neigiamą kontrolinę grupę sudarė pažeidimai be konstrukto (negydyta, n = 4). Po implantacijos girmelė buvo atstatyta, kelio sąnario kapsulė užsiūta pertraukiamomis 3–0 tirpstančiomis siūlėmis (Ethicon, Johnson & Johnson Medical, Somerville, NJ, JAV). Oda buvo susiūta 4–0 odos išsisine siūle (Ethicon) ir dezinfekuota.

5.6.1. Pirminis tyrimas: 6 mėnesių *in vivo* tyrimo dizainas

Tyrime buvo naudojami devyni triušiai, turintys 18 abipusių osteochondrinių defektų. Chirurginės procedūros buvo atliekamos operacinėje, laikantis aseptikos taisyklių. Anestezija buvo sukelta, leidžiant anestetikus į raumenis, o jos palaikymas – leidžiant į veną. Kelio sąnariai buvo atveriami šoniniu paragirneliniu pjūviu ir vidine girmelės dislokacija. Kritinio dydžio osteochondrinis defektas (skersmuo: 3 mm; gylis: 2 mm) buvo sukurtas elektriniu gražtu kelio vidinio šlaunikaulio gumburo srityje, gaunančioje atraminį krūvį.

Siekiant pritvirtinti ir stabilizuoti karkasus defekte, buvo formuojamas polimerizuotas fibrininis krešulys. Prieš implantuojant krešulį, kiekvienas sukurtas pažeidimas buvo plaunamas steriliu buferiniu tirpalu. Fibrino krešulio formavimui buvo sumaišyta 1 ml autologinės kraujo plazmos, 250 µl trombino ir 250 µl CaCl₂. Jis buvo inkubuotas 5 minutes kambario temperatūroje prieš pat implantuojant jį į pažeidimą.

Po intervencijos triušiai buvo laikomi įprastomis sąlygomis, jiems buvo leidžiama laisvai judėti atskiruose narvuose. Triušiams buvo atlikta eutanazija po 6 mėnesių, o kelio sąnario komplekso mėginiai paimti ištyrimui.

5.6.2. Galutinis tyrimas: 3 mėnesių *in vivo* tyrimo dizainas

Šiame tyrime buvo naudojamos devynios, 10 savaičių, imunosupresinės žiurkės (NIHRNU-M, NTac: NIH-Foxn1rnu; Taconic, NY, JAV). Per inhalacinę kaukę gyvūnams buvo skiriamos anestezijos dujos, kurių sudėtyje yra 3 proc. izoflurano ir deguonies dujų mišinys. Kelio sąnariai buvo operuojami, atliekant šoninį parapatelarinį pjūvį. Dislokavus girmelę į vidinę pusę, prieita prie sąnarinio paviršiaus. Kritinis osteochondrinis pažeidimas (diametras: 1,5 mm, gylis: 1 mm) buvo sukurtas krūviui tenkančioje skridinio vagos vietoje. Prieš karkasų implantaciją defektas buvo plaunamas steriliu fosfatinu buferiniu tirpalu. Siekiant fiksuoti karkasus arba užpildyti defektus be

karkasų, į defektą buvo leidžiami fibrino klijai (Tisseel, Baxter, Glendale, CA, JAV).

Po intervencijos žiurkės buvo laikomos bendruose narvuose ir leidžiamas laisvas judėjimas. Žiurkėms buvo atlikta eutanazija praėjus 3 mėnesiams po operacijos, o kelio sąnario komplekso mėginiai paimti tolimesniems tyrimams.

5.7. Makroskopinis ilgalaikio tyrimo vertinimas

Pirminio ir galutinio tyrimų metu du nepriklausomi tyrėjai atliko makroskopinį vertinimą pagal modifikuotą *Oswestry Arthroscopy Score* (OAS) skalę gyvūnų ir žmogaus ląstelėlių tyrimams.

OAS vertinimo sistemą sudaro atskirų regeneravusios kremzlės parametrų įvertinimas: transplantato lygis, integracija su aplinkine kremzle, kremzlės paviršiaus išvaizda ir regeneravusio audinio spalva. Sąnario kremzlės audinio kietumo vertinimas kabliuku buvo pakeistas objektyvesniu elektromechaninio parametro įvertinimu. Tačiau šis metodas nebuvo naudojamas galutinėje studijoje su žmogaus ląstelėmis dėl nepakankamo žiurkės kelio sąnario kremzlės paviršiaus ploto.

5.7.1. Pirminis tyrimas: regeneravusios kremzlės elektromechaninis įvertinimas *in vivo*

Regeneravusio kremzlės audinio elektromechaninės savybės buvo įvertintos naudojant rankinį artroskopinį įspaudikli-indentatorių (Arthro-BST, Biomomentum Inc., Laval, Kvebekas) [91]. Neigiamai įkrautos proteoglikano molekulės palaiko pusiausvyrą kartu su mobiliosiomis, teigiamai įkrautomis jonų molekulėmis, esančiomis sąnarinės kremzlės TLM kolageno tinklo intersticiniame skystyje. Dėl kremzlės išorinio spaudimo atsiranda intersticinio skysčio tėkmė, todėl judantys teigiamai įkrauti jonai pasislenka fiksuotų neigiamų krūvių atžvilgiu. Dėl šios tėkmės susidaro srauto potencialai, patikimai atspindintys kremzlės sudėtį ir funkciją [91–93].

Aukštesnis elektromechaninis potencialas (EP) parodo padidėjusį tarp-ląstelinio audinio irimą, prastesnes biomechanines kremzlės savybes ir jos gebėjimą atlaikyti dideles apkrovas. Žemas EP, priešingai, rodo stiprias elektromechanines savybes ir gebėjimą atlaikyti didelius krūvius.

Vidinio šlaunikaulio gumburo EP buvo matuojamas prieš operaciją ir praėjus 6 mėnesiams po operacijos. Šlaunikaulio sąnarys buvo paimtas ištyrimui, pjaunant aukščiau šlaunikaulio gumburo, o EP matavimai buvo pakartoti 3 kartus tiriamosiose grupėse.

5.8. Regeneravusios kremzlės histologinis vertinimas

Pirminio ir galutinio tyrimų metu tolimoji šlaunikaulio dalis buvo pjauta virš gumburo, fiksuota 10 proc. neutraliu buferiniu formalino tirpalu ir įlieta į parafino blokus. 6 µm storio pjūviai buvo deparafinuoti ir dažyti Toluidino mėlynuoju (Fisher Scientific, Pitsburgas, PA, JAV) ir Safranin-O dažais (Fisher Scientific), siekiant įvertinti glikozaminoglikanų, proteoglikanų ir kolageno pasiskirstymą regeneravusioje kremzlėje [94]. Histologinių pjūvių nuotraukos buvo vertinamos, naudojant skaitmeninį mikroskopą (Olympus BX61, Olympus, Tokijas, Japonija) su fotoaparatu (Olympus DP72, Olympus). Aklausias vertinimas atliktas naudojant *O'Driscoll* vertinimo skalę [95]. Aukštesnis balas rodo geresnę kremzlės regeneraciją, o 24 yra didžiausias galimas balas.

5.9. Statistinis vertinimas

Pirminio ir galutinio tyrimo metu kiekybiniai duomenys buvo išreikšti vidurkiu su standartiniu nuokrypiu. Statistiniai skaičiavimai buvo atlikti, naudojant GraphPad Prism 7.04.

5.9.1. Pirminė studija: Statistinis vertinimas

Statistiniai rezultatai buvo gauti naudojant neparametrinį Kruskal-Wallis daugybinį palyginimo testą ir pateikti kaip vidurkis ir standartinis nuokrypis (SD). Statistinis reikšmingumas tarp tyrimo grupių yra pažymėtas (*), kuris reiškia, jog $p < 0,05$ ir (**), kuris reiškia, jog $p < 0,01$.

5.9.2. Galutinė studija: Statistinis vertinimas

Statistiniai rezultatai buvo gauti naudojant vienpusį ANOVA su Tukey daugkartiniu palyginimo testu. Rezultatai pateikiami kaip vidutinė reikšmė su skliausteliuose nurodytu standartiniu nuokrypiu (SD). Statistinis reikšmingumas tarp grupių žymimas (*), kuris reiškia, jog $p < 0,05$ ir (**), kuris reiškia, jog $p < 0,01$.

6. Rezultatai

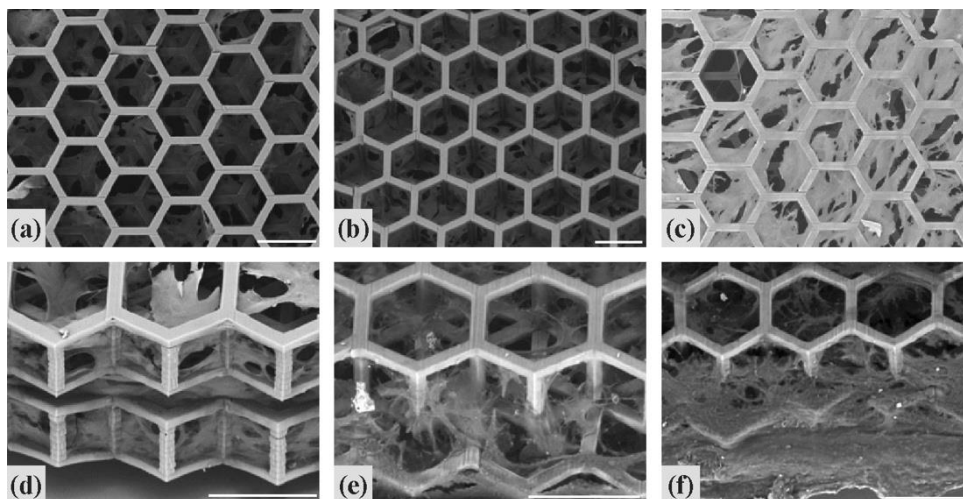
6.1. Pirminės studijos rezultatai

6.1.1. Vienasluoksnių ląstelių morfologija ir gyvybingumas

Vienasluoksnės kultūros metu buvo stebėta chondrocitų fenotipo kitimo dinamika. Ląstelės palaipsniui prarado savo natūralią apvalią formą ir tapo plokštesnės, įgijo į fibroblastus panašios ląstelės formą. Chondrocitų gyvybingumas prieš sėjimą ant karkasų buvo aukštas ir svyravo tarp 98–100 proc.

6.1.2. Pirminės studijos ląstelių sėjimo ir trijų dimensijų kultūros vertinimas

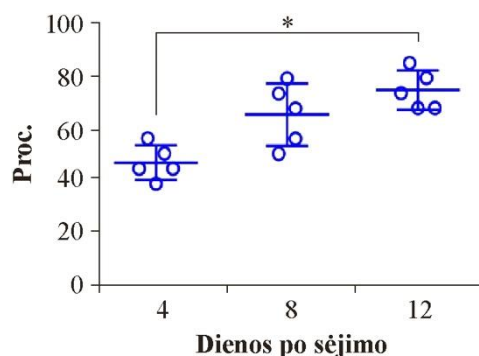
Ląstelės, pasėtos ant šešiakampio HOI, buvo glaudžiai sukibusios su horizontaliomis ir vertikaliomis karkaso sijomis. Ląstelių dauginimasis ir TLM gamyba karkasuose išliko iki 12-os dienos. Ovalios ir pailgos formos ląstelės buvo matomos ant horizontalių ir vertikalių sijų. Jungtys tarp netoliese esančių sijų daugiausia buvo sudaromos apraizgant ir sujungiant šalia esančias vertikaliąsias sijas. Ląstelių skaičius ir jungiantysis TLM padengė visus HOI konstrukto sluoksnius, jo gausėjimas tęsėsi ne mažiau kaip iki 12-os dienos, užpildydamas konstrukto vidinę erdvę ir padengdamas didžiąją poros skersmens dalį. Ląstelių augimas HOI pateiktas 6.1.2.1 pav.



6.1.2.1 pav. Ląstelės ir tarpusavyje jungiantis TLM pasiskirstymas visame trijų dimensijų šešiakampio pavidalo HOI SEM nuotraukos 4-ą (a), 8-ą (b) ir 12-ą (c) dienomis

Pailgos ir ovalios formos ląstelės prilipo ir sujungė horizontalius ir vertikalius karkasų sijas. Apvyniodami ir sujungdami šalia esančias sijas, ląstelės ir nusodintas TLM kiekis palaipsniui peraugo visus tris HOI sluoksnius, užpildydami didžiąją poros tūrio dalį 12-ą dieną. Priartin-tas vaizdas iš šono rodomas 4-ą (d), 8-ą (e) ir 12-ą (f) dienomis. Mastelis: 100 μm .

Padidėjęs porų padengimas buvo pastebimas visose trijų dimensijų kultūrose ne mažiau kaip iki 12-os dienos prieš implantaciją. Padengimas reikšmingai pagerėjo 12-ą dieną, palyginti su 4-a diena ($p = 0,0114$), ir uždengė $71 \pm 6,5$ proc. vienos poros skersmens. Poros padengimo ląstelėmis dinamika pateikta 6.1.2.2 pav.

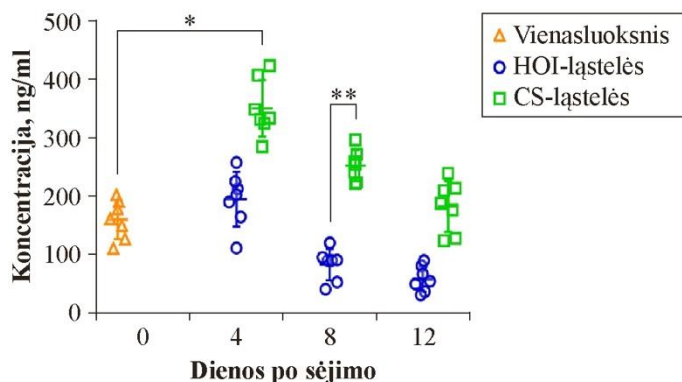


6.1.2.2 pav. HOI konstrukto porų padengimo sodintomis ląstelėmis dinamika

Užpildytų porų procentas žymiai padidėjo nuo 4-os iki 12-os dienos, tuo parodant biologiškai suderinamas morfologines sąlygas nuolatiniam ląstelių dauginimuisi. * $p < 0,05$.

6.1.3. Trijų dimensijų kultūros karkasų stiprumo vertinimas

HOI konstruktas su ląstelėmis palaikė kremzlinio audinio formavimąsi įprastomis auginimo sąlygomis. Tai buvo nustatyta, įvertinus trijų dimensijų kultūros II tipo kolageno baltymo išskyrimą į terpę bei palyginus išsiskyrimo aktyvumą su vienasluoksnių ląstelių, naudojamų karkasų sėjimui, išskyrimo lygiu. II tipo kolageno baltymo išskyrimo dinamika iki 12-os dienos yra pateikta 6.1.3.1 pav.

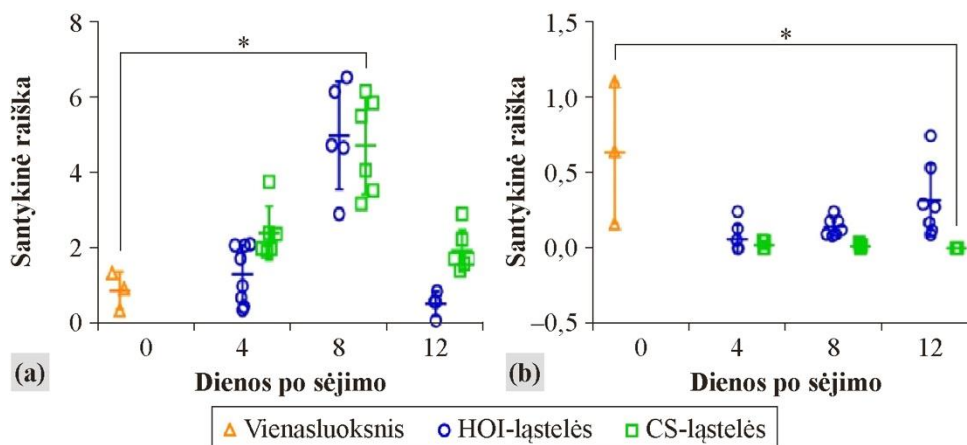


6.1.3.1 pav. II tipo kolageno baltymo išskyrimas, matuotas ELISA metodu vienasluoksnio, HOI ir CS grupėse vienasluoksnio ir po sėjimo 4-ą, 8-ą ir 12-ą dienomis

Abi grupės išlaikė išskiriamo baltymo kiekį nuo 4-os iki 12-os dienos, nors ir stebėtas nežymus išskyrimo sumažėjimas viso periodo metu. CS turėjo aukštesnį pradinį II tipo kolageno išskyrimo pajėgumą 4-ą ir 8-ą dienomis, palyginti su atitinkamai vienasluoksniomis ląstelėmis ir HOI. * $p < 0,05$, ** $p < 0,01$.

Baltymų išskyrimas HOI konstrukto su ląstelėmis grupėje nesumažėjo iki 12-os dienos, tačiau buvo stebėta nereikšmingo mažėjimo tendencija. Baltymų išskyrimas pagerėjo 4-ą dieną CS su ląstelėmis grupėje ($p = 0,03$), kuris reikšmingai nesumažėjo iki 12 dienos. Kai karkasai su ląstelėmis buvo lyginami tarpusavyje, CS-ląstelių grupėje 8 dieną buvo pastebėtas didesnis II tipo kolageno baltymo išskyrimo kiekis ($p = 0,0045$), parodantis aukštesnę pradinę ląstelių ir karkaso biologinio suderinamumo fazę CS su ląstelėmis grupėje. 12-ą dieną buvo pastebėtas skaitinis CS su ląstelėmis konstrukto pranašumas, palyginti su HOI su ląstelėmis konstrukto grupe tą pačią dieną.

Kremzlinio audinio COL2A1 geno raiška buvo padidėjusi abiejose grupėse iki 8-os dienos, tačiau nereikšmingai sumažėjo 12-ą dieną abiejuose grupėse. COL2A1 geno raiškos dinamika yra pateikta 6.1.3.2 pav. (a).



6.1.3.2 pav. (a) COL2A1 ir (b) COL10A1 genų raiškos modeliai, vertinti RT-kPCR metodu vienasluoksnyje, HOI ir CS grupėse 4-ą, 8-ą ir 12-ą dienomis

Chondrogenezė abiejose grupėse buvo padidėjusi iki 8-os dienos. (a) Vidutinis COL2A1 geno raiškos lygis padidėjo HOI 4-ą ir 8-ą dienomis. CS išlaikė aukščiausią raišką iki 8-os dienos, palyginti su vienasluoksniomis ląstelėmis. (b) Vidutinė fibroblastinės COL10A1 geno raiška buvo sumažėjusi abiejose konstrukto grupėse iki 12-os dienos. CS su ląstelėmis, kurių COL10A1 raiška buvo mažesnė 12-ą dieną, palyginti su vienasluoksniomis ląstelėmis. COL10A1 geno raiška CS buvo mažesnė, palyginti su HOI 12-os dienos. $*p < 0,05$.

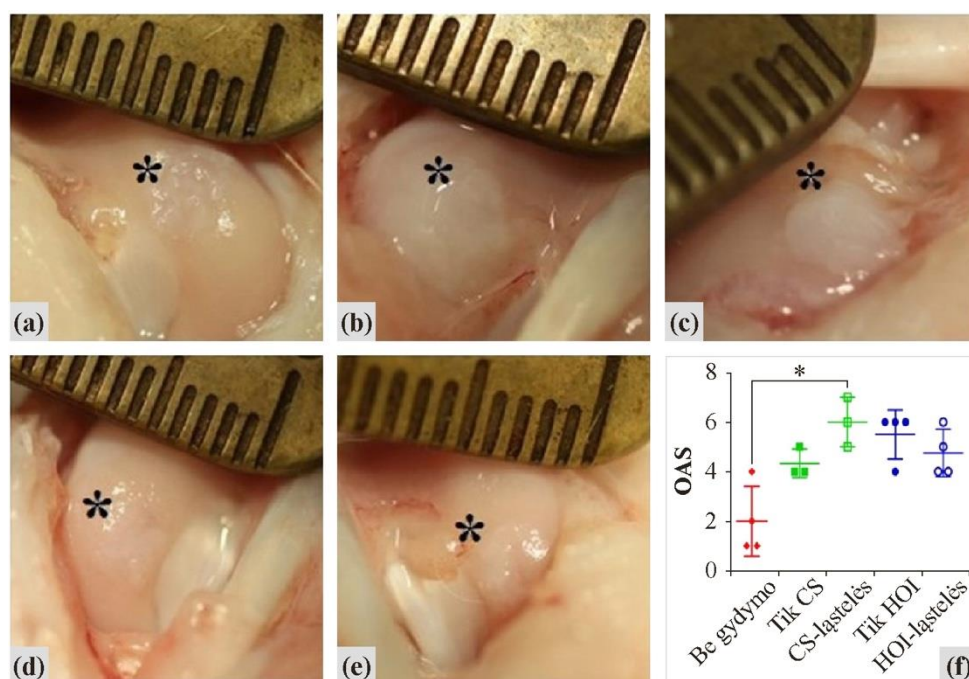
Nors vidutinis COL2A1 geno raiškos lygis padidėjo HOI-ląstelės grupėje 4-ą ir 8-ą dienomis, jis buvo panašus į sėjimo dienos rodiklius. CS-ląstelės grupė išlaikė aukštesnę vidutinę COL2A1 raiškos lygį iki 12-os dienos, palyginti su vienasluoksnių ląstelių geno raiška, tačiau jis žymiai pagerėjo 8-ą kultūros dieną ($p = 0,031$). Reikšmingų skirtumų tarp abiejų konstrukto nepastebėta; tačiau vidutinės vertės buvo mažesnės HOI-ląstelės grupėje, palyginti su CS-ląstelės grupe.

Vidutinis fibroblastinio COL10A1 geno raiškos lygis buvo sumažėjęs HOI-ląstelės ir CS-ląstelės grupėse, tokiu būdu palaikant ląstelių rediferenciaciją genotipiniu lygmeniu. COL10A1 geno raiška yra pateikta 6.1.3.2 pav. (b).

Vertinant fibroblastinio geno raišką, CS-ląstelės grupėje COL10A1 raiška buvo mažesnė nei vienasluoksnių ląstelių grupės ir dar labiau sumažėjo 12-ą kultūros dieną ($p = 0,035$).

6.1.4. Makroskopinis OAS vertinimas *in vivo*

6 mėnesius po operacijos triušio kelio sąnariuose nebuvo stebėta patinimo, uždegiminių požymių ar imuninės reakcijos į implantuotus konstruktus. CS-ląstelės grupė turėjo aukščiausią vidutinę OAS balo vertę tarp visų tyrimo grupių. Makroskopinis vertinimas yra pateiktas 6.1.4.1 pav.



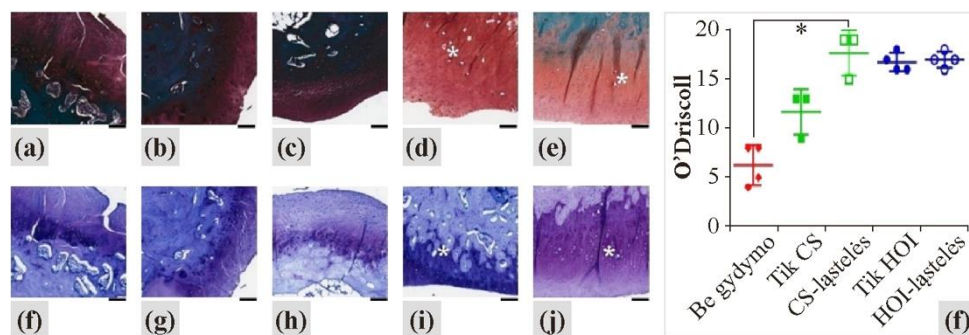
6.1.4.1 pav. Makroskopinis eksperimentinių grupių įvertinimas praėjus 6 mėnesiams po operacijos: (a) be gydymo, (b) tik CS, (c) CS-ląstelių, (d) tik HOI ir (e) HOI-ląstelių grupėse, apskaičiuojant (f) OAS balo vertes

CS-ląstelės turėjo aukščiausią vidutinę (f) OAS rezultatą tarp visų eksperimentinių grupių. Tik HOI ir HOI-ląstelės grupės turėjo skaitinį pranašumą, palyginti su negydyta grupe. Kremzlės regeneracija (žvaigždutė), buvo akivaizdi visose gydymo grupėse, tačiau smulkios pavienės atplaišos kremzlės paviršiuose buvo matomos visose HOI ir HOI-ląstelės grupėse, o lygesnis kremzlės paviršius buvo matomas visose CS grupėse. * $p < 0,05$.

CS-ląstelės grupės OAS įvertinimas parodė, kad regeneravęs kremzlinis audinys yra panašiausias į hialininę kremzlę, palyginti su negydytos grupės rezultatu ($p = 0,035$). Kitos eksperimentinės grupės tarpusavyje reikšmingai nesiskyrė; tačiau pastebėta tendencija, kad OAS rezultatai buvo geresni HOI ($p = 0,076$) ir HOI-ląstelės ($p = 0,69$) grupėse, palyginti su negydyta grupe. Prastesniam makroskopiniam vertinimui HOI grupėse daugiausia įtakos turėjo didesnis kremzlės atplaišų kiekis sąnariname paviršiuje, palyginti su lygesniu kremzlės paviršiumi CS grupėse.

6.1.5. Histologinis vertinimas *in vivo*

Sąnarinės kremzlės regeneracijos histologinis vertinimas buvo geresnis visose gydytose grupėse, palyginti su negydyta grupe, 6 mėnesiai po implantacijos. Tačiau tik CS-ląstelės grupėje histologiniai rezultatai buvo reikšmingai geresni už neigiamą kontrolės ($p = 0,035$) grupę. Taip pat buvo nustatyta aiški HOI-ląstelės grupės geresnės regeneracijos tendencija, palyginti su negydyta grupe ($p = 0,057$). Kitos tyrimo grupės buvo panašios tarpusavyje, tačiau tik HOI grupė turėjo polinkį į geresnę histologinę regeneraciją, palyginti su negydyta grupe ($p = 0,1$). Nė vienoje grupėje subchondrinis kaulas nebuvo atkurtas, o nežymūs pokremzlinės ribos netolygūs kontūrai buvo stebimi visose grupėse. HOI struktūriniai elementai buvo išsklaidyti recipiento kremzliniame ir pokremzliniame sluoksniuose, tačiau nebuvo pastebėta jokių infekcijos, donoro audinio atmetimo ar imuninio atsako histologiniuose eksperimentinių grupių mėginiuose. Histologinis regeneravusios kremzlės vertinimas yra pateiktas 6.1.5.1 pav.



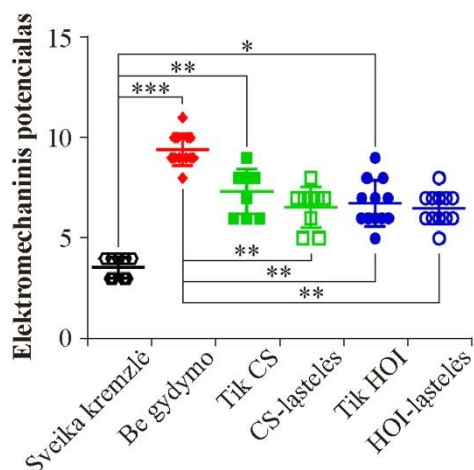
6.1.5.1 pav. Histologinis eksperimentinių grupių įvertinimas, praėjus 6 mėnesiams po operacijos: (a) be gydymo, (b) tik CS, (c) CS-ląstelių, (d) tik HOI ir (e) HOI-ląstelių grupėse, apskaičiuojant (f) histologinio balo (O'Driscoll) vertes

Histologinis balas pagerėjo visose gydymo grupėse, palyginti su negydyta grupe. Teigiama tendencija buvo pastebėta HOI-ląstelės ir HOI grupėse, palyginti su negydyta grupe. HOI struktūriniai elementai (žvaigždutė) buvo stebimi kremzliniame ir pokremzliniame sluoksnyje. CS-ląstelės grupė buvo pranašesnė, palyginti su negydyta grupe. * $p < 0,05$. Mastelis: 200 μm .

6.1.6. Elektromechaninis vertinimas *in vivo*

EP regeneravusios kremzlės vietoje buvo žemesnis visose tyrimo grupėse, palyginti su negydyta grupe, rodantis geresnės kokybės sąnarinės kremzlės regeneraciją gydytose grupėse.

Daug prastesnės nei sveikos kremzlės elektromechaninės savybės buvo nustatytos CS ($p = 0,002$), HOI ($p = 0,022$) ir negydytose grupėse ($p = 0,0009$). Tačiau HOI-ląstelių ($p = 0,0014$) ir HOI ($p = 0,0059$) grupių EP reikšmės buvo geresnės, palyginti su negydytos grupės reikšmėmis. EP buvo panašus tarp CS-ląstelės ($p = 0,069$) ir HOI-ląstelės ($p = 0,066$) grupių. Elektromechaninis kremzlės vertinimas yra pateiktas 6.1.6.1 pav.



6.1.6.1 pav. Elektromechaninių regeneravusios kremzlės savybių 6 mėnesiai po pirminės operacijos įvertinimas

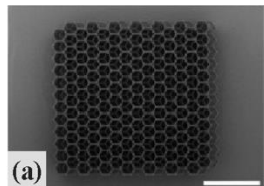
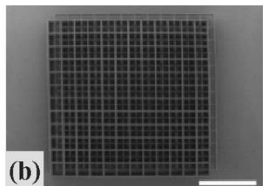
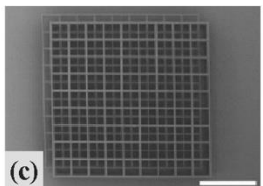
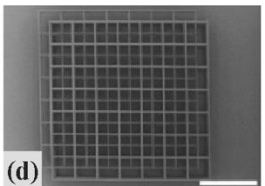
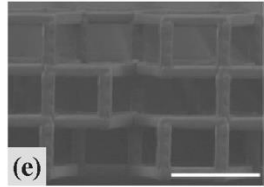
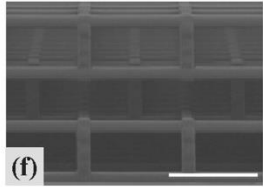
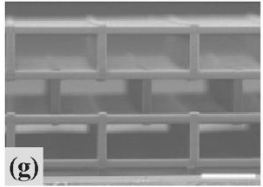
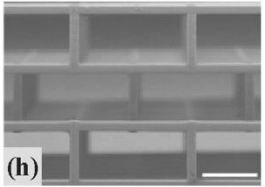
(a) Be gydymo, (b) tik CS, (c) CS-ląstelės, (d) tik HOI ir (e) HOI-ląstelės grupėse su Arthro-BST. EP išmatuotas sveikojoje, HOI, HOI-ląstelės ir CS-ląstelės grupėse, buvo žemesnis už negydytą grupę, taigi, šių grupių regeneravusi kremzlė buvo geresnės kokybės. HOI-ląstelės ir CS-ląstelės grupės pasižymėjo geresnėmis elektromechaninėmis savybėmis ir buvo palyginamos su (s) sveikąja kremzle. * $p < 0,05$; ** $p < 0,01$; *** $p < 0,001$.

6.2. Galutinės studijos rezultatai

6.2.1. Biomechaninis vertinimas

HOI-H ir HOI-T karkasų morfologinės charakteristikos buvo panašios, kad būtų galima įvertinti poros formos įtaką biomechaninėms savybėms. Morfologinės karkasų savybės yra pateikiamos 6.2.1.1 lentelėje.

6.2.1.1 lentelė. HOI karkasų morfologinės SEM fotografijos (a–d) iš viršaus ir (e–h) iš šono

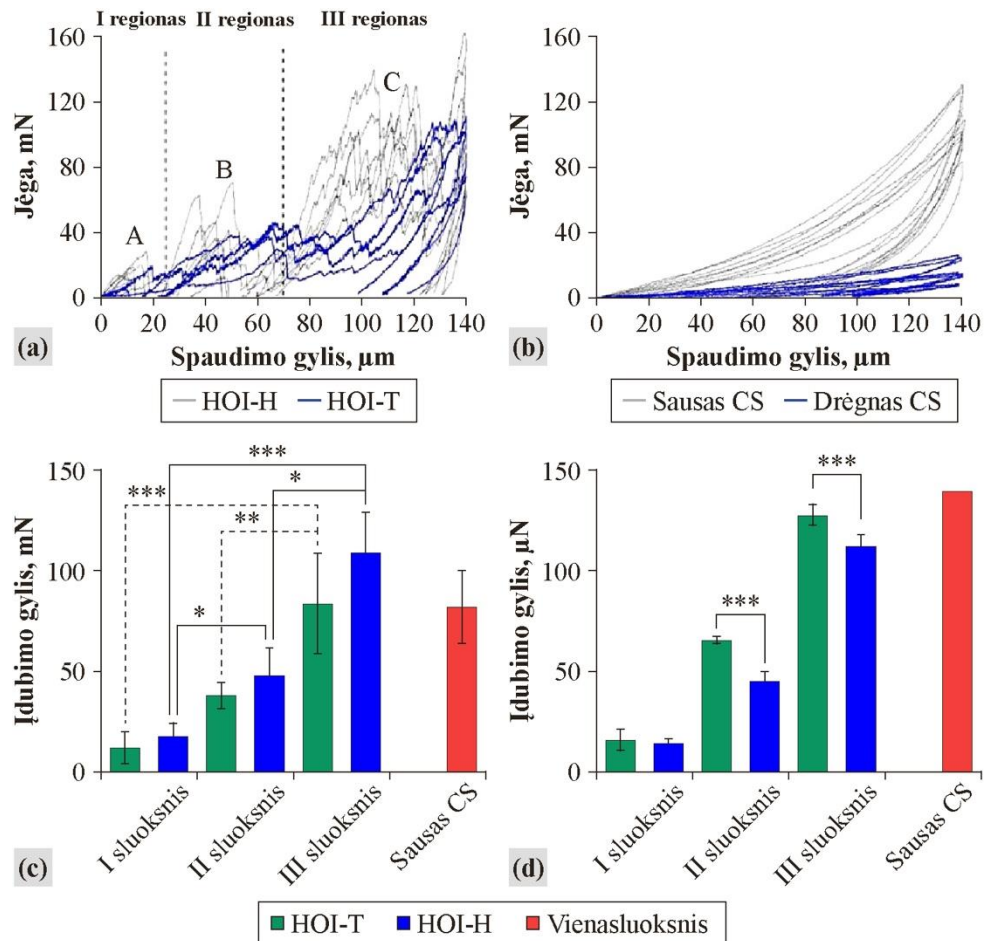
Karkaso tipas	HOI-H	HOI-T	HOI-T1.5	HOI-T2
	 (a)	 (b)	 (c)	 (d)
	 (e)	 (f)	 (g)	 (h)
Karkaso dydis (P×I×A), μm ³	1511×1567×195	1515×1515×195	1582.5×1582.5×262.5	1590×1590×330
Šoninė pora (I×A), μm ²	49×45	105×45	150×67.5	195×90
Viršutinė pora (I×A), μm ²	42×49	45×45	67×67	90×90
Poringumas, proc.	87	89	94	96

Poros formos įtaka ląstelių augimui buvo vertinama tiriant (a, e) HOI-H ir (b, f) HOI-T karkasus. Poros dydžio poveikis ląstelių augimui buvo nustatytas tiriant (c, g) HOI-T1.5 ir (d, h) HOI-T2 karkasus. Mastelis: (a–d) – 500 μm, (e–h) – 100 μm.

Netaisyklingos formos biomechaninio atsako kreivės buvo sugeneruotos mechaniniu įspaudikliu ir išreikštos santykiu tarp taikytos gniuždymo jėgos ir įspaudimo gylio. HOI-H ir HOI-T įspaudimo kreivės parodė, kad gniuždymo jėgos padidėjo, pasiekdamos A, B ir C viršūnes trijų iš eilės regionų gylyje nuo HOI viršaus iki apačios. Jėgos ir spaudimo gylio kreivės pateiktos 6.2.1.1 pav. (a, b).

Lūžių pobūdis tarp HOI buvo skirtingas ir buvo išreikštas didesniu gyliu, kurį reikia pasiekti maksimaliai jėgai II ir III lygmenyse HOI-T, palyginti su HOI-H. Lūžę karkaso elementai skirtingai sukrito abiejose grupėse, tokiu būdu padidindami suminę įspaudimo jėgą kiekviename sluoksnyje. Spaudimo jėga ir gylis kiekviename sluoksnyje yra pateikti 6.2.1.1 pav. (c, d).

Buvo stebėta akivaizdi didesnio kietumo (H_{IT}) ir modulio (E_{IT}) HOI-H tendencija, palyginti su HOI-T. Abu HOI karkasai išlaikė tą patį H_{IT} ir E_{IT} , kai buvo laikomi skystoje terpėje (duomenys nepateikti). Priešingai, sausos būklės CS buvo užfiksuotas staigus ir stabilus gniuždymo jėgos pakilimas, o šlapios būklės CS užfiksavo reikšmingą jėgos sumažėjimą iki 140 μ m spaudimo gylio. Šios sąlygos imitavo klinikinį CS taikymą prieš implantaciją ir parodė mažesnę atsparumą šlapios būklės CS. Be to, implantacijai paruošto CS H_{IT} ir E_{IT} buvo žymiai prastesni nei HOI-T ir HOI-H. H_{IT} ir E_{IT} vidutinės matavimų reikšmės yra pateiktos 6.2.1.1 pav. (e).



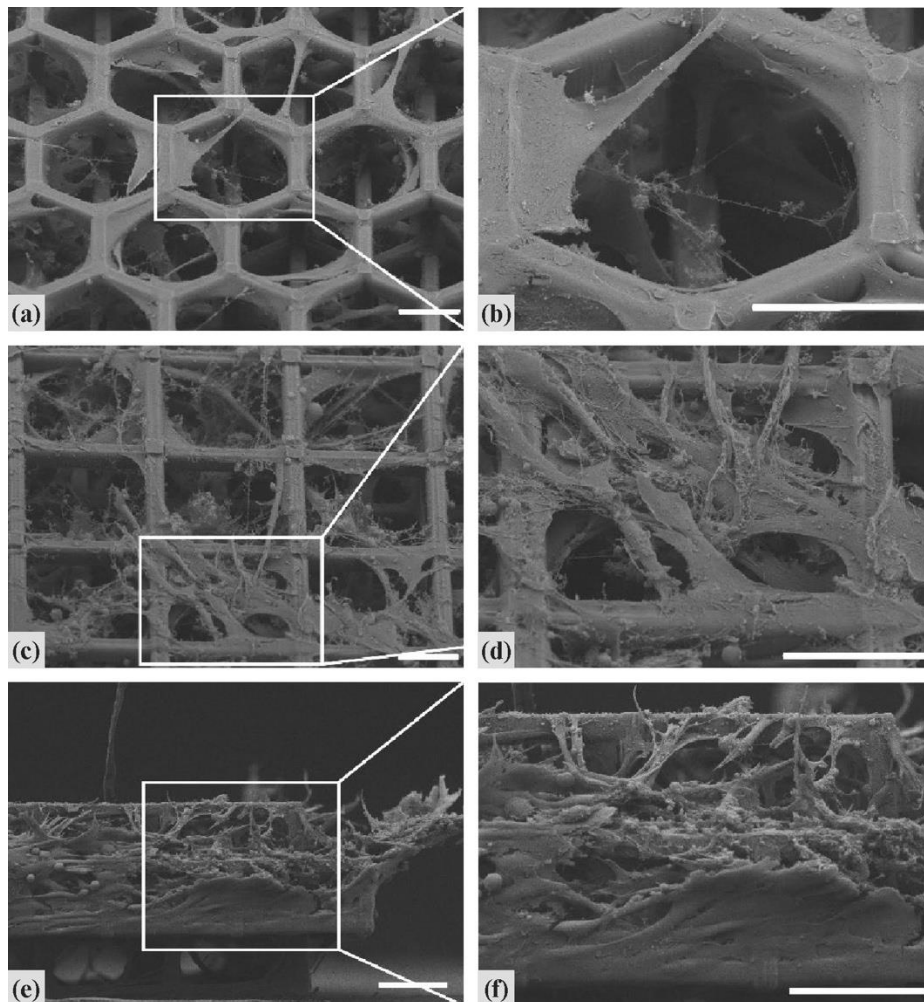
	H_{IT} , MPa	E_{IT} , GPa
HOI-H	0,91 (0,35)	0,047 (0,024)
HOI-T	0,77 (0,16)	0,021 (0,007)
Sausas CS	0,92 (0,16)	0,0132 (0,0031)
Šlapias CS	0,15 (0,06)***	0,0013 (0,0005)***

6.2.1.1 pav. Jėgos ir įdubimo gylio kreivės, gautos atliekant mikrospaudimo tyrimą HOI ir CS karkasams

(a) HOI-T ir HOI-H karkasų lūžių pobūdis buvo skirtingas, o (b) sausos ir šlapios CS deformacijos parodė mažesnę šlapios CS mechaninį atsparumą. (c, d) Žymiai didesnė jėga buvo užfiksuota pereinant į gilesnius HOI karkasų sluoksnius ir buvo panaši į sausos CS. (e) Pastebėtas aukštesnio H_{IT} ir E_{IT} santykis HOI-H grupėje, palyginti su HOI-T. Šlapios CS H_{IT} ir E_{IT} buvo žymiai prastesni nei visų išbandytų karkasų. * $p < 0,05$; ** $p < 0,01$; *** $p < 0,0001$.

6.2.2. Biologinio suderinamumo vertinimas ir priklausomybė nuo poros formos

HOI-H konstrukto ląstelių prilipimas ir padidėjęs TLM nusėdimas buvo išlaikytas iki 7-ųjų dienų *in vitro*, nuolat ilgėjant TLM pluoštams tarp statmenų sijų. Ląstelių ir HOI-H karkasų biologinio suderinamumo SEM fotografijos yra pateiktos 6.2.2.1 pav. (a, b).



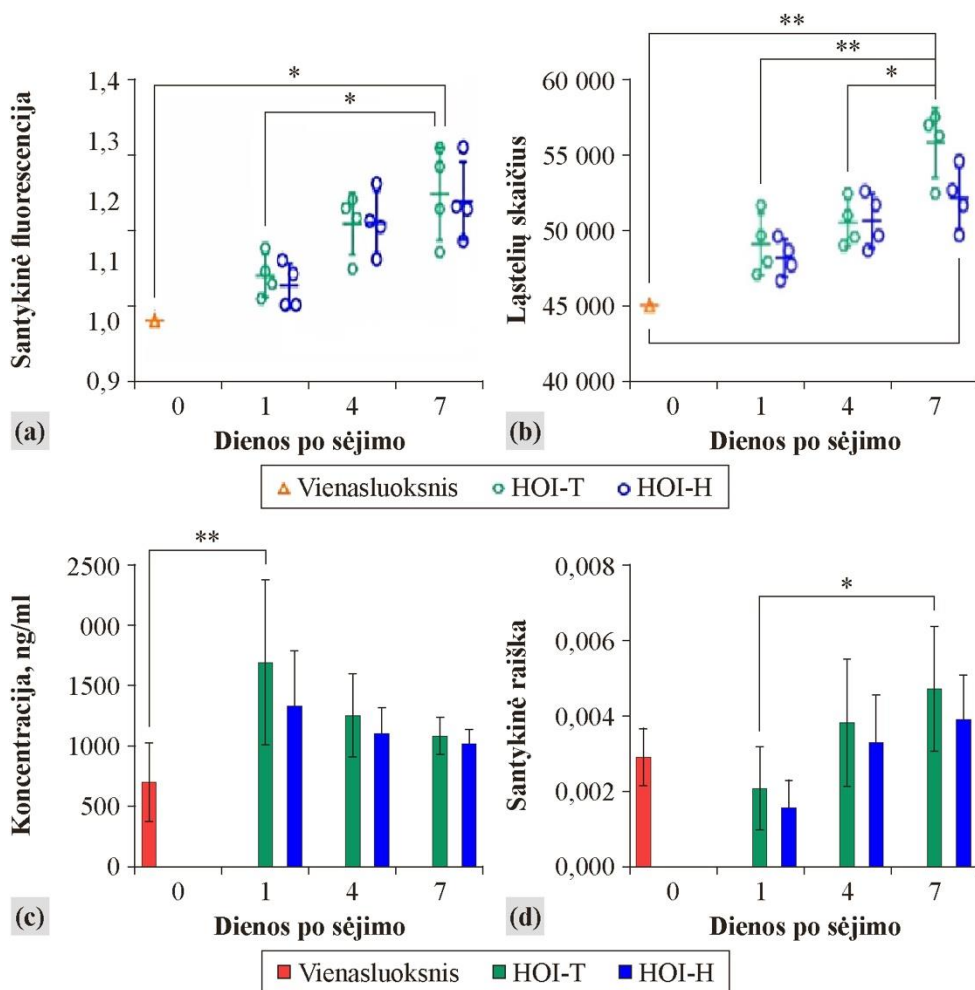
6.2.2.1 pav. *Chondrocitų pasiskirstymas (a, b) HOI-H karkase bei (c, d) horizontalioje ir (e, f) vertikalioje HOI-T karkaso plokštumoje 7-ą dieną po sėjimo*

Pailgos ir ovalios formos ląstelės, apvyniotos ir sujungiančios horizontalius ir vertikalius HOI-T karkasų sijas. Išskirtas TLM peraugo visus tris sluoksnius, užpildydamos didžiąją dalį poros tūrio 7-ą dieną. Mastelis: (a–d) 50 μm , (e, f) 100 μm .

Ląstelės, pasėtos ant HOI-T, prilipo prie horizontalių ir vertikalų karkasų sijų. Pailgėjusių ir sferinės formos ląstelių vešėjimas abiejuose karkasuose buvo palaikomas iki 7-ųjų dienų *in vitro* ir rodė ląstelių rediferenciaciją. Gretimi karkaso sluoksniai buvo sujungti ląstelėmis ir TLM, kurie apraizgė visus HOI sluoksnius ir užpildė didžiąją poros erdvę 7-ą dieną, ypač HOI-T. Ląstelių ir HOI-T karkasų biologinio suderinamumo SEM fotografijos yra pateiktos 6.2.2.1 pav. (c–f).

Ant HOI-T ir HOI-H pasėtų ląstelių metabolinis aktyvumas pagerėjo, palyginti su vienasluoksnėmis ląstelėmis, naudojamomis sėjimui. Nors ląstelių metabolinis aktyvumas reikšmingai pagerėjo nuo 1-os iki 7-os dienos HOI-T ir HOI-H grupėse, jis buvo panašus tarp dviejų grupių visuose tyrimo taškuose. Nepaisant to, tik HOI-T grupės ląstelių metabolinis aktyvumas pagerėjo 7-ą dieną, palyginti su vienasluoksnėmis ląstelėmis, o HOI-H grupėje buvo stebima aiški pagerėjimo tendencija ($p = 0,057$). Metabolinio ląstelių aktyvumo ir poros formos priklausomybė yra pateikta 6.2.2.2 pav. (a).

Panašiai ląstelių skaičius padidėjo HOI-T ir HOI-H grupėse 7-ą dieną, palyginti su vienasluoksnių kultūros ląstelių skaičiumi. Nors ląstelių skaičius buvo panašus tarp grupių visuose tyrimo taškuose, tačiau didesnio ląstelių skaičiaus tendencija buvo nustatyta HOI-T grupėje, palyginti su HOI-H. Pagerėjęs metabolinis aktyvumas lėmė didesnę ląstelių skaičių ir aktyvesnę vešėjimą abiejuose HOI konstruktuose. Ląstelių skaičiaus ir poros formos priklausomybė yra pateikta 6.2.2.2 pav. (b).



6.2.2.2 pav. (a) Metabolinis aktyvumas, (b) ląstelių skaičius, (c) II tipo kolageno baltymo išskyrimas ir (d) COL2A1 geno raiška 1-ą, 4-ą ir 7-ą dienomis po HOI-T ir HOI-H pasėjimo chondrocitais

Panašus metabolinio aktyvumo ir ląstelių skaičiaus pagerėjimas iki 7-os dienos buvo stebimas abiejuose konstruktuose, palyginti su vienasluoksnio ląstelėmis. Baltymo išskyrimas pagerėjo pirmąją dieną HOI-T grupėje, palyginti su ląstelėmis, naudojamomis sėjimui, o chondrogenzė buvo palaikoma iki 7-os dienos. Vidutinės baltymų išskyrimo vertės buvo didesnės HOI-T grupėje, palyginti su HOI-H, visuose tirtuosiuose taškuose. Santykinė COL2A1 geno raiška pagerėjo tik HOI-T iki 7-os dienos. * $p < 0,05$; ** $p < 0,01$.

6.2.3. Trijų dimensijų ląstelių rediferenciacija ir poros formos priklausomybė

Pagerėjęs II tipo kolageno baltymo išskyrimas 1-ą trimatės kultūros dieną buvo stebėtas HOI-T-ląstelės grupėje, palyginti su vienasluoksnėmis ląstelėmis. Sumažėjęs, tačiau nuolatinis kremzlinio audinio formavimasis buvo nustatytas iki 7-os dienos įprastomis auginimo sąlygomis HOI-T-ląstelės grupėje.

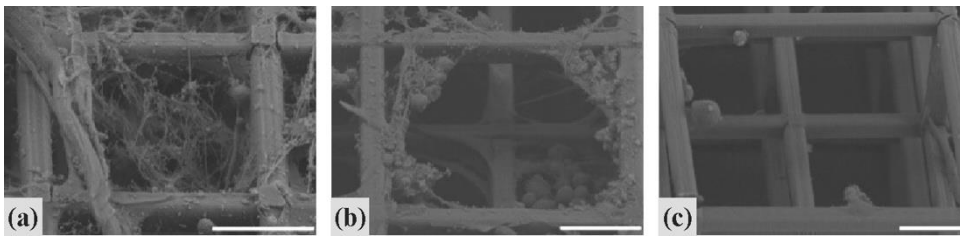
Kremzlei būdingo II tipo kolageno baltymo išskyrimas buvo pastovus iki 7-os dienos HOI-H-ląstelės grupėje; tačiau jis buvo panašus į vienasluoksnių kultūros ląstelių išskiriamo baltymo kiekį viso laikotarpio metu. Iki 7-os dienos abiejose karkasų grupėse buvo stebėtas nereikšmingas baltymų išskyrimo sumažėjimas. Vidutinės baltymų išskyrimo vertės buvo nereikšmingai didesnės HOI-T grupėje visuose tyrimo taškuose, palyginti su HOI-H grupe. II tipo kolageno baltymo išskyrimo ir poros formos priklausomybė yra pateikta 6.2.2.2 pav. (c).

Buvo nustatytas COL2A1 geno raiškos padidėjimas iki 7-os dienos HOI-H ir HOI-T grupėse. Vidutinės genų raiškų vertės abiejose eksperimentinėse grupėse buvo panašios į vienasluoksnių ląstelių vertes per visą auginimo laikotarpį. Nepaisant to, reikšmingas pagerėjimas iki 7-os dienos buvo nustatytas tik HOI-T grupėje.

Reikšmingų skirtumų tarp dviejų karkasų nepastebėta, tačiau vidutinės genų raiškos vertės buvo didesnės HOI-T grupėje, palyginti su HOI-H grupe. Aukštesnės HOI-T karkaso geno raiškos vertės rodo kvadratinės poros pranašumą prieš šešiakampės formą. COL2A1 geno raiška ir poros formos priklausomybė yra pateikta 6.2.2.2 pav. (d).

6.2.4. Trimatė ląstelių rediferenciacija ir poros dydžio priklausomybė

Siekiant nustatyti poros dydžio įtaką ląstelių vešėjimui, antruoju tyrimo etapu HOI-T viršutinės ir šoninės poros buvo padidintos faktoriais – 1,5 (HOI-T1,5) ir 2 (HOI-T2). Pagamintų HOI morfologinės savybės yra pateiktos 6.2.1.1 lentelėje. Pailgėjusios ir ovalios formos ląstelių vešėjimas buvo panašus HOI-T ir HOI-T1.5 konstruktuose *in vitro* ir buvo palaikomas iki 7-os dienos. Ląstelės ir jų išskiriamas TLM buvo nustatyti statmenose ir lygiagrečiose karkasų plokštumose, taip parodant morfologinių karkaso savybių tinkamumą TLM formavimuisi. Ląstelių pasiskirstymas HOI-T ir HOI-T1.5 konstruktuose yra pateiktas 6.2.4.1 pav. (a, b).

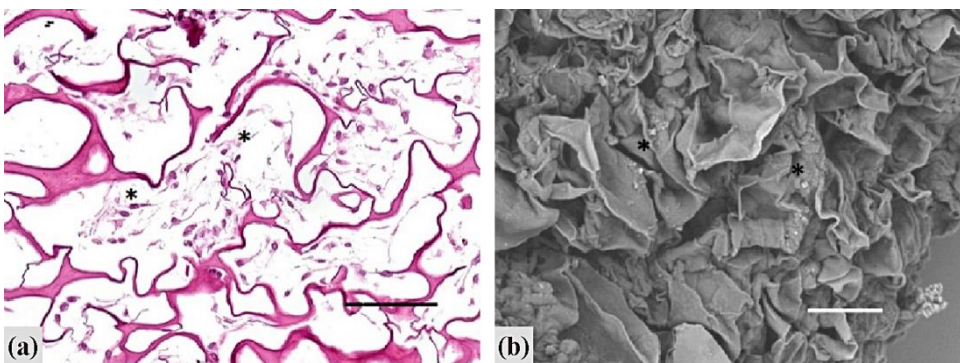


6.2.4.1 pav. *Ląstelių pasiskirstymas tetragoninėse (a) HOI-T, (b) HOI-T1.5 ir (c) HOI-T2 porose 7-ą dieną po sėjimo*

Pailgos ir ovalios formos ląstelės ir išsiskyręs TLM buvo nustatyti statmenose ir lygia-grečiose plokštumose HOI-T ir HOI-T1.5 karkasuose. Ant HOI-T2 sijų nustatytas tik pavienių ląstelių prilipimas. Mastelis: 50 μm .

HOI-T2 konstruktas nepalaikė ląstelių augimo ir TLM gamybos, o visuose tiriamuosiuose HOI-T2 konstruktuose buvo stebėtas tik pavienis ląstelių sukibimas su nedideliu kiekiu TLM. Ląstelių pasiskirstymas HOI-T2 konstruktuose yra pateikiamas 6.2.4.1 pav. (c).

Ląstelės sujungė CS konstrukto kolageno linkius ir raukšles, jos buvo atsitiktinai pasiskirsčiusios paviršiniame ir viduriniame CS konstrukto sluoksniuose. Ląstelių pasiskirstymas CS konstrukte yra pateiktas 6.2.4.2 pav.



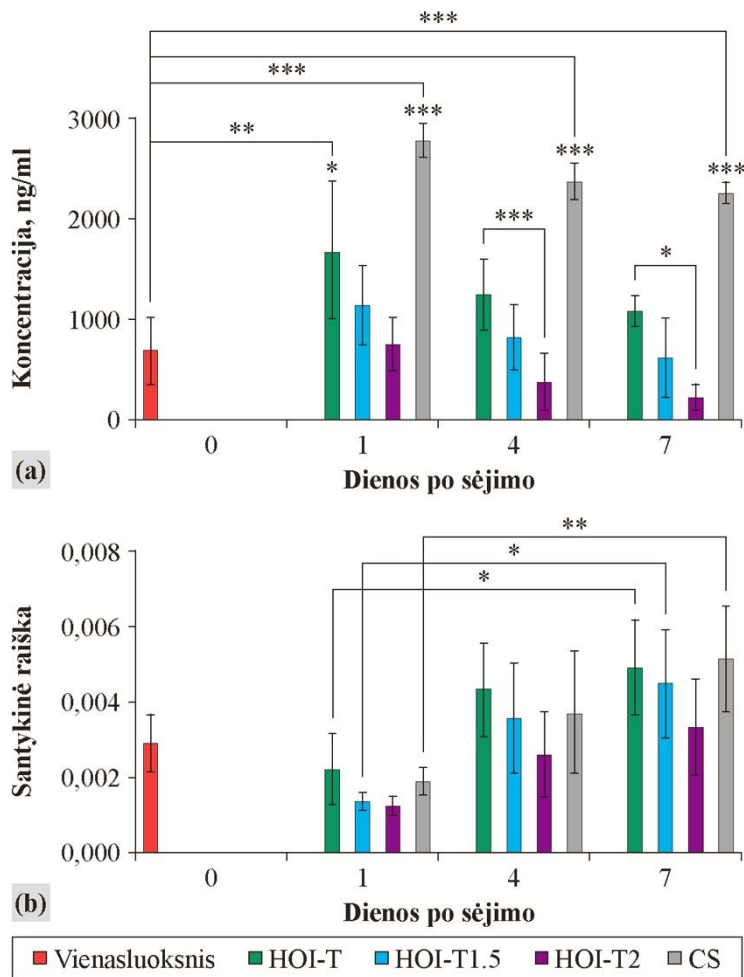
6.2.4.2 pav. *Pasėtų žmogaus chondrocitų pasiskirstymas CS karkase 7-ą dieną*

Reprezentatyvus (a) histologinis (hematoksilinas ir eozinas) ir (b) SEM vaizdas iš arti parodo chondrocitų (žvaigždutė) pasiskirstymą paviršiniuose ir viduriniuose kolageno karkaso sluoksniuose, sujungiančiuose netoliese esančias karkaso raukšles. Mastelis: 50 μm .

Vidutinės II tipo kolageno baltymo išskyrimo vertės pagerėjo pirmą dieną HOI-T, HOI-T1.5 ir HOI-T2 grupėse, tačiau reikšmingai pagerėjo tik HOI-T grupėje. Po vienos dienos auginimo HOI-T baltymų išskyrimas buvo reikšmingai geresnis nei HOI-T1.5 ir HOI-T2. Be to, HOI-T biocheminiai parametrai buvo geresni nei HOI-T2 4-ą ir 7-ą dienomis. Panašiai baltymų išskyrimas sumažėjo ir CS konstrukte, grupėje iki 7-os dienos, vis dėlto ji buvo pranašesnė už kitas tyrimo HOI grupes visuose tyrimo taškuose. Taigi, morfologiniai karkaso parametrai ir specifinis poros dydis turi įtakos biocheminiam HOI-T pranašumui prieš HOI-T1.5 ir HOI-T2 bent pirmą dieną po *in vitro* auginimo trumpalaikiu, klinikiniam implantavimui priimtinu laikotarpiu. II tipo kolageno baltymo išskyrimas yra pateiktas 6.2.4.3 pav. (a).

Vidutinės COL2A1 geno raiškos vertės buvo padidėjusios iki 7-os auginimo dienos HOI-T ir HOI-T1.5 grupėse. Visos trijų dimensijų kultūros auginimo metu vidutinės geno raiškos vertės HOI grupėse buvo panašios į vienasluoksnių kultūros ląstelių genų raišką. COL2A1 geno raiška pagerėjo CS grupėje 7-ą dieną, palyginti su 1-a diena, tačiau buvo panaši į visas HOI grupes visuose tyrimo taškuose. II tipo kolageno geno santykinė raiška yra pateikta 6.2.4.3 pav. (b).

HOI konstruktai su padidintomis poromis buvo palyginami tarpusavyje, tačiau didesnės vidutinės vertės nedidintos poros HOI-T grupėje rodo teigiamą tendenciją tolimesniam šių konstrukčių naudojimui *in vivo*, palyginti su HOI-T1.5 ir HOI-T2 konstruktais.



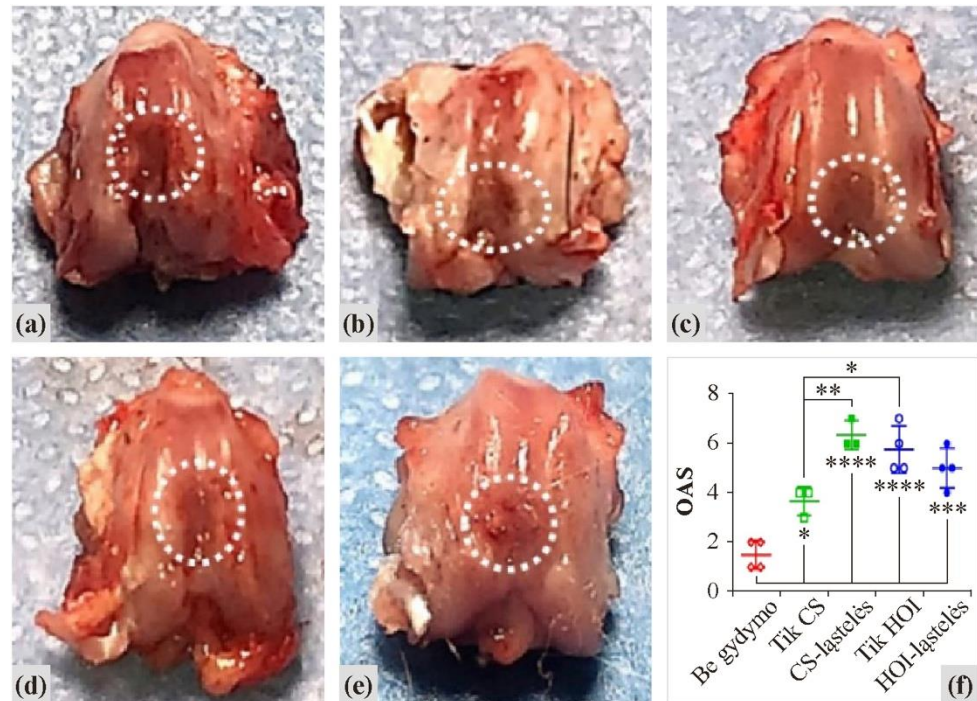
6.2.4.3 pav. Poros skalės ir biologinio suderinamumo priklausomybė, remiantis II tipo kolageno baltymo (a) išskyrimu ir (b) raiška HOI-T, HOI-T1.5 ir HOI-T2 karkasuose 1-q, 4-q ir 7-q dienomis

Išskyrimas pagerėjo HOI-T grupės pirmąją dieną, palyginti su ląstelėmis, naudojamomis sėjimui, ir buvo pranašesnė už HOI-T1.5 ir HOI-T2. CS karkaso baltymo išskyrimas buvo pranašesnis nei bet kurios kitos HOI grupės. Vidutinės COL2A1 geno raiškos vertės pagerėjo HOI-T ir HOI-1,5T grupėse ir buvo panašios į CS. * $p < 0,05$; ** $p < 0,01$; *** $p < 0,001$.

6.2.5. Makroskopinis regeneravusios kremzlės vertinimas *in vivo*

3 mėnesius po operacijos nebuvo stebėta kelio sąnario patinimo, uždegiminių ar imuninių reakcijų į implantuotus konstruktus. OAS nustatyta vertė pagerėjo visose tyrimo grupėse, palyginti su negydyta grupe. Įdomu tai, kad ląstelių pridėjimas HOI grupėje šiek tiek pablogino makroskopinį vertinimą, palyginti su HOI be ląstelių grupe. Nė viena iš HOI konstrukto

grupių neatkūrė lygaus kremzlės paviršiaus ir transplantato vienodo lygio su šeimininko kremzlės lygiu. Integracija ir kremzlės spalva buvo panašios tarp tyrimo grupių. CS ląstelių grupė regeneravo labiausiai į hialininę kremzlę panašų audinį, palyginti su negydyta grupe, vertinant lygų regeneravusios kremzlės paviršių ir vienodą transplantato lygį su šeimininko kremzlės lygiu. Nepaisant to, CS be ląstelių grupės makroskopinis vertinimas buvo prastesnis už HOI be ląstelių grupės, daugiausia dėl didesnio kiekio atplaišų CS grupės kremzlės paviršiuje, palyginti su lygesniu kremzlės paviršiumi abiejose HOI grupėse. Makroskopinis regeneravusios kremzlės įvertinimas *in vivo* yra pateiktas 6.2.5.1 pav.

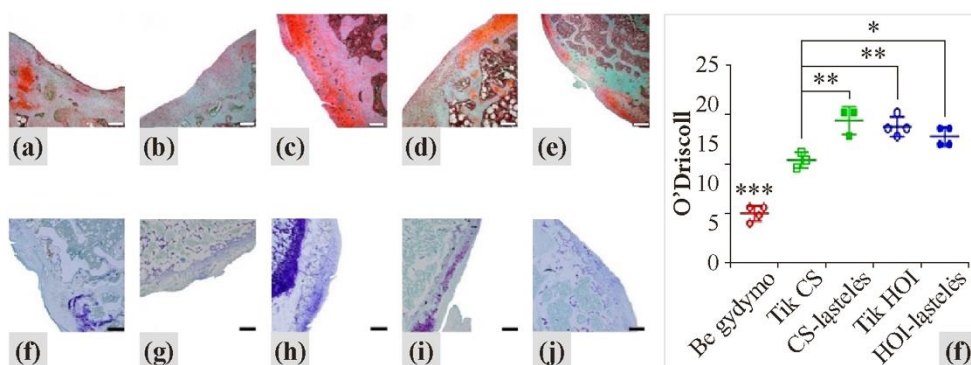


6.2.5.1 pav. Makroskopinis (OAS) eksperimentinių grupių vertinimas 3 mėnesius po gydymo: (a) negydyta, (b) tik CS, (c) CS-ląstelės, (d) tik HOI ir (e) HOI-ląstelės grupėse

Tik HOI ir HOI-ląstelės grupės turėjo aiškią geresnio makroskopinio regeneracinės kremzlės (punktyru pažymėtas apskritimas) vertinimo tendenciją, palyginti su negydyta grupe. Smulkios atplaišos buvo matomos tik HOI ir HOI-ląstelės grupėse, o kremzlės paviršius buvo lygesnis visose CS grupėse. CS-ląstelės grupė turėjo aukščiausią vidutinį OAS rezultatą tarp visų eksperimentinių grupių. Statistinis reikšmingumas: * $p < 0,05$; ** $p < 0,01$; *** $p < 0,001$; **** $p < 0,0001$.

6.2.6. Histologinis regeneravusios kremzlės vertinimas

3 mėnesiai po operacijos histologijos balas reikšmingai pagerėjo visose gydytose tyrimo grupėse, palyginti su negydyta kontroline grupe. Ląstelių pridėjimas HOI grupei nepagerino kremzlės histologinio atkūrimo. HOI be ląstelių grupėje buvo stebėta regeneravusio kremzlės audinio abipusė visiška integracija į šeimininko kremzlę, palyginti su HOI su ląstelių grupės daline integracija. Kiti parametrai buvo panašūs tarp HOI grupių. Histologijos balas HOI be ląstelių grupėje buvo pranašesnis, palyginti su CS be ląstelių grupe. Tam daugiausia įtakos turėjo lygesnis kremzlės paviršius HOI grupėje, o CS be ląstelių grupėje buvo stebėti pavieniai patologiniai įtrūkimai regeneravusios kremzlės paviršiuje. CS su ląstelėmis grupėje buvo nustatyta geriausia skaitinė kremzlės regeneracija, vertinant >75 proc. regeneravusios kremzlės ploto užpildymą chondrocitais ir abipusę visišką regeneracinio audinio integraciją į šeimininko kremzlės audinį. Nė vienoje grupėje nebuvo stebėtas visiškas pokremzlinio kaulo atkūrimas, bet tik nežymūs pokremzlinės zonos kontūro pokyčiai buvo matomi visose grupėse. Histologinis kremzlės regeneracijos įvertinimas yra pateiktas 6.2.6.1 pav.



6.2.6.1 pav. Eksperimentinių grupių histologinis įvertinimas

3 mėnesiai po gydymo: (a, f) be gydymo, (b, g) tik CS, (c, h) CS-ląstelės, (d, i) tik HOI ir (e, j) HOI-ląstelės

Histologinis rezultatas pagerėjo visose gydymo grupėse, palyginti su negydyta grupe, vertinant pagal (a–e) Safranino O ir (f–j) Toluidino mėlynojo dažymą. Ląstelių pridėjimas prie HOI kremzlės regeneracijos dar labiau nepagerino, daugiausia dėl ląstelių sankaupų karkase. CS išlaikė kiek geresnį kremzlės atkūrimą ir buvo panaši į HOI karkasus sekimo periodu. Mastelis: (a–e) 100 μ m; (f–j) 200 μ m. Statistinis reikšmingumas: * $p < 0,05$; ** $p < 0,01$; *** $p < 0,0001$.

7. Išvados

1. Sukurti pirminiai mikrostruktūrizuoti HOI ir triušių chondrocitai yra biologiškai suderinami iki 12-os dienos *in vitro* studijose.
2. Pirminis SKT yra saugus ir efektyvus ilgalaikiame triušio sąvarnės kremzlės pažeidimo modelyje.
3. Biologinis suderinamumas tarp žmogaus chondrocitų ir optimizuotų HOI išlieka iki 7-os dienos *in vitro* studijose bei priklauso nuo HOI poros formos ir dydžio.
4. Optimizuotas SKT yra saugus ir efektyvus ilgalaikiame žiurkės sąvarnės kremzlės pažeidimo modelyje. Papildymas chondrocitais pagerina kremzlės regeneraciją, naudojant CS, tačiau neturi teigiamos įtakos, naudojant HOI-T.

8. Rekomendacija

Didžiausią efektyvumą *in vitro* ir *in vivo* turėjęs kolageninis karkasas su ląstelėmis gali būti naudojamas klinikinėje praktikoje kaip saugus ir efektyvus audinių inžinerijos produktas, skirtas kremzlės regeneracijai. Tačiau optimalus būsimos gamybos procesas (transportavimo terpė, laikas, kultivavimo procedūra, trimatės kultivavimo sąlygos, standartizuotų procesų kontrolė ir kt.) turi būti nustatytas, remiantis šio projekto metu atliktais tyrimais.

REFERENCES LIST

1. Bohndorf K. Injuries at the articulating surfaces of bone (chondral, osteochondral, subchondral fractures and osteochondrosis dissecans). *Eur J Radiol* [Internet]. 1996 Mar 1;22(1):22–9.
2. Curl WW, Krome J, Gordon ES, Rushing J, Smith BP, Poehling GG. Cartilage injuries: a review of 31,516 knee arthroscopies. *Arthroscopy* [Internet]. 1997 Aug; 13(4):456–60.
3. Buckwalter JA, Mankin HJ. Articular cartilage: tissue design and chondrocyte-matrix interactions. *Instr Course Lect*. 1998;47:477–86.
4. Eyre D. Articular cartilage and changes in Arthritis: Collagen of articular cartilage. *Arthritis Res Ther* [Internet]. 2001;4(1):30.
5. Bhosale AM, Richardson JB. Articular cartilage: Structure, injuries and review of management. *Br Med Bull*. 2008;87(1):77–95.
6. Hunziker EB. Articular cartilage repair: basic science and clinical progress. A review of the current status and prospects. *Osteoarthr Cartil*. 2002 Jun;10(6):432–63.
7. Benthien JP, Schwaninger M, Behrens P. We do not have evidence based methods for the treatment of cartilage defects in the knee. *Knee Surg Sports Traumatol Arthrosc*. 2011 Apr;19(4):543–52.
8. MacLulaitis R, D'Apote L, Buchanan A, Pioppo L, Schneider CK. Clinical development of advanced therapy medicinal products in Europe: Evidence that regulators must be proactive. *Mol Ther* [Internet]. 2012;20(3):479–82.
9. European Medicines Agency. Guideline on human cell-based medicinal products. *Ema*. 2008;EMA(May):EMA/CHMP/410869/2006.
10. European Medicines Agency (EMA). ICH guideline Q10 on pharmaceutical quality system. 2014;44(1):1–20.
11. Morrison SJ, Shah NM, Anderson DJ. Regulatory mechanisms in stem cell biology. *Cell* [Internet]. 1997 Feb 7;88(3):287–98.
12. Langer R, Tirrell DA. Designing materials for biology and medicine. *Nature*. 2004 Apr;428(6982):487–92.
13. Dhandayuthapani B, Yoshida Y, Maekawa T, Kumar DS. Polymeric scaffolds in tissue engineering application: A review. *Int J Polym Sci*. 2011;2011(ii).
14. Murphy CM, O'Brien FJ. Understanding the effect of mean pore size on cell activity in collagen-glycosaminoglycan scaffolds. Vol. 4, *Cell Adhesion & Migration*. 2010. p. 377–81.
15. Tayalia P, Mendonca CR, Baldacchini T, Mooney DJ, Mazur E. 3D Cell-Migration Studies using Two-Photon Engineered Polymer Scaffolds. *Adv Mater* [Internet]. 20(23):4494–8.
16. Weiß T, Schade R, Laube T, Berg A, Hildebrand G, Wyrwa R, et al. Two-Photon Polymerization of Biocompatible Photopolymers for Microstructured 3D Biointerfaces. *Adv Eng Mater* [Internet]. 13(9):B264–73.
17. Ajeti V, Lien C-H, Chen S-J, Su P-J, Squirrell JM, Molinarolo KH, et al. Image-inspired 3D multiphoton excited fabrication of extracellular matrix structures by modulated raster scanning. *Opt Express* [Internet]. 2013;21(21):25346–55.
18. Marino A, Filippeschi C, Genchi GG, Mattoli V, Mazzolai B, Ciofani G. The Osteoprint: a bioinspired two-photon polymerized 3-D structure for the enhancement of bone-like cell differentiation. *Acta Biomater*. 2014 Oct;10(10):4304–13.

19. Zhu J, Marchant RE. Design properties of hydrogel tissue-engineering scaffolds. Vol. 8, *Expert review of medical devices*. 2011. p. 607–26.
20. O'Brien FJ. Biomaterials & scaffolds for tissue engineering. *Mater Today* [Internet]. 2011;14(3):88–95.
21. Murphy S V, Atala A. 3D bioprinting of tissues and organs. *Nat Biotechnol*. 2014 Aug;32(8):773–85.
22. Terzaki K, Kissamitaki M, Skarmoutsou A, Fotakis C, Charitidis CA, Farsari M, et al. Pre-osteoblastic cell response on three-dimensional, organic-inorganic hybrid material scaffolds for bone tissue engineering. *J Biomed Mater Res A*. 2013 Aug;101(8):2283–94.
23. Griffon DJ, Sedighi MR, Schaeffer D V, Eurell JA, Johnson AL. Chitosan scaffolds: interconnective pore size and cartilage engineering. *Acta Biomater*. 2006 May;2(3):313–20.
24. Dai W, Kawazoe N, Lin X, Dong J, Chen G. The influence of structural design of PLGA/collagen hybrid scaffolds in cartilage tissue engineering. *Biomaterials*. 2010 Mar;31(8):2141–52.
25. Annabi N, Nichol JW, Zhong X, Ji C, Koshy S, Khademhosseini A, et al. Controlling the porosity and microarchitecture of hydrogels for tissue engineering. *Tissue Eng Part B Rev*. 2010 Aug;16(4):371–83.
26. K pyl  E, Aydogan DB, Virjula S, Vanhatupa S, Miettinen S, Hyttinen J, et al. Direct laser writing and geometrical analysis of scaffolds with designed pore architecture for three-dimensional cell culturing. *J Micromechanics Microengineering* [Internet]. 2012;22(11):115016.
27. Bhat S, Tripathi A, Kumar A. Supermacro porous chitosan–agarose–gelatin cryogels: in vitro characterization and in vivo assessment for cartilage tissue engineering. Vol. 8, *Journal of the Royal Society Interface*. 2011. p. 540–54.
28. Gao Y, Liu S, Huang J, Guo W, Chen J, Zhang L, et al. The ECM-Cell Interaction of Cartilage Extracellular Matrix on Chondrocytes. Vol. 2014, *BioMed Research International*. 2014.
29. Hendriks J, Riesle J, Blitterswijk CA van. Co-culture in cartilage tissue engineering. *J Tissue Eng Regen Med*. 2010;4(7):524–31.
30. Benya PD, Shaffer JD. Dedifferentiated chondrocytes reexpress the differentiated collagen phenotype when cultured in agarose gels. *Cell*. 1982 Aug;30(1):215–24.
31. Do A-V, Khorsand B, Geary SM, Salem AK. 3D Printing of Scaffolds for Tissue Regeneration Applications. Vol. 4, *Advanced healthcare materials*. 2015. p. 1742–62.
32. Goldring MB. Chondrogenesis, chondrocyte differentiation, and articular cartilage metabolism in health and osteoarthritis. *Ther Adv Musculoskelet Dis* [Internet]. 2012 Jun 1;4(4):269–85.
33. Chen FS, Frenkel SR, Di Cesare PE. Repair of articular cartilage defects: part I. Basic Science of cartilage healing. *Am J Orthop (Belle Mead NJ)* [Internet]. 1999 Jan;28(1):31–3.
34. Berninger MT, Wexel G, Rummeny EJ, Imhoff AB, Anton M, Henning TD, et al. Matrix-assisted Autologous Chondrocyte Transplantation for Remodeling and Repair of Chondral Defects in a Rabbit Model. *J Vis Exp* [Internet]. 2013;(75):1–6.
35. Buckwalter JA, Annunziato A, Clark C. Articular Cartilage and Meniscal Considerations. *Bone*. :3–11.
36. Vannini F, Battaglia M, Buda R, Cavallo M, Giannini S. “One step” treatment of juvenile osteochondritis dissecans in the knee: clinical results and T2 mapping characterization. *Orthop Clin North Am* [Internet]. 2012/03/14. 2012 Apr;43(2):237–vi.

37. Steadman JR, Briggs KK, Rodrigo JJ, Kocher MS, Gill TJ, Rodkey WG. Outcomes of microfracture for traumatic chondral defects of the knee: average 11-year follow-up. *Arthroscopy* [Internet]. 2003;19(5):477–84.
38. Steinwachs MR, Guggi T, Kreuz PC. Marrow stimulation techniques. *Injury* [Internet]. 2008 Apr;39 Suppl 1:S26–31.
39. Bedi A, Feeley BT, Williams 3rd RJ. Management of articular cartilage defects of the knee. *J Bone Joint Surg Am* [Internet]. 2010 Apr;92(4):994–1009.
40. Orth P, Gao L, Madry H. Microfracture for cartilage repair in the knee: a systematic review of the contemporary literature. *Knee Surg Sports Traumatol Arthrosc* [Internet]. 2019/01/18. 2020 Mar;28(3):670–706.
41. Weber AE, Locker PH, Mayer EN, Cvetanovich GL, Tilton AK, Erickson BJ, et al. Clinical Outcomes After Microfracture of the Knee: Midterm Follow-up. *Orthop J Sport Med* [Internet]. 2018 Feb 9;6(2):2325967117753572–2325967117753572.
42. Gille J, Behrens P, Volpi P, de Girolamo L, Reiss E, Zoch W, et al. Outcome of Autologous Matrix Induced Chondrogenesis (AMIC) in cartilage knee surgery: data of the AMIC Registry. *Arch Orthop Trauma Surg* [Internet]. 2012/10/16. 2013 Jan;133(1):87–93.
43. Kusano T, Jakob RP, Gautier E, Magnussen RA, Hoogewoud H, Jacobi M. Treatment of isolated chondral and osteochondral defects in the knee by autologous matrix-induced chondrogenesis (AMIC). *Knee Surg Sports Traumatol Arthrosc* [Internet]. 2011/12/25. 2012 Oct;20(10):2109–15.
44. Benthien JP, Behrens P. Autologous matrix-induced chondrogenesis (AMIC). A one-step procedure for retropatellar articular resurfacing. *Acta Orthop Belg* [Internet]. 2010 Apr;76(2):260–3.
45. Anders S, Volz M, Frick H, Gellissen J. A Randomized, Controlled Trial Comparing Autologous Matrix-Induced Chondrogenesis (AMIC®) to Microfracture: Analysis of 1- and 2-Year Follow-Up Data of 2 Centers. *Open Orthop J* [Internet]. 2013 May 3;7:133–43.
46. Erggelet C, Vavken P. Microfracture for the treatment of cartilage defects in the knee joint - A golden standard? *J Clin Orthop trauma* [Internet]. 2016/06/28. 2016;7(3):145–52.
47. Hangody L, Füles P. Autologous osteochondral mosaicplasty for the treatment of full-thickness defects of weight-bearing joints: ten years of experimental and clinical experience. *J Bone Joint Surg Am* [Internet]. 2003;85-A Suppl:25–32.
48. Solheim E, Hegna J, Øyen J, Harlem T, Strand T. Results at 10 to 14 years after osteochondral autografting (mosaicplasty) in articular cartilage defects in the knee. *Knee* [Internet]. 2013/03/06. 2013 Aug;20(4):287–90.
49. Hangody L, Dobos J, Baló E, Pánics G, Hangody LR, Berkes I. Clinical experiences with autologous osteochondral mosaicplasty in an athletic population: a 17-year prospective multicenter study. *Am J Sports Med* [Internet]. 2010/04/01. 2010 Jun;38(6):1125–33.
50. de Windt TS, Vonk LA, Brittberg M, Saris DBF. Treatment and Prevention of (Early) Osteoarthritis Using Articular Cartilage Repair—Fact or Fiction? A Systematic Review. *Cartilage* [Internet]. 2013 May 8;4(3_suppl):5S-12S.
51. Manning WK, Bonner Jr. WM. Isolation and Culture of Chondrocytes From Human Adult Articular Cartilage. *Arthritis Rheum*. 1967;10(3):235–9.
52. Ma B, Leijten JCH, Wu L, Kip M, van Blitterswijk CA, Post JN, et al. Gene expression profiling of dedifferentiated human articular chondrocytes in monolayer culture. *Osteoarthr Cartil*. 2013;21(4):599–603.

53. von der Mark K, Gauss V, von der Mark H, Müller P. Relationship between cell shape and type of collagen synthesised as chondrocytes lose their cartilage phenotype in culture. *Nature* [Internet]. 1977 Jun 9;267(5611):531–2.
54. Grogan SP, Barbero A, Diaz-Romero J, Cleton-Jansen A-M, Soeder S, Whiteside R, et al. Identification of markers to characterize and sort human articular chondrocytes with enhanced in vitro chondrogenic capacity. *Arthritis Rheum* [Internet]. 2007 Feb;56(2):586–95.
55. Bastiaansen-Jenniskens YM, Koevoet W, de Bart ACW, van der Linden JC, Zuurmond AM, Weinans H, et al. Contribution of collagen network features to functional properties of engineered cartilage. *Osteoarthr Cartil* [Internet]. 2007/08/21. 2008 Mar;16(3):359–66.
56. Salvat C, Pigenet A, Humbert L, Berenbaum F, Thirion S. Immature murine articular chondrocytes in primary culture: a new tool for investigating cartilage. *Osteoarthr Cartil* [Internet]. 2005 Mar;13(3):243–9.
57. Caron MMJ, Emans PJ, Coolsen MME, Voss L, Surtel DAM, Cremers A, et al. Redifferentiation of dedifferentiated human articular chondrocytes: Comparison of 2D and 3D cultures. *Osteoarthr Cartil* [Internet]. 2012;20(10):1170–8.
58. Sasazaki Y, Seedhom BB, Shore R. Morphology of the bovine chondrocyte and of its cytoskeleton in isolation and in situ: are chondrocytes ubiquitously paired through the entire layer of articular cartilage? *Rheumatology* [Internet]. 2008;47(11):1641–6.
59. Guerne PA, Blanco F, Kaelin A, Desgeorges A, Lotz M. Growth factor responsiveness of human articular chondrocytes in aging and development. *Arthritis Rheum* [Internet]. 1995 Jul;38(7):960–8.
60. Gomez-Camarillo MA, Almonte-Becerril M, Vasquez Tort M, Tapia-Ramirez J, Kouri Flores JB. Chondrocyte proliferation in a new culture system. *Cell Prolif* [Internet]. 2009/02/18. 2009 Apr;42(2):207–18.
61. Wu G-H, Hsu S-H. Review: Polymeric-Based 3D Printing for Tissue Engineering. *J Med Biol Eng* [Internet]. 2015/06/10. 2015;35(3):285–92.
62. Danilevicius P. Micro-structured polymer scaffolds fabricated by direct laser writing for tissue engineering. *J Biomed Opt* [Internet]. 2012;17(8):081405.
63. Malinauskas M, Farsari M, Piskarskas A, Juodkasis S. Ultrafast laser nanostructuring of photopolymers: A decade of advances. *Phys Rep* [Internet]. 2013;533(1):1–31.
64. Malinauskas M, Rekštytė S, Lukoševičius L, Butkus S, Balčiūnas E, Pečiukaiytė M, et al. 3D Microporous Scaffolds Manufactured via Combination of Fused Filament Fabrication and Direct Laser Writing Ablation. Vol. 5, *Micromachines*. 2014.
65. Mobasher A, Kalamegam G, Musumeci G, Batt ME. Chondrocyte and mesenchymal stem cell-based therapies for cartilage repair in osteoarthritis and related orthopaedic conditions. *Maturitas* [Internet]. 2014;78(3):188–98.
66. Farjanel J, Schürmann G, Bruckner P. Contacts with fibrils containing collagen I, but not collagens II, IX, and XI, can destabilize the cartilage phenotype of chondrocytes. *Osteoarthr Cartil* [Internet]. 2001;9 Suppl A:S55–63.
67. Oliveira SM, Ringshia RA, Legeros RZ, Clark E, Yost MJ, Terracio L, et al. An improved collagen scaffold for skeletal regeneration. *J Biomed Mater Res A* [Internet]. 2010 Aug;94(2):371–9.
68. Stenhamre H, Nannmark U, Lindahl A, Gatenholm P, Brittberg M. Influence of pore size on the redifferentiation potential of human articular chondrocytes in poly(urethane urea) scaffolds. *J Tissue Eng Regen Med*. 2011 Jul;5(7):578–88.

69. Matsiko A, Gleeson JP, O'Brien FJ. Scaffold mean pore size influences mesenchymal stem cell chondrogenic differentiation and matrix deposition. *Tissue Eng Part A*. 2015 Feb;21(3–4):486–97.
70. Wang C-C, Yang K-C, Lin K-H, Liu H-C, Lin F-H. A highly organized three-dimensional alginate scaffold for cartilage tissue engineering prepared by microfluidic technology. *Biomaterials*. 2011 Oct;32(29):7118–26.
71. Wang C-C, Yang K-C, Lin K-H, Wu C-C, Liu Y-L, Lin F-H, et al. A biomimetic honeycomb-like scaffold prepared by flow-focusing technology for cartilage regeneration. *Biotechnol Bioeng*. 2014 Nov;111(11):2338–48.
72. LU XINL, MOW VANC. Biomechanics of Articular Cartilage and Determination of Material Properties. *Med Sci Sport Exerc* [Internet]. 2008;40(2).
73. Nwe N, Furuike T, Tamura H. The Mechanical and Biological Properties of Chitosan Scaffolds for Tissue Regeneration Templates Are Significantly Enhanced by Chitosan from *Gongronella butleri*. Vol. 2, *Materials*. 2009.
74. Spiller KL, Maher SA, Lowman AM. Hydrogels for the Repair of Articular Cartilage Defects. *Tissue Eng Part B Rev* [Internet]. 2011 Apr 21;17(4):281–99.
75. Sophia Fox AJ, Bedi A, Rodeo SA. The basic science of articular cartilage: Structure, composition, and function. *Sports Health*. 2009;1(6):461–8.
76. Mow VC, Guo XE. Mechano-Electrochemical Properties Of Articular Cartilage: Their Inhomogeneities and Anisotropies. *Annu Rev Biomed Eng* [Internet]. 2002 Aug 1;4(1):175–209.
77. Franz T, Hasler EM, Hagg R, Weiler C, Jakob RP, Mainil-Varlet P. In situ compressive stiffness, biochemical composition, and structural integrity of articular cartilage of the human knee joint. *Osteoarthr Cartil* [Internet]. 2001;9(6):582–92.
78. Armstrong CG, Mow VC. Variations in the intrinsic mechanical properties of human articular cartilage with age, degeneration, and water content. *JBJS* [Internet]. 1982;64(1).
79. Sim S, Chevrier A, Garon M, Quenneville E, Yaroshinsky A, Hoemann CD, et al. Non-destructive electromechanical assessment (Arthro-BST) of human articular cartilage correlates with histological scores and biomechanical properties. *Osteoarthr Cartil* [Internet]. 2014;22(11):1926–35.
80. Changoor A, Coutu JP, Garon M, Quenneville E, Hurtig MB, Buschmann MD. Streaming potential-based arthroscopic device is sensitive to cartilage changes immediately post-impact in an equine cartilage injury model. *J Biomech Eng*. 2011 Jun;133(6):061005.
81. Mickevicius T, Pockevicius A, Kucinskas A, Gudas R, MacIulaitis J, Noreikaite A, et al. Impact of storage conditions on electromechanical, histological and histochemical properties of osteochondral allografts. *BMC Musculoskelet Disord*. 2015;16(1).
82. Abedian R, Willbold E, Becher C, Hurschler C. In vitro electro-mechanical characterization of human knee articular cartilage of different degeneration levels: A comparison with ICRS and Mankin scores. *J Biomech* [Internet]. 2013;46(7):1328–34.
83. Pettersson S, Wetterö J, Tengvall P, Kratz G. Cell expansion of human articular chondrocytes on macroporous gelatine scaffolds—impact of microcarrier selection on cell proliferation. *Biomed Mater* [Internet]. 2011;6(6):65001.
84. Gigante A, Bevilacqua C, Cappella M, Manzotti S, Greco F. Engineered articular cartilage: influence of the scaffold on cell phenotype and proliferation. *J Mater Sci Mater Med* [Internet]. 2003 Aug;14(8):713–6.

85. Riesle J, Hollander AP, Langer R, Freed LE, Vunjak-Novakovic G. Collagen in tissue-engineered cartilage: Types, structure, and crosslinks. *J Cell Biochem* [Internet]. 1998 Dec 1;71(3):313–27.
86. Gneccchi M, Melo LG. Bone marrow-derived mesenchymal stem cells: isolation, expansion, characterization, viral transduction, and production of conditioned medium. *Methods Mol Biol* [Internet]. 2009;482:281–94.
87. Barner-Kowollik C, Bastmeyer M, Blasco E, Delaittre G, Muller P, Richter B, et al. 3D Laser Micro- and Nanoprinting: Challenges for Chemistry. *Angew Chem Int Ed Engl*. 2017 Dec;56(50):15828–45.
88. Jonušauskas L, Juodkasis S, Malinauskas M. Optical 3D printing: bridging the gaps in the mesoscale. *J Opt* [Internet]. 2018 May 1;20(5):053001.
89. Ovsianikov A, Viertl J, Chichkov B, Oubaha M, MacCraith B, Sakellari I, et al. Ultra-low shrinkage hybrid photosensitive material for two-photon polymerization microfabrication. *ACS Nano*. 2008;2(11):2257–62.
90. Gille J, Kunow J, Boisch L, Behrens P, Bos I, Hoffmann C, et al. Cell-laden and cell-free matrix-induced chondrogenesis versus microfracture for the treatment of articular cartilage defects: A histological and biomechanical study in sheep. *Cartilage*. 2010;1(1):29–42.
91. Garon M, Légaré A, Guardo R, Savard P, Buschmann MD. Streaming potentials maps are spatially resolved indicators of amplitude, frequency and ionic strength dependant responses of articular cartilage to load. *J Biomech* [Internet]. 2002;35(2):207—216.
92. Chen AC, Nguyen TT, Sah RL. Streaming potentials during the confined compression creep test of normal and proteoglycan-depleted cartilage. *Ann Biomed Eng* [Internet]. 1997;25(2):269–77.
93. Schagemann JC, Rudert N, Taylor ME, Sim S, Quenneville E, Garon M, et al. *Bilayer Implants : Electromechanical Assessment of Regenerated Articular Cartilage in a Sheep Model*. 2016;
94. Schmitz N, Laverty S, Kraus VB, Aigner T. Basic methods in histopathology of joint tissues. *Osteoarthr Cartil* [Internet]. 2018;18(2010):S113–6.
95. O’Driscoll SW, Keeley FW, Salter RB. The chondrogenic potential of free autogenous periosteal grafts for biological resurfacing of major full-thickness defects in joint surfaces under the influence of continuous passive motion. An experimental investigation in the rabbit. *J Bone Joint Surg Am*. 1986 Sep;68(7):1017–35.
96. Hissnauer TN, Baranowsky A, Pestka JM, Streichert T, Wiegandt K, Goepfert C, et al. Identification of molecular markers for articular cartilage. *Osteoarthr Cartil*. 2010;18(12):1630–8.
97. Brittberg M, Recker D, Ilgenfritz J, Saris DBF. Matrix-Applied Characterized Autologous Cultured Chondrocytes Versus Microfracture: Five-Year Follow-up of a Prospective Randomized Trial. *Am J Sports Med*. 2018;46(6):1343–51.
98. McManus CJ, May GE, Spealman P, Shteyman A. Ribosome profiling reveals post-transcriptional buffering of divergent gene expression in yeast. Vol. 24, *Genome Research*. 2014. p. 422–30.
99. Selden C, Fuller B. Role of Bioreactor Technology in Tissue Engineering for Clinical Use and Therapeutic Target Design. *Bioengineering* [Internet]. 2018;5(2):32.
100. Ye K, Traianedes K, Robins SA, Choong PFM, Myers DE. Osteochondral repair using an acellular dermal matrix-pilot in vivo study in a rabbit osteochondral defect model. *J Orthop Res* [Internet]. 2018;1–10.

101. Sherwood JK, Riley SL, Palazzolo R, Brown SC, Monkhouse DC, Coates M, et al. A three-dimensional osteochondral composite scaffold for articular cartilage repair. *Biomaterials*. 2002;23(24):4739–51.
102. Pan Z, Duan P, Liu X, Wang H, Cao L, He Y, et al. Effect of porosities of bilayered porous scaffolds on spontaneous osteochondral repair in cartilage tissue engineering. *Regen Biomater* [Internet]. 2015 Mar 6;2(1):9–19.
103. Wang Y, Meng H, Yuan X, Peng J, Guo Q, Lu S, et al. Fabrication and in vitro evaluation of an articular cartilage extracellular matrix-hydroxyapatite bilayered scaffold with low permeability for interface tissue engineering. *Biomed Eng Online*. 2014;13(1):1–18.
104. Duan P, Pan Z, Cao L, He Y, Wang H, Qu Z, et al. The effects of pore size in bilayered poly(lactide-co-glycolide) scaffolds on restoring osteochondral defects in rabbits. *J Biomed Mater Res Part A* [Internet]. 2014;102(1):180–92.
105. Madry H, van Dijk CN, Mueller-Gerbl M. The basic science of the subchondral bone. *Knee Surgery, Sport Traumatol Arthrosc*. 2010;18(4):419–33.
106. Malinauskas LJ and SJ and M. Optical 3D printing: bridging the gaps in the mesoscale. *J Opt* [Internet]. 2018;20(5):53001.
107. Edwards SL, Church JS, Alexander DLJ, Russell SJ, Ingham E, Ramshaw JAM, et al. Modeling tissue growth within nonwoven scaffolds pores. *Tissue Eng Part C Methods* [Internet]. 2010/10/01. 2011 Feb;17(2):123–30.
108. Sun T, Smallwood R, MacNeil S. Development of a mini 3D cell culture system using well defined nickel grids for the investigation of cell scaffold interactions. *J Mater Sci Mater Med* [Internet]. 2009/02/20. 2009 Jul;20(7):1483–93.
109. Engelmayr Jr GC, Papworth GD, Watkins SC, Mayer Jr JE, Sacks MS. Guidance of engineered tissue collagen orientation by large-scale scaffold microstructures. *J Biomech* [Internet]. 2005/07/25. 2006;39(10):1819–31.
110. Di Luca A, Lorenzo-Moldero I, Mota C, Lepedda A, Auhl D, Van Blitterswijk C, et al. Tuning Cell Differentiation into a 3D Scaffold Presenting a Pore Shape Gradient for Osteochondral Regeneration. *Adv Healthc Mater*. 2016;5(14):1753–63.
111. Accardo A, Blatché M-C, Courson R, Loubinoux I, Thibault C, Malaquin L, et al. Multiphoton Direct Laser Writing and 3D Imaging of Polymeric Freestanding Architectures for Cell Colonization. *Small* [Internet]. 2017/05/30. 2017 Jul;13(27):10.1002/smll.201700621.
112. Hippler M, Lemma ED, Bertels S, Blasco E, Barner-Kowollik C, Wegener M, et al. 3D Scaffolds to Study Basic Cell Biology. *Adv Mater* [Internet]. 2019/02/21. 2019 Jun;31(26):e1808110–e1808110.
113. Accardo A, Blatché M-C, Courson R, Loubinoux I, Vieu C, Malaquin L. Two-photon lithography and microscopy of 3D hydrogel scaffolds for neuronal cell growth. *Biomed Phys Eng Express* [Internet]. 2018;4(2):27009.
114. Lemma ED, Spagnolo B, De Vittorio M, Pisanello F. Studying Cell Mechanobiology in 3D: The Two-Photon Lithography Approach. *Trends Biotechnol* [Internet]. 2018/10/18. 2019 Apr;37(4):358–72.
115. Greenbaum D, Williams K, Greenbaum D, Colangelo C, Williams K, Gerstein M. Comparing protein abundance and mRNA expression levels on a genomic scale. *Comparing protein abundance and mRNA expression levels on a genomic scale*. 2003;(FEBRUARY).
116. Loh QL, Choong C. Three-Dimensional Scaffolds for Tissue Engineering Applications: Role of Porosity and Pore Size. *Tissue Eng Part B Rev* [Internet]. 2013;19(6):485–502.

117. Mačiulaitis J, Rekštytė S, Ūsas A, Jankauskaitė V, Gudas R, Malinauskas M, et al. Characterization of tissue engineered cartilage products: Recent developments in advanced therapy. *Pharmacol Res.* 2016;113.
118. Danilevicius P, Georgiadi L, Pateman CJ, Claeysens F, Chatzinikolaidou M, Farsari M. The effect of porosity on cell ingrowth into accurately defined, laser-made, polylactide-based 3D scaffolds. *Appl Surf Sci [Internet]*. 2015;336:2–10.
119. Trautmann A, Rūth M, Lemke HD, Walther T, Hellmann R. Two-photon polymerization based large scaffolds for adhesion and proliferation studies of human primary fibroblasts. *Opt Laser Technol [Internet]*. 2018;106:474–80.
120. Gelse K, Pöschl E, Aigner T. Collagens - Structure, function, and biosynthesis. *Adv Drug Deliv Rev.* 2003;55(12):1531–46.
121. Pan Z, Duan P, Liu X, Wang H, Cao L, He Y, et al. Effect of porosities of bilayered porous scaffolds on spontaneous osteochondral repair in cartilage tissue engineering. *Regen Biomater [Internet]*. 2015;2(1):9–19.
122. Divieto C, Sassi MP. A first approach to evaluate the cell dose in highly porous scaffolds by using a nondestructive metabolic method. Vol. 1, *Future Science OA*. London, UK; 2015.
123. Gálisová A, Fábryová E, Sticová E, Kosinová L, Jiráťová M, Herynek V, et al. The Optimal Timing for Pancreatic Islet Transplantation into Subcutaneous Scaffolds Assessed by Multimodal Imaging. Vol. 2017, *Contrast Media & Molecular Imaging*. 2017.
124. Salzmann GM, Niemeyer P, Hochrein A, Stoddart MJ, Angele P. Articular Cartilage Repair of the Knee in Children and Adolescents. *Orthop J Sport Med.* 2018;6(3):1–12.
125. Hunziker EB, Lippuner K, Keel MJB, Shintani N. An educational review of cartilage repair: Precepts & practice - myths & misconceptions – progress & prospects. *Osteoarthr Cartil [Internet]*. 2015;23(3):334–50.
126. Rekštytė S, Mačiulaitis J, Mačiulaitis R, Malinauskas M. Fabrication of 3D micro-structured scaffolds by direct laser writing in pre-polymers for in vitro and in vivo studies. In: *ProcSPIE [Internet]*. 2017.
127. Livak KJ, Schmittgen TD. Analysis of relative gene expression data using real-time quantitative PCR and the 2⁻(-Delta Delta C(T)) Method. *Methods.* 2001 Dec;25(4):402–8.

PUBLICATIONS LIST

1. Mačiulaitis, Justinas; Miškinienė, Milda; Rekštytė, Sima; Bratchikov, Maksim; Darinskas, Adas; Šimbelytė, Agnė; Daunoras, Gintaras; Laurinavičienė, Aida; Laurinavičius, Arvydas; Gudas, Rimtautas; Malinauskas, Mangirdas; Mačiulaitis, Romaldas. Osteochondral repair and electromechanical evaluation of custom 3D scaffold microstructured by direct laser writing lithography // *Cartilage*. Thousand Oaks : Sage Publications. ISSN 1947-6035. eISSN 1947-6043. 2019, first on line, p. 1-11.
2. Mačiulaitis, Justinas; Rekštytė, Sima; Bratčikov, Maksim; Gudas, Rimtautas; Malinauskas, Mangirdas; Počkevičius, Alius; Ūsas, Arvydas; Rimkūnas, Augustinas; Jankauskaitė, Virginija; Grigaliūnas, Valdas; Mačiulaitis, Romaldas. Customization of direct laser lithography-based 3D scaffolds for optimized in vivo outcome // *Applied surface science*. Amsterdam : Elsevier Science. ISSN 0169-4332. eISSN 1873-5584. 2019, vol. 487, p. 692-702.
3. Mačiulaitis, Justinas; Deveikytė, Milda; Rekštytė, Sima; Bratchikov, Maksim; Darinskas, Adas; Šimbelytė, Agnė; Daunoras, Gintaras; Laurinavičienė, Aida; Laurinavičius, Arvydas; Gudas, Rimtautas; Malinauskas, Mangirdas; Mačiulaitis, Romaldas. Preclinical study of SZ2080 material 3D microstructured scaffolds for cartilage tissue engineering made by femtosecond direct laser writing lithography // *Biofabrication*. Bristol : IOP Pub. ISSN 1758-5082. 2015, vol. 7, no. 1, p. 1-1.

CONFERENCE PRESENTATIONS

1. Mačiulaitis, Justinas; Gudas, Rimtautas; Rekštytė, Sima; Malinauskas, Mangirdas; Rimkūnas, Augustinas; Grigaliūnas, Valdas; Jankauskaite, Virginija; Bratchikov, Maksim; Mačiulaitis, Romaldas. Tiesioginio lazerinio rašymo būdu pagamintos 3D membranos ikiklinikinė 6 mėnesių saugumo ir efektyvumo studija // Ligonį tausojanti chirurgija ir regeneracinė medicina ortopedijoje ir traumatologijoje : XIV-asis Lietuvos ortopedų traumatologų draugijos suvažiavimas : tezių knyga : 2018 m. balandžio 27–28 d. Vilnius ; [Suvažiavimo organizacinis komitetas: Giedrius Kvederas, Aleksas Makulavičius, Alfredas Smailys [ir kt.]]. Vilnius : Lietuvos ortopedų traumatologų draugija, 2018. ISBN 9786099602509. p. 43-44. (Lietuvos Vaikų Ortopedų traumatologų draugijos sekcija).
2. Rimkūnas, Augustinas; Mačiulaitis, Justinas; Rekštytė, Sima; Malinauskas, Mangirdas; Gudas, Rimtautas; Mačiulaitis, Romaldas. Microstructured three dimensional scaffolds for articular cartilage regeneration. An in vitro study // IHS Conference abstract book / Lithuanian University of Health Sciences. Student Scientific Society ; [Edited by Elvinas Monstavičius, Cover by Kamilė Krauledaitė]. Kaunas : Lithuanian University of Health Sciences. 2018, p. 744-746. (Posters).
3. Rekštytė, Sima; Mačiulaitis, Justinas; Mačiulaitis, Romaldas; Malinauskas, Mangirdas. Didelio našumo trimačių mikrostruktūrizuotų karkasų lazerinis formavimas kremzlės regeneracijos tyrimams in vitro ir in vivo = High throughput laser fabrication of 3D microstructured scaffolds for cartilage regeneration studies in vitro and in vivo // 42-oji Lietuvos nacionalinė fizikos konferencija: 2017 m. spalio 4–6 d., Vilnius: programa ir pranešimų tezės / Vilniaus universitetas. Fizinių ir technologijos mokslų centras. Kauno technologijos universitetas. Lietuvos fizikų draugija. Vilnius: Vilniaus universitetas, 2017. ISBN 9786094598807. p. 259-259: pav. DOI: 10.15388/proceedings/LNFK.42.
4. Rekštytė, Sima; Mačiulaitis, Justinas; Mačiulaitis, Romaldas; Malinauskas, Mangirdas. Fabrication of 3D microstructured scaffolds by direct laser writing in pre-polymers and their performance in cartilage regeneration in vitro and in vivo // CLEO@/Europe-EQEC 2017 : Conference on Lasers and Electro-Optics/Europe and the European Quantum Electronics Conference, 25–29 June 2017, Munich (ICM), Germany. New York : IEEE, 2017. ISBN 9781509067367, 1p.
5. Justinas Mačiulaitis, Rimtautas Gudas, Arvydas Ūsas, Sima Rekštytė, Mangirdas Malinauskas, Romaldas Mačiulaitis. Three dimensional

scaffolds microfabricated by a direct laser writing lithography in a long term preclinical study., 24 – 27 June 2016, Sorrento, Italy.

6. Daunoras, Gintaras; Mačiulaitis, Justinas; Grigonis, Aidas; Šernienė, Loreta; Mačiulaitis, Romaldas. Evaluation of the clinical indicators under different types of organic and organic-inorganic scaffold implantation into the knee joints, using in vivo rabbit model // International Scientific Conference “Nutrition, Health and Quality of Food of Animal Origin – Challenges and Opportunities”, the conference is devoted to the 20th anniversary of Laboratory of Poultry Nutrition and Products Quality: Book of Proceedings : Kaunas, 25 September, 2014 = Tarptautinė mokslinė konferencija "Gyvūnų mityba, sveikata, produkcijos kokybė – problemos ir sprendimai" : tezių knyga : 2014 rugsėjo 25 d., Kaunas, skirta Lietuvos sveikatos mokslų universiteto Veterinarijos akademijos Paukščių lesalų ir paukštininkystės produktų laboratorijos prie Gyvulininkystės katedros įkūrimo 20-čiui paminėti / Lithuanian University of Health Sciences. Veterinary Academy. Hohenheim University, Germany. University of Veterinary Medicine, Vienna, Austria; [Scientific Committee: Rolandas Stankevičius, Antanas Sederevičius, Rainer Mosenthin, Michael A. Grashorn, Qendrim Zebeli, Romas Gružas]. Kaunas : Lietuvos sveikatos mokslų universitetas, 2014. ISBN 9789955153634. p. 125-128.



Original Article

Osteochondral Repair and Electromechanical Evaluation of Custom 3D Scaffold Microstructured by Direct Laser Writing Lithography

CARTILAGE
1–11
© The Author(s) 2019
Article reuse guidelines:
sagepub.com/journals-permissions
DOI: 10.1177/1947603519847745
journals.sagepub.com/home/CAR

Justinas Maciulaitis¹ , Milda Miskiniene², Sima Rekštytė³, Maksim Bratchikov⁴, Adas Darinskas², Agne Simbelyte⁵, Gintaras Daunoras⁶, Aida Laurinaviciene⁵, Arvydas Laurinavicius⁵, Rimtautas Gudas¹, Mangirdas Malinauskas³, and Romaldas Maciulaitis⁷

Abstract

Objective. The objective of this study was to assess a novel 3D microstructured scaffold seeded with allogeneic chondrocytes (cells) in a rabbit osteochondral defect model. **Design.** Direct laser writing lithography in pre-polymers was employed to fabricate custom silicon-zirconium containing hybrid organic-inorganic (HOI) polymer SZ2080 scaffolds of a predefined morphology. Hexagon-pored HOI scaffolds were seeded with chondrocytes (cells), and tissue-engineered cartilage biocompatibility, potency, efficacy, and shelf-life *in vitro* was assessed by morphological, ELISA (enzyme-linked immunosorbent assay) and PCR (polymerase chain reaction) analysis. Osteochondral defect was created in the weight-bearing area of medial femoral condyle for *in vivo* study. Polymerized fibrin was added to every defect of 5 experimental groups. Cartilage repair was analyzed after 6 months using macroscopical (Oswestry Arthroscopy Score [OAS]), histological, and electromechanical quantitative potential (QP) scores. Collagen scaffold (CS) was used as a positive comparator for *in vitro* and *in vivo* studies. **Results.** Type II collagen gene upregulation and protein secretion was maintained up to 8 days in seeded HOI. *In vivo* analysis revealed improvement in all scaffold treatment groups. For the first time, electromechanical properties of a cellular-based scaffold were analyzed in a preclinical study. Cell addition did not enhance OAS but improved histological and QP scores in HOI groups. **Conclusions.** HOI material is biocompatible for up to 8 days *in vitro* and is supportive of cartilage formation at 6 months *in vivo*. Electromechanical measurement offers a reliable quality assessment of repaired cartilage.

Keywords

chondrocytes, cells, electromechanics, biomechanics, *in vivo*, biomechanics, tissue engineering, repair, autologous chondrocyte, grafts

Introduction

Advancements in biomaterial fabrication and tissue engineering procedures have enabled a wide spread of technologies for articular cartilage regeneration.¹ Scaffold-based tissue engineering approach has long been a reasonable approach to restore or improve damaged cartilage tissue in the field of regenerative orthopedics.² To improve scaffold biological activity, a selection of biomaterials and manufacturing methods have been analyzed, both of which are essential initial elements for a successful subsequent *in vivo* application.³

A cellular component is often included in the fabricated scaffold, thus resulting in a tissue-engineered product (TEP). A positive feedback from scaffolding materials results in a cellular activation and improved potency of a TEP *in vitro*.

This is mainly influenced by a number of factors, such as fabrication method, material, and morphological parameters of a scaffold.⁴ Biocompatibility of the scaffold can then be determined by efficacy and potency studies *in vitro*, which are mostly dependent on adequate amount and type of cells seeded and culture methods.⁵ Despite the emergence of stem cells in orthopedic regenerative medicine, somatic cells have convincingly supported a long-term positive preclinical and clinical data for articular cartilage defect treatment.⁶ In addition, different approaches to reduce the use of a 2-stage matrix-applied chondrogenesis procedure by combining somatic and stem cells and excluding the need for cultivation has still yet to prove for the long-term clinical outcome.^{7,8}

Direct laser writing in pre-polymers (DLW-PP) technique (also known as 2-photon polymerization [2PP] or multi-photon processing [MPP]) is especially attractive for

the fabrication of scaffolds in tissue engineering applications as it enables the predefinition of precise geometry and dimensions.^{9,12} Versatility of the fabrication method enables the creation of scaffolds, which can be tailored to an individual patient. In addition, recent research on the through-put-augmenting techniques of the DLW-PP has resulted in speeding-up the fabrication of microstructured objects, successfully mitigating the main disadvantage of point-by-point fabrication that was once a bottleneck of this technique.^{11,13,14} *In vitro* biocompatibility of the HOI material used for the scaffold fabrication has been shown previously, while effectiveness and safety evaluation relied on preliminary *in vivo* studies.^{15,16} TEPs prepared for clinical use must be cultivated for a certain period of time before implantation to ensure optimal potency. Thus, interruptions and delays of transplantation procedure might require prolonged cultivation and adequate evaluation of shelf-life as represented by sustained efficacy and potency *in vitro*.¹⁷

A quick and reliable method to objectively evaluate several key parameters of cartilage quality, including cellular viability and histological and biomechanical parameters, has been proposed by analyzing the electromechanical properties of cartilage.¹⁸ Cartilage repair quality, by means of electromechanical properties, after treatment with a cellular-based TEP, has not yet been evaluated in any of the preclinical studies reported in the literature.

The primary objective of this work was to compare the biocompatibility of 3D customized DLW-PP scaffold to a routinely used commercially available CS *in vitro*. The secondary objective was to evaluate repaired cartilage quality in a long-term *in vivo* preclinical model.

Materials and Methods

Scaffold Manufacturing

The 3D microstructured polymeric scaffolds were fabricated by employing the DLW-PP technique. Computer models were designed using conventional CAD software or specially designed 3DPoli package (Femtika, Vilnius, Lithuania) and created by focusing a femtosecond laser

beam into the volume of a photosensitive pre-polymer. Polymerization reaction is initiated due to multi-photon absorption localized within the vicinity of the focal volume, which turns a gel-like material into a solid state. Subsequently, different parts of the material are exposed to the laser light point-by-point until a scaffold of specific microarchitecture is materialized. The DLW-PP setup employed an ultrafast laser, which provided 300 fs, 200 kHz, and 515 nm pulsed light radiation (Pharos, Light Conversion, Vilnius, Lithuania). More specific details about the setup and fabrication process can be found elsewhere.¹¹ The material chosen for the scaffold fabrication was a hybrid organic-inorganic silicon-zirconium containing photopolymer SZ2080 (FORTH-IESL, Heraklion, Greece), which consists of 20% inorganic and 80% organic parts.¹⁹ To make the material more sensitive to the laser light, it was photo-sensitized with 1% of 2-benzyl-2-(dimethylamino)-4'-morpholinobutyrophenone (IRG, Sigma Aldrich, St. Louis, MO) photo-initiator.

HOI scaffolds were fabricated as hexagonal structures and consisted of 3 identical layers. Each layer had an offset of half a period in relation to the lower layer. The overall scaffolds dimensions were $2.1 \times 2.1 \times 0.21 \text{ mm}^3$ and single hexagon diameter was predefined at $100 \mu\text{m}$ wide. Height and width of the rod constituting a scaffold structure was set at $15 \mu\text{m}$. Predetermined scaffold top pore characteristics were described as a distance between 2 parallel rods and were set at $42 \times 49 \mu\text{m}^2$, which reflected the actual narrowest passage from top to bottom of the scaffold. The typical side pore was set at $51 \times 54 \mu\text{m}^2$ in width and length, respectively (Fig. 1a and b).

A commercially available collagen sponge (CS, Septodont, Maidstone, UK) was used as a direct comparator. CS is composed of native, non-denatured, freeze-dried collagen of bovine origin type I collagen (Fig. 1c). CS was cut to the same dimensions to be compared with each other.

CS scaffolds were individually received under sterile conditions, while HOI scaffolds were chemically disinfected in 70% ethanol solution overnight and UV irradiated for 2 hours. The next day scaffolds were washed in

¹Institute of Sports, Lithuanian University of Health Sciences, Kaunas, Lithuania

²Laboratory of Immunology, National Institute of Cancer, Vilnius, Lithuania

³Laser Research Center, Faculty of Physics, Vilnius University, Vilnius, Lithuania

⁴Department of Physiology, Biochemistry, Microbiology and Laboratory Medicine, Institute of Biomedical Sciences, Faculty of Medicine, Vilnius University, Vilnius, Lithuania

⁵National Center of Pathology, Affiliate of Vilnius University Hospital Santaros Klinikos, Vilnius, Lithuania

⁶Non-infectious Disease Department, Lithuanian University of Health Sciences, Kaunas, Lithuania

⁷Institute of Physiology and Pharmacology, Medical Academy, Lithuanian University of Health Sciences, Kaunas, Lithuania

Supplementary material for this article is available on the *Cartilage* website at <https://journals.sagepub.com/home/CAR>.

Corresponding Author:

Justinas Maciulaitis, Institute of Sports, Lithuanian University of Health Sciences, Tilzes st. 18, 9 House, Kaunas 47181, Lithuania.
Email: justinas.maciulaitis@gmail.com

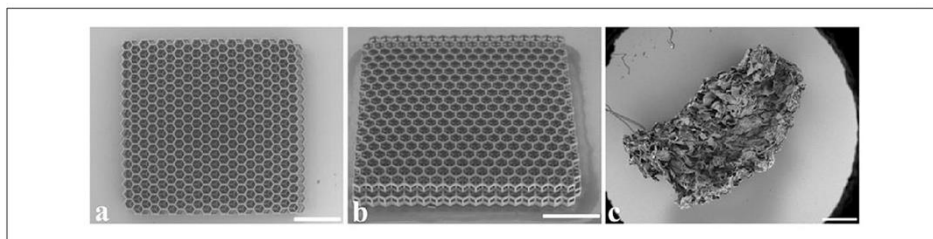


Figure 1. SEM images of manufactured HOI top (a), side (b) view and CS (c). Three layers consisting of 13 and 14 hexagonal chambers in width and length, respectively, with the single hexagon diameter of 100 μm wide. Side pore width and height throughout the scaffold was 51 and 54 μm , respectively. CS is composed of native, non-denaturated, freeze-dried collagen of bovine origin type I collagen. Scale bar: 500 μm .

phosphate-buffered saline (PBS) solution and left to dry for subsequent cell seeding.

Scaffold Morphology Analysis

Scanning electron microscopy (SEM) on HOI and CS was performed by Hitachi TM-1000 (Hitachi High-Technologies Co., Tokyo, Japan), as previously described.¹⁶

A cell filling of HOI pores was calculated as a percentage of empty and filled pore areas from SEM photographs by 2 researchers at days 4, 8, and 12. CS cell distribution was evaluated at day 12 prior to implantation by histological staining with hematoxylin and eosin dye (H&E).

Cell Isolation, Culture, and Posology

All experimental procedures were approved and conducted according to the standard guidelines and protocols by the Animal Health and Welfare Department, State Food and Veterinary Service of the republic of Lithuania. New-Zealand rabbits (male and female; 4-5 months old; 3-4 kg body weight) were housed separately in cages under ordinary conditions ($21 \pm 1^\circ\text{C}$, 12/12 light/dark and a 45% relative humidity) with free access to food and water.

Rabbit chondrocytes were isolated as previously described.¹⁶ Briefly, allogeneic rabbit articular cartilage biopsy from the non-weight-bearing area was minced and digested by 2.5% trypsin (Gibco, Invitrogen, Carlsbad, CA), followed by overnight collagenase XI (Sigma Aldrich) digestion. Isolated cells were plated, cultured, and harvested when 80% confluence was reached. Cells were grown in DMEM/F12 (Hyclone, Logan, UT) supplemented with 10% fetal calf serum (Lonza, Basel, Switzerland), 100 U/mL⁻¹ penicillin and 100 $\mu\text{g}/\text{mL}^{-1}$ streptomycin (Sigma) at 37°C in a humid atmosphere with 5% CO₂.

Scaffolds were soaked in proliferation medium 1 day before seeding. Posology was carried by calculating a cell

dose required for seeding and was based on the volume of the defect and the corresponding scaffold used. After trypsinization with 0.25% trypsin, third passage cells were counted and resuspended in vials with culture medium at 10⁷ in 1 mL concentration. Cells were seeded in 10 μL doses on presterilized HOI and CS in a dropwise fashion, resulting in 10⁵ cells per scaffold. Seeded scaffolds were placed for 2 hours in the CO₂ incubator to allow cellular adhesion before the remaining medium was added.

Seeded scaffolds were cultured up to 12 days. The medium was changed every 3 to 4 days. Scaffolds with cells were harvested after 4, 8, and 12 days of culture and sent for *in vitro* analysis. Also, on the day 12 of culturing, scaffolds were prepared for *in vivo* implantation.

Protein Secretion Analysis

Type II collagen production was analyzed at 4, 8, and 12 days after seeding using enzyme-linked immunosorbent assay kit (rabbit collagen type II ELISA kit, BioSite). The test was performed on 7 samples per condition, according to manufacturer's protocol. The optical density absorbance was read at 450 nm in a microplate reader (Multiskan GO, Thermo Scientific). A standard curve was plotted as the relative optical density of each standard solution versus the respective concentration of the standard solution. Type II collagen concentration of the samples was interpolated from the standard curve.

Gene Expression Analysis

For the chondrogenic gene mRNA analysis, we examined COL2A1 (type II collagen) and COL10A1 (type X collagen) mRNAs' expression dynamics of cells at day 0 before the seeding on scaffolds and on days 4, 8, and 12 *in vitro*. The total RNA was extracted from the samples using an ISOLATE II RNA Micro Kit (Biolone, London, UK) according to the

manufacturer's instructions. Designed primer pairs, probes, and the condition of amplification are represented in the supplementary data (Suppl. Table S1). To analyze the data obtained, the $2^{-\Delta\Delta C_T}$ method was applied for the relative gene expression data evaluation. European rabbit GAPDH gene expression was used for data normalization.

Long-Term *In Vivo* Biocompatibility

Nine rabbits containing 18 bilateral osteochondral defects were used in the study. Surgical procedures were performed aseptically in an operating theatre. Anesthesia was induced intramuscularly and maintained intravenously. Knee joints were approached via the lateral parapatellar approach, followed by medial patellar dislocation. Critical size osteochondral defect (diameter: 3 mm; depth: 2 mm) was created through the articular cartilage and subchondral bone at the weight-bearing area of the medial femoral condyle using an electric drill.

Every defect was extensively washed with saline before implanting a polymerized fibrin clot. Briefly, a mixture 1 mL of autologous blood plasma, 250 μ L of thrombin, and 250 μ L of CaCl_2 were mixed to prepare the fibrin clot. It was incubated for 5 minutes at room temperature just before adding it to the defect to secure the scaffold or fill the scaffold-free defect.

Osteochondral defects were divided into experimental groups based on the randomly received treatment: defects treated using HOI hexagon-pored scaffolds with cultured cells (HOI-cells, $n = 4$) and without cells (HOI-only, $n = 4$). Similarly, positive control groups included collagen scaffolds with cultured cells (CS-cells, $n = 3$) and without cells (CS-only, $n = 3$). Negative control group comprised defects without scaffolds (scaffold-free, $n = 4$). After the implantation patella was relocated, knee capsule was closed with interrupted 3-0 resorbable Monocryl suture (Ethicon, Johnson & Johnson Medical, Somerville, NJ). Overlying skin was approximated with 4-0 subcutaneous continuous suture (Ethicon) and disinfected.

After intervention, the rabbits were housed under regular conditions and were allowed to move freely in individual cages. Rabbits were euthanized after 6 months and samples for subsequent examination were collected.

Macroscopic Evaluation of Repair Cartilage

Two independent researchers performed macroscopic grading according to a modified Oswestry Arthroscopy Score (OAS) at 6 months after implantation. The OAS system comprises a distinct evaluation of several cartilage repair parameters: graft level, integration with surrounding cartilage, appearance of the surface, and color of the repair tissue. Stiffness on probing was excluded from the original scoring system in our study, because a more objective

electromechanical parameter of the repair tissue was evaluated. The maximum OAS score of 8 represents normal cartilage (supplementary data, Suppl. Table S2).

Electromechanical Analysis of Repair Cartilage

Electromechanical properties of the repair tissue were evaluated with Arthro-BST device (Biomomentum Inc., Laval, Quebec, Canada) 6 months after implantation, as previously described.²⁰ Briefly, negatively charged proteoglycan molecules in the collagen network are balanced by mobile positive ions in an interstitial fluid. Cartilage compression results in interstitial fluid movement; thus, mobile positive ions are displaced relative to the fixed negative charges. This flow generates streaming potentials which reflect cartilage composition and function.²¹⁻²³

A higher electromechanical QP mainly reflects increased extracellular matrix disintegration and inferior load-bearing capacity of the cartilage, while low QP indicates strong electromechanical properties and superior load-bearing capacity. However, low QP can similarly be at the lower end of the scale, due to a cartilage thinning until reaching no electromechanical response with complete cartilage loss and bone exposure.²⁴

Measurements of the weight-bearing area on lateral femoral condyle were made during the surgery at 6 months after implantation, following femoral joint harvest and were used as a healthy cartilage control ($n = 9$). QP measurements were recorded 3 times on each control and treated defect to obtain median values.

Histological Analysis of Repair Cartilage

For histological analysis, distal ends of femurs were cut above the condyles, fixed in a 10% neutral buffered formalin solution, and embedded in paraffin blocks. Five-micrometer-thick serial sections were deparaffinized and stained with toluidine blue and Safranin-O stain (both Fisher Scientific, Pittsburgh, PA).²⁵ Sections were analyzed using a digital image microscope (Olympus BX61, Center Valley, PA) equipped with a camera (Olympus DP72, Olympus, Japan) to assess glycosaminoglycans, proteoglycans, and collagen production. Images were scored blindly using a modified O'Driscoll histological scoring system.²⁶ Higher score indicated superior cartilage repair, with a total maximal score of 24 (supplementary data, Suppl. Table S3). Immunological reaction of host tissue to the scaffold at the implantation site was evaluated from histological sections by infiltration of inflammatory cells.

Statistical Analysis

The quantitative data are expressed as a mean (standard deviation). Statistics were performed using GraphPad Prism 7.04. Statistical results were obtained using Kruskal-Wallis

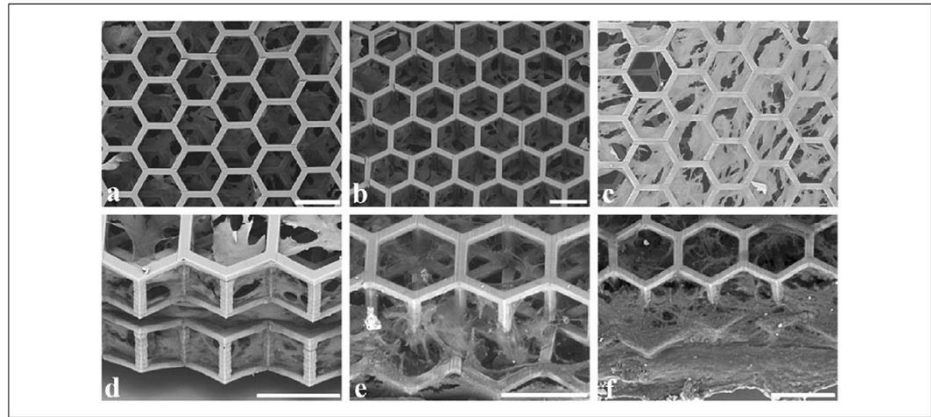


Figure 2. Cells and interconnecting ECM distribution throughout 3-dimensional hexagonal-pored HOI as a percentage of empty and filled pore areas from SEM photographs at days 4 (a), 8 (b), and 12 (c). Elongated and oval-shaped cells continuously adhered and interconnected horizontal and vertical rods of the scaffold. By wrapping and bridging nearby rods, cells, and deposited ECM content incrementally have outgrown all 3 layers of HOI filling most of the pore volume at day 12. Close-up view from the side is displayed at day 4 (d), 8 (e), and 12 (f). Scale bar: 100 μm .

multiple comparison test and presented as the mean and standard deviation (SD). Statistical significance between experimental groups is indicated with (*), which represents a $P < 0.05$ and (**) representing $P < 0.01$.

Results

Cell Seeding and 3D Growth Analysis

Cells seeded on hexagonal-pored HOI exhibited a continuous adherence to the horizontal and vertical rods of the scaffold. Proliferation of cells and extracellular matrix (ECM) production within the scaffold have maintained up to 12 days *in vitro*. The cells could be seen positioned on horizontal and vertical rods, elongated or oval-shape. Connections between nearby rods were mainly made by wrapping and bridging the interconnected nearby perpendicular rods. Cell number and interconnecting ECM content have outgrown all the layers of HOI and kept increasing up to day 12, filling the void space and covering most of the pore diameter at day 12 (Fig. 2).

Incremental pore coverage was evident throughout the cultures up to day 12 prior to the implantation. It improved significantly at day 12 compared to day 4 ($P = 0.0114$) and covered $71 \pm 6.5\%$ of a single pore (Fig. 3).

A positive control of cell-seeded CS revealed random cell distribution from top to bottom and interconnection of nearby collagen folds and creases. Despite all the voids clearly occupied by cells, the bottom layer of CS had fewer cells compared to the top and middle layers (supplementary

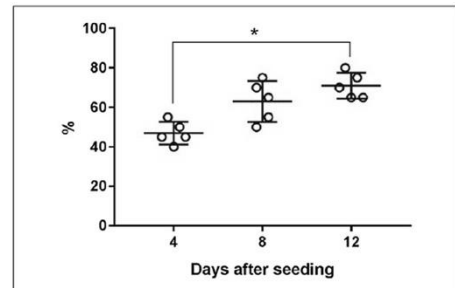


Figure 3. Dynamics of HOI pore coverage by seeded cells. Percentage of filled pore has increased significantly from days 4 to 12, revealing biocompatible morphological conditions for sustained cell proliferation. * $P < 0.05$.

data, Suppl. Fig. S1). Significantly more iterative pore morphology in HOI allowed superior and more even cell distribution throughout the scaffold compared to CS. Both scaffolds kept physical integrity and did not lose material during *in vitro* culture.

Cell Seeded Scaffold Potency Analysis

HOI with cells sustained chondrogenesis under regular culture conditions, by measuring type II collagen secretion to

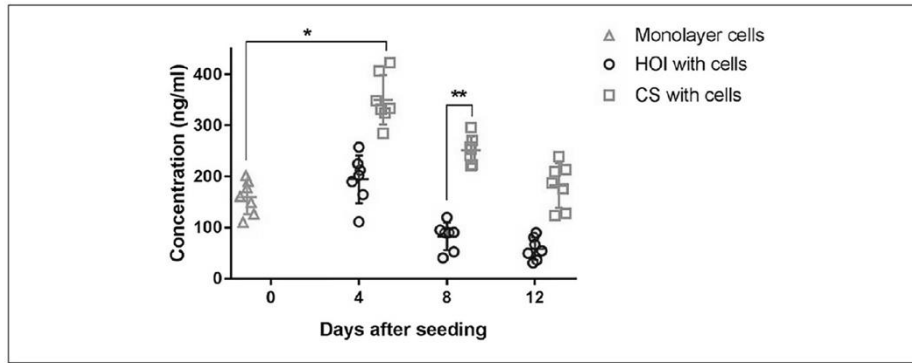


Figure 4. Type II collagen protein secretion, as measured by ELISA in monolayer, HOI, and CS groups at days 0, 4, 8, and 12. Both groups retained the level of secreted protein from days 4 to 12, with a numerical decrease throughout the period. CS had the superior initial type II collagen secretion capacity at day 4 and at day 8, when compared to monolayer cells and HOI, respectively. * $P < 0.05$, ** $P < 0.01$.

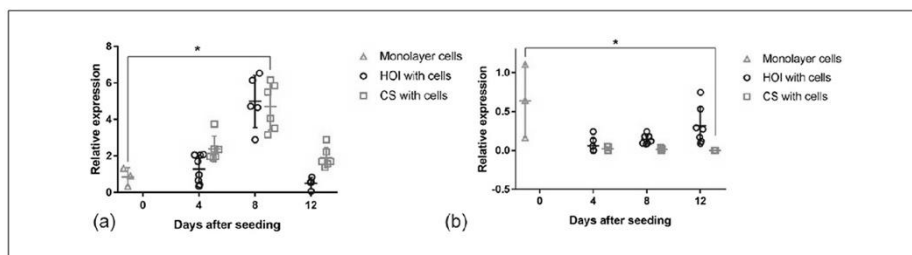


Figure 5. COL2A1 (a) and COL10A1 (b) genes expression patterns, measured by RT-PCR in monolayer, HOI and CS groups at days 0, 4, 8, and 12. Chondrogenesis was upregulated in both groups up to day 8. (a) Mean expression level of COL2A1 increased in HOI at days 4 and 8. CS retained superior expression up to day 8, compared to monolayer cells. (b) Mean expression of fibroblastic COL10A1 was downregulated in both scaffold groups up to day 12. CS with cells expressed less COL10A1 at day 12 compared to monolayer cells. COL10A1 expression in CS was lower compared to HOI at day 12. * $P < 0.05$.

the media when compared to the secretion level of cells that were used for scaffold seeding (monolayer cells) (Fig. 4).

Protein excretion in HOI-cells group retained its level up to day 12; however, a slight decrease was evident throughout the period. Protein secretion improved at day 4 ($P = 0.03$) in CS-cells, then retained its previous level up to day 12. Numerical protein secretion decrease was also noted in CS-cells up to day 12. When scaffolds with cells were compared to each other, a greater amount of type II collagen secretion was noted in CS-cells group at day 8 ($P = 0.0045$), highlighting a superior initial phase of cell-scaffold biocompatibility in this group. A numerical superiority was noted in CS-cells at day 12, when compared to HOI-cells at the respective endpoint of the study.

Chondrogenic COL2A1 expression was upregulated in both groups up to day 8 with a numerical decrease at day 12 in both groups (Fig. 5a).

Even though the mean level of COL2A1 expression increased in HOI-cells at days 4 and 8, it was comparable to day 0 ($P = 0.11$). CS-cells retained superior mean level of expression up to day 12, when compared to the gene expression of monolayer cells; however, it improved significantly in the middle of culture period at day 8 ($P = 0.0306$). No significant differences among the 2 scaffolds were observed; however, mean values were lower in HOI-cells group, compared to CS-cells.

Mean expression of fibroblastic COL10A1 was downregulated in HOI-cells and CS-cells groups, thus supporting

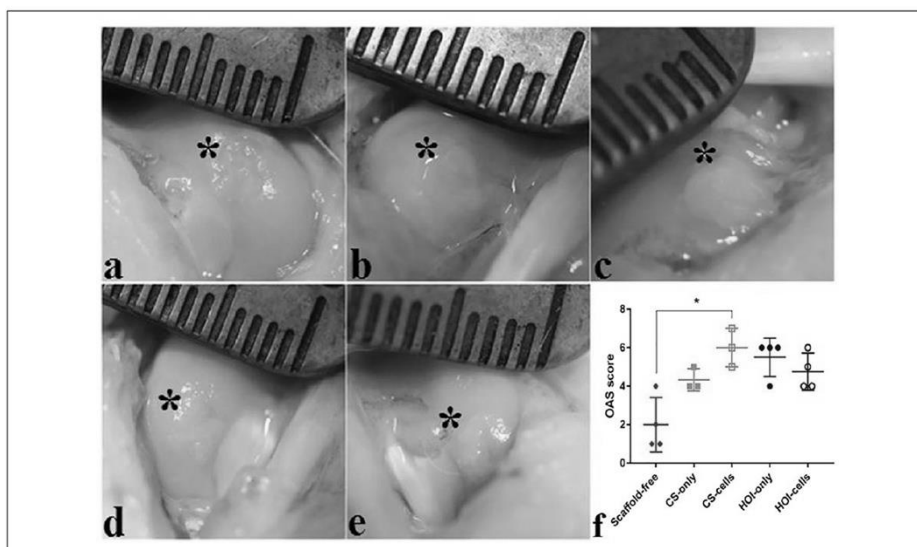


Figure 6. Macroscopic evaluation of experimental groups at 6 months after treatment in (a) scaffold-free, (b) CS-only, (c) CS-cells, (d) HOI-only, and (e) HOI-cells groups. CS-cells had the highest mean (f) OAS score among all experimental groups. HOI-only and HOI-cells had a tendency for superiority compared to scaffold-free group. Cartilage repair was evident in all treated groups (*); however, fine fronds on the cartilage surface were evident in all of HOI-only and HOI-cells defects, while smoother cartilage surface was exhibited throughout CS groups. * $P < 0.05$.

cell redifferentiation on a genotypic level (Fig. 5b). However, COL10A1 expression remained numerically lower throughout the culture period only in HOI-cells group, thus supporting the improved chondrogenic characteristic. CS-cells group was superior compared to monolayer cells by numerically lower fibroblastic expression values. In addition, it improved significantly, by expressing less COL10A1 at day 12 ($P = 0.0355$). CS-cells scaffold expressed less fibroblastic gene than HOI-cells group at day 12 ($P = 0.0077$). *In vitro* potency analysis values are set in supplementary data (Suppl. Table S4).

Macroscopic Evaluation

No swelling, signs of inflammatory, or immune responses to implanted materials on operated knees were observed at 6 months after implantation. CS-cells group had the highest mean OAS score among all experimental groups (Fig. 6).

CS-cells group OAS evaluation revealed the most hyaline-like cartilage, when compared to scaffold-free group ($P = 0.0347$). Other experimental groups did not differ among each other significantly; however, a tendency for superior outcome in HOI-only ($P = 0.076$) and HOI-cells ($P = 0.69$)

compared to scaffold-free group was also noted. A numerically inferior outcome in HOI groups was mainly influenced by more fine fronds on the cartilage surface when compared to a smoother cartilage surface in CS groups. Macroscopic values are set in supplementary data (Suppl. Table S5).

Histological Analysis

Mean cartilage repair scores were superior in all treatment groups compared to the scaffold-free group at 6 months; however, a significantly superior histological outcome was scored in CS-cell ($P = 0.035$) group only (Fig. 7).

A clear numerical advantage of HOI-cell group over scaffold-free group was also noted ($P = 0.057$). Other experimental groups were comparable among each other; however, HOI-only group had a tendency for superior histological restoration compared to the control group, as well ($P = 0.103$). Restoration of subchondral bone was not achieved in any of the samples, with slight contour changes throughout experimental groups. HOI structural elements were dispersed in cartilage and subchondral bone layers enfolded in the host tissue. No evidence of infection, donor tissue rejection, or immune response was noted in any

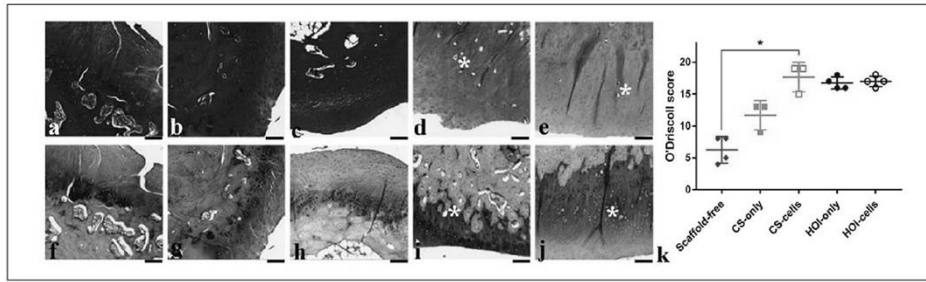


Figure 7. Histological evaluation of experimental groups at 6 months after treatment in (a, f) scaffold-free, (b, g) CS-only (c, h), CS-cells (d, i), HOI-only, and (e, j) HOI-cells groups, as evaluated by a modified O'Driscoll score. (k) Histological score improved in all treatment groups compared to the scaffold-free group as assessed by (a-e) Safranin O and (f-j) toluidine blue staining. A positive tendency was noted in HOI-cell and HOI-only groups over scaffold-free group. HOI structural elements (*) were evident in cartilage and subchondral layer. CS-cells group was superior compared to control group. * $P < 0.05$. Scale bar: 200 μm .

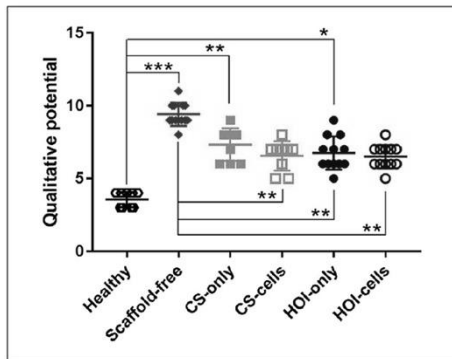


Figure 8. Electromechanical measurement in cartilage-treated areas with Arthro-BST. Electromechanical parameter measured at HOI-only, HOI-cells, and CS-cells groups was lower than scaffold-free group, thus resulting in superior repair in these groups. HOI-cells and CS-cells exhibited improved values of electromechanical parameter and were comparable to healthy cartilage. * $P < 0.05$, ** $P < 0.01$, *** $P < 0.001$.

histological samples of experimental groups. Histological values are set in supplementary data (Suppl. Table S5).

Electromechanical Testing

Electromechanical parameter measured at the cartilage repair sites treated with HOI-only, HOI-cells, and CS-cells groups were lower than untreated scaffold-free group, resulting in superior repair for scaffold-based groups, especially cell-seeded scaffolds (Fig. 8).

Significantly inferior electromechanical properties were noted in CS-only ($P = 0.002$), HOI-only ($P = 0.022$), and in scaffold-free ($P < 0.0001$) groups compared to healthy cartilage. However, HOI scaffolds with cells ($P = 0.0014$) or without ($P = 0.0059$) exhibited improved values of electromechanical parameter compared to scaffold-free group. Despite the noninferiority between healthy cartilage values compared to CS-cell ($P = 0.069$) and HOI-cell ($P = 0.066$) groups, the best repair potential has been shown for cell seeded groups, as expressed by improved intrinsic electromechanical properties of cartilage. Electromechanical values are set in supplementary data (Suppl. Table S5).

Discussion

This study demonstrated a sustained cartilage repair at 6 months after 3D HOI scaffold implantation. This was supported by macroscopical, histological, and electromechanical analysis. To our knowledge, this is the first *in vivo* study to analyze electromechanical properties of a TEP in a long-term preclinical study.

Chondrocytes have long been a first choice of cells for articular cartilage repair, due to their genotypic and phenotypic compliance to the cartilage treatment area. Morphological, genotypic, and phenotypic profiles of chondrocytes have been well established and *in vivo* efficacy of cellular TEPs has been proven in long-term *in vivo* human studies.²⁷⁻²⁹

Physical and chemical properties of TEP influence cell attachment and the resultant potency *in vitro* and efficacy *in vivo*. DLW-PP and SZ2080 material enable predetermining parameters such as pore size, shape, and porosity, which would support the ingrowth of cells and extracellular matrix ECM deposition. A described discrepancy among gene expression and protein secretion prompted PCR (polymerase

chain reaction) and ELISA (enzyme-linked immunosorbent assay) analysis *in vitro*.³⁰ Despite the decline of protein secretion, HOI retained the same protein translation level as that of monolayer chondrocytes used for seeding. A period up to day 4 should be analyzed in detail, to determine if the spike of gene expression has occurred earlier. From the clinical translation perspective, most scaffolds tend to be cultured for a very brief period after seeding, with the focus on accelerated implantation. This enables faster and more qualitative *in vivo* redifferentiation, even compared to recently introduced bioreactors, which are still ways of addressing functional and structural mimics of *in vivo* conditions, after prolonged *in vitro* culture.³¹

Cell-based cartilage regeneration has been best established for chondral defects, requiring additional bone grafting for subchondral lesions.³² Despite a complicated osteochondral defect used in our study, improvement at 6-month follow-up was evident in most of the experimental groups, especially HOI and CS scaffold groups with cells. Both HOI groups had a tendency for better OAS compared to a scaffold-free group, mainly because of superior tissue integration and smoother cartilage surface in the defect area. Interestingly, OAS score was numerically inferior in a HOI group with cells, when compared to HOI without cells, representing superior macroscopical outcome in HOI without cells group. This might be the result of cells' interference in a scaffold full integration by suppressing the attractiveness of host tissue cells. A recent study showed an increased fibrosis in a cell-based scaffold, compared to cell-free scaffold, suggesting an inhibitory cell effect on host tissue integration.³³ The property of cell migration toward scaffold should be analyzed in the future studies.

Histologically cell groups had a tendency for superiority over cell-free groups, mainly influenced by the hyaline-like cellular morphology and over 75% of area filled with chondrocytes, both of which are influenced by the addition of cells. HOI structural elements were enfolded both in cartilaginous and subchondral layers, with no signs of inflammation. Nevertheless, subchondral bone was not fully restored and slight bone plate changes were evident throughout all of the samples. Biphasic scaffolds with different mechanical and spatial parameters have been proposed to provide a superior osteochondral repair.³⁴ Strategies for choosing the right morphological scaffold parameters vary among groups.³⁵⁻³⁷ In addition, the subchondral interface between bone marrow and calcified cartilage layer containing vessels and innervation must be addressed as well.³⁸

An increasing number of *in vivo* experimental TEP studies have prompted a need for a quick and reliable assessment of treatment outcome, other than invasive diagnostic methods, especially in long-term preclinical studies. Electromechanical properties have been shown to reflect cartilage quality and correlate to histological and biomechanical parameters,

apoptosis, and inversely correlate to chondrocyte viability.^{18,20,39} In addition, electromechanical analysis has been shown to be more sensitive than invasive biomechanical testing.⁴⁰ In our study, we have observed higher electromechanical potential in the repair cartilage compared to healthy cartilage, revealing incomplete cartilage regeneration. Nevertheless, scaffold groups with cells had a significantly higher score compared to scaffold-free groups, translating to better cartilage quality. In addition, inferiority to a healthy cartilage was only marginal in both groups with cells, revealing satisfactory *in vivo* cartilage regeneration. Results from Arthro-BST were comparable to histological results of cartilage repair quality in our study. Inclusion of QP measurement has already been applied in explanted human osteochondral cores, and correlation to other cartilage quality parameters have suggested a possible use of this technique to detect underlying cartilage defects, otherwise not visible with a macroscopic analysis.¹⁸ Electromechanical measurement can serve as a diagnostic *in vivo* method to quantify damaged and regenerated cartilage, by reflecting essential cartilage quality parameters.

Acknowledgments and Funding

The author(s) disclosed receipt of the following financial support for the research, authorship, and/or publication of this article: This research was funded by a grant (No. SEN-20/2015) from the Research Council of Lithuania.

Declaration of Conflicting Interests

The author(s) declared no potential conflicts of interest with respect to the research, authorship, and/or publication of this article.

Ethical Approval

Ethical approval for this study was obtained from Animal Health and Welfare Department, State Food and Veterinary Service of the republic of Lithuania (G2-36).

Animal Welfare

The present study followed international, national, and/or institutional guidelines for humane animal treatment and complied with relevant legislation.

ORCID iD

Justinas Maciulaitis  <https://orcid.org/0000-0002-1265-8657>

References

1. Armiento AR, Stoddart MJ, Alini M, Eglin D. Biomaterials for articular cartilage tissue engineering: learning from biology. *Acta Biomater.* 2018;65:1-20. doi:10.1016/j.actbio.2017.11.021
2. Dhandayuthapani B, Yoshida Y, Maekawa T, Kumar DS. Polymeric scaffolds in tissue engineering application: a review. *Int J Polym Sci.* 2011;2011:290602. doi:10.1155/2011/290602

3. Maciulaitis J, Rekstyte S, Usas A, Jankauskaitė V, Gudas R, Malinauskas M, *et al.* Characterization of tissue engineered cartilage products: recent developments in advanced therapy. *Pharmacol Res.* 2016;113(pt B):823-32. doi:10.1016/j.phrs.2016.02.022
4. Carletti E, Motta A, Migliaresi C. Scaffolds for tissue engineering and 3D cell culture. *Methods Mol Biol.* 2011;695:17-39. doi:10.1007/978-1-60761-984-0_2
5. Bueno EM, Laevsky G, Barabino GA. Enhancing cell seeding of scaffolds in tissue engineering through manipulation of hydrodynamic parameters. *J Biotechnol.* 2007;129(3):516-31. doi:10.1007/s1027-01259-71. doi:10.1177/0363546509346395
6. Brittberg M. Cell carriers as the next generation of cell therapy for cartilage repair: a review of the matrix-induced autologous chondrocyte implantation procedure. *Am J Sports Med.* 2010;38(6):1259-71. doi:10.1177/0363546509346395
7. Nazempour A, Van Wie BJ. Chondrocytes, mesenchymal stem cells, and their combination in articular cartilage regenerative medicine. *Ann Biomed Eng.* 2016;44(5):1325-54. doi:10.1007/s10439-016-1575-9
8. Salzmann GM, Calek AK, Preiss S. Second-generation autologous minced cartilage repair technique. *Arthrosc Tech.* 2017;6(1):e127-e131. doi:10.1016/j.eats.2016.09.011
9. Ovsianikov A, Mironov V, Stampf J, Liska R. Engineering 3D cell-culture matrices: multiphoton processing technologies for biological and tissue engineering applications. *Expert Rev Med Devices.* 2012;9(6):613-33. doi:10.1586/erd.12.48
10. Selimis A, Mironov V, Farsari M. Direct laser writing: principles and materials for scaffold 3D printing. *Microelectron Eng.* 2015;132(C):83-9. doi:10.1016/j.mee.2014.10.001
11. Rekstyte S, Maciulaitis J, Maciulaitis R, Malinauskas M. Fabrication of 3D micro-structured scaffolds by direct laser writing in pre-polymers for in vitro and in vivo studies. *Proc SPIE.* 2017;10094. doi:10.1117/12.2249579
12. Malinauskas M, Zukauskas A, Hasegawa S, Hayasaki Y, Mizzeikis V, Buividas R, *et al.* Ultrafast laser processing of materials: from science to industry. *Light Sci Appl.* 2016;5(8):e16133. doi:10.1038/lsa.2016.133
13. Ricci D, Nava MM, Zandrini T, Cerullo G, Raimondi MT, Osellame R. Scaling-up techniques for the nanofabrication of cell culture substrates via two-photon polymerization for industrial-scale expansion of stem cells. *Materials (Basel).* 2017;10(1):E66. doi:10.3390/ma10010066
14. Trautmann A, Rüth M, Lemke HD, Walther T, Hellmann R. Two-photon polymerization based large scaffolds for adhesion and proliferation studies of human primary fibroblasts. *Opt Laser Technol.* 2018;106:474-80. doi:10.1016/j.optlastec.2018.05.008
15. Danilevicius P, Rekstyte S, Balciunas E, Kraniauskas A, Jarasiene R, Sirmenis R, *et al.* Micro-structured polymer scaffolds fabricated by direct laser writing for tissue engineering. *J Biomed Opt.* 2012;17(8):081405-1. doi:10.1117/1.JBO.17.8.081405
16. Maciulaitis J, Deveikyte M, Rekstyte S, Bratchikov M, Darinskas A, Šimbelytė A, *et al.* Preclinical study of SZ2080 material 3D microstructured scaffolds for cartilage tissue engineering made by femtosecond direct laser writing lithography. *Biofabrication.* 2015;7(1):015015. doi:10.1088/1758-5090/7/1/015015
17. Coopman K, Medcalf N. From production to patient: challenges and approaches for delivering cell therapies. In: *StemBook.* Amsterdam, Netherlands: IOS Press; 2014. doi:10.3824/stembook.1.97.1
18. Changoor A, Couto JP, Garon M, Quenneville E, Hurtig MB, Buschmann MD. Streaming potential-based arthroscopic device is sensitive to cartilage changes immediately post-impact in an equine cartilage injury model. *J Biomech Eng.* 2011;133(6):61005. doi:10.1115/1.4004230
19. Skarmoutsou A, Lolas G, Charitidis CA, Chatzizokolaidou M, Vamvakaki M, Farsari M. Nanomechanical properties of hybrid coatings for bone tissue engineering. *J Mech Behav Biomed Mater.* 2013;25:48-62. doi:10.1016/j.jmbm.2013.05.003
20. Mickevicius T, Pockevicius A, Kucinskas A, Gudas R, Maciulaitis J, Noreikaite A, *et al.* Impact of storage conditions on electromechanical, histological and histochemical properties of osteochondral allografts. *BMC Musculoskelet Disord.* 2015;16(1):314. doi:10.1186/s12891-015-0776-y
21. Garon M, Légaré A, Guardo R, Savard P, Buschmann MD. Streaming potentials maps are spatially resolved indicators of amplitude, frequency and ionic strength dependent responses of articular cartilage to load. *J Biomech.* 2002;35(2):207-16. doi:10.1016/S0021-9290(01)00197-x
22. Schagemann JC, Rudert N, Taylor ME, Sim S, Quenneville E, Garon M, *et al.* Bilayer implants: electromechanical assessment of regenerated articular cartilage in a sheep model. *Cartilage.* 2016;7(4):346-60. doi:10.1177/1947603515623992
23. Chen AC, Nguyen TT, Sah RL. Streaming potentials during the confined compression creep test of normal and proteoglycan-depleted cartilage. *Ann Biomed Eng.* 1997;25(2):269-77.
24. Sim S, Hadjab I, Garon M, Quenneville E, Lavigne P, Buschmann MD. Erratum to: development of an electromechanical grade to assess human knee articular cartilage quality. *Ann Biomed Eng.* 2017;45(10):2422. doi:10.1007/s10439-017-1879-4
25. Schmitz N, Laverty S, Kraus VB, Aigner T. Basic methods in histopathology of joint tissues. *Osteoarthritis Cartilage.* 2010;18(Suppl 3):S113-S116. doi:10.1016/j.joca.2010.05.026
26. O'Driscoll SW, Keeley FW, Salter RB. The chondrogenic potential of free autogenous periosteal grafts for biological resurfacing of major full-thickness defects in joint surfaces under the influence of continuous passive motion. An experimental investigation in the rabbit. *J Bone Joint Surg Am.* 1968;68(7):1017-35.
27. Hissnauer TN, Baranowsky A, Pestka JM, Streichert T, Wiegandt K, Goepfert C, *et al.* Identification of molecular markers for articular cartilage. *Osteoarthritis Cartilage.* 2010;18(12):1630-8. doi:10.1016/j.joca.2010.10.002
28. Grogan SP, Barbero A, Diaz-Romero J, Cleton-Jansen AM, Soeder S, Whiteside R, *et al.* Identification of markers to characterize and sort human articular chondrocytes with enhanced in vitro chondrogenic capacity. *Arthritis Rheum.* 2007;56(2):586-95. doi:10.1002/art.22408
29. Brittberg M, Recker D, Ilgenfritz J, Saris DBF. SUMMIT Extension Study Group Matrix-applied characterized autologous cultured chondrocytes versus microfracture: five-year

- follow-up of a prospective randomized trial. *Am J Sports Med.* 2018;46(6):1343-51. doi:10.1177/0363546518756976
30. McManus CJ, May GE, Spealman P, Shteyman A. Ribosome profiling reveals post-transcriptional buffering of divergent gene expression in yeast. *Genome Res.* 2014;24(3):422-30. doi:10.1101/gr.164996.113
31. Selden C, Fuller B. Role of bioreactor technology in tissue engineering for clinical use and therapeutic target design. *Bioengineering (Basel).* 2018;5(2):E32. doi:10.3390/bioengineering5020032
32. Salzmann GM, Niemeyer P, Hochrein A, Stoddart MJ, Angele P. Articular cartilage repair of the knee in children and adolescents. *Orthop J Sport Med.* 2018;6(3):2325967118760190. doi:10.1177/2325967118760190
33. Ye K, Traianedes K, Robins SA, Choong PFM, Myers DE. Osteochondral repair using an acellular dermal matrix-pilot in vivo study in a rabbit osteochondral defect model. *J Orthop Res.* 2018;36(7):1919-28. doi:10.1002/jor.23837
34. Sherwood JK, Riley SL, Palazzolo R, Brown SC, Monkhouse DC, Coates M, et al. A three-dimensional osteochondral composite scaffold for articular cartilage repair. *Biomaterials.* 2002;23(24):4739-51.
35. Pan Z, Duan P, Liu X, Wang H, Cao L, He Y, et al. Effect of porosities of bilayered porous scaffolds on spontaneous osteochondral repair in cartilage tissue engineering. *Regen Biomater.* 2015;2(1):9-19. doi:10.1093/rb/rbv001
36. Wang Y, Meng H, Yuan X, Peng J, Guo Q, Lu S, et al. Fabrication and in vitro evaluation of an articular cartilage extracellular matrix-hydroxyapatite bilayered scaffold with low permeability for interface tissue engineering. *Biomed Eng Online.* 2014;13:80. doi:10.1186/1475-925X-13-80
37. Duan P, Pan Z, Cao L, He Y, Wang H, Qu Z, et al. The effects of pore size in bilayered poly(lactide-co-glycolide) scaffolds on restoring osteochondral defects in rabbits. *J Biomed Mater Res A.* 2014;102(1):180-92. doi:10.1002/jbm.a.34683
38. Madry H, van Dijk CN, Mueller-Gerbl M. The basic science of the subchondral bone. *Knee Surg Sport Traumatol Arthrosc.* 2010;18(4):419-33. doi:10.1007/s00167-010-1054-z
39. Sim S, Chevrier A, Garon M, Quenneville E, Yaroshinsky A, Hoemann CD, et al. Non-destructive electromechanical assessment (Arthro-BST) of human articular cartilage correlates with histological scores and biomechanical properties. *Osteoarthritis Cartilage.* 2014;22(11):1926-35. doi:10.1016/j.joca.2014.08.008
40. Changoor A, Coutu JP, Garon M, Quenneville E, Hurtig MB, Buschmann MD. Streaming potential-based arthroscopic device is sensitive to cartilage changes immediately post-impact in an equine cartilage injury model. *J Biomech Eng.* 2011;133(6):61005.



Full length article

Customization of direct laser lithography-based 3D scaffolds for optimized *in vivo* outcome



Justinas Maciulaitis^{a,*}, Sima Rekštytė^b, Maksim Bratchikov^c, Rimtautas Gudas^a, Mangirdas Malinauskas^b, Alius Pocekevicius^d, Arvydas Usas^c, Augustinas Rimkunas^c, Virginija Jankauskaite^f, Valdas Grigaliunas^g, Romaldas Maciulaitis^c

^a Department of Sports Medicine, Medical Academy, Lithuanian University of Health Sciences, Kaunas, Lithuania

^b Laser Research Center, Faculty of Physics, Vilnius University, Vilnius, Lithuania

^c Department of Physiology, Biochemistry, Microbiology and Laboratory Medicine, Institute of Biomedical Sciences, Faculty of Medicine, Vilnius University, Vilnius, Lithuania

^d Department of Veterinary Pathobiology, Veterinary Academy, Lithuanian University of Health Sciences, Kaunas, Lithuania

^e Institute of Physiology and Pharmacology, Medical Academy, Lithuanian University of Health Sciences, Kaunas, Lithuania

^f Department of Production Engineering, Faculty of Mechanical Engineering and Design, Kaunas University of Technology, Kaunas, Lithuania

^g Institute of Mechatronics, Kaunas University of Technology, Kaunas, Lithuania

ARTICLE INFO

Keywords:

Direct laser writing lithography
Biomaterials
SZ2080
Artificial scaffolds
Tissue engineering

ABSTRACT

Direct laser writing 3D lithography in pre-polymers was employed to microstructure custom 3D silicon-zirconium hybrid organic-inorganic polymer SZ2080 scaffolds (HOI) of varying morphology for cartilage repair in a preclinical xenogenic model. Scaffolds were fabricated to contain tetragonal and hexagonal pores, followed by pore scaling of 1.5 and 2 times. HOI scaffolds were seeded with human chondrocytes (cells) and biocompatibility was analyzed *in vitro*. Tissue engineered cartilage (TEC) potency, efficacy and shelf-life *in vitro* was assessed by morphological, biomechanical, metabolic activity, cell count, ELISA and PCR analysis. Optimal HOI scaffold was implanted in a long-term preclinical osteochondral defect of immunodeficient rat model and analyzed for the translated efficacy in experimental groups. Collagen scaffold was a positive comparator for *in vitro* and *in vivo* studies. Treatment efficacy was evaluated after 3 months using standardized macroscopical and histological scores. Biocompatibility was superior in tetragon-pored scaffold (HOI-T) compared to hexagon-pored HOI *in vitro*. Cartilage tissue formation in HOI with tetragonal pores scaled 1.5 times was comparable to HOI-T at least for up to 7 days *in vitro*. HOI-T with and without cells improved cartilage repair and were comparable to collagen scaffold *in vivo* at 3-months follow-up.

1. Introduction

Articular cartilage lesions are amongst the major health problems for active population [1]. Avascular origin of the cartilage greatly limits the innate capacity for qualitative regeneration [2,3]. Sustained injury to the osteochondral region often leads to a spontaneous repair, however structural and functional properties of the formed tissue are inferior compared to native cartilage [4]. This leads to a repaired cartilage deterioration and progression toward osteoarthritis [5].

Different treatment methods to manage a sustained osteochondral injury have been introduced [6], however complete restoration of cartilage tissue has not yet been achieved. Recently, scaffold and cellular based tissue engineering have progressed rapidly and currently

hold a promise as a useful tool in the field of regenerative orthopedics and especially, cartilage repair.

Similarly, to any medical product, quality parameters for tissue engineered cartilage (TEC) must be established, as well. Safety and efficacy profiles highly depend on characterization of cellular, non-cellular components and the interaction in between.

Biomaterials and fabrication methods are essential elements to enhance seeded cell proliferation, interaction and deposition of extracellular matrix (ECM) at the time of TEC manufacturing [7]. Natural collagen-based scaffolds possess inherent bioactive properties, to facilitate cell and material interaction, thus enhancing chondrogenic activity [8,9]. Similarly, additive manufacturing of synthetic scaffolds, such as direct laser writing in pre-polymers (DLW-PP) is being carefully

* Corresponding author.

E-mail address: justinas.maciulaitis@ismuni.lt (J. Maciulaitis).

<https://doi.org/10.1016/j.apsusc.2019.05.065>

Received 21 September 2018; Received in revised form 3 May 2019; Accepted 7 May 2019

Available online 08 May 2019

0169-4332/ © 2019 Elsevier B.V. All rights reserved.

investigated in tissue engineering due to its three-dimensional (3D) structuring capability, high spatial resolution, scaling flexibility and diversity of processable materials [10–14].

TEC biocompatibility is highly dependent on scaffold biomechanical and physical features *in vitro* [15,16]. Customization of scaffolds with highly predictable physical characteristics, such as mechanical rigidity, pore size, porosity and pore interconnectivity is enabled by the ability to adjust parameters of synthetic polymeric feed material [17–19]. These critical structural parameters provide a homogenous distribution of cells and nutrient transfer within the scaffold [20,21]. In addition, phenotype formation and superior production of ECM proteins can be influenced by the custom design of pore morphology [22]. Scaffold biomechanics can be similarly affected by the surrounding liquid medium, especially the soft natural collagen-based scaffolds, thus reducing biomechanical properties of the scaffold prior to implantation.

The ability of chondrocytes to effectively adhere to the scaffold is highly dependent on cell viability. In addition, viable cell proliferation is indicative of the ability to deposit ECM on the scaffold, thus identification of optimal biomaterial morphological parameters is essential for specific cellular processes [23]. Similarly, TEC potency *in vitro* is established by cartilaginous protein expression and secretion [24]. A lost ability of monolayer cells to express hyaline cartilage genes could be reversed in a 3D culture [25]. Therefore, upregulation of genes encoding hyaline cartilage specific type-II collagen is indicative of the cell redifferentiation and functionality of TEC *in vitro*.

With a variety of technologies available for scaffold fabrication, clinical usage of effective scaffold is still limited due to inconsistent manufacturing methods, insufficient characterization and lack of pre-clinical studies for safety and efficacy evaluation [26]. This supports the use of DLW-PP lithography technique and the design of appropriate scaffold morphology for a subsequent TEC testing in a preclinical setting. Thus, the formation of cartilage tissue *in vitro* and the regenerative potential *in vivo* by the TEC with human cells was compared between currently used medical implants and the state-of-the-art DLW-PP 3D lithography technique in this xenogeneic preclinical study.

2. Materials and methods

2.1. Scaffold manufacturing

A high power and energy Yb:KGW femtosecond laser system (Pharos, Light Conversion, Vilnius, Lithuania), generating 1030 nm central wavelength and 300 fs duration pulses with adjustable repetition rate in the 1 to 200 kHz range was used to fabricate 3D scaffolds of silicon-zirconium containing hybrid material. The wavelength was frequency-doubled to 515 nm and the repetition rate set to 200 kHz for the fabrication of presented scaffolds. The positioning of the focal spot inside the pre-polymer was implemented by using the infinite field of view regime exploiting the synchronized motion of the galvanometer scanners (Scanlab, Munich, Germany) and linear stages (Aerotech, Pittsburgh, PA, USA), allowing the usage of high-speed scanning capabilities. The principle of synchronization is based on distributing the focal spot movement inside the pre-polymer so that linear stages are responsible for long continuous movements while the scanners are more involved in fast movements and trajectory corrections when needed. This allows employing the high velocity of the stages and in the same time overcoming the defects that would arise due to inertia during acceleration/deceleration as deviations of the set velocity are compensated by the scanners via a feedback loop. The developed continuous laser 3D writing technique is studied and presented in details elsewhere [27].

In addition, despite the bigger scaffold size than the working range of the used 0.8 NA objective (Carl Zeiss AG, Oberkochen, Germany), the need for stitching was avoided. The scaffold geometry was programmed and the whole fabrication process was controlled by a 3DPoli software package (Femtika, Vilnius, Lithuania) [28–30].

As a structuring material we used hybrid organic-inorganic pre-polymer [31], photo-sensitized with 1% of 2-benzyl-2-(dimethylamino)-4'-morpholinobutyrophenone (IRG, Sigma Aldrich, St. Louis, MO, USA) photo-initiator. Pre-polymer was created for DLW-PP applications, therefore is characterized by its superb 3D micro-/nano-structuring properties. Also, biocompatibility of this material and animal cells was demonstrated in our previous preclinical cartilage regeneration study [32].

The sample preparation for the laser structuring was performed by the following process. The required area ($\sim 1.5 \times 1.5 \text{ cm}^2$, depending on the amount of needed scaffolds) of the cover glass was covered with the liquid pre-polymer and heated on a hot-plate at 40–70–90 °C (20 min each) with a 5-minute ramp before each temperature raise to avoid bubble formation. Due to loss of the solvent liquid material turns into a gel during this pre-bake step. The pre-bake step is necessary to evaporate the solvent which would otherwise inhibit the polymerization reaction and/or cause micro explosions due to overheating [31]. Afterwards, another layer of the pre-polymer was put on top of the pre-heated one and the heating step was run again. Therefore, several consequent processes of heating on the hot-plate were performed to achieve the height of pre-polymer drop exceeding the predetermined scaffold height. Subsequently, complete solvent evaporation from the volume of the pre-polymer was achieved by incubating the samples overnight at 70–75 °C.

The scaffolds with hexagonal pores and tetragonal pores were realized by exposing to $P = 420 \mu\text{W}$ and $P = 520 \mu\text{W}$ average optical powers corresponding to $I = 2.5 \text{ TW}/\text{cm}^2$ and $I = 3.1 \text{ TW}/\text{cm}^2$ at the focal spot in the sample. Depending on the scaffold type and porosity the fabrication took from 11 min (for the highest porosity HOI-T2 scaffolds) up to 38 min (for HOI-H scaffolds).

After laser exposure the samples were developed in 4-methyl-2-pentanone for at least 60 min and then moved into a clean developer bath and left for additional 3 h. The procedure was repeated at least twice with a couple of hours in between the solvent change to make sure that all of the non-polymerized material is washed away. Since SZ2080 is solid gel during laser fabrication, the scaffolds were manufactured in the volume of the pre-polymer, so after development the scaffolds were not stuck to the glass substrate. Alternatively, the weak adherence during subsequent stages of sample preparation for the implantation could be easily overcome by gentle probing with a scalpel/tweezers.

A commercially available bilayer collagen scaffold (CS, Chondro-Gide, Geistlich Biomaterials, Wollhusen, Switzerland) was cut to the same dimensions as HOI and used as a direct comparator. CS is made of highly refined porcine collagen and has been shown to be effective for treating traumatic cartilage defects [33].

CS scaffolds were individually packed under sterile conditions, while HOI scaffolds were chemically disinfected in 70% ethanol solution overnight and UV irradiated for 2 h, after drying. The next day scaffolds were washed in phosphate buffered saline solution (Sigma Aldrich, St. Louis, MO, USA) and left to dry for subsequent cell seeding. Scaffold pore shaping and scaling: Computer models of four different types of scaffolds were created and then used for fabrication. In the first stage of experiment, tetragon-pored scaffold (HOI-T) and hexagon-pored scaffold (HOI-H) were investigated for the pore shape influence to cell growth.

HOI-T and HOI-H were comprised of hollow-sided rectangular and honeycomb prisms, respectively and put one next to another to form a single layer of the scaffold. Each scaffold had three such layers stacked one atop another. Each layer had an offset in both directions to the previous layer in HOI-T, thus four square shape top pores were formed throughout the scaffold. Contrarily, an offset in one direction to the previous layer was made in HOI-hexa, thus three rhombus shape top pores were formed throughout the scaffold.

In the second stage of experiment, top and side pores of HOI-T were scaled by the factors of 1.5 (HOI-T1.5) and 2 (HOI-T2) for the

determination of pore size effect on cell proliferation. Size of the scaffold was kept as similar as possible ($\approx 1.5 \times 1.5 \text{ mm}^2$) and only the overall height of the scaffold and a number of individual cell units was minutely changed. The rod width and height was kept constant – 15 μm in all cases.

2.2. Scaffold morphological analysis

Scanning electron microscopy (SEM) of HOI was performed by Hitachi TM-1000 (Hitachi High-Technologies Co., Tokyo, Japan), as previously described [32]. Briefly, scaffolds were washed and fixed in 2.5% glutaraldehyde solution. After series of ethanol dehydration, they were dried and coated with 20 μm gold. Manufactured and cell seeded HOI scaffolds were analyzed after 7 days of culture.

2.3. Biomechanical analysis

Microindentation (MCT Micro Combi Tester, Anton Paar, Graz, Austria) of HOI-T, HOI-H and CS was performed according to Oliver and Pharr method [34]. Rockwell C diamond cone spherical indenter with radius of 200 μm was used for indentation. The strength of the scaffolds was tested in the direction parallel to the pore channels at the 30 $\mu\text{m}/\text{min}$ loading/unloading rates and 20 holding time at peak load. During test ceramic scaffolds were crushed layer by layer up to the defined maximal contact depth of 140 μm . The mean crushing force of ceramic scaffold was determined from load-indentation depth curves. Indentation curves were divided to regions 1, 2 and 3, each corresponding to the respective top, middle and bottom scaffold layer. Maximal forces obtained in each HOI layer are represented by the respective peak A, B and C. CS and HOI scaffolds biomechanical behaviour was represented by a single peak at the maximal indentation depth for dry and wet states. Indentation hardness (H_{IT}) was measured by the indenter penetration depth under the applied force throughout the test cycle, and thus reflecting plastic and elastic deformation of the material tested. Similarly, an indentation modulus (E_{IT}) was calculated, which determine the stiffness of contact with the material.

2.4. Cell isolation, culture and posology

All experimental procedures were approved and conducted according to the standard guidelines and protocols set by the Kaunas Regional Biomedical Research Ethics Committee. An informed signed content was obtained from the patient. Human cartilage tissue was collected during routine knee reconstruction surgery procedure as a waste material. Briefly, a biopsy was washed extensively, predigested with protease (Sigma) for 2 h and collagenase A (Worthington biochemical, Lakewood, NJ) overnight. Isolated cells were plated and cultured in Dulbecco's modified eagle medium (DMEM, Thermo Fisher, Hyclone, Logan, UT, USA) supplemented with 20% fetal bovine serum (Sigma), 100 U/ml^{-1} penicillin and 100 $\mu\text{g}/\text{ml}^{-1}$ streptomycin (Sigma) at 37 $^{\circ}\text{C}$ in a humid atmosphere with 5% CO_2 . Cells were harvested when reached 80% confluence.

Scaffolds were soaked in proliferation medium one day before seeding. Posology was determined based a cell dose required for seeding and was referenced to 1×10^6 cells to 1 cm^2 area of scaffold. Manufactured HOI and CS scaffold parameters are set at $1.5 \times 1.5 \text{ mm}^2$ in area, therefore, the proposed cell dosage of 4.5×10^4 cells per scaffold tested corresponds to the projected treatment posology.

After trypsinisation with 0.25% trypsin (Gibco, Invitrogen, Carlsbad, CA, USA), third passage cells were counted and resuspended in vials with culture medium. Cells were seeded in 40 μl doses on presterilized HOI and C scaffolds in a dropwise fashion. Seeded scaffolds were placed for 2 h in the CO_2 incubator to allow cellular adhesion before the remaining medium was added.

Seeded scaffolds were cultured up to 7 days. Medium was changed every 2–3 days. Scaffolds with cells were harvested after 1, 4 and 7 days

of culture and sent for *in vitro* analysis. Also, on the day 7 of culturing, scaffolds were prepared for *in vivo* implantation.

2.5. Metabolic activity and cell count analysis

An assay for human chondrocytes growth in HOI-T and HOI-H was performed using Presto Blue Cell Viability Reagent (Invitrogen, CA, USA) according to the manufacturer's recommendations. Presto Blue is a non-cytotoxic, resazurin based metabolic assay to determine cell viability. It measures mitochondrial ability of cells to reduce the non-fluorescent, blue resazurin to pink resorufin, thus biocompatibility of cells and manufactured scaffold could be evaluated [35]. Briefly, the assay was performed on four samples per endpoint on days 1, 4 and 7 post-seeding. Each scaffold was submerged in 10% Presto Blue solution and incubated for 30 min at 37 $^{\circ}\text{C}$. Samples were collected and read on a plate reader (Multiskan GO, Thermo Scientific) with the excitation wavelength set to 570 nm. A standard curve of absorbance vs. metabolic activity ratio of samples and monolayer cells was plotted. Similarly, a standard curve of absorbance vs. cell density was used to estimate cell count in scaffolds.

2.6. Biochemical analysis

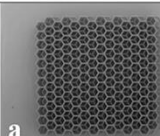
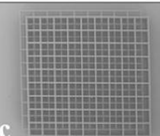
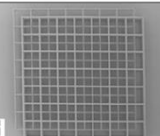
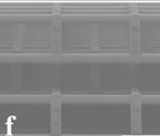
Type II collagen production evaluation was performed on the cells ($n = 4$) used for seeding on the scaffolds and the seeded scaffolds at days 1 ($n = 12$), 3 ($n = 9$) and 7 ($n = 5$) after seeding using enzyme-linked immunosorbent assay kit (human collagen type II ELISA kit, BioSite), according to manufacturer's protocol. The optical density absorbance was read at 450 nm in microplate reader (Multiskan GO, Thermo Scientific). A standard curve was plotted as the relative optical density of each standard solution vs. the respective concentration of the standard solution. Type II collagen concentration of the samples was interpolated from the standard curve.

2.7. Gene expression analysis

For the chondrogenic gene mRNA analysis, we examined type-II collagen (COL2A1) mRNAs' expression dynamics of cells at day 0 before the seeding on scaffolds and on days 1, 4 and 7 *in vitro*, as previously described. The total RNA from the samples was extracted using an ISOLATE II RNA Micro Kit (Bioline Reagents Ltd., London, UK) according to the manufacturer's instructions. Elution was performed with 10 μl RNase-free water included in the kit. SensiFAST Probe No-ROX One-Step Kit (Bioline Reagents Ltd., London, UK), primers and hydrolyzation probes (Biologio B.V., Nijmegen, Netherlands) were used for one-step RT-qPCR. The primer and probe sequences (Table S2, Supporting Information) were designed using Vector NTI Advance™ program (Thermo Fisher Scientific, Waltham, MA, USA) for sequences alignment and FastPCR online (<http://primerdigital.com/tools/pcr.html>) java applet for primers test. All multiplex one-step reactions were carried out in a total volume of 15 μl using 6.75 μl of the isolated RNA sample and primers at a concentration of 200 nM each, and probes at a concentration of 100 nM each. The multiplex one-step RT-qPCR assays were performed employing a real-time thermocycler Rotor-Gene Q 5plex model with software version 1.7 (Qiagen GmbH, Hilden, Germany) under the following conditions: first strand cDNA was synthesized at 45 $^{\circ}\text{C}$ for 20 min (1 cycle) and then denatured at 95 $^{\circ}\text{C}$ for 2 min (1 cycle); followed by 50 cycles of denaturation at 95 $^{\circ}\text{C}$ for 10 s and annealing/extension at 60 $^{\circ}\text{C}$ for 1 min.

The expression of β -actin mRNA was used as an internal standard for normalization of the target mRNA levels between different samples. The $2^{-\Delta\Delta C_T}$ algorithm was applied for calculation of the relative quantities of PCR amplification product reflecting the relative levels of target mRNA [36].

Table 1
Morphological (a,b,c,d) top-view and (e,f,g,h) side-view SEM images of HOI scaffolds. Pore shape influence to cell growth was analyzed in (a,c) HOI-H and (b,f) HOI-T scaffolds. Pore size effect on cell proliferation was determined in (c,g) HOI-T1.5 and (d,h) HOI-T2 images. Scale bar: a,b,c,d – 500 μm , e,f,g,h – 100 μm .

Scaffold type	HOI-H	HOI-T	HOI-T1.5	HOI-T2
				
				
Scaffold size (W×L×H), μm^3	1511×1567×195	1515×1515×195	1582.5×1582.5×262.5	1590×1590×330
Side pore (L×H), μm^2	49×45	105×45	150×67.5	195×90
Top pore (L×H), μm^2	42×49	45×45	67×67	90×90
Porosity, %	87	89	94	96

2.8. Repair of osteochondral defects

All experimental procedures were approved and conducted according to the standard guidelines and protocols by the Animal Health and Welfare Department, State Food and Veterinary Service. Nine, 10-week-old nude rats (NIHRNU-M, NTac:NIH-Foxn1^{rmu}; Taconic, NY, USA) were used in this study. The animals were anesthetized through an inhalation mask after exposure to 3% isoflurane and O₂ gas. The knee joint was approached by lateral parapatellar approach, and the trochlear groove was exposed by medial patellar dislocation. Critical size osteochondral defect (diameter: 1.5 mm, depth: 1 mm) was created through the articular cartilage and subchondral bone at the weight-bearing area of the trochlear groove. Defect was extensively washed with saline before scaffold implantation. Fibrin glue (Tisseel, Baxter, Glendale, CA) was added to the defect to secure the scaffold or fill the scaffold-free defect.

Osteochondral defects were divided into groups based on the treatment received: defects treated using HOI-T with cultured cells (HOI-cells, $n = 4$) and without cells (HOI-only, $n = 4$). Similarly, positive control groups included CS with cultured cells (CS-cells, $n = 3$) and without cells (CS-only, $n = 3$). Negative control group comprised defects with fibrin glue only (scaffold-free, $n = 4$). After the implantation patella was relocated, knee capsule was closed with interrupted 3-0 resorbable sutures (Ethicon, Johnson & Johnson Medical, Somerville, NJ). Overlying skin was approximated with 4-0 subcutaneous continuous suture (Ethicon) and disinfected.

After intervention, rats were housed and allowed to move freely within their cages. Rats were euthanized 3 months after surgery and samples for subsequent examination were collected.

2.9. Macroscopic evaluation

Macroscopic grading was carried out by two independent researchers and evaluated using a modified Oswestry Arthroscopy score (OAS) at 3 months after implantation. OAS evaluation system is comprised of key cartilage regeneration parameters: graft level, integration with surrounding cartilage, appearance of the surface and color of the repair tissue. Stiffness on probing was excluded from the original scoring system in our study. The maximum score of 8 represents normal cartilage (Table S3, Supporting information).

2.10. Histological analysis

Distal ends of femurs were cut above the condyles, fixed in a 10% neutral buffered formalin solution and embedded in paraffin blocks. 6 μm thick serial sections were deparaffinized and stained with Toluidine blue and Safranin-O stain (both Fisher Scientific, Pittsburgh, PA, USA) to assess glycosaminoglycans, proteoglycans and collagen production in repaired cartilage [37]. Sections were analyzed using a digital microscope (Olympus BX61, Center Valley, PA) with a camera (Olympus DP72, Olympus, Japan) and scored blindly using O'Driscoll histological scoring system (Table S4, supporting information) [38]. Higher score indicated superior cartilage repair, with 24 representing the maximum score.

2.11. Statistical analysis

Statistics were performed using GraphPad Prism 7.04. Statistical results were obtained using one-way ANOVA with Tukey's *post hoc* multiple comparison test. Results are presented as the mean and bracketed standard deviation (SD). Statistical significance between the groups is indicated with (*) which represents a $p < 0.05$ and (**) representing $p < 0.01$.

3. Results

3.1. Biomechanical analysis

Morphological characteristics of constructed HOI-H and HOI-T scaffolds were comparable to allow analysis of pore shape influence on biomechanical properties (Table 1).

Biomechanical response curves of irregular shape were generated by the indenter tip, as expressed by the obtained crushing force vs. indentation depth. Indentation curves of HOI-H and HOI-T demonstrated that the crushing force increased reaching peaks A, B and C at the depth of three consecutive regions from HOI top to bottom (Fig. 1(a,b)).

Fracture pattern was different amongst HOI scaffolds and was represented by a greater depth required to reach a maximum peak force in HOI-T, compared to HOI-H (Fig. 1(c)). Accumulated fractured parts precipitated in a different fashion in both scaffolds, thus increasing indentation force in a layer by layer fashion (Fig. 1(d)). A clear tendency for superior hardness and modulus in HOI-H compared to HOI-T

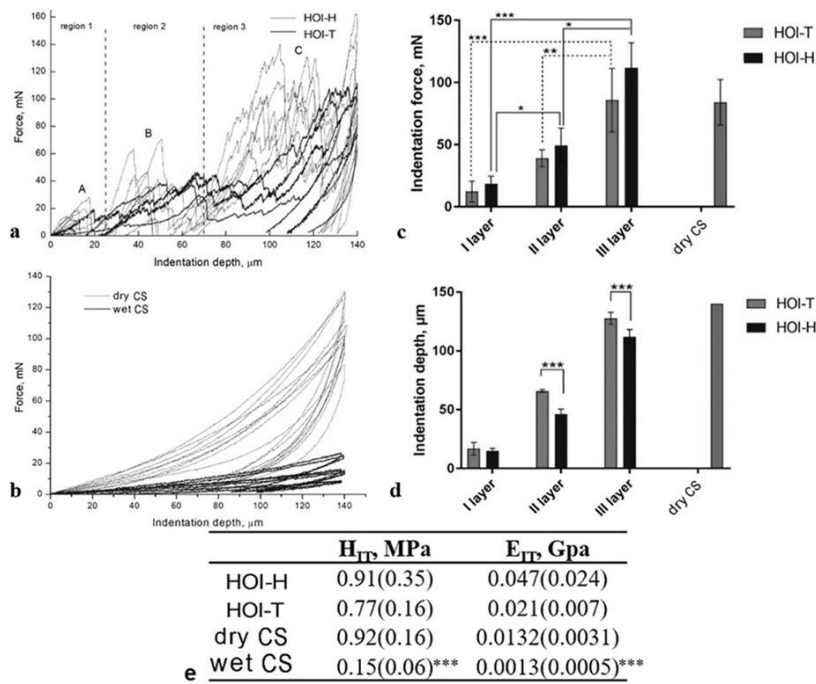


Fig. 1. Force-indentation depth curves obtained during microindentation test performed on HOI and CS. (a) Fracture pattern was different amongst HOI-T and HOI-H scaffolds while (b) dry and wet CS deformation patterns indicated reduced resistance for a wet CS. (c,d) Significantly higher force was registered with advancing to deeper layers of HOI scaffolds and was comparable to dry CS. (e) A tendency for superior H_{IT} and E_{IT} in HOI-H compared to HOI-T was noted. H_{IT} and E_{IT} of wet CS was significantly inferior to all scaffolds tested. * $p < 0.05$; ** $p < 0.01$; *** $p < 0.0001$.

was evident (Fig. 1(e)). Both HOI scaffolds retained the same H_{IT} and E_{IT} when kept in a wet state (data not shown). On the contrary, a steep and steady incline of crushing force was registered for dry-state CS, while wet-state CS registered a significant force reduction through 140 μm in depth. This simulated a clinical application prior CS implantation and indicated a reduced resistance for a wet-state CS. In addition, H_{IT} and E_{IT} of CS prepared for implantation was significantly inferior to HOI-T and HOI-H. Indentation force and depth values are set in supporting information of table S1.

3.2. Biocompatibility analysis and pore shape dependence

HOI-H cell adherence and increased ECM deposition was maintained up to 7 days *in vitro* by elongated matrix fibers in-between perpendicular rods (Fig. 2(a,b)).

Similarly, cells seeded on HOI-T adhered to the horizontal and vertical rods of the scaffold. Proliferation of elongated and spherical shape cells within both scaffolds was sustained up to 7 days *in vitro* and signified cell redifferentiation. Adjacent rods were interconnected by cells and ECM which have outgrown all the layers of HOI and filled the greater part of pore void at day 7, especially in HOI-T (Fig. 2(c,d)).

Cells seeded on HOI-T and HOI-H improved their metabolic activity compared to cells used for seeding (monolayer cells) (Fig. 3(a)).

Even though, the metabolic cellular improvement from day 1 to day 7 in both HOI-T and HOI-H groups was significant, it was comparable

amongst two groups at all endpoints. Nevertheless, only cells in HOI-T group improved at day 7, compared to monolayer cells, while HOI-T showed a clear tendency for improvement ($p = 0.057$).

Similarly, cell number increased in HOI-T and HOI-H at day 7, compared to monolayer cells count and was comparable amongst groups in all endpoints (Fig. 3(b)). However, a tendency for higher count of cells was noted in HOI-T group, compared to HOI-H. Improved metabolic activity translated to higher count of cells, thus supporting cellular proliferation on both HOI scaffolds, with a tendency for superiority in HOI-T group.

3.3. 3D cell redifferentiation and pore shape dependence

An improved type-II collagen protein secretion at day 1 was noted in HOI-T group, compared to monolayer cells. Reduced, yet sustained chondrogenesis was evident up to day 7 under regular culture conditions in HOI-T group (Fig. 3(c)).

Similarly, protein secretion retained its level up to day 7 in HOI-H group; however, it was comparable to secretion levels of monolayer cells throughout the period. A decrease in protein secretion was noted in both scaffold groups up to day 7, albeit not significant. Mean protein secretion values were greater in HOI-T group in all endpoints, when scaffolds with cells were compared to each other, albeit not significantly. Therefore, a superior initial phase of HOI-T scaffold and cells biocompatibility indicates at least a numerical superiority of tetragon-

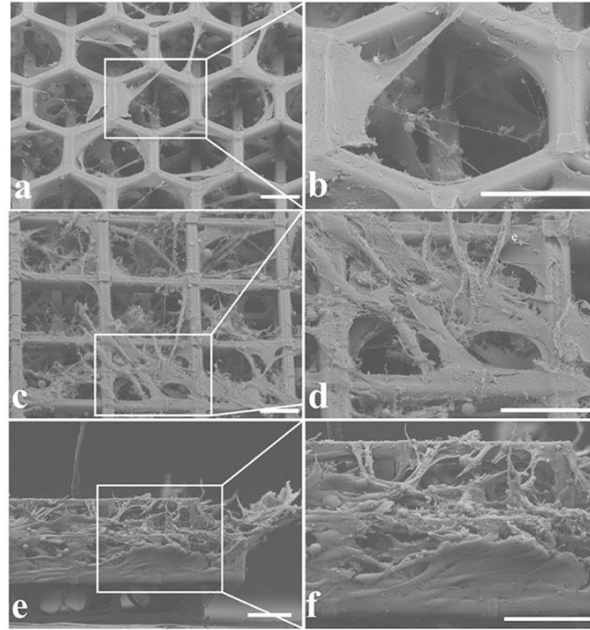


Fig. 2. Horizontal distribution of seeded cells and top view of (a,b) HOI-H scaffold at day 7 post seeding. Elongated and oval-shaped cells wrapped and bridged (c,d) horizontal and (e,f) vertical rods of the HOI-T scaffold and deposited ECM have outgrown all three layers, filling most of the pore volume at day 7. Scale bar: (a,b,c,d) 50 μm , (e,f) 100 μm .

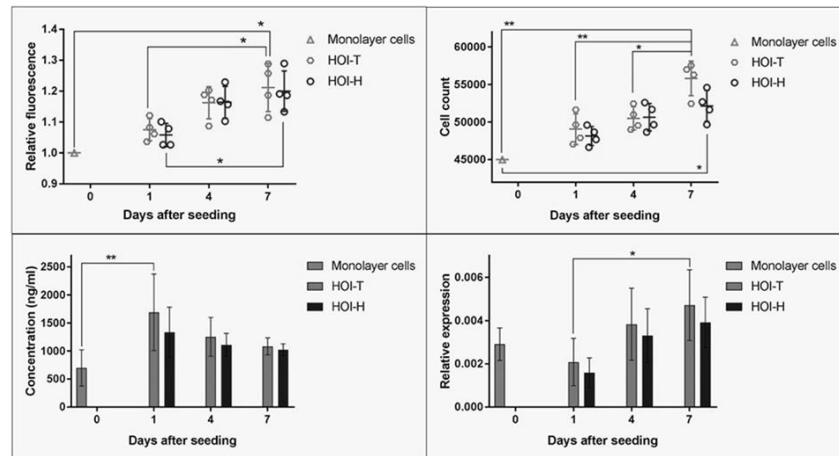


Fig. 3. (a) Metabolic activity and (b) count of cells seeded on HOI-T and HOI-H at days 1, 4 and 7. Similar improvement of metabolic activity and cell count up to day 7 was seen in both scaffolds, compared to cells used for seeding (cell control). Pore shape and biocompatibility dependence as represented by (c) type-II collagen protein secretion and (d) expression of HOI-T and HOI-H seeded with cells at days 1, 4 and 7 after seeding. Secretion improved at day 1 in HOI-T group, compared to cells used for seeding and sustained chondrogenesis up to day 7. Mean protein secretion values were higher in HOI-T group compared to HOI-H at all endpoints. Relative COL2A1 expression improved only in HOI-T up to day 7. * $p < 0.05$; ** $p < 0.01$.

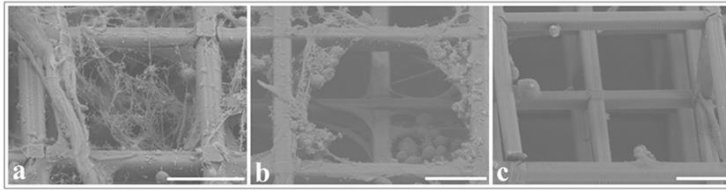


Fig. 4. Cells distribution in a tetragonal pore of (a) HOI-T, (b) HOI-T1.5 and (c) HOI-T2 at day 7 post seeding. Elongated and oval shape cells and the secreted ECM were noted on perpendicular and parallel planes within the HOI-T and HOI-T1.5 scaffolds. Only sporadic cell adherence was noted on the HOI-T2 rods. Scale bar: 50 μ m.

over hexagon-pored HOI.

COL2A1 was upregulated up to day 7 in HOI-H and HOI-T groups (Fig. 3(d)). Mean values of gene expression were comparable to values of monolayer cells in both groups throughout the culture period. Nevertheless, a significant improvement up to day 7 was noted only in HOI-T group.

No significant differences amongst two scaffolds were observed, however mean values of gene expression were higher in HOI-T group, compared to HOI-H group, thus supporting a tendency for superiority of tetragon- over hexagon-pored HOI.

3.4. 3D cell redifferentiation and pore scale dependence

In the second stage of experiment, top and side pores of HOI-T were scaled by the factors of 1.5 (HOI-T1.5) and 2 (HOI-T2) for the determination of pore size effect on cell proliferation (Table 1e,f,g,h). A comparable proliferation of elongated and oval shape cells within the HOI-T and HOI-T1.5 was sustained up to 7 days *in vitro* (Fig. 4(a,b)).

Cells and the secreted ECM were noted on perpendicular and parallel planes of scaffolds, thus supporting the predefined distance between the rods. HOI-T2 did not support cell growth and ECM production. Only sporadic cell adherence was noted on the rods, with little ECM production in all HOI-T2 scaffolds tested (Fig. 4(c)). Cells were randomly distributed in the superficial and middle layers of CS, interconnecting collagen folds and creases (Fig. S1, Supporting information).

Mean values of type-II collagen protein secretion improved at day 1 in HOI-T, HOI-T1.5 and HOI-T2 groups, however only HOI-T had a significant improvement (Fig. 5(a)).

Protein secretion numerically diminished in all HOI groups up to day 7, indicating decreased, yet sustained release of protein in culture media. HOI-T had significantly superior protein secretion compared to HOI-T1.5 and HOI-T2 after one day in culture. In addition, HOI-T retained its biochemical superiority over HOI-T2 at days 4 and 7. Similarly, mean values of protein secretion numerically diminished in a positive comparator CS group up to day 7, nevertheless it was superior to any other HOI group at all endpoints. Therefore, a biochemical

superiority of HOI-T scaffold over HOI-T1.5 and HOI-T2 at least 1-day after the *in vitro* culture is of morphological nature and indicates an advantage of specific pore size in a short-term, yet for clinical implantation acceptable period.

Mean values of COL2A1 expression were upregulated up to day 7 of culture in HOI-T and HOI-T1.5 groups (Fig. 5(b)). Mean values of gene expression throughout the culture period were comparable to monolayer cells in all HOI groups. COL2A1 expression improved in CS group at day 7 compared to day1, yet was similar to all HOI groups at all endpoints.

HOI scaffolds of scaled pores were comparable amongst each other, however higher mean values supported a tendency for gene expression superiority of HOI-T scaffolds over HOI-T1.5 and HOI-T2.

3.5. Macroscopic evaluation of repair cartilage

No swelling, signs of inflammatory or immune responses to implanted materials on operated knees were observed. *Oswestry Arthroscopy Score* (macroscopic score) improved in all groups compared to scaffold-free group (Fig. 6(f)).

Interestingly, addition of cells in HOI group marginally impaired macroscopic evaluation compared to HOI-only group. None of the HOI scaffolds restored a smooth cartilage surface and graft level, integration and coloration resulted relatively the same. CS-cells group revealed the most hyaline-like cartilage, when compared to scaffold-free group, as evident by the leveled graft with the surrounding cartilage and the smooth appearance of surface throughout all samples. However, CS-only was inferior to HOI-only group, mainly due to more fine fronds on the cartilage surface when compared to a smoother cartilage surface in both HOI groups.

3.6. Histological analysis of repair

O'Driscoll score improved significantly in all treatment groups compared to scaffold-free group at 3 months (Fig. 7(k)).

Cell addition in HOI group did not improve cartilage repair quality.

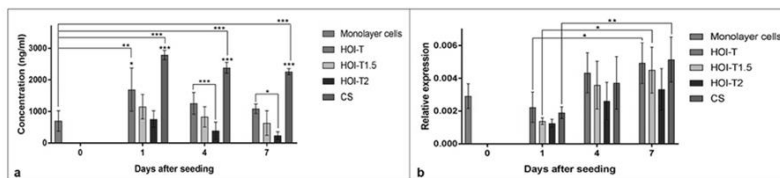


Fig. 5. Pore scale and biocompatibility dependence as represented by (a) type-II collagen protein secretion and (b) expression of HOI-T, HOI-T1.5 and HOI-T2 seeded with cells at days 1, 4 and 7. Secretion improved at day 1 in HOI-T group, compared to cells used for seeding and was superior to HOI-T1.5 and HOI-T2. CS protein secretion was superior than any other HOI group. Mean COL2A1 expression values improved in HOI-T and HOI-T1.5T groups and was comparable to CS. * $p < 0.05$, ** $p < 0.01$, *** $p < 0.001$.

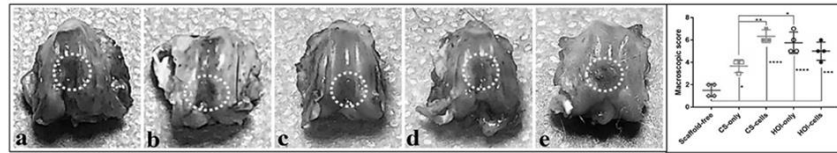


Fig. 6. Macroscopic evaluation of experimental groups at 3 months after treatment in (a) scaffold-free, (b) CS-only, (c) CS-cells, (d) HOI-only and (e) HOI-cells groups. HOI-only and HOI-cells had a clear tendency for superior macroscopic evaluation of repair cartilage (dotted circle) compared to scaffold-free group. Fine fronds on the cartilage surface were evident in all of HOI-only and HOI-cells defects, when smoother cartilage surface was exhibited throughout CS groups. CS-cells had the highest mean OAS score amongst all experimental groups, as evident by cartilage defect filling. Statistical significance * $p < 0.05$, ** $p < 0.01$, *** $p < 0.001$, **** $p < 0.0001$.

HOI-only group revealed that both sides of repair tissue integrated with host cartilage, compared to HOI-cells group partial integration. Other parameters were comparable amongst the HOI groups. O'Driscoll score in HOI-only group was superior compared to CS-only group and was mainly influenced by the smoother cartilage surface in HOI-only group, whereas isolated pathological fissures on the repair cartilage surface were evident in CS-only group. CS-cells group revealed the best numerical cartilage regeneration amongst all groups tested, as evident by > 75% of repair area filled with cells and both sides of repair tissue integrated with host cartilage in all samples. Complete restoration of subchondral bone was not seen in any of the samples, with slight tidemark contour changes evident throughout experimental groups.

4. Discussion

This study demonstrated a sustained cartilage formation *in vitro* and a repair at 3 months *in vivo* xenogenic model, after custom 3D silicon-zirconium hybrid organic-inorganic polymer SZ2080 scaffold (HOI) seeding with human chondrocytes. This was supported by scaffold-cell biocompatibility and redifferentiation *in vitro* and macroscopical and histological analysis *in vivo*. This is the first *in vivo* study to analyse a TEC manufactured by DLW-PP technology and subsequently seeded with human cells in a long term preclinical study. In addition, pore shape and size has been analyzed in search for improved cartilage formation outcome. HOI cartilage formation ability was compared to a positive comparator collagen-based scaffold.

Biomechanical properties of the scaffold are an important characteristic of potent TEC formation and are dependent on the material used and morphology design [8,15]. In addition, sufficient biomechanics of TEC *in vitro* enables the prediction of sufficient cell redifferentiation to sustain heavy loads *in vivo* [8,38]. Pore shape, size, interconnectivity and other morphological scaffold parameters are

known to play a crucial role in biomechanical properties of the scaffold [39]. In this study, HOI scaffolds were subjected to quasi-static indentation loading from top to bottom, until failure by cracking of the three horizontal rod layers. At regions 2 and 3, or middle and bottom scaffold layers, several higher peaks were observed, which could be related to the increased loading of the previously fractured scaffold rods. Incremental amount of fractured rods influenced the number of peaks; therefore, two peaks were commonly visible in the second region, while no < 3 clearly expressed peaks were registered in the third region. However, crushing force peaks were not so clearly expressed in HOI-T compared to HOI-H in the second and third region which could be related to the higher HOI-T porosity and a different collapse pattern of fractured rods. In addition, influence of pore shape on the fracture pattern significantly increased in the second and third regions of HOI, with HOI-T revealing less resistance to the fracture under loading, compared to HOI-H. Since force is distributed over the rods, the hexagon-pored HOI with higher amount of rods could withstand 30–35% higher average force. Different indentation pattern in CS was represented by irregular shapes and wide variability of response curves. Generally, the force increases up to maximal values as indentation depth increases. However, the average values of force significantly depended on the water amount in the specimen volume. Submerging CS in proliferation medium represents an actual clinical situation prior to implantation, however hardness of the CS, became significantly reduced by then. In addition, this reduction is significantly inferior to both HOI scaffolds, which retained their H_{IT} and E_{IT} in the same clinical setting, i.e. wet state.

Fabrication and characterization of a porous scaffold has been a central focus of manufacturing a TEC, because of the impact that pore shape, size, porosity and interconnectivity have on cellular responses, such as cell proliferation, metabolic activity and ECM secretion *in vitro* [8,19,30,40]. Pore shape and size plays a vital role in chondrocyte

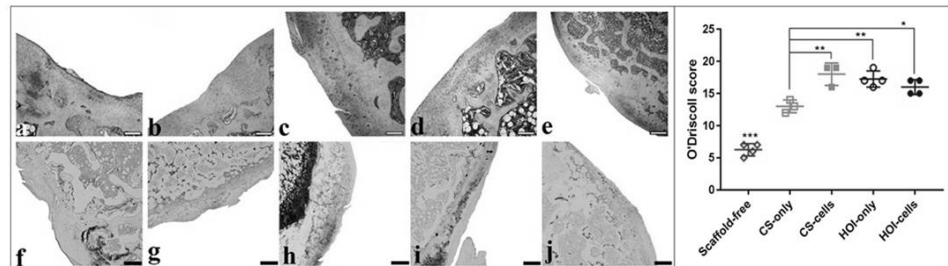


Fig. 7. Histological evaluation of experimental groups at 3 months after treatment in (a, f) scaffold-free, (b, g) CS-only, (c, h) CS-cells, (d, i) HOI-only and (e, j) HOI-cells groups. Histological score improved in all treatment groups compared to scaffold-free group as assessed by (a–e) Safranin O and (f–j) Toluidine blue staining. Cell addition to the HOI did not further improve cartilage repair, mainly due to more cell clustering in HOI-cell. CS retained numerically superior cartilage repair and was comparable to HOI scaffolds at the follow-up. Scale bar: a–e 100 μ m; f–j 200 μ m. Statistical significance * $p < 0.05$, ** $p < 0.01$, *** $p < 0.0001$.

infiltration, as the geometry dictates the cell distribution and the resultant pattern of extracellular matrix embedded cells. Single chondrocyte size depends on the area of cartilage and usually takes up the volume of 200–2000 μm^3 , which correspond to 7–15 μm in diameter. Having the ability to easily migrate through the larger pore, chondrocyte spanning throughout the scaffold predominantly depends on the cell-scaffold interaction. As the angle between rods widens, the cell-rod interaction is impeded and subsequent cell-cell interactions are initiated. This decreases the stability of the structure and the proliferation of new ECM [41]. Therefore, shorter inter-rod distances in tetragonal scaffolds and the resulting additional sites for cell attachment to support the proliferation of cells might favor pore coverage by the secreted ECM and cells [42,43].

Morphological scaffold properties such as, high porosity, regularly interconnected pores have been shown to improve chondrocytic phenotype and secrete an abundance of ECM in chitosan and alginate scaffolds [19,44]. Influence of varying pore sizes have also been investigated, revealing superior biomechanical and physical properties in scaffolds with uniform pore sizes, homogenous environment and high interconnectivity throughout the scaffold [45]. In addition, Wang et al. showed that particular pore shape can support normal phenotype with enhanced functional production of ECM. Di Luca et al., suggested a benefit of different pore shapes for osteochondral repair [46]. Uniformity in pore size, shape and high porosity can be effectively achieved using the DLW-PP technique, with key parameters controlled by a precise and flexible microfabrication. Kapyla et al. fabricated scaffolds with custom pore sizes, porosity and interconnectivity using the DLW-PP technique, providing a novel approach for studying the effect of scaffold architecture on cell behaviour *in vitro* [22]. Although for quite some time now DLW-PP has been known as a promising technology for creating tailored 3D scaffolds with high precision, however, they are most often sub-mm in size and their use is usually limited to *in vitro* cell biology studies [47–51].

In our study we have fabricated tetragon- and hexagon-pored HOI to determine pore shape influence on the cartilage formation *in vitro*. HOI-T and HOI-H improved metabolic cell activity and count up to day 7. In addition, only cells cultured in tetragon-pored HOI improved activity and total number compared to monolayer cells used for seeding. Pore morphology was significantly more iterative in HOI and allowed more equal cell distribution throughout the scaffold compared to CS. A superior COL2A1 gene expression was similarly upregulated in tetragon-pored scaffold at least up to day 7. A superior initial culturing phase of HOI-T biocompatibility indicated at least a numerical superiority of tetragon- over hexagon-pored scaffolds. A previously described discrepancy amongst gene expression and protein translation *in vitro* prompted a coupled PCR and ELISA analysis *in vitro* and was evident in our study as well [52]. An inverse correlation of mRNA transcription and protein translation in our study has been described previously and is not yet sufficiently defined [53].

Different approaches have been applied to generate three-dimensional microstructures for cartilage regeneration, such as salt leaching, gas foaming, phase separation, and freeze-drying in the past. Conventional manufacturing methods result in the span of 70–860 μm and 30–95% pore size and porosity, respectively [54]. However, precise control of scaffold micro-architecture could only be achieved by rapid customized fabrication, such as DLW, through computer-aided design [55]. Danilevicius et al. showed an optimal pre-osteoblastic cell in-growth and proliferation on microstructured DLW scaffolds containing 70 μm squared pores of 86% porosity [56]. Trautmann et al. micro-structured stable and reproducible scaffolds of 10–90 μm squared pore sizes. They determined a pore size of 90 μm to support the best adhesion and growth of fibroblast cells in the specimens [57]. Precisely micro-structured pore shapes and sizes require a different design approach compared to conventional methods. The reduced surface volume for the cell attachment and the fragile mechanical properties of DLW scaffolds must be offsetted by the calculated pore morphological and scaffold

structural properties and must not compromise the ingrowth and proliferation of cells. Thus, smaller pore characteristics coupled with improved scaffold structural properties could support the highly custom and sustainable scaffold for tissue engineering.

Complex intermolecular cross-links between transcription, translation, post-translational modifications, secretion and extracellular processing of collagens are a prerequisite for enabling effective protein secretion and a stable network formation [58]. Addition of growth medium supplements that catalyze gene splicing, polyadenylation, hydroxylation and other posttranscriptional modifications might enhance the intermolecular connections and type-II collagen secretion by the scaffolds. We also speculate that a 7-day timeframe serves more for a shelf-life decision making than for clinical surrogacy in the long term. Despite the decline of protein secretion, HOI sustained superior protein translation compared to monolayer cells used for seeding.

Physical properties of TEC influence cell attachment and a subsequent potency *in vitro*. When impact of pore size was evaluated, a sustained cell proliferation was noted in HOI-T and HOI-T1.5 scaffolds with $45 \times 45 \mu\text{m}^2$ and $67 \times 67 \mu\text{m}^2$ in pore sizes, respectively. Despite the reduced type-II collagen protein secretion up to 7 days *in vitro*, initially protein secretion was superior in HOI-T group, compared to other HOI scaffolds. In addition, expression was upregulated in all groups, with a tendency for superiority in HOI-T scaffolds compared to HOI-T1.5 and HOI-T2. Our study supported the findings of Duan et al. who observed 100–200 μm^2 pores in the chondral layer to produce the best results *in vivo* compared to smaller or larger pore sizes [59]. Wang et al. demonstrated a requisite for sufficient porosity to support the effective permeability and cell migration throughout the scaffold [60]. Pan and the group showed a scaffold of 92% porosity in the cartilage layer that yielded the best *in vivo* efficacy [61]. Despite the 96% porosity in our HOI-T2 scaffold, the void in between the rods might have been too large for the amount of cells seeded, thus greater count of cells might have improved attachment. Therefore, parameters of scaffold pore size, porosity and surface area must be coupled to the cell dosage, as well. Posology of the seeded cells must be addressed in the early stages of preclinical study to guarantee the effectiveness of treatment [62]. The treated cartilage defect area is not plain, but rather organized spatially, therefore manufactured scaffold size area might be better substituted with a volume when optimal cell dosing is anticipated. Cartilage thickness differences between species must be estimated to obtain the most accurate dose for successful clinical translation.

An accelerated TEC implantation has been proven in other clinical areas and is the focus in cartilage clinical translation, as well [63]. Therefore, TEC tend to be cultured *in vitro* for a very short period after seeding, thus enabling faster and more qualitative *in vivo* re-differentiation and preventing the tissue of becoming too dense *in vitro* that would restrict nutritional and oxygen flow [64]. Therefore, in our study, the initially sustained, yet not improved in protein secretion level, *in vitro* potency of HOI scaffolds, was supported by improved gene expression. Thus early implantation after cell seeding could support the subsequent redifferentiation and cartilage formation *in vivo*.

An initial swelling of operated knees later subsided and no signs of immune reaction to implanted materials on operated knees were observed at the late follow-up. Both HOI-T groups with and without cells improved cartilage repair *in vivo* at 3-month follow-up according to macroscopic and histologic evaluation compared to a scaffold-free group. This was mainly influenced by the superior tissue integration and smoother cartilage surface in the defect area in both HOI groups. Interestingly, HOI-cells group had a numerically inferior result compared to HOI-only group. This might have been influenced by the seeded cells interference for full scaffold integration and suppression of host cell migration toward TEC. A recent study showed an increased fibrosis in a cell based scaffold, compared to a cell-free scaffold [65], suggesting an inhibitory donor cell effect on tissue integration. CS-cells group revealed the best numerical cartilage regeneration amongst all groups tested; however, subchondral bone was not restored completely.

Cell based cartilage regeneration has been mostly applied for localized chondral defects, while subchondral lesions require additional bone substitution [66]. This might be improved by employing a biphasic scaffold to fully restore osteochondral segment [67,68]. In addition, the subchondral interface between bone marrow and calcified cartilage layer containing vessels and innervation, must be addressed, as well [69].

Basic and clinical research teams have enabled translation of scientifically proven preclinical data to clinical trials utilizing TECs. Despite the clinical success of natural materials-based scaffolds in cartilage tissue engineering, customized synthetic scaffolds are proving to possess a greater potential for superior *in vitro* and clinical outcome. DLW-PP technique enables fabrication of optimal predetermined parameters to micron accuracy in a real-time fashion. The potency and efficacy of custom fabricated scaffolds can be constantly improved to achieve optimal TECs for patients suffering of cartilage defects by genuine osteochondral tissue regeneration.

5. Conclusions

In this study, custom designed HOI scaffolds 3D microstructured by DLW-PP lithography and seeded with human cells were analyzed for influence of pore shape and scale differences *in vitro* and the translated efficacy *in vivo*. HOI-T and HOI-H improved metabolic activity of seeded monolayer cells *in vitro*. Tetragon-pored HOI had a tendency for superior biocompatibility, cartilage specific protein secretion and gene expression compared to hexagon-pored HOI scaffolds. Tetragonal pore sized $45 \times 45 \mu\text{m}^2$ scaffold was comparable to a $67 \times 67 \mu\text{m}^2$ pore sized scaffold by protein secretion and gene expression for at least up to 7 days *in vitro*. All HOI scaffolds improved cartilage repair *in vivo* at 3-month follow-up. Cell addition to the regular tetragon-pored HOI did not further improve cartilage repair *in vivo*. Collagen scaffold retained numerically superior cartilage repair and was comparable to HOI scaffolds at the follow-up. The study supported hypothesis that pore shape and size influence cell proliferation *in vitro* and gave new insight into cartilage repair with HOI scaffolds seeded with human cells *in vivo*.

Declaration of Competing Interest

None.

Acknowledgements

This research was funded by a grant (No. SEN-20/2015) from the Research Council of Lithuania.

Appendix A. Supplementary data

Supplementary data to this article can be found online at <https://doi.org/10.1016/j.apsusc.2019.05.065>.

References

- [1] Bohndorf K. Injuries at the articulating surfaces of bone (chondral, osteochondral, subchondral fractures and Osteochondrosis dissecans). *Eur. J. Radiol.* [Internet]. 1996 Mar 1;22(1):22–9.
- [2] J.A. Buckwalter, H.J. Mankin. Articular cartilage: tissue design and chondrocyte-matrix interactions. *Instr. Course Lect.* 47 (1998) 477–486.
- [3] D. Eyre. Articular cartilage and changes in arthritis: collagen of articular cartilage. *Arthritis Res Ther* 4 (1) (2001) 30 [Internet].
- [4] A.M. Bhosale, J.B. Richardson. Articular cartilage: structure, injuries and review of management. *Br. Med. Bull.* 87 (1) (2008) 77–95.
- [5] E.B. Hunziker. Articular cartilage repair: basic science and clinical progress. A review of the current status and prospects. *Osteoarthr. Cartil.* 10 (6) (2002) 432–463 Jun.
- [6] J.P. Benthien, M. Schwanger, P. Behrens. We do not have evidence based methods for the treatment of cartilage defects in the knee. *Knee Surg. Sports Traumatol. Arthrosc.* 19 (4) (2011) 543–552. Apr.
- [7] R. Langer, D.A. Tirrell. Designing materials for biology and medicine. *Nature* 428 (6982) (2004) 487–492. Apr.
- [8] B. Dhandayuthapani, Y. Yoshida, T. Maekawa, D.S. Kumar. Polymeric scaffolds in tissue engineering application: a review. *Int J Polym Sci.* 2011 (ii) (2011).
- [9] Murphy CM, O'Brien FJ. Understanding the effect of mean pore size on cell activity in collagen-glycosaminoglycan scaffolds. Vol. 4. *Cell Adhes. Migr.*. 2010. p. 377–81.
- [10] Tayalia P, Mendonca CR, Baldacchini T, Mooney DJ, Mazur E. 3D cell-migration studies using two-photon engineered polymer scaffolds. *Adv. Mater.* [Internet]. 20(23):4494–8. Available from: <https://onlinelibrary.wiley.com/doi/abs/10.1002/adma.200801319>.
- [11] Weiß T, Schade R, Laube T, Berg A, Hildebrand G, Wyrwa R, et al. Two-photon polymerization of biocompatible photopolymers for microstructured 3D biointerfaces. *Adv. Eng. Mater.* [Internet]. 13(9):B264–73. Available from: <https://onlinelibrary.wiley.com/doi/abs/10.1002/adem.201080090>.
- [12] V. Ajeti, C.-H. Lien, S.-J. Chen, P.-J. Su, J.M. Squirrell, K.H. Molinarolo, et al. Image-inspired 3D multiphoton excited fabrication of extracellular matrix structures by modulated raster scanning. *Opt. Express* 21 (21) (2013) 25346–25355 Internet. Available from: <http://www.opticsexpress.org/abstract.cfm?URI=oe-21-21-25346>.
- [13] A. Marino, C. Filippeschi, G.G. Genchi, V. Mattoli, B. Mazzolai, G. Giofani. The Osteoprint: a bioinspired two-photon polymerized 3-D structure for the enhancement of bone-like cell differentiation. *Acta Biomater.* 10 (10) (2014) 4304–4313 Oct.
- [14] Danilevicius P, Reksyte S, Balciunas E, Kraniuskauskas A, Jarasiene R, Sirmenis R, Baltrukiene D, Bukelskiene V, Gadosas R, Malinauskas M. Micro-structured polymer scaffolds fabricated by direct laser writing for tissue engineering. *J. Biomed. Opt.*. 2012 Aug;17(8):081405-1. doi:<https://doi.org/10.1117/1.JBO.17.8.081405>.
- [15] J. Zhu, R.E. Marchant. Design properties of hydrogel tissue-engineering scaffolds. *Expert review of medical devices* 8 (2011) 607–626.
- [16] F.J. O'Brien. Biomaterials & scaffolds for tissue engineering. *Mater. Today* 14 (3) (2011) 88–95 Internet. Available from: <http://www.sciencedirect.com/science/article/pii/S136970211170058X>.
- [17] S.V. Murphy, A. Atala. 3D bioprinting of tissues and organs. *Nat. Biotechnol.* 32 (8) (2014) 773–785. Aug.
- [18] K. Terzaki, M. Kissamitaki, A. Skarmoutsou, C. Fotakis, C.A. Charitidis, M. Farsari, et al. Pre-osteoblastic cell response on three-dimensional, organic-inorganic hybrid material scaffolds for bone tissue engineering. *J. Biomed. Mater. Res. A* 101 (8) (2013) 2283–2294. Aug.
- [19] D.J. Griffon, M.R. Sedighi, D.V. Schaeffer, J.A. Eurell, A.L. Johnson. Chitosan scaffolds: interconnective pore size and cartilage engineering. *Acta Biomater.* 2 (3) (2006) 313–320 May.
- [20] W. Dai, N. Kawazoe, X. Lin, J. Dong, G. Chen. The influence of structural design of PEG/collagen hybrid scaffolds in cartilage tissue engineering. *Biomaterials* 31 (8) (2010) 2141–2152 Mar.
- [21] N. Annabi, J.W. Nichol, X. Zhong, C. Ji, S. Koshy, A. Khademhosseini, et al. Controlling the porosity and microarchitecture of hydrogels for tissue engineering. *Tissue Eng Part B Rev* 16 (4) (2010) 371–383. Aug.
- [22] E. Käpylä, D.B. Aydogan, S. Virjula, S. Vanhatupa, S. Miettinen, J. Hyttinen, M. Kellomaki. Direct laser writing and geometrical analysis of scaffolds with designed pore architecture for three-dimensional cell culturing. *J. Micromechanics Microengineering* 22 (2012) 115016.
- [23] Y. Gao, S. Liu, J. Huang, W. Guo, J. Chen, L. Zhang, J. Peng, A. Wang, Y. Wang, W. Xu, S. Lu, M. Yuan, Q. Guo. The ECM-cell interaction of cartilage extracellular matrix on chondrocytes. *Biomed. Res. Int.* 2014 (2014) 648459. <https://doi.org/10.1155/2014/648459> (Epub 2014 May 18).
- [24] J. Hendriks, J. Riesle, Bitterswijk C.A. van, Co-culture in cartilage tissue engineering. *J. Tissue Eng. Regen. Med.* 1 (3) (2007) 170–178 May-Jun.
- [25] P.D. Benya, J.D. Shaffer. Dedifferentiated chondrocytes reexpress the differentiated collagen phenotype when cultured in agarose gels. *Cell* 30 (1) (1982) 215–224. Aug.
- [26] A.-V. Do, B. Khorsand, S.M. Geary, A.K. Salem. 3D printing of scaffolds for tissue regeneration applications. *Advanced healthcare materials* 4 (2015) 1742–1762.
- [27] L. Jonusauskas, D. Gailevičius, S. Reksyte, T. Baldacchini, S. Juodkazis, M. Malinauskas. Mesoscale Laser 3D Printing. *Opt. Express* 27 (11) (2019) 15205–15221.
- [28] Malinauskas M, Farsari M, Piskarskas A, Juodkazis. Ultrafast laser nanostructuring of photopolymers: a decade of advances. *Phys. Rep.*. 2013;533(1):1–31.
- [29] C. Barner-Kowollik, M. Bastmeyer, E. Blasco, G. Delaitre, P. Muller, B. Richter, et al. 3D laser micro- and nanoprinting: challenges for chemistry. *Angew Chem Int Ed Engl.* 56 (50) (2017) 15828–15845. <https://doi.org/10.1002/anie.201704695> Dec 11. (Epub 2017 Nov 15).
- [30] L. Jonusauskas, S. Juodkazis, M. Malinauskas. Optical 3D printing: bridging the gaps in the mesoscale. *J. Opt.* 20 (2018) 053001.
- [31] A. Ovsianikov, J. Viertel, B. Chichkov, M. Oubaha, B. MacCraith, I. Sakellari, A. Giakoumaki, D. Gray, M. Vamvakaki, M. Farsari, C. Fotakis. Ultra-low shrinkage hybrid photosensitive material for two-photon polymerization microfabrication. *ACS Nano* 2 (11) (2008) 2257–2262. <https://doi.org/10.1021/nr800451w> Nov 25.
- [32] Maciulaitis J, Deveikiyte M, Reksyte S, Bratichkov M, Darinskas A, Simbelyte A, Daunoras G, Laurinaviciene A, Laurinavicius A, Gudas R, Malinauskas M, Maciulaitis R. Preclinical study of SZ2080 material 3D microstructured scaffolds for cartilage tissue engineering made by femtosecond direct laser writing lithography. *Biofabrication*. 2015 Mar 23;7(1):015015. doi:<https://doi.org/10.1088/1758-5090/7/1/015015>.
- [33] J. Gille, J. Kunow, L. Boisch, P. Behrens, I. Bos, C. Hoffmann, W. Koller, M. Russliess, B. Kurz. Cell-laden and cell-free matrix-induced chondrogenesis versus microfracture for the treatment of articular cartilage defects. *Cartilage* 1 (1) (2010)

- 29–42. <https://doi.org/10.1177/1947603509358721> Jan.
- [34] W.C. Oliver, G.M. Pharr, Measurement of hardness and elastic modulus by instrumented indentation: advances in understanding and refinements to methodology, *J. Mater. Res.* 19 (1) (2004) 3–20 Jan.
- [35] J. O'Brien, I. Wilson, T. Orton, F. Pognan, Investigation of the Alamar blue (resazurin) fluorescent dye for the assessment of mammalian cell cytotoxicity, *Eur. J. Biochem.* 267 (17) (2000) 5421–5426 Sep.
- [36] K.J. Livak, T.D. Schmittgen, Methods. Analysis of relative gene expression data using real-time quantitative PCR and the $2^{-\Delta\Delta CT}$ method, *Dec* 25 (4) (2001) 402–408.
- [37] N. Schmitz, S. Laverty, V.B. Kraus, T. Aigner, Basic methods in histopathology of joint tissues, *Osteoarthr. Cartil.* 18 (Suppl. 3) (2010) S113–S116. <https://doi.org/10.1016/j.joca.2010.05.026> Oct.
- [38] S.W. O'Driscoll, F.W. Keeley, R.B. Salter, The chondrogenic potential of free autogenous periosteal grafts for biological resurfacing of major full-thickness defects in joint surfaces under the influence of continuous passive motion. An experimental investigation in the rabbit, *J. Bone Joint Surg. Am.* 68 (7) (1986) 1017–1035 Sep.
- [39] S. Bhat, A. Tripathi, A. Kumar, Supermacroporous chitosan–agarose–gelatin cryogels: in vitro characterization and in vivo assessment for cartilage tissue engineering, *J. R. Soc. Interface* 8 (2011) 549–554.
- [40] H. Stenhamre, U. Nannmark, A. Lindahl, P. Gatenholm, M. Brittberg, Influence of pore size on the redifferentiation potential of human articular chondrocytes in poly (urethane urea) scaffolds, *J. Tissue Eng. Regen. Med.* 5 (7) (2011) 578–588 Jul.
- [41] S.L. Edwards, S.J. Church, D.L.J. Alexander, S.J. Russell, E. Ingham, J.A.M. Ramshaw, Modeling tissue growth within nonwoven scaffolds pores, *Tissue Eng Part C Methods* 17 (2) (2011) 123–130. <https://doi.org/10.1089/ten.tec.2010.0182> Feb.
- [42] T. Sun, R. Smallwood, S. MacNeil, Development of a mini 3D cell culture system using well defined nickel grids for the investigation of cell scaffold interactions, *J Mater Sci Mater Med* 20 (7) (2009) 1483–1493 Jul.
- [43] G.C. Engelmayr Jr., G.D. Papworth, S.C. Watkins, J.E. Mayer Jr., M.S. Sacks, Guidance of engineered tissue collagen orientation by large-scale scaffold microstructures, *J. Biomech.* 39 (10) (2006) 1819–1831.
- [44] C.-C. Wang, K.-C. Yang, K.-H. Lin, H.-C. Liu, F.-H. Lin, A highly organized three-dimensional alginate scaffold for cartilage tissue engineering prepared by microfluidic technology, *Biomaterials* 32 (29) (2011) 7118–7126 Oct.
- [45] C.-C. Wang, K.-C. Yang, K.-H. Lin, C.-C. Wu, Y.-L. Liu, F.-H. Lin, et al., A biomimetic honeycomb-like scaffold prepared by flow-focusing technology for cartilage regeneration, *Biotechnol. Bioeng.* 111 (11) (2014) 2338–2348 Nov.
- [46] A. Di Luca, I. Lorenzo-Moldero, C. Mota, A. Lepedda, D. Auhl, C. Van Blitterswijk, et al., Tuning cell differentiation into a 3D scaffold presenting a pore shape gradient for osteochondral regeneration, *Adv Health Mater* 5 (14) (2016) 1753–1763.
- [47] A. Accardo, M.C. Blatché, R. Courson, C. Thibault, I. Malaquin, et al., Multiphoton direct laser writing and 3D imaging of polymeric freestanding architectures for cell colonization, *Small* 13 (27) (2017). <https://doi.org/10.1002/smll.201700621> Jul.
- [48] Hippler M, Lemma ED, Bertels S, Blasco E, Barner-Kowollik C, Wegener M et al. 3D scaffolds to study basic cell biology. *Adv. Mater.* 2019 Feb 21:e1808110. doi:<https://doi.org/10.1002/adma.201808110>.
- [49] Accardo A, Blatché MC, Courson R, Loubinoux I, Vieu C and Malaqui M. Two-photon lithography and microscopy of 3D hydrogel scaffolds for neuronal cell growth. *Biomed. Phys. Eng. Express* 4 027009.
- [50] E.D. Lemma, B. Spagnolo, M. De Vittorio, F. Pisanello, Studying cell mechanobiology in 3D: the two-photon lithography approach, *Trends Biotechnol.* 37 (4) (2019) 358–372. <https://doi.org/10.1016/j.tibtech.2018.09.008> Apr.
- [51] A. Accardo, M.C. Blatché, R. Courson, I. Loubinoux, C. Vieu, I. Malaquin, Direct laser fabrication of free-standing PEGDA-hydrogel scaffolds for neuronal cell growth: engineering 3D biocompatible microenvironments, *Mater. Today* 21 (3) (2018) 315–316. <https://doi.org/10.1016/j.mattod.2018.02.004> April.
- [52] C.J. McManus, G.E. May, P. Spielman, A. Shetyan, Ribosome profiling reveals post-transcriptional buffering of divergent gene expression in yeast, *Genome Res.* 24 (2014) 422–430.
- [53] D. Greenbaum, C. Colangelo, K. Williams, M. Gerstein, Comparing protein abundance and mRNA expression levels on a genomic scale, *Genome Biol.* 4 (9) (2003) 117 (Epub 2003 Aug 29).
- [54] Q.L. Loh, C. Choong, Three-dimensional scaffolds for tissue engineering applications: role of porosity and pore size, *Tissue Eng Part B Rev* 19 (6) (2013) 485–502. <https://doi.org/10.1089/ten.TEB.2012.0437> Dec.
- [55] J. Mačulaitis, S. Reksytė, A. Ūsas, V. Jankauskaitė, R. Gudas, M. Malinauskas, R. Mačulaitis, Characterization of tissue engineered cartilage products: recent developments in advanced therapy, *Pharmacol. Res.* 113 (Pt B) (2016 Nov) 823–832. <https://doi.org/10.1016/j.phrs.2016.02.022>.
- [56] Danilevicius P, Leoni G, Pateman JC, Claeysens F, Chatzinkolaïdou, M, Farsari M., The effect of porosity on cell ingrowth into accurately defined, laser-made, polylactide-based 3D scaffolds *Appl. Surf. Sci.*, Volume 336, p. 2–10. <https://doi.org/10.1016/j.apsusc.2014.06.012>.
- [57] Trautmann A, Růth M, Lemke HD, Walther T, Hellmann R. Two-photon polymerization based large scaffolds for adhesion and proliferation studies of human primary fibroblasts. *Opt. Laser Technol.*, Volume 106, p. 474–480. <https://doi.org/10.1016/j.optlastec.2018.05.008>.
- [58] K. Gelse, E. Püschel, T. Aigner, Collagens—structure, function, and biosynthesis, *Adv. Drug Deliv. Rev.* 55 (12) (2003) 1531–1546 Nov 28.
- [59] P. Duan, Z. Pan, L. Cao, Y. He, H. Wang, Z. Qu, et al., The effects of pore size in bilayered poly(lactide-co-glycolide) scaffolds on restoring osteochondral defects in rabbits, *J Biomed Mater Res Part A* 102 (1) (2014) 180–192 Internet. Available from: <http://doi.wiley.com/10.1002/jbm.a.34683>.
- [60] Y. Wang, H. Meng, X. Yuan, J. Peng, Q. Guo, S. Lu, et al., Fabrication and in vitro evaluation of an articular cartilage extracellular matrix-hydroxyapatite bilayered scaffold with low permeability for interface tissue engineering, *Biomed. Eng. Online* 13 (1) (2014) 1–18.
- [61] Z. Pan, P. Duan, X. Liu, H. Wang, L. Cao, Y. He, et al., Effect of porosities of bilayered porous scaffolds on spontaneous osteochondral repair in cartilage tissue engineering, *Regen Biomater* 2 (1) (2015) 9–19 Internet. Available from: <https://academic.oup.com/rb/article-lookup/doi/10.1093/rb/rbv001>.
- [62] C. Divioto, M.P. Sassi, A First Approach to Evaluate the Cell Dose in Highly Porous Scaffolds by Using a Nondestructive Metabolic Method, vol. 1, Future Science OA, London, UK, 2015.
- [63] A. Gálisová, E. Fábryová, E. Sticová, L. Kosinová, M. Jiráťová, V. Herynek, et al., The optimal timing for pancreatic islet transplantation into subcutaneous scaffolds assessed by multimodal imaging, *Contrast Media & Molecular Imaging* 2017 (2017).
- [64] C. Seiden, B. Fuller, Role of bioreactor technology in tissue engineering for clinical use and therapeutic target design, *Bioengineering* 5 (2) (2018) 32 <https://doi.org/10.3390/bioengineering5020032>.
- [65] K. Ye, K. Trainees, S.A. Robins, P.F.M. Choong, D.E. Myers, Osteochondral repair using an acellular dermal matrix-pilot in vivo study in a rabbit osteochondral defect model, *J. Orthop. Res.* (2018) 1–10 Internet. Available from: <http://doi.wiley.com/10.1002/jor.22837>.
- [66] G.M. Salzmann, P. Niemyer, A. Hochrein, M.J. Stoddart, P. Angele, Articular cartilage repair of the knee in children and adolescents, *Orthop J Sport Med* 6 (3) (2018) 1–12.
- [67] E.B. Hunziker, K. Lippuner, M.J.B. Keel, N. Shintani, An educational review of cartilage repair: precepts & practice - myths & misconceptions - progress & prospects, *Osteoarthr. Cartil.* 23 (3) (2015) 334–350 Internet. (Available from: <https://doi.org/10.1016/j.joca.2014.12.011>).
- [68] J.K. Sherwood, S.L. Riley, R. Palazzolo, S.C. Brown, D.C. Monkhouse, M. Coates, et al., A three-dimensional osteochondral composite scaffold for articular cartilage repair, *Biomaterials* 23 (24) (2002) 4739–4751.
- [69] H. Madry, C.N. van Dijk, M. Mueller-Gerbl, The basic science of the subchondral bone, *Knee Surgery, Sport Traumatol Arthrosc* 18 (4) (2010) 419–433.

Biofabrication



PAPER

RECEIVED
19 October 2014REVISED
6 February 2015ACCEPTED FOR PUBLICATION
11 February 2015PUBLISHED
23 March 2015

Preclinical study of SZ2080 material 3D microstructured scaffolds for cartilage tissue engineering made by femtosecond direct laser writing lithography

Justinas Mačiulaitis^{1,2,3}, Milda Deveikytė⁴, Sima Rekštytė⁵, Maksim Bratchikov^{6,7}, Adas Darinskas^{1,4,11}, Agnė Šimbelytė^{4,8,9}, Gintaras Daunoras¹⁰, Aida Laurinavičienė^{8,9}, Arvydas Laurinavičius^{8,9}, Rimtautas Gudas^{2,3}, Mangirdas Malinauskas⁵ and Romaldas Mačiulaitis¹¹ Institute of Physiology and Pharmacology, Medical Academy, Lithuanian Health Science University, Mickėvičiaus 9, LT-44307 Kaunas, Lithuania² Institute of Sports, Medical Academy, Lithuanian University of Health Science, Kalniečių 231, LT-44307 Kaunas, Lithuania³ Orthopaedic and Trauma Department, Lithuanian Health Science University, Mickėvičiaus 9, LT-44307 Kaunas, Lithuania⁴ Stem Cell Bank Ltd, Linkmenų str. 28, LT-08317, Vilnius, Lithuania⁵ Laser Research Center, Department of Quantum Electronics, Faculty of Physics, Vilnius University, Saulėtekio Ave. 10, LT-10223 Vilnius, Lithuania⁶ Immunology Department, State Research Institute Centre for Innovative Medicine, Vilnius University, Moleėtų pl. 29, LT-08409, Vilnius, Lithuania⁷ Department of Physiology, Biochemistry, Microbiology and Laboratory Medicine, Faculty of Medicine, Vilnius University, M. K. Čiurlionio 21, LT-03101 Vilnius, Lithuania⁸ Department of Pathology, Forensic Medicine and Pharmacology, Faculty of Medicine, Vilnius University, M. K. Čiurlionio 21, LT-03101 Vilnius, Lithuania⁹ National Center of Pathology, Affiliate of Vilnius University Hospital Santariškių Klinikos, P. Baublio 5, LT-08406 Vilnius, Lithuania¹⁰ Non-infectious Disease Department, Veterinary Academy, Lithuanian Health Science University, Mickėvičiaus 9, LT-44307 Kaunas, Lithuania¹¹ Laboratory of Immunology, Vilnius University, Institute of Oncology, Santariškių 1, LT-08660, Vilnius, Lithuania

E-mail: justinas.maciulaitis@yahoo.com, adas@arbata.org, mangirdas.malinauskas@ff.vu.lt and romaci11@gmail.com

Keywords: direct laser writing lithography, biomaterials, SZ2080, artificial scaffolds, tissue engineering, *in vitro*, *in vivo*

Abstract

Over the last decade DLW employing ultrafast pulsed lasers has become a well-established technique for the creation of custom-made free-form three-dimensional (3D) microscaffolds out of a variety of materials ranging from proteins to biocompatible glasses. Its potential applications for manufacturing a patient's specific scaffold seem unlimited in terms of spatial resolution and geometry complexity. However, despite few exceptions in which live cells or primitive organisms were encapsulated into a polymer matrix, no demonstration of an *in vivo* study case of scaffolds generated with the use of such a method was performed. Here, we report a preclinical study of 3D artificial microstructured scaffolds out of hybrid organic-inorganic (HOI) material SZ2080 fabricated using the DLW technique. The created $2.1 \times 2.1 \times 0.21 \text{ mm}^3$ membrane constructs are tested both *in vitro* by growing isolated allogeneic rabbit chondrocytes (Cho) and *in vivo* by implanting them into rabbit organisms for one, three and six months. An *ex vivo* histological examination shows that certain pore geometry and the pre-growing of Cho prior to implantation significantly improves the performance of the created 3D scaffolds. The achieved biocompatibility is comparable to the commercially available collagen membranes. The successful outcome of this study supports the idea that hexagonal-pore-shaped HOI microstructured scaffolds in combination with Cho seeding may be successfully implemented for cartilage tissue engineering.

1. Introduction

Within a few years after the initial demonstration of DLW in polymers based on nonlinear light-matter

interaction [1] the potential applications in biomedicine were observed [2–4]. The novel technique immediately attracted researchers due to its 3D structuring capability, spatial resolution, scaling

flexibility and diversity of processable materials [5–8]. Currently, self-assembled or commercially available DLW set-ups are standard tools in modern laboratories of various fields. A few very interesting implementations in micro-fluidics have been reported [9–11], and also specific cell studies have been performed [12–14]. Femtosecond pulsed lasers are advantageous due to their non-damaging material behavior, enabling encapsulation of alive cells [15] or even whole organisms [16], as well as offering a possibility to 3D micro-/nano-structure non-photosensitized (pure) materials [17]. Additionally, DLW polymer structuring can be combined with the laser induced forward transfer (LIFT) technique, thus resulting in straight-forward printing of single cells to laser pre-fabricated 3D scaffolds [18]. Recently, the method has been employed for the structuring of hyaluronic acid [19] and polylactic acid bioresorbable materials [20].

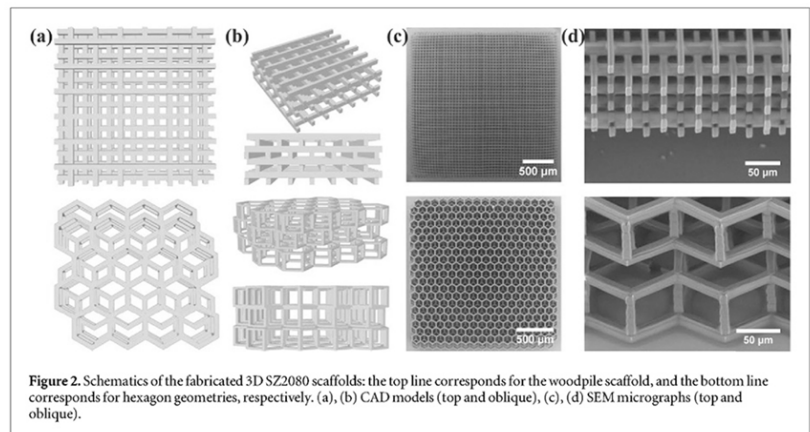
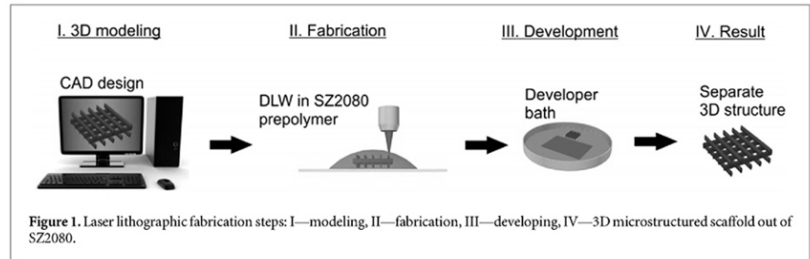
Strangely, though the technique shows unmatched versatility in producing custom-made scaffolds or real-time manufacturing of implants for individual patients, the structures fabricated this way are still not studied *in vivo* in model organisms. Despite numerous investigations into single-cell behavior and the colonization of various cell lines on DLW-made scaffolds, the only report proving the applied materials' biocompatibility is of non-structured bulk pieces [21]. It should be stressed that the technique has matured enough to capacitate real-time fabrication of cm³ scale 3D microstructured scaffolds [22, 23] out of biocompatible—and bioinert as well as biodegradable—materials [24]. Assuming that the manufacturing of a single scaffold 30 × 30 × 3 mm³ (already sufficient for a human patient) can take less than 24 h, it is not the bottleneck to start the practical application in medical surgery. To support the fulfilment of the idea one should emphasize that the price of such an implant is already below the cost of the surgery itself. Thus, DLW as a tool for custom-made 3D microstructured scaffold fabrication has no direct limitations, which was noted a decade ago when the technique emerged [25]. Furthermore, several methods have already been proposed for the increase of fabrication throughput (active [26] and passive [27]); approaches have also been proposed for the expansion of the dimensions of the object by using the liquid photoresist itself as the immersion fluid between the objective and substrate [28] or by using a special sample-objective holder [29].

This gap between the vision of the technique's biomedical application and practical implementation has encouraged our group to target the experimental research work toward *in vivo* study of 3D scaffolds seeded with Cho. We have chosen SZ2080 as a widely used and biocompatible material which is exceptional for its DLW structuring and mechanical properties [30, 31]. To make the research work impactful for practice, a clinical case of an osteochondral injury problem was selected. In the preclinical study rabbits were

used as model animals, and two types of scaffold geometries were implemented. The obtained results were compared to a commercially available collagen membrane seeded with Cho at one, three and six months post-implantation in order to get reliable *in vivo* results. Below, we present osteochondral health problems and currently existing methods to treat them.

Osteochondral injuries represent one of the major health problems in the active population [32, 33]. Adult articular cartilage is an avascular tissue with limited cartilage capacity for self-repair [34, 35]. In the event of an injury, the local defect is repaired with a neo-cartilage fibrous tissue, which is structurally inferior to the native cartilage [36]. This leads to a rapid deterioration and progression toward osteoarthritis [37]. Type-II collagen is the principal molecular component in mature cartilage [35]. Different methods to treat osteochondral injuries are being applied today [38]. Cartilage tissue engineering is an effective method for hyaline and hyaline-like cartilage regeneration. There is a large number of reports available on successful cartilage tissue regeneration using Cho in combination with natural or synthetic 3D scaffolds [39–41], among them hybrid printing for improving mechanical and biological properties [42]. It is of high importance that 3D culturing of dedifferentiated cells allows for increased type-II collagen reexpression [43]. An artificial scaffold is used as a niche for cells to adopt a natural cartilage phenotype. Porosity that allows diffusion of nutrients and waste products is highly influential to the cell survival rate [40, 44–46]. Fibrin as a carrier had been previously used with success [47, 48]. Efforts are being made to find new 3D carriers for cell experiments *in vitro* and *in vivo*. DLW structuring enables tuning-in-practice of all the important 3D scaffold parameters: mechanical, biological and chemical properties of fabricated structures. This encourages employing the DLW technique for scaffold fabrication: selecting suitable scaffold material and designing appropriate geometry as well as testing the product in a preclinical study [49]. Special attention is paid to HOI polymers, namely ORMOCERS [50] and ORMOSILs [51].

In this study we aim at practically determining the potential of DLW lithography with the use of currently accessible techniques for the applications of 3D scaffold design and study at a preclinical level. Thus, this study was designed to provide an answer on the feasibility of such templates as Cho carriers to form hyaline cartilage *in vitro* and to test the healing potential of articular cartilage defects in a preclinical rabbit model. For the control we use a collagen sponge, which is a widely applied, biocompatible material, although it presents weak mechanical rigidity properties [52–54]. Sponges had been shown to be good carriers for Cho redifferentiation [53, 54]. The experiment was designed as a comparative study *in vivo* of currently used medical implants and the state-of-the-art DLW lithography technique.



2. Materials and methods

2.1. SZ2080 scaffold and collagen membrane preparation

3D polymeric scaffolds were fabricated using the DLW technique: a laser beam is tightly focused into the volume of a photosensitive pre-polymer, thus initiating a polymerization reaction, turning a liquid (or gel-like) material into a solid state [55]. Using specially designed software, a computer model of a scaffold with a desired geometry is created. The pre-polymer sample is then translated in respect of the laser beam, according to this model, thus point-by-point exposing different parts of the material to the laser light, yielding a functional polymeric object of specific micro-architecture. This technique enables fabrication of unique scaffolds with geometry and dimensions targeted for an individual patient [22]. The employed ultrafast laser provided 300 fs, 200 kHz and 515 nm pulsed light radiation (Pharos, Light Conversion). Sample positioning synchronization with beam deflection was realized using a custom assembled femtosecond laser system for the laboratory (Femto-LAB, Altechna R&D). The detailed description of the set-up can be found elsewhere [56]. The material

chosen for the scaffolds was a HOI sol-gel photopolymer SZ2080 [30] (IESL FORTH, Greece), which consists of 20% inorganic and 80% organic parts. The sequence of the fabrication is given in figure 1.

The fabricated SZ2080 scaffolds were mathematically precise structures, rigid and non-immunogenic, however not yet tested for cartilage tissue regeneration. For this study the suitability of the HOI scaffold type was assessed by testing two structurally distinct types of pore geometries: square and hexagon (figure 2). A more detailed study on pore geometry, pore size and general porosity of the designed model and the fabricated scaffold is presented elsewhere [57]. The first one had a woodpile structure and consisted of 17 layers of parallel rods that were rotated by 90° in each next layer and were shifted by half a period in each alternate layer. The rod height and width was 15 and 10 μm, respectively, with a 50 μm period, thus making the pore size 40 × 40 μm². For the fabrication of a single scaffold layer the laser beam was scanned in parallel along its length 28 times, with separation between the scans of 0.35 μm. The woodpile-type scaffold dimensions were 2.5 × 2.5 × 0.22 mm³. The second-type scaffolds had the honeycomb (hexagon) structure. They consisted of three self-repeating layers

of hollow-sided honeycombs, each layer with an offset of half a period in one direction with relation to the previous layer. The apothem of the hexagon was $50\ \mu\text{m}$; the width and height of the side hole was 51 and $54\ \mu\text{m}$, respectively, and the overall scaffold dimensions were $2.1 \times 2.1 \times 0.21\ \text{mm}^3$. The scaffold was fabricated in a layer-by-layer fashion using two methods: (a) raster scanning to fabricate the columns and scanning concentric hexagons with decreasing apothem when fabricating hexagon parts, with the distance between adjacent lines set to $0.5\ \mu\text{m}$, or (b) fabricating from a STL (stereo lithography) format file, with a hatching distance set to $0.35\ \mu\text{m}$. No noticeable difference in structural quality depending on fabrication strategy was observed. However, fabrication-wise, we determined that raster scanning allowed higher sample translation velocities in comparison to directly imported STL: $7\ \text{mm s}^{-1}$ and $2\ \text{mm s}^{-1}$, respectively. This corresponded to $\sim 2.5\ \text{h}$ and $\sim 6\ \text{h}$ scaffolds' fabrication durations. A further increase of scanning speed resulted in deterioration of geometrical rigidity, which, on the other hand, and, to some extent, can be sacrificed for the sake of manufacturing throughput. As an indirect comparator a commercially available collagen membrane (CM) composed of type-I collagen (Septodont, UK) was used. The length, width and height were $5\ \text{mm}$ each.

2.2. Monolayer and scaffold cell cultures

An articular cartilage biopsy (size $2\text{--}5\ \text{mm}^3$) was removed from the non-weight bearing area of the knee of New Zealand white rabbits and placed immediately in Dulbecco's modified eagle medium (DMEM). The samples were cut into small pieces and minced finely. The Cho were isolated by trypsin 2.5% /EDTA 0.05% (Gibco) solution after $20\ \text{min}$ in room temperature, followed by collagenase XI digestion. The isolated cells were then cultured in DMEM/F12 (HyClone) supplemented with 10% fetal calf serum (FCS), $100\ \text{U ml}^{-1}$ penicillin and $100\ \mu\text{g ml}^{-1}$ streptomycin. The cells were incubated at $37\ ^\circ\text{C}$ in a $5\% \text{CO}_2$ incubator. When the cells reached 80% confluence, they were harvested by trypsinisation; the medium was refreshed, and the samples were sent for biochemical analysis. Rabbit Cho were cultivated in a monolayer up to the 3rd passage. 1st (P1), 2nd (P2) and 3rd (P3) passage cells were sent for further analysis. The P3 cells were seeded on HOI and CM scaffolds (10^5 and 10^6 cells, respectively) and cultured for up to 14 days. The culture medium was changed every $2\text{--}3$ days. At 14 days of *in vitro* three-dimensional culturing, the scaffolds were harvested for subsequent analysis and *in vivo* implantation.

2.3. Scanning electron microscope (SEM) inspection

The HOI with Cho scaffolds were washed three times with phosphate buffered saline (PBS) and fixed in PBS containing 2.5% glutaraldehyde. They were then

dehydrated in increasing concentrations of ethanol (from 25% and 75% to 96%), dried and coated with a $20\text{--}50\ \text{nm}$ thick layer of gold (Quorum Q150R S Rotary-pumped sputter coater) and examined under a scanning electron microscope (SEM) (Hitachi TM-1000). Pore coverage by Cho in a HOI scaffold was conducted independently by two researchers using SEM photographs. The membrane filling density and increment of cell count during the culture were evaluated and counted as a percentage of pore coverage at days $3, 7$ and 14 (prior to implantation).

2.4. Experimental design

27 New Zealand adult male rabbits ($4\text{--}5$ months old, $3\text{--}4\ \text{kg}$ body weight) were used in the study. They were housed separately in cages and allowed ad libitum rabbit feed (T-2, Biofabrikas, Ukmerge dist., Lithuania) and tap water during the experiment. The vivarium was maintained at a temperature of $21\ ^\circ\text{C}$ with a relative humidity of 45% and with a $12/12$ light/dark period. The surgical procedures were performed in an operating theatre under intravenous anesthesia and sterile conditions. The rabbits were given intramuscular anesthesia for induction and intravenous anesthesia for maintained sedation. Using a surgical drill bit, a bilateral osteochondral defect $3\ \text{mm}$ in diameter was created at the weight-bearing area of the medial femoral condyle, thus producing 54 defects. For every experimental and control group defect a polymerized fibrin clot was used. Blood plasma ($1\ \text{ml}$), thrombin ($250\ \mu\text{l}$) and CaCl_2 ($250\ \mu\text{l}$) were mixed in a petri dish. It was incubated at room temperature for five minutes prior to implantation.

The defects were treated with CM and polymerized fibrin (experimental group #1, EG1), CM seeded with Cho and polymerized fibrin (experimental group #2, EG2), a HOI membrane and polymerized fibrin (experimental group #3, EG3), a HOI membrane seeded with Cho and polymerized fibrin (experimental group #4, EG4) and polymerized fibrin only (control group, CG). The study was conducted according to the standard guidelines and protocols approved by Lithuanian State Food and Veterinary Service.

2.5. Histology, immunohistology

Animals were sacrificed at $1, 3$ and 6 months post-operatively. The knee joints were approached via the lateral parapatellar approach. After gross examination, pictures were taken of treated defects. The femurs were cut above the condyles, fixed in a 10% neutral buffered formalin solution, embedded in paraffin blocks and cut to serial $2\text{--}3\ \mu\text{m}$ thick sections (microtome RM 2145, Leica). The demineralised sections were stained with hematoxylin and eosin, toluidine blue and safranin O to assess glycosaminoglycans (GAGs), proteoglycans (PGs) and collagen production in the matrix. Type-II and type-I collagen expression were

detected by immunohistochemical analysis using an anti-human collagen type-II (clone II-4CII) and a mouse monoclonal anti-collagen type-I antibody (clone 2H12B4, ABCAM), respectively. Purified IgG (MP Biomedicals, LLC) was used for the negative control. Briefly, the sections were blocked with a peroxidase-blocking reagent (EnVision Flex SM801, DAKO) for 15 min and rinsed with a wash buffer (EnVision Flex, DAKO). The sections were digested with a pepsin solution (DAKO S3002) at 37 °C for 10 min and rinsed with a wash buffer (EnVision Flex, DAKO). The sections were visualized using a detection system (EnVision Flex K8002, DAKO) after incubation with primary antibody collagen type-II or collagen type-I for 60 min. The sections were subsequently washed with tris-buffered saline/tween (TBST) before incubation with a secondary antibody (EnVision FLEX/HRPSM802, DAKO) for 30 min at room temperature and rinsed with a wash buffer (EnVision Flex, DAKO). The cell nuclei were counter-stained using DAB + Chromogen (EnVision Flex, DAKO) for 10 min. The sections were analyzed using a microscope (Olympus BX41, Center Valley, PA). The slides were scored blindly by two investigators using a modified O'Driscoll histological scoring system, with a total maximal score of 23 [58]. The host response to the scaffold at the implantation site was evaluated morphologically by infiltration of inflammatory cells (i.e. leukocytes and macrophages).

2.6. Real-time reverse transcription (RT) polymerase chain reaction analysis

2.6.1. RNA extraction

The total RNA from the samples was extracted using an ISOLATE II RNA Micro Kit (Bioline, England) according to the manufacturer's instructions. Elution was performed with 10 μ l RNase-free water included in the kit. One-step RTqPCR was performed using a Rotor-Gene Q 5-plex model (QIAGEN, Germany). Rotor-Gene Q Series Software 1.7 was used for the process. SensiFAST Probe No-ROX One-Step Kit (Bioline, England), primers and hydrolyzation probes (Integrated DNA technologies, USA) were used for one-step RT-qPCR. Each 15 μ l reaction for type-II collagen (COL2A1) mRNA expression quantification contained 400 nM of Col2 F primer, 400 nM of Col2 R primer, 200 nM of GAPDH F primer, 200 nM of GAPDH R primer, a 100 nM of Col2 Z probe, a 100 nM of GAPDH Z probe and 2 μ l of RNA. Each 15 μ l reaction for type-X collagen (COL10A1) mRNA expression quantification contained 200 nM of Col10 F primer, 200 nM of Col10 R primer, 200 nM of GAPDH F primer, 200 nM of GAPDH R primer, a 100 nM of Col10 Z probe, a 100 nM of GAPDH Z probe and 2 μ l of RNA. Designed primer pairs, probes and the condition of amplification are represented in the supplementary data.

2.6.2. Data analysis

The 2⁻ddCT method was applied for the relative gene expression data evaluation. *Oryctolagus cuniculus* GAPDH gene expression was used for the data normalization.

For the particular chondrogenic gene mRNA analysis, we examined COL2A1 (*Col2*) and COL10A1 (*Col10*) mRNAs' expression dynamics of: *in vitro* monolayer (prior to seeding); the three-dimensional cultures of HOI scaffold and CM (after seeding) and prior to implantation; *in vivo* at 1, 3 and 6 months post-implantation. For the monolayer cultures we analyzed samples of passages 1 (P1), 2 (P2) and 3 (P3) mRNA expressions, which were compared to that of passage 0 (P0). The CM with Cho scaffolds were sent for examination at days 1, 7, 14 and 21. HOI scaffolds with chondrocytes—at days 3, 7, and 14.

2.7. Statistical evaluation

The results were calculated using descriptive parametric and non-parametric analysis as relevant and were presented as the mean \pm SD for descriptive statistics. The differences were analyzed using Student's t-test. The results were considered statistically significant when $p < 0.05$ and were considered as showing the trend if p was between 0.05 and 0.1.

3. Results

3.1. Cell morphology and viability in monolayer

During the monolayer culture the Cho showed typical phenotypic changes. The cells progressively lost their natural round shape and became flattened, fibroblast-like cells. The viability of the Cho prior to seeding on membranes was consistently high, ranging from 98% to 100% (supplementary data).

3.2. SEM analysis of scaffolds with chondrocytes (Cho)

After 14 days of three-dimensional CM and Cho culturing, the cells were seen to be randomly distributed on the top and near-surface levels. Due to a dense net of collagen sponge fibers, deeper layers could not be effectively evaluated. Very few elongated Cho and scarce extracellular matrix (ECM) fibers were seen at the surface of the membrane (figures 3(a) and (b)). This figure illustrates the final CM scaffold prior to *in vivo* implantation.

The first day after the Cho had been seeded on a square-pore-type HOI scaffold, no cells' filling of scaffold pores could be visualized (supplementary data). The same image was seen throughout the next few days. The cells were seen to be attached to the flask in the monolayer around the borders of the square-pore-type membrane. In contrast, cho seeded on the hexagonal-pore-type HOI scaffold exhibited continuous adherence to the layers of hollow-sided honeycombs. Interactions between Cho and the HOI scaffold were

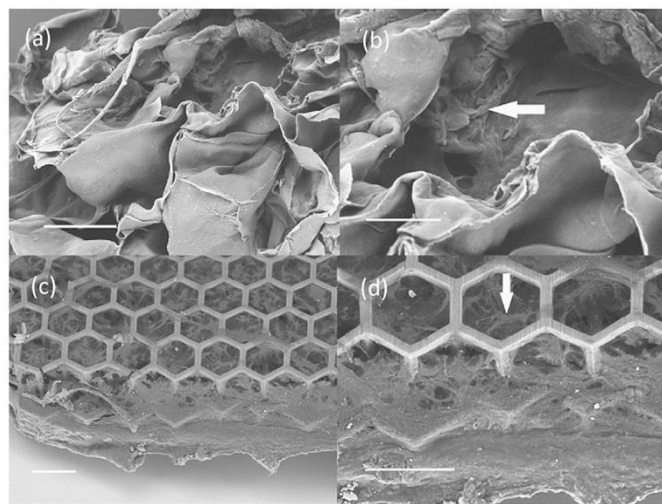


Figure 3. (a), (b) SEM images of a CM seeded with 10^6 Cho in a $60 \mu\text{l}$ culture medium at day 14 prior to implantation at two different magnifications. Few Cho are visible near the surface of the CM. (c), (d) SEM images of a hexagon-pore-type HOI scaffold seeded with 10^6 Cho in a $2 \mu\text{l}$ culture medium 14 days *in vitro* prior to *in vivo* implantation at two different magnifications. Cho (white arrows) and ECM can be seen at every layer of the HOI scaffold. Scale bar: (a), (c) $100 \mu\text{m}$, (b) $50 \mu\text{m}$.

shown as a function of the attachment and distribution continuity of cells on the surface and within the membrane. Thus, we continued experimenting with the hexagon-pore-type HOI scaffold. Proliferation of Cho within the scaffold, extracellular ECM production and the dynamics of incremental pore coverage were evident throughout three-dimensional cultures up to day 14 prior to the implantation (supplementary data). After 14 days of three-dimensional HOI with Cho culturing, cells were seen to have outgrown every layer of the scaffold with the interconnecting ECM (figures 3(c) and (d)). This figure illustrates the final scaffold prior to *in vivo* implantation. The cells could be seen elongated and positioned randomly throughout the scaffold, but they covered the whole pore diameter. After a continuous increment of pore coverage throughout the three-dimensional hexagonal scaffold culture, on day 14 (D14) Cho covered $76.6 \pm 10.4\%$ ($p < 0.05$ D7 vs. D3 and D14 vs. D3; $p = \text{n.s}$ D14 vs. D7) of a single pore (supplementary data).

Both scaffolds did not show signs of degradation throughout the *in vitro* culture. No significant cell death was observed during scaffold culturing.

3.3. Gene expression

3.3.1. Monolayer

Col2 and *Col10* expression at P1, P2 and P3 was examined (table 1 and supplementary data). The mean mRNA expression values showed numerical decline of

Col2 and an increase of fibroblastic *Col10*. The changes in *Col2* and *Col10* mRNA expressions illustrate clear dedifferentiation typically seen in monolayer cultures. Similar trends were observed in distinct monolayer culture lines throughout a two week assessment period (data not shown). After comparing the aforementioned gene expressions of one passage to P0 (i.e. P1 vs. P0, P2 vs. P0 and P3 vs. P0), a steady dedifferentiation and decreased chondrogenic marker expression process was evident: the *Col2* mRNA expression was 4.1, 32.7 and 25.3 times lower compared to normal cartilage in P1 (mean culture time of 16.4 ± 7.4 days), P2 (mean culture time of 22.8 ± 6.3 days) and P3 (mean culture time of 31.7 ± 10.8 days), respectively. The *Col10* mRNA expression was lower by 114.9, 101 and 39.8 times in P1, P2 and P3, respectively.

3.3.2. CM with chondrocytes (Cho) *in vitro*

The three-dimensional culture of the CM with Cho resulted in statistical trends for increased mean COL2A1 mRNA values vs. 2D (0.29 ± 0.13 vs. 0.08 ± 0.08 , $p = 0.05$) as well as low numerical Col10 mRNA values that cannot be equivocally interpreted (supplementary data). Similarly, we observed a certain numerical tendency in the increase of Col2 as well as a certain decrease of Col 10 mRNA expressions in a longitudinal assessment throughout the observed three week period (data not shown).

Table 1. Type-II and type-X collagen mRNA expression dynamics in a monolayer (P1 to P3) and 3D collagen membrane seeded with P3 Cho *in vitro* (prior to implantation) and *in vivo*.

Environment	Type-II collagen mRNA mean (SD)	Type-X collagen mRNA mean (SD)
<i>In vitro</i> (at week 2)		
2D	P1 (<i>n</i> = 5)	0.240 (0.419)
	P2 (<i>n</i> = 5)	0.031 (0.035)
	P3 (<i>n</i> = 5)	0.034 (0.073)
2D/3D (CM)	Pre-seeding (2D) (<i>n</i> = 3)	0.083 (0.081)
	Pre-implantation (3D) (<i>n</i> = 4)	0.290 (0.132) ^b
<i>In vivo</i> (at month 3)		
	CM only (EG1, <i>n</i> = 3)	0.200 (0.002)
	CM with chondrocytes (EG2, <i>n</i> = 3)	0.392 (0.044) ^c
	HOI only (EG3, <i>n</i> = 4)	1.256 (1.594)
HOI with chondrocytes (EG4, <i>n</i> = 3)		0.198 (0.041)
	Control group (CG, <i>n</i> = 2)	0.759 (0.541) ^d
<i>In vivo</i> (at month 6)		
	CM only (EG1, <i>n</i> = 3)	0.252 (0.012) ^e
	CM with chondrocytes (EG2, <i>n</i> = 3)	0.887 (0.095) ^{e,f}
	HOI only (EG3, <i>n</i> = 3)	1.761 (0.765)
HOI with chondrocytes (EG4, <i>n</i> = 4)		1.483 (0.614) ^{e,f}
	Control group (CG, <i>n</i> = 5)	0.680 (0.379)

2D—two-dimensional microenvironment; 3D—three-dimensional microenvironment; CM—collagen membrane; EG—experimental group; ND—not detected; P1—first passage; P2—second passage; P3—third passage; HOI—hybrid organic-inorganic scaffold.

^a $p < 0.05$ (Col10 P3 vs. P1).

^b $p = 0.05$ (Col2 3D vs. 2D).

^c $p < 0.05$ (Col2 at month 3 EG1 vs. EG2).

^d one unexplained outlying value was observed.

^e $p < 0.05$ (Col2 EG1, EG2 and EG4 at month 6 vs. month 3).

^f $p < 0.05$ (Col2 EG1 vs. EG2 and EG4 at month 6).

3.3.3. HOI with chondrocytes (Cho) *in vitro*

A steady increment of type-II collagen mRNA expression values was evident in a single sample from 0.001 to 0.226 (226 times). This indicates a redifferentiation trend toward hyaline-like cartilage. The type-X collagen mRNA expression values slightly increased in a single sample from 0.0026 to 0.0069 (2.6 times), thus showing isolated signs of fibrogenesis.

3.3.4. *In vivo* study

We evaluated COL2A1 and COL10A1 mRNA expression values in five experimental groups at 3 and 6 months after implantation (table 1). The study revealed rather clear increases in the Col2 expression within a 6 month period, reaching numerically higher mean COL2A1 mRNA expression values compared to the control group in both Cho-containing groups EG2 and EG4 as well as in the EG3 group, i.e. ~ 0.9 , ~ 1.5 and ~ 1.8 vs. ~ 0.7 , respectively. In addition, the EG1 group showed statistically significant lower values than both experimental groups with seeded Cho and a certain numerical inferiority to all other groups at 6 months post-implantation. The type-X collagen mRNA values were below detection limits in all groups tested for both time periods *in vivo*.

3.4. *In vitro* histology of scaffolds

The Cho of the third passage were seeded onto CM and HOI membranes and evaluated histologically for hyaline cartilage specific matrix staining.

During the CM seeded with the Cho culture, continuous incremental visualization of cartilage specific GAGs was evident up to D14 (supplementary data). At D14, prior to implantation, Cho were seen interconnected and attached to the membrane. An extracellular matrix was produced; immunohistochemical staining showed no type-II collagen at D14. The type-I collagen remained weakly stained throughout the scaffold culture. However, toluidine blue revealed staining of specific glycosaminoglycan molecules in the cartilage.

At D14 of the HOI membrane with the Cho scaffold culture prior to implantation, cells revealed a round shape and extracellular matrix adjacent to the fragmented HOI membrane (supplementary data). The type-I collagen staining was not clearly visible; however, hyaline-like cartilage-specific staining of PGs and GAGs by means of toluidine blue and safranin O was clearly evident.

3.5. Gross examination

Minimal initial swelling on the operated knee, which later subsided, was observed 1-2 days postoperatively. No signs of inflammatory or immune response to the implanted material at the day of examination were evident. In the control group treated only with fibrin polymerization, a 1 month gross examination showed incomplete cartilage tissue filling, with the defect clearly visible (figure 4(a)). At three months the defect

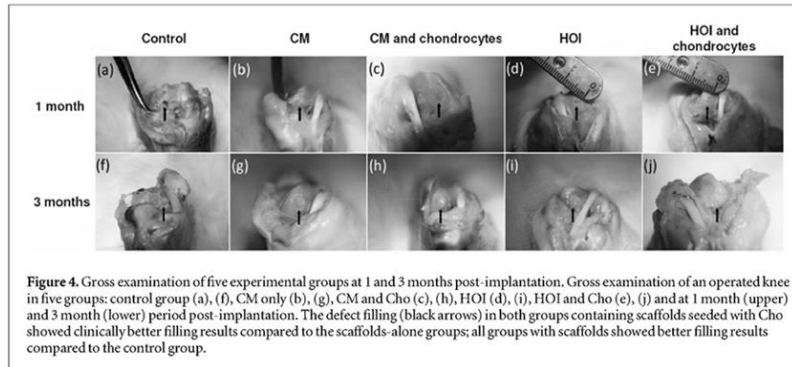


Figure 4. Gross examination of five experimental groups at 1 and 3 months post-implantation. Gross examination of an operated knee in five groups: control group (a), (f), CM only (b), (g), CM and Cho (c), (h), HOI (d), (i), HOI and Cho (e), (j) and at 1 month (upper) and 3 month (lower) period post-implantation. The defect filling (black arrows) in both groups containing scaffolds seeded with Cho showed clinically better filling results compared to the scaffolds-alone groups; all groups with scaffolds showed better filling results compared to the control group.

was partially filled, with soft cartilage-like tissue in the lesser part of the defect (figure 4(f)).

In experimental group #1 (the CM only group) the greater part of the 1 month defect was filled with soft tissue without good lateral integration with the adjacent cartilage (figure 4(b)); it improved at 3 months with cartilage-like tissue filling the greater part of the defect with little depressions at the defect margins (figure 4(g)).

In the experimental group #2, CM seeded with chondrocytes, defect at 1 month showed better filling than that of group #3. Cartilage-like fibrous tissue could be observed throughout the repair zone with good integration in the surrounding tissue, however a slight depression at the center of the defect could be seen (figure 4(c)). At 3 months the defect was fully covered by soft whitish cartilage-like tissue with a slight hypertrophy evident throughout the defect (figure 4(h)).

In experimental group #3 (the HOI membrane only group) at one month, the defect was filled with soft cartilage-like tissue with nearly good integration between the neocartilage and surrounding cartilage; however, slight depression could be seen in the middle of the defect (figure 4(d)). At 3 months the neo-cartilage was almost fully integrated with the host cartilage throughout the defect, with whitish cartilage-like tissue; however, rough surface was observed (figure 4(i)).

In experimental group #4 (HOI seeded with Cho) the defect at 1 month was filled with neo-cartilage with nearly good integration to the surrounding cartilage with little depression in the center of the defect that was still evident (figure 4(e)). At 3 months, newly formed cartilage-like tissue had good integration with the adjacent cartilage and displayed cartilage-like color and texture. No hypertrophy was seen throughout the defect area (figure 4(j)).

3.6. Histological examination after 3 months *in vivo*

Healthy articular cartilage has its own specific histological architecture (supplementary data).

Five experimental groups underwent histological evaluation.

In the control group treated with fibrin polymerization only, at 3 months the lesions were covered with connective tissue (figures 5(a)–(d)). Very little matrix staining was observed. Fibrous tissue was dominating the whole defect, with cellular orientation of repaired tissue of no particular organization.

Experimental group #1 showed an empty defect filling with a similar ratio of type-II and type-I collagen staining, resulting in a fibrous tissue. Surface irregularities could be seen throughout the group. As in the control group, the lesions were partially covered with connective tissue; no hyaline-like cartilage tissue formation was seen (figures 5(e)–(h)).

In experimental group #2 at 3 months the defects showed a better filling of connective tissue, with more intense staining of type-II collagen and less staining of type-I collagen in comparison to experimental group #1. Type-II collagen and histochemical staining revealed increased hyaline cartilage-like formation and increased GAGs and PGs deposition at the surface of the defect compared to the control group. However, the cells appeared randomly orientated as seen with extracellular matrix staining by toluidine blue and safranin O (figure 5(i)–(l)).

Experimental group #3 showed better filling of the defect, with slight irregularities at the surface compared to the control group. Repaired tissues showed partial detachment from the subchondral bone and adjacent host cartilage; the repair tissue did not have a clear zonal organization. However, cartilage-like tissue ECM staining was evident (figures 5(m)–(p)).

Experimental group #4 revealed similar type-II and type-I collagen staining compared to the HOI membrane only but had a better organized cellular distribution and histoarchitecture. At 3 months post-

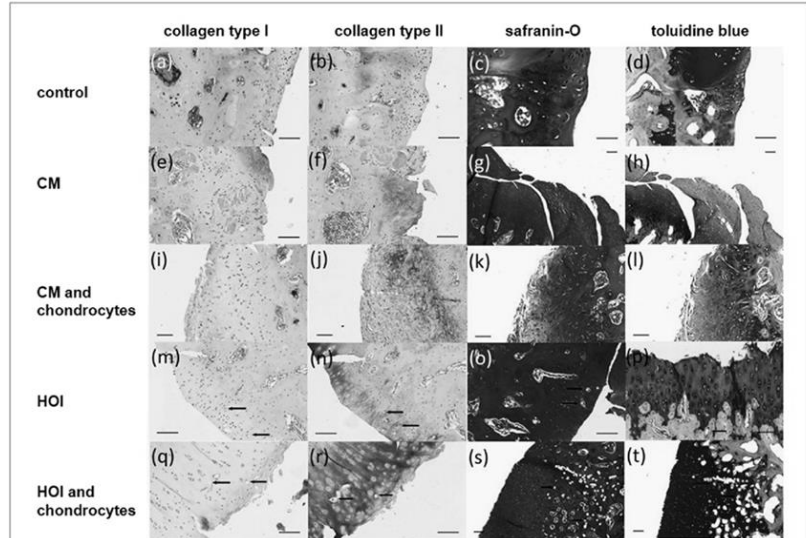


Figure 5. Histological examination of five experimental groups at 3 months post-implantation. Histological examination of cartilage tissue regeneration in the control group (a)–(d), in CM only (e)–(h), in CM with Cho (i)–(l), in HOI (m)–(p), in HOI with Cho (q)–(t) at a 3 month period post-implantation by means of immune staining against type-I and type-II collagens and histochemical staining with safranin O and toluidine blue. The histology showed better defect filling results in both groups of scaffolds and Cho compared to the scaffolds-alone groups; all the groups with scaffolds showed better defect filling results compared to the control group. The arrows depict fragmented HOI. Scale bar: 100 μ m.

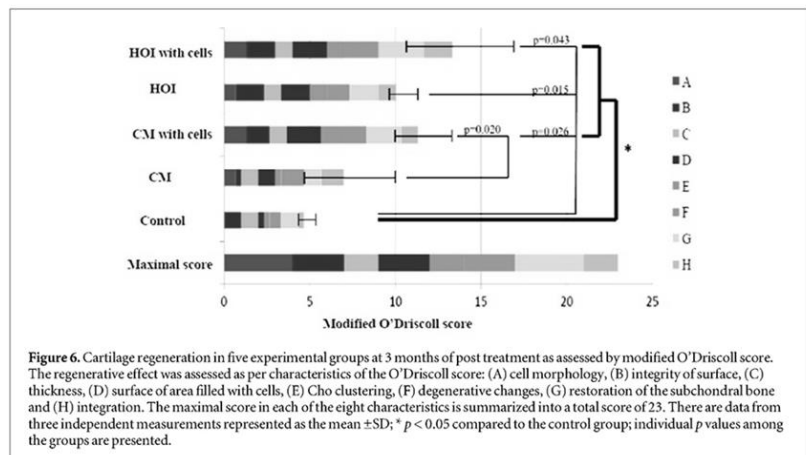


Figure 6. Cartilage regeneration in five experimental groups at 3 months of post treatment as assessed by modified O'Driscoll score. The regenerative effect was assessed as per characteristics of the O'Driscoll score: (A) cell morphology, (B) integrity of surface, (C) thickness, (D) surface of area filled with cells, (E) Cho clustering, (F) degenerative changes, (G) restoration of the subchondral bone and (H) integration. The maximal score in each of the eight characteristics is summarized into a total score of 23. There are data from three independent measurements represented as the mean \pm SD; * $p < 0.05$ compared to the control group; individual p values among the groups are presented.

implantation, remnants of the HOI membrane were clearly visible at the subchondral line, with no severe signs of tissue reaction nor evident inflammatory cell immigration (figures 5(q)–(t)).

For experimental groups #3 and #4, inflammatory reactions were analyzed assessing immune cell

infiltration events. However, histological examination revealed that the scaffold did not provoke a foreign body reaction with infiltration of any inflammatory type cells, i.e. leukocytes and macrophages.

Type-II and type-I collagen expression and GAGs deposition were evaluated in all repair tissues. The

culturing [74]. We used it for a non-direct comparison. An increased number of Cho was seen during the *in vitro* sponge culture, indicating favorable conditions for cell proliferation and the production of proteoglycans. The type-II collagen numerical increment was evident by mRNA expression analysis, although it was not apparent by immunohistochemical collagen type-II staining up to D14. Similarly as for HOI scaffold the same reasoning is relevant for this discrepancy. Cell-seeding density has been shown to influence the outcome of *in vitro* engineered tissue [75]. Because of different cell-seeding concentrations, we were not able to compare two membranes directly. However, PCR data shows a tendency toward chondrogenic tissue formation at both cell-seeding formulations. It is important to note that a lower count of Cho seeded on a HOI membrane allowed for a greater cartilage-specific genotypic change as indirectly compared to the collagen scaffold. Immunohistological analysis revealed a weakened chondrogenic phenotype over a 14 days of an *in vitro* scaffold culture in both matrices as compared to healthy cartilage. However, histochemical analysis showed retention of GAGs by means of toluidine blue and safranin O staining. Further studies are needed to assess the chondrogenic factors' influence on HOI scaffolds and Cho redifferentiation as well as the ability to retain the chondrogenic phenotype during a prolonged time in a scaffold culture. In the present *in vivo* study, we used a rabbit model for three-dimensionally cultured Cho implantation. This study showed rather diverging results comparing one and 3 months data: CM with Cho showed superior type-II collagen expression compared to CM only at both endpoints, while the HOI membrane with Cho was comparable at lower numerical levels to the HOI membrane alone at 1 and 3 months except for the HOI membrane alone at which an unexpected increase of collagen type-II expression is observed at the 3 month endpoint. This may be due to unique features of the HOI membrane to attract host Cho for cartilage regeneration, while seeded allogeneic Cho within the HOI might interfere with attraction of host cells. This short term *in vivo* observation cannot be overemphasized, and longer term studies are of great importance.

The histological observation of regenerated tissues throughout experimental groups with Cho showed numerically better results when compared to its respective groups without Cho and were significantly better than the control group. At 3 months after implantation, CM cultured Cho had a superior repair tissue compared to the control and CM without cells. No delaminations of CM were observed histologically in this study. Although macroscopically defects were filled with repair tissue, irregularities at the surface in both groups were evident, as seen in figure 4. Improvement in both membrane groups without the cells was not significant and may be explained by the insufficient effect of bone marrow stem cells that infiltrate

the subchondral defect [35]. No inflammatory reactions were observed throughout the HOI membrane groups. The scaffold was seen to disintegrate during the examination. This may be due to histological preparation of the samples, which requires mechanical dissection of paraffin blocks. Frozen blocks should be considered in the future studies. The modified O'Driscoll score was significantly better in experimental groups treated with seeded scaffolds compared to unseeded groups and the control group. This study demonstrated that direct laser polymerization is a valuable method to create a scaffold of various formations. Loss of the chondrogenic phenotype during the monolayer culture can be recovered through three-dimensional cultures with a HOI and collagen membranes, and the phenotype can be maintained at least 3 months after implantation. The differences observed between the investigated scaffold groups need further investigation. Our hexagonal HOI scaffold in combination with Cho may be successfully implemented in cartilage tissue engineering applications.

5. Conclusions

For the first time ultrafast pulse DLW lithography was employed for the fabrication of 3D microstructured scaffolds, and their biocompatibility was tested *in vivo* using rabbits. Osteochondral injury was chosen as the study problem. Common HOI material SZ2080 was used for the microstructuring. A woodpile and a mesh of 3D hexagons geometries were manufactured, and prior to implantation into 27 rabbits for up to 6 months they were seeded with Cho for two weeks. The results were compared to the same procedure with a collagen scaffold. Ultrafast pulsed lasers became a well-established technique for the creation of custom-made free-form 3D micro scaffolds from a variety of materials ranging from proteins to biocompatible glasses. Its potential applications for the manufacturing of patient specific scaffold seem unlimited in terms of spatial resolution and geometry complexity. However, despite few exceptions in which live cells or primitive organisms were encapsulated into a polymer matrix, no demonstration of an *in vivo* study case of scaffolds generated with such a method was performed. Here, we report a preclinical study of 3D artificial microstructured scaffolds of HOI material SZ2080 fabricated using the DLW technique. The created $2.1 \times 2.1 \times 0.21 \text{ mm}^3$ membrane constructs are tested both *in vitro* by growing isolated allogeneic rabbit Cho and *in vivo* by implantation into rabbit organisms for 6 months. An *Ex vivo* histological examination shows that optimization of pore geometry and pre-growing of Cho prior to implantation significantly improves the performance of the created 3D scaffolds. A HOI membrane with Cho allowed for a better macroscopical and histological evaluation, which was in accordance with PCR results obtained

defects treated with scaffolds containing cells demonstrated superior tissue formation compared to its respective group of implanted scaffold only. The subchondral bone tissue is still seen undergoing remodeling throughout groups at 3 months postoperatively.

The different parameters of the modified O'Driscoll histological scoring system [56] were evaluated, as seen in figure 6. The histological score in group #4 revealed statistically significantly better repair compared to the control group (the mean O'Driscoll scores were 13.3 ± 3.1 and 4.7 ± 0.6 ($p < 0.05$) in group #4 and the control group, respectively) and were numerically higher compared to group #3 (mean score was 10.0 ± 1.0 , $p = 0.118$). The experimental group #2s resultant defect repair was also statistically significantly superior compared to group #1 and the control group: the mean O'Driscoll scores were 11.7 ± 2.1 , 7.4 ± 2.1 and 4.7 ± 0.6 ($p < 0.05$) in groups #2 and #1 and the control group, respectively.

4. Discussion

Articular cartilage repair still remains a major problem in healthcare. Previous studies have demonstrated the efficacy of somatic cells combined with three-dimensional scaffolds for treatment of large osteochondral defects in knee joints [59]. The rigid biocompatible scaffold allows for the Chos' proliferation, migration, redifferentiation and subsequent cartilage formation. After the Chos' adherence to the surrounding scaffold, the reexpression of hyaline cartilage-specific genes indicates that the scaffold is suitable for *in vivo* implantation [60, 61]. When trying to elucidate the true effect of the implanted scaffold, the articular osteochondral model has its drawback of reaching through the vascularized subchondral bone, which might repair itself spontaneously [62, 63]. Rabbit articular cartilage of 0.2-0.3 mm thickness makes it difficult to effectively produce a pure chondral defect. The contribution of host cells infiltrating from bone marrow to tissue defect should be elucidated in further studies. No data related to combination of this type of scaffold and Cho were found. SZ2080 material has been shown to provide adequate response for tissue engineering for rabbit stem cells *in vitro* [64] as well as whole animals *in vivo* [21]. DLW in photopolymers is distinguished by a possibility to precisely fabricate fully 3D microstructures with a freely chosen geometry out of a vast selection of materials. *In vitro* and *in vivo* biocompatibility tests have shown that various photosturucturable polymers used in DLW are biocompatible, making it an attractive technique for fabrication of polymeric scaffolds for tissue engineering applications [22]. The studies show that it is possible to structure hydrogels that already contain living cells without any damage [15]. This allows precise spatial encapsulation of the cells inside the scaffold during the fabrication process. The limiting factor here is photoinitiators

used to photosensitize the materials as they are very chemically reactive and can result in the formation of reactive oxygen, which is harmful to cells. However, this limitation could be circumvented by employing the fabrication of pure materials without the use of any photoinitiators [17]. The primary focuses of this study were to test the feasibility of HOI and collagen scaffolds in combination with allogeneic Cho to form cartilage-like tissue *in vitro* and *in vivo*. For newly formed tissue evaluation we used collagen type-II protein, which is a known hyaline cartilage specific marker [43], and collagen type-X, a fibroblastic marker [65]. Many studies have previously shown the benefits of chondrogenic factors such as Sox9, Bmp-2 or Tgf for *in vitro* cultures [66, 67]. We were interested in exclusively a three-dimensional scaffold influence toward retaining chondrogenic lineage. Multiple studies indicate that Cho lose their phenotype during a monolayer culture, which is highly dependent on time in a culture. Cho morphologically and functionally dedifferentiate, becoming fibroblast-like cells [68]. Type-II collagen expression in our experiment decreased in accordance with these studies [69, 70], while type-X collagen showed an insignificant increment in value. It is important to ensure that expanded Cho retain their phenotypic function. Redifferentiation to the chondrogenic phenotype is induced after three-dimensional scaffold cultures [43]. Many studies support the use of scaffolds of different 3D origins [71, 72]. Ideally, the scaffold would resemble the environment of a native cartilage with Cho far apart from each other [73]. In this study we fabricated a HOI scaffold using direct laser polymerization. SZ2080 has been shown to be biocompatible in previous reports [21]. A HOI membrane was made of two types of pores: woodpile and honeycomb. Further scaffold culturing with Cho in a woodpile-type membrane revealed that cells failed to integrate and were seen in a monolayer. This may be due to narrow inside structures, which are not compatible for Cho migration throughout, thus leaving cells unable to adequately integrate to the scaffold. A hexagon-type pore seemed appropriate for cells to proliferate. Its rigid structure enabled the attachment of Cho and the production of ECM that covered every layer of the hexagon-type membrane. The increment of pore coverage revealed remarkable growth at D8 with continuing growth for a period up to the end of the observation at D14. The cells at the bottom layer of the scaffold showed signs of adherence to the culture flask as well. Up to 14 days of *in vitro* HOI scaffold culture PCR data revealed a 226 times increment of type-II collagen reexpression albeit in one sample. The toluidine blue and safranin-O stainings were positive despite the absence of collagen type-II positive immunohistochemical staining. This indicates that Cho in a HOI membrane retained their ability to produce GAGs. In addition to the HOI membrane, we tested a collagen membrane, which has suitable properties for the three-dimensional

from samples at 3 months after implantation. The HOI membrane loaded with Cho had the most hyaline-like tissue compared to other groups. The achieved biocompatibility is comparable to the commercially available collagen membrane. A successful outcome of this study supports the idea that hexagonal-pore-shaped HOI microstructured scaffolds in combination with Cho seeding may be successfully implemented for the cartilage tissue engineering.

Thus, here we showed for the first time that novel, specially shaped SZ2080 material is a biocompatible material for Cho in a 3D environment and enables them to recover the chondrogenic phenotype, which is otherwise diminished during culturing in a monolayer. The biocompatibility was sustained throughout the long-term *in vivo* study. This feature of maintaining chondrogenicity is at least non-inferior to standard 3D forming of biocompatible materials, such as collagenous scaffolds, and is a promising feature for effective exploitation of Cho for tissue regeneration. It seems that a laser-formed HOI scaffold is more efficient in producing a chondrogenic environment compared to standard collagenous scaffolds. Future studies should involve further improvement of *in vitro* and *in vivo* outcomes by preventing cells from elongation and by adding growth factors to the medium; long-term durability of the HOI membrane after implantation and its effect on cartilage regeneration; adding human somatic and stem cells cultures for *in vitro* and *in vivo* analysis and their functionality in larger animals and humans.

Acknowledgments

This work was supported by the research grant received from Lithuanian Academy of Science Project No. MIP050/2012. SR and MM acknowledge financial support by EC's Seventh Framework Programme (LASERLABEUROPE, Grant Agreement No. 228334, OPTOBIO). SR and MM dedicate this work to Mr Paulius Danilevičius (VU LRC and FORTH-IESL) who, due to his early accidental death, could not reach practical realization of *in vivo* studies of fs laser-made 3D polymer micro-scaffolds.

References

- [1] Kawata S, Sun H B, Tanaka T and Takada T 2001 Finer features for functional microdevices *Nature* 412 697–8
- [2] Ovsianikov A, Schlie S, Ngezhahyo A, Haverich A and Chichkov B N 2007 Two-photon polymerization technique for microfabrication of CAD-designed 3D scaffolds from commercially available photosensitive materials *J. Tissue Eng. Regen. Med.* 1 443–9
- [3] Gittard S D, Ovsianikov A, Chichkov B N, Doraiswamy A and Narayan R J 2010 Two-photon polymerization of microneedles for transdermal drug delivery *Expert Opin. Drug Deliv.* 7 513–33
- [4] Wiesbauer M, Wollhofen R, Vasic B, Schilcher K, Jacak J and Klar T A 2013 Nano-anchors with single protein capacity produced with STED lithography *Nano Lett.* 13 5672–8
- [5] Tayalia P, Mendonca C R, Baldacchini T, Mooney D J and Mazur E 2008 3D cell-migration studies using two-photon engineered polymer scaffolds *Adv. Mat.* 20 4494–8
- [6] Weiss T, Schade R, Laube T, Berg A, Hildebrand G, Wyrwa R, Schnabelrauch M and Liefelth K 2011 Two-photon polymerization of biocompatible photopolymers for microstructured 3D biointerfaces *Adv. Eng. Mat.* 13 B264–73
- [7] Ajeti V, Lien C H, Chen S J, Su P J, Squirrel J M, Molinarolo K H, Lyons G E, Eliceiri K W, Ogle B M and Campagnola P J 2013 Image-inspired 3D multiphoton excited fabrication of extracellular matrix structures by modulated raster scanning *Opt. Express* 21 25346–55
- [8] Marino A, Filippeschi C, Genchi G G, Mattoli V, Mazzalai B and Ciofani G 2014 The osteoprint: a bio-inspired two-photon polymerized 3D structure for the enhancement of bone-like cell differentiation *Acta Biomaterialia* 10 4304–13
- [9] Amato L, Gu Y, Bellini N, Eaton S M, Cerullo G and Osellame R 2012 Integrated three-dimensional filter separates nanoscale from microscale elements in a microfluidic chip *Lab. Chip.* 12 1135–42
- [10] Sugioka K and Cheng Y 2014 Ultrafast lasers-reliable tools for advanced materials processing *Light Sci. Appl.* 3 149
- [11] Galanopoulos S, Chatzidai N, Melissinaki V, Selimis A, Schizas C, Farsari M and Karalekas D 2014 Design, fabrication and computational characterization of a 3D micro-valve built by multi-photon polymerization *Micromachines* 5 505–14
- [12] Seidlits S K, Schmidt C E and Shear J B 2009 High-resolution patterning of hydrogels in three dimensions using direct-write photofabrication for cell guidance *Adv. Func. Mat.* 19 3543–51
- [13] Greiner A M, Richter B and Bastmeyer M 2012 Micro-Engineered 3D scaffolds for cell culture studies *Macromolecular Biosci.* 12 1301–14
- [14] Raimondi M T, Michele M, Nava M, Eaton S M, Bernasconi A, Vishnubhatla K C, Cerullo G and Osellame R 2014 Optimization of femtosecond laser polymerized structural niches to control mesenchymal stromal cell fate in culture *Micromachines* 5 341–58
- [15] Ovsianikov A et al 2014 Laser photofabrication of cell-containing hydrogel constructs *Langmuir* 30 3787–94
- [16] Torgersen J et al 2014 Photo-sensitive hydrogels for three-dimensional laser microfabrication in the presence of whole organisms *J. Biomed. Opt.* 17 105008
- [17] Rekštyte S, Malinauskas M and Juodkazi S 2013 Three-dimensional laser micro-sculpturing of silicone: towards biocompatible scaffolds *Opt. Express* 21 17028–41
- [18] Ovsianikov A, Gruene M, Paum M, Koch L, Maiorana F, Wilhelm M, Haverich A and Chichkov B 2010 Laser printing of cells into 3D scaffolds *Biofabrication* 2 014104
- [19] Kufelt O, El-Tamer A, Schring C, Schlie S, Wolter S and Chichkov B N 2014 Hyaluronic acid based materials for scaffolding via two-photon polymerization *Biomacromolecules* 15 650–9
- [20] Danilevičius P, Georgiadi L, Pateman C J, Claeysens F, Chatzinikolaidou M and Farsari M 2014 The effect of porosity on cell ingrowth into accurately defined, laser-made, polylactide-based 3D scaffolds *Appl. Surf. Sci.* in press doi:10.1016/j.apsusc.2014.06.012
- [21] Malinauskas M et al 2012 *In vitro* and *in vivo* biocompatibility study on laser 3D microstructurable polymers *Appl. Phys. A* 108 751–9
- [22] Danilevičius P, Rekštyte S, Balčiūnas E, Kraniuskas A, Jarašienė R, Širmenis R, Baltrušienė D, Bukelskienė V, Gadonas R and Malinauskas M 2012 Microstructured polymer scaffolds fabricated by direct laser writing for tissue engineering *J. Biomed. Optics* 17 081405

- [23] Buckmann T, Thiel M, Kadic M, Schittny R and Wegener M 2014 An elasto-mechanical unfeelability cloak made of pentamode metamaterials *Nature Commun.* 5 4130
- [24] Melissinaki V, Gill A, Ortega I, Vamvakaki M, Ranella A and Haycock J W Fotakis C, Farsari M and Claeysens F 2011 Direct laser writing of 3D scaffolds for neural tissue engineering applications *Biofabrication* 3 045005
- [25] Farsari M and Chichkov B N 2009 Materials processing: two-photon fabrication *Nature Photon.* 3 450–2
- [26] Gittard S D, Nguyen A, Obata K, Koroleva A, Narayan R J and Chichkov B N 2011 Fabrication of microscale medical devices by two-photon polymerization with multiple foci via a spatial light modulator *Biomed. Opt. Express* 2 3167–78
- [27] Stankevicius E, Gertus T, Rutkauskas M, Gedvilas M, Raciukaitis G, Gadonas R, Smilgevičius V and Malinauskas M 2012 Fabrication of micro-tube arrays in photopolymer SZ2080 by using three different methods of a direct laser polymerization technique *J. Micromech. Microneng.* 22 065022
- [28] Buckmann T, Stenger N, Kadic M, Kaschke J, Frolich A, Kennerknecht T, Eber C, Thiel M and Wegener M 2012 Tailored 3D mechanical metamaterials made by dip-in direct-laser-writing optical lithography *Adv. Mat.* 24 2710–4
- [29] Obata K, El-Tamer A, Koch L, Hinze U and Chichkov B N 2013 High-aspect 3D two-photon polymerization structuring with widened objective working range (WOW-2PP) *Light Sci. Appl.* 2 e116
- [30] Ovsianikov A, Viertel J, Chichkov B, MacCraith M O B, Sakellari I, Giakoumaki A, Gray D, Vamvakaki M, Farsari M and Fotakis C 2008 Ultra-low shrinkage hybrid photosensitive material for multiphoton polymerization microfabrication *ACS Nano* 2 2257–62
- [31] Psycharakis S, Tosca A, Melissinaki V, Giakoumaki A and Ranella A 2011 Tailor-made three-dimensional hybrid scaffolds for cell cultures *Biomed. Mater.* 6 045008
- [32] Bohndorf K 1996 Injuries at the articulating surfaces of bone (chondral, osteochondral, subchondral fractures and osteochondrosis dissecans) *Eur. J. Radiol.* 22 247
- [33] Gudas R, Simonaityte R, Cekanaukas E and Mickevicius T 2011 Concomitant autologous chondrocyte implantation with osteochondral grafting for treatment of a massive osteochondral defect in the bilateral knees of a child *Medicina* 47 170–3
- [34] Buckwalter J A and Mankin H J 1997 Articular cartilage: tissue design and chondrocyte-matrix interactions *J. Bone Joint Surg.* 79 600–11
- [35] Eyre D 2002 Articular cartilage and changes in arthritis: collagen of articular cartilage *Arthritis Res.* 4 30–5
- [36] Bedi A, Feeley B T and Williams R J III 2010 Management of articular cartilage defects of the knee *J. Bone Joint Surg. Am.* 92 994–1009
- [37] Hunziker E B 2002 Articular cartilage repair: basic science and clinical progress. A review of the current status and prospects *Osteoarthr. Cartil.* 10 432–63
- [38] Benthien J P, Schwanninger M and Behrens P 2011 We do not have evidence based methods for the treatment of cartilage defects in the knee *Knee Surg. Sports Traumatol. Arthrosc.* 19 543–52
- [39] Portocarrero G, Collins G and Livingston A T 2013 Challenges in cartilage tissue engineering *J. Tissue Sci. Eng.* 4 e120
- [40] Nuernberger S, Cyran N, Albrecht C, Redl H, Vecsei V and Marlovits S 2011 The influence of scaffold architecture on chondrocyte distribution and behaviour in matrix-associated chondrocyte transplantation grafts *Biomaterials* 32 1032–40
- [41] Johnstone B et al 2013 Tissue engineering for articular cartilage repair—state of the art *Eur. Cells Mat.* 25 248–67
- [42] Xu T, Binder K W, Albanna M Z, Dice D, Zhao W, Yoo J J and Atala A 2013 Hybrid printing of mechanically and biologically improved constructs for cartilage tissue engineering applications *Biofabrication* 5 015001
- [43] Benya P D and Shafer J D 1982 Differentiated chondrocytes reexpress the differentiated collagen phenotype when cultured in agarose gels *Cell* 30 215–24
- [44] Freed L E, Marquis J C, Nohria A, Emmanuel J, Mikos A G and Langer R 1993 Neocartilage formation *in vitro* and *in vivo* using cells cultured on synthetic biodegradable polymers *J. Biomed. Mater. Res.* 27 11–23
- [45] Freed L E, Engelmayr G C Jr, Borenstein J T, Moutos F T and Guilak F 2009 Advanced material strategies for tissue engineering scaffolds *Adv. Mater.* 21 3410–8
- [46] Ahmed T A E and Hincke M T 2010 Strategies for articular cartilage lesion repair and functional restoration *Tissue Eng. Part B Rev.* 16 305–29
- [47] Itay S, Abramovici A and Nevo Z 1987 Use of cultured embryonal chick epiphyseal chondrocytes as grafts for defects in chick articular cartilage *Clin. Orthop. Relat. Res.* 220 284–303
- [48] Wysocka A, Mann K, Bursig H, Dec J and Gazdzik T S 2010 Chondrocyte suspension in fibrin glue *Cell Tissue Bank* 11 209–15
- [49] Selimis A, Mironov V and Farsari M 2015 Direct laser writing: principles and materials for scaffold 3D printing *Microelectron. Eng.* 132 83–9
- [50] Schlie S, Ngezhayoh A, Ovsianikov A, Fabian T, Kolb H-A, Haferkamp H and Chichkov B N 2007 Three-dimensional cell growth on structures fabricated from ORMOCER® by two-photon polymerization technique *J. Biomater. Appl.* 22 275–87
- [51] Terzaki K, Kissamitaki M, Skarmoutsou A, Fotakis C, Charitidis C A, Farsari M, Vamvakaki M and Chatziniokolaidou M 2013 Pre-osteoblastic cell response on three-dimensional, organic-inorganic hybrid material scaffolds for bone tissue engineering *J. Biomed. Mater. Res. A* 101A 2283–94
- [52] Malafaya P B, Silva G A and Reis R L 2007 Natural-origin polymers as carriers and scaffolds for biomolecules and cell delivery in tissue engineering applications *Adv. Drug Deliv. Rev.* 59 207–33
- [53] Ben-Yishay A, Grande D A, Schwartz R E, Menche D and Pitman M D 1995 Repair of articular cartilage defects with collagen-chondrocyte allografts *Tissue Eng.* 1 119–33
- [54] Frenkel S R, Toolan B, Menche D, Pitman M I and Pachence J M 1997 Chondrocyte transplantation using a collagen bilayer matrix for cartilage repair *J. Bone Joint Surg.* 79 831–6
- [55] Malinauskas M, Farsari M, Piskarskas A and Juodkazis S 2013 Ultrafast laser nanostructuring of photopolymers: a decade of advances *Phys. Rep.* 533 1–31
- [56] Malinauskas M, Kiršanskė G, Reksytė S, Jonavičius T, Kazulionytė E, Jonušauskas L, Žukauskas A, Gadonas R and Piskarskas A 2012 Nanophotonic lithography: a versatile tool for manufacturing functional three-dimensional micro-/nano-objects *Lith. J. Phys.* 52 312–26
- [57] Kapyla E, Aydoğan D B, Virjula S, Vanhatupa S, Miettinen S, Hyttinen J and Kellomaki M 2012 Direct laser writing and geometrical analysis of scaffolds with designed pore architecture for three-dimensional cell culturing *J. Micromech. Microeng.* 22 115016
- [58] O'Driscoll S W, Keeley F W and Salter R B 1986 The chondrogenic potential of free autogenous periosteal grafts for biological resurfacing of major full-thickness defects in joint surfaces under the influence of continuous passive motion: an experimental investigation in the rabbit *J. Bone Joint Surg. Am.* 68 1017–35
- [59] Ossendorf C, Kaps C, Kreuz P C, Burmester G R, Sittlinger M and Ergelet C 2007 Treatment of posttraumatic and focal osteoarthritic cartilage defects of the knee with autologous polymer-based three-dimensional chondrocyte grafts: 2-year clinical results *Arthritis Res. Ther.* 9 R41
- [60] Hauselmann H J, Masuda K, Hunziker E B, Neidhart M, Mok S S, Michel B A and Thonar E J 1996 Adult human chondrocytes cultured in alginate form a matrix similar to native human articular cartilage *Am. J. Physiol.* 27 742–52
- [61] Grigolo B, Roseti L, Fiorini M, Fini M, Giavaresi G and Aldini N N 2001 Transplantation of chondrocytes seeded on a hyaluronan derivative (hya-11) into cartilage defects in rabbits *Biomaterials* 22 2417–24

- [62] Kim H K, Moran M E and Salter R B 1991 The potential for regeneration of articular cartilage in defects created by chondral shaving and subchondral abrasion: an experimental investigation in rabbits *J. Bone Joint Surg. Am.* **73** 1301–15
- [63] Shapiro F, Koide S and Glimcher M J 1993 Cell origin and differentiation in the repair of full-thickness defects of articular cartilage *J. Bone Joint Surg. Am.* **75** 532–53
- [64] Malinauskas M et al 2014 3D microporous scaffolds manufactured via combination of fused filament fabrication and direct laser writing ablation *Micromachines* **5** 839–58
- [65] Valverde F G et al 2010 Defects in articular cartilage metabolism and early arthritis in fibroblast growth factor receptor 3 deficient mice *Hum. Mol. Gen.* **15** 1783–92
- [66] Kan A et al 2009 Screening of chondrogenic factors with a real-time fluorescence-monitoring cell line ATDC5-C2ER *Arthritis Rheum.* **60** 3314–23
- [67] Danisovic L, Varga I and Polak S 2011 Growth factors and chondrogenic differentiation of mesenchymal stem cells *Tissue Cell* **44** 69–73
- [68] Nadzir M M, Kino-Oka M, Maruyama N, Sato Y and Kim M H 2009 Comprehension of terminal differentiation and dedifferentiation of chondrocytes during passage cultures *J. Biosci. Bioeng.* **112** 395–401
- [69] Marlovits S, Hombauer M, Truppe M, Vecsei V and Schlegel W 2004 Changes in the ratio of type-I and type-II collagen expression during monolayer culture of human chondrocytes *J. Bone Joint Surg. Br.* **86** 286–95
- [70] Chou A I, Bansal A, Miller G J and Nicoll S B 1976 The effect of serial monolayer passaging on the collagen expression profile of outer and inner annulus fibrosus cells *Spine* **31** 1875–81
- [71] Tortelli F and Cancedda R 2009 Three-dimensional cultures of osteogenic and chondrogenic cells: a tissue engineering approach to mimic bone and cartilage *in vitro Eur. Cells Mat.* **17** 1–14
- [72] Wang H and Blitterswijk C A 2010 The role of three-dimensional polymeric scaffold configuration on the uniformity of connective tissue formation by adipose stromal cells *Biomaterials* **31** 4322–9
- [73] Gilmore R S and Palfrey A J 1988 Chondrocyte distribution in the articular cartilage of human femoral condyles *J. Anat.* **157** 23–31
- [74] Legendre F et al 2013 Enhanced hyaline cartilage matrix synthesis in collagen sponge scaffolds by using siRNA to stabilize chondrocytes phenotype cultured with bone morphogenetic protein-2 under hypoxia *Tissue Eng. Part C Methods* **19** 550–67
- [75] Mandl E W, Verhaar J A and Osch G J 2004 Multiplication of human chondrocytes with low seeding densities accelerates cell yield without losing redifferentiation capacity *Tissue Eng.* **10** 109–18

ANNEXES

Annexe 1

State Food and Veterinary Service Permit

VALSTYBINĖ MAISTO IR VETERINARIJOS TARNYBA LEIDIMAS ATLIKTI BANDYMO SU GYVŪNAIS PROCEDŪRŲ PROJEKTĄ

2015-12-08 Nr. G2-36
Vilnius

Vadovaujantis Lietuvos Respublikos gyvūnų gerovės ir apsaugos įstatymo 16 straipsnio 4 dalimi, Mokslo ir mokymo tikslais naudojamų gyvūnų laikymo, priežiūros ir naudojimo reikalavimais, patvirtintais Valstybinės maisto ir veterinarijos tarnybos direktoriaus 2012 m. spalio 31 d. įsakymu Nr. B1-866 „Dėl Mokslo ir mokymo tikslais naudojamų gyvūnų laikymo, priežiūros ir naudojimo reikalavimų patvirtinimo“, Europos konvencija dėl eksperimentiniais ir kitais mokslo tikslais naudojamų stuburinių gyvūnų apsaugos (OL 2004 m. specialusis leidimas, 15 skyrius, 4 tomas, p. 325) ir remiantis Lietuvos bandomųjų gyvūnų naudojimo etikos komisijos prie Valstybinės maisto ir veterinarijos tarnybos 2015-11-25 išvada Nr. 17 „Dėl leidimo atlikti bandymus su gyvūnais“,
le i d ž i a m a

Lietuvos sveikatos mokslų universiteto Veterinarijos akademijai,

(tikro subjekto (-ų), kuriam (-iems) išduotas leidimas atlikti bandymus su gyvūnais procedūrų projektą)

Tilžės g. 18, LT-47181 Kaunas, 302536989.

adresas (-ai), kodas (-ai) juridinių asmenų registre)

atlikti bandymo su gyvūnais procedūrų projektą

„3D mikrostruktūrizuotų ir kologeninių konstruktu su chondrogeninėmis ląstelėmis sukūrimas ir jų transliacinis panaudojimas kremzlės regeneracijai“.

(bandymo su gyvūnais procedūrų projekto pavadinimas, vadovai, naudojami gyvūnai)

projekto vadovas Romualdas Mačiulaitis, naudojant 30 žiurkių, 6 triušius.

Lietuvos sveikatos mokslų universiteto Veterinarijos akademijoje, Tilžės g. 18, LT-47181 Kaunas.

(bandymo su gyvūnais procedūrų projekto atlikimo vietos pavadinimas, adresas)

Leidimas atlikti bandymo su gyvūnais procedūrų projektą galioja iki 2018 m. spalio 1 d.

Direktoriaus pavaduotojas



Vidmantas Paulauskas

Kaunas Regional Biomedical Research Ethics Committee Permit



KAUNO REGIONINIS BIOMEDICININIŲ TYRIMŲ ETIKOS KOMITETAS
Lietuvos sveikatos mokslų universitetas, A. Mickevičiaus g. 9, LT-44307 Kaunas, tel. (+370) 37 32 68 89; el. paštas: kaunorbtek@ismuni.lt

LEIDIMAS ATLIKTI BIOMEDICININĮ TYRIMĄ

2016-05-03 Nr. BE-2-22

Biomedicininio tyrimo pavadinimas: "Žmogaus kelio sąnarinės kremzlės gyvybingumo tyrimas. Chondrocitų išskyrimas ir charakterizavimas"	
Protokolo Nr.:	16/02/24-1
Data:	2016-02-24
Versija:	CHONDRO2
Asmens informavimo forma	Versija Nr. P-CONSENT3, 2016-04-27
Pagrindinis tyrėjas:	Doc. Arvydas Ūsas
Biomedicininio tyrimo vieta:	LSMUL VŠĮ Kauno klinikos,
Įstaigos pavadinimas:	Ortopedijos traumatologijos klinika
Adresas:	Eivenių g. 2, LT-50009, Kaunas, Lietuva

Išvada:

Kauno regioninio biomedicininių tyrimų etikos komiteto posėdžio, įvykusio 2016 m. balandžio mėn. 5 d. (protokolo Nr. BE-10-7) sprendimu pritarta biomedicininio tyrimo vykdymui.

Mokslinio eksperimento vykdytojai įsipareigoja: (1) nedelsiant informuoti Kauno Regioninį biomedicininių Tyrimų Etikos komitetą apie visus nenumatytus atvejus, susijusius su studijos vykdymu, (2) iki sausio 15 dienos – pateikti metinį studijos vykdymo apibendrinimą bei, (3) per mėnesį po studijos užbaigimo, pateikti galutinį pranešimą apie eksperimentą.

Kauno regioninio biomedicininių tyrimų etikos komiteto nariai			
Nr.	Vardas, Pavardė	Veiklos sritis	Dalyvavo posėdyje
1.	Prof. Romaldas Mačiulaitis	Klinikinė farmakologija	taip
2.	Prof. Edgaras Stankevičius	Fiziologija, farmakologija	taip
3.	Doc. Eimantas Peičius	Filosofija	taip
4.	Dr. Ramunė Kasperavičienė	Kalbotyra	ne
5.	Med. dr. Jonas Andriūškevičius	Chirurgija	taip
6.	Agnė Krušinskaitė	Teisė	taip
7.	Prof. Skaidrius Miliuskas	Pulmonologija, vidaus ligos	ne
8.	Med. dr. Rokas Bagdonas	Chirurgija	ne
9.	Eglė Vaižgelienė	Visuomenės sveikata	taip

Kauno regioninis biomedicininių tyrimų etikos komitetas dirba vadovaudamasis etikos principais nustatytais biomedicininių tyrimų Etikos įstatyme, Helsinkio deklaracijoje, vaistų tyrinėjimo Geros klinikinės praktikos taisyklėmis.

Pirmininkas



Prof. Romaldas Mačiulaitis

CURRICULUM VITAE

Name, Surname: Justinas Mačiulaitis
Address: The Institute of Physiology and Pharmacology,
A. Mickevičiaus 9, LT-49264 Kaunas, Lithuania
Phone: +370 685 04325
E-mail: justinas.maciulaitis@gmail.com

Work Experience:

- September 2017–Present Orthopaedic Surgeon, JSC “Gijos Klinikos”
Outpatient consultations for patients suffering orthopaedic disorders. Specialisation – knee cartilage pathology and ortho-biological treatment.
- September 2016–2019 Clinical trial investigator, Hospital of Lithuanian University of Health Sciences, Orthopaedic and Traumatology department
Investigator in advanced therapeutic medicinal product trial for cartilage repair. Duties include performing surgeries, clinical effectiveness evaluation and documentation.
- August 2015–Present Junior researcher, Lithuanian University of Health Sciences, Medical Academy, Sports Institute, Regenerative Medicine
Fundamental and applied research in regenerative medicine. Main focus areas include musculoskeletal and renal systems. Disease modelling in preclinical animal models. Developmental steps of somatic and stem cell products, including biopsy tissue procurement, cell isolation, cultivation, purification, differentiation and final formulation. Characterisation studies of identity, potency, purity and toxicology assays.
- 2015–Present Combined advanced therapeutic medicinal product preclinical and clinical development
Hospital of Lithuanian University of Health Sciences, Orthopaedic and Traumatology department
Lithuanian University of Health Sciences, Medical Academy, Sports Institute, Regenerative Medicine
Lithuanian University of Health Sciences, Medical Academy, Physiology Pharmacology department
Vilnius University, Faculty of Physics, Laser Research Center
Kaunas technology university, Faculty of Design and Technologies
Combined tissue engineered product of somatic cell and scaffold developmental studies in preclinical model and clinical models. Translational research included active substance and a medical device characterisation, biocompatibility, safety and efficacy studies.

2012–2014	<p>Combined advanced therapeutic medicinal product preclinical development Hospital of Lithuanian University of Health Sciences, Orthopaedic and Traumatology department Lithuanian University of Health Sciences, Medical Academy, Sports Institute, Regenerative Medicine Lithuanian University of Health Sciences, Medical Academy, Physiology Pharmacology department Vilnius University, Faculty of Physics, Laser Research Center <i>Combined tissue engineered product of somatic cell / stem cell and microstructured scaffold developmental studies in preclinical model. Translational research included active substance and a medical device characterisation studies.</i></p>
April 2009–August 2009	<p>Junior researcher, intern Stem Cell Research Center at University of Pittsburgh, PA, USA School of Medicine, Department of Orthopaedic Surgery <i>Stem cell isolation, cultivation, differentiation, characterisation, biological assays. Cell therapy application in preclinical animal musculoskeletal models.</i></p>
2008–2009	<p>Junior researcher, intern Kaunas University of Medicine, Cardiology institute Vilnius University, Immunology department <i>Isolation, cultivation, differentiation, characterisation of stem cells derived from different tissues. Application in preclinical renal models.</i></p>
Education and Training:	
Since March 2017	<p>Translational research and development of innovative technologies, Agency for Science, Innovation and Technology</p>
Since 2015	<p>PhD student in Regenerative medicine, Lithuanian University of Health Sciences, Medical Academy, Sports Institute</p>
2010–2015	<p>Orthopaedics and Traumatology Residency, Lithuanian University of Health Sciences, Medical Academy,</p>
2003–2009	<p>Orthopaedics and Traumatology Department MD, Kaunas University of Medicine</p>

PADĖKA

Kai 2007-ųjų metų vasarą kartu su tėčiu prof. Romaldu Mačiulaičiu, prof. Rimtautu Gudu susitikome pas prof. Emilį Čekanauską svečiuose, dar nežinojau, kad tai buvo mano naujos, bet, mano akimis žiūrint, nedidelės kelionės pradžia.

Jei būčiau žinojęs tai, ką žinau dabar, ar būčiau pradėjęs šiuos pažangios terapijos vaistų vystymo darbus, apie kuriuos supratau tiek nedaug?

Daug kas sako, kad darbo kryptis biologinė, ne medicininė. Vis dėlto šį darbą sunku priskirti vienai ar dviem temoms, todėl ir padėkoti už pagalbą norėčiau medicinos, fizikos, veterinarijos, farmacijos, molekulinės biologijos ir raudonųjų biotechnologijų specialistams svariai prisidėjusiems prie rezultatų gavimo.

Prof. Rimtautui Gudiui ir prof. Romaldui Mačiulaičiui – Jūsų patarimais ir išvalgomis vadovavausi bręsdamas kaip mokslininkas, žmogus ir asmenybė. Pradėjau daugiau klausti, ne *Kas?* ir *Kaip?*, o *Kodėl?* Ačiū.

Lietuvos sveikatos mokslų universiteto ligoninės Kauno klinikų Ortopedijos traumatologijos klinikos kolegoms už įsimintinus rezidentūros metus, kurie perkėlė mane iš jaunystės į suaugusiųjų gyvenimą. Suteikė galimybę matyti tuos pacientus, dėl kurių ir dirbame. Ačiū.

Vilniaus universiteto Lazerinių tyrimų centro kolegoms dr. Simai Rekštytei ir prof. Mangirdui Malinauskui už atviras akis ir skrupulingus mikrostruktūrizavimo darbus. Leido mums visiems pajauti tarpdiscipliniškumo jėgą. Ačiū.

Lietuvos sveikatos mokslų universiteto Biologinių tyrimų centrui už tiriamųjų operacijas ir priežiūrą. Anestezijos specifiką gali išmokti, bet išbandyti naujų metodikų, atliekant naujo pobūdžio operacijas, reikia drąsos. Ačiū.

Visiems mokslinės ir eksperimentinės plėtros projektų dalyviams, kurių pagalba buvo įgyvendinti šie darbai – didelis Ačiū už Jūsų kompetencijas ir skirtą laiką. Iš kiekvieno Jūsų išmokau to, ką pritaikiau ir tebetaikau savo profesiniame ir asmeniniame gyvenime. Ačiū.

Didelis ačiū, recenzentui prof. Giedriui Barauskui už disertacinio darbo pakėlimą į kitą lygį. Profesoriaus išvalgos leido pamatyti darbą prezidentinės ložės kampu. Ačiū.

Mama Violeta, Tėtis Romas, Sesuo Gintarė – jūs su manimi 35 metai. Liksiu Jums skoloje amžinai. Žmona Rūta ir dukrytė Eglutė – mūsų pradžia labai graži ir man neįkainojamai prasminga. Ačiū už Jūsų paramą ir stiprybę.

Prabėgus trylikai metų, jei tai ką žinau dabar, ar būčiau pradėjęs šiuos darbus. Be abejonės.